JOURNAL OF CONDENSED MATTER NUCLEAR SCIENCE

Experiments and Methods in Cold Fusion

VOLUME 1, APRIL 2007

JOURNAL OF CONDENSED MATTER NUCLEAR SCIENCE

Experiments and Methods in Cold Fusion

JOURNAL OF CONDENSED MATTER NUCLEAR SCIENCE

Volume 1, April 2007

Orders, claims, author inquiries and journal inquiries

Please contact the Editor in Chief, CMNSEditor@iscmns.org or webmaster@iscmns.org

J. Condensed Matter Nucl. Sci. 1 (2007) 1–154

JOURNAL OF CONDENSED MATTER NUCLEAR SCIENCE

Volume 1 2007

CONTENTS

PREFACE

Cold Fusion was publicly announced on March 23, 1989 by Professors Martin Fleischmann and Stan Pons. Now, 18 years later the first volume of a refereed scientific journal, entirely devoted to this field is being published. During all these years hundreds of scientists have worked passionately to prove that the two inventors were right. They faced a number of scientific challenges, the exciting side of their endeavour. Working in t*erra incognita* was their source of hope and joy. Going where nobody else had gone before, where the most extravagant theory had to be considered. Doing things that were supposed to do nothing, and yet continuing in spite of failures. These people deserve our admiration. Hopefully one day they will be acknowledged as scientific pioneers. In addition to the scientific challenges, they had to fight two more battles; one was the lack of recognition by their peers, and the other the difficulty of publishing their findings in reputed journals.

It will take still more time before the scientific community recognizes the importance and validity of Condensed Matter Nuclear Science. My personal experience, after giving a number of talks and seminars, is that young people are a lot more open to these new ideas than older and established scientists. Therefore, there is hope. However, we need a place where essential aspects of the field can be easily located. I am very proud to be the first editor of this journal that will hopefully become the reference for this field. I would like to thank my colleagues and the associate editors who have entrusted me with this position.

This journal is wide open to new ideas: experimental as well as theoretical. We are engaged in a field where it is difficult to know if classical physics as taught at the university is capable of understanding Condensed Matter Nuclear Science or whether a new science needs to be developed. Only future will tell. This first volume contains a majority of theoretical papers. Even though theories are important in understanding Condensed Matter Nuclear Science, what will certainly be most persuasive in the broader scientific community is a good and reproducible experiment.

In the beginning years of Cold Fusion, attention was concentrated on excess heat, neutron production and helium detection mostly during electrolysis in the palladium heavy water system. Later on, it was discovered that other metals and hydrogen could be used. Excess heat has been measured by many scientists, helium-4 detected in a dozen laboratories, low-level neutrons measured with difficulties in few cases. However, in addition to what was expected, transmutation of elements also has been detected. Recently, new triggering techniques have been developed from gas phase to plasma discharges, complex non-dc electrical stimulation and ultrasound activation.

At 18 it is time to enter adulthood and be free of the pains and accidental conditions of birth. In most countries this is the age of independence from one's parents. It is my hope that the field has at last reached this point. Hopefully this journal will provide stimulation and encouragement, as well as serve to document the second phase of the cold fusion revolution.

Jean-Paul Biberian
April 2007

J. Condensed Matter Nucl. Sci. 1 (2007) 1–5

Letter to the Editor

Palladium Fission Triggered by Polyneutrons

John C. Fisher *

600 Arbol Verde, Carpinteria, CA, 93013, USA

Abstract

Polyneutron theory is applied to experiments of Iwamura et al. that show evidence for titanium and for an anomalous iron isotope ratio in palladium cathodes following electrolysis. Theory and experiment are in reasonable agreement. Experiments are suggested for additional testing of the theory.

Keywords: Fission, LENR reaction, Liquid drop model, Palladium, Polyneutron

Iwamura et al. [1] have conducted electrolysis experiments in which deuterium was introduced into a palladium cathode. During electrolysis they observed excess heat generation and X-ray emission that they attributed to nuclear reactions. Following electrolysis, investigation of the cathode revealed a significant signal for titanium and an anomalous iron isotope ratio. In the subsequent experiments [2] where deuterium was diffused into a palladium diaphragm they confirmed the anomalous iron isotope ratio. Evidence for titanium and for iron suggests that these isotopes may have arisen from fission of palladium in the cathode. Although this interpretation seems at first to be physically impossible, it may be that interactions with polyneutrons can enable fission to occur.

Fission reactions that yield titanium, iron, and other isotopes with mass numbers comparable to half that of palladium are exothermic, but do not occur under normal circumstances. According to the liquid drop model of nuclei the criterion for spontaneous fission is

$$\frac{Z^2}{A} > \frac{2a_s}{a_c}, \tag{1}$$

where Z is the nuclear charge, A the nucleon number, a_s the surface energy coefficient, and a_c is the Coulomb energy coefficient [3]. For ordinary nuclei the drop model coefficients are $a_s = 16.8$ MeV and $a_c = 0.72$ MeV and the corresponding criterion for spontaneous fission is $Z^2/A > 47$. For ^{102}Pd we have $Z^2/A = 21$, well short of the required 47. An extrapolation to $Z = 46$ based on data for $Z > 89$ suggests a palladium fission half-life of about 10^{60} years. It follows that a significant reduction in surface energy is required if palladium fission is to occur.

*E-mail: jcfisher@fisherstone.com

Polyneutron theory offers a possibility for the required reduction in surface energy. Polyneutrons are hypothetical neutron aggregates having densities comparable with ordinary nuclei. I have proposed that in LENR reactions they grow in size to hundreds of neutrons, and that they bind to ordinary nuclei in reactions responsible for nuclear energy production, helium production, palladium transmutation, and other nuclear phenomena [4]. For this binding energy to be the cause of surface energy reduction, the configuration of the polyneutron-nucleus composite must be that of a shell nucleus, with a polyneutron forming a neutron shell around an ordinary nucleus as core. If the energy of the outer surface of the shell plus the interfacial energy between the shell and the core nucleus together amount to less than 45% of the surface energy of a free nucleus, then $Z^2/A < 21$ and palladium fission is assured. I assume this to be so and consider the consequences.

Fission reactions are of the following form:

$$^{A}\mathrm{Pd} + {}^{B}\mathrm{n} \rightarrow ({}^{A}\mathrm{Pd}\ {}^{B}\mathrm{n}) \rightarrow ({}^{C}\mathrm{X}^{B-\alpha}\mathrm{n}) + {}^{D}\mathrm{Y} + \Delta E_{\mathrm{s}} + \Delta E,$$
$$\alpha = C + D - A. \tag{2}$$

In this reaction the symbol $({}^{A}\mathrm{Pd}\ {}^{B}\mathrm{n})$ stands for a shell nucleus with B neutrons in the shell surrounding ${}^{A}\mathrm{Pd}$ as core. Because polyneutrons are large I expect that $B > A$ and the polyneutron shell is larger than the palladium core. The nuclei ${}^{C}\mathrm{X}$ and ${}^{D}\mathrm{Y}$ are the fission products. The $({}^{C}\mathrm{X}^{B-\alpha}\mathrm{n})$ is a shell nucleus with $B - \alpha$ neutrons in the shell. ΔE_{s} is the net surface energy released on formation of the final composite. ΔE is the remainder of energy released in the reaction. The quantity α is the number of neutrons that are transferred from the polyneutron to the fission products. I assume that the polyneutron halo is attached to a single fission fragment. This is plausible provided that the interfacial energy between shell and core depends on the thickness of the shell and does not reach its minimum value until the shell reaches a thickness of several neutrons. As a consequence, considering the sizes of palladium nuclei and the estimated sizes of free polyneutrons in the reactions under consideration, the energy is a minimum when all neutrons are concentrated in a single shell. I assume that chance decides which fission fragment is free and which is a shell nucleus core.

Reaction energies ΔE are calculated using the standard mass excesses for ordinary nuclei [5], and the formula

$$\Delta({}^{A}\mathrm{n}) - \Delta({}^{A-\alpha}\mathrm{n}) = 1.143\alpha \tag{3}$$

for the differences between polyneutron mass excesses [4]. I assume even values for A and α because of the high mass excesses expected for polyneutrons containing an odd neutron.

The following calculations illustrate the method:

$$^{102}\mathrm{Pd} + {}^{A}\mathrm{n} \longrightarrow {}^{56}\mathrm{Cr} + {}^{52}\mathrm{Ti} + {}^{A-6}\mathrm{n} + \Delta E_{\mathrm{s}} + \Delta E,$$
$$\Delta E = \Delta(^{102}\mathrm{Pd}) - \Delta(^{56}\mathrm{Cr}) - \Delta(^{52}\mathrm{Ti}) + 6(1.143) = 23.679\ \mathrm{MeV},$$

$$^{106}\mathrm{Pd} + {}^{A}\mathrm{n} \longrightarrow {}^{56}\mathrm{V} + {}^{54}\mathrm{V} + {}^{A-4}\mathrm{n} + \Delta E_{\mathrm{s}} + \Delta E,$$
$$\Delta E = \Delta(^{106}\mathrm{Pd}) - \Delta(^{56}\mathrm{V}) - \Delta(^{54}\mathrm{V}) + 4(1.143) = 10.660\ \mathrm{MeV}. \tag{4}$$

There are about a thousand such reactions with energies ΔE in the range from zero to 24 MeV. They occur with probabilities that depend on how exothermic they are. I expect that the probability increases exponentially with ΔE and that reactions with small ΔE can be neglected. As a rough approximation I consider only the 94 reactions having $\Delta E > 18$ MeV and I give them equal weight. This assumes that the unknown energy ΔE_{s} is approximately the same

Mass number	Final product	1.02% ^{102}Pd	11.14% ^{104}Pd	22.33% ^{105}Pd	Weighted totals
42	Ar	3	–	–	3
44	Ca	3	–	–	3
46	Ca	7	–	–	7
47	Ti, K→ Ti (8d)	3, 2	–	–	3, 2
48	Ti, Ca	1, 6	0, 4	0, 3	1, 119
49	Ti	5	1	2	61
50	Ti	8	4	1	75
51	V	12	–	1	35
52	Cr	7	2	2	74
53	Cr	12	–	2	57
54	Cr	8	3	–	42
55	Mn	12	–	1	35
56	Fe	6	3	2	84
57	Fe	5	–	1	27
58	Fe	7	1	–	18
59	Fe → Co (44d)	6	–	1	28
60	Fe	6	2	1	51
61	Ni	5	1	1	38
62	Ni	3	2	1	48
63	Ni	3	–	1	25
64	Ni	6	1	–	17
65	Cu	1	–	–	1
66	Zn	4	–	–	4
68	Zn	3	–	–	3
Total		144	24	20	861

for all fission reactions and that it does not affect their ranking. The 188 fission fragments are classified in the following table.

The first column gives the mass number of the fission fragment.

Many fragments are radioactive and undergo one or more beta decays before reaching stability. The second column identifies the isotopes that are present 1 day after electrolysis, by which time most beta decay has ceased. Except for mass numbers 47 and 59 all tabulated fission products are stable or have half-lives greater than 30 years.

The third column summarizes the fragments expected from fission of ^{102}Pd. The largest signals are for Cr (27 fragments with mass numbers 52–54), for Fe (30 fragments with mass numbers 57–60 declining to 24 fragments after decay of ^{59}Fe), and Ti (17 fragments with mass numbers 47–50 rising to 19 after decay of ^{47}K).

The fourth and fifth columns summarize the fragments expected from fission of ^{104}Pd and ^{105}Pd. There are no fission reactions with $\Delta E > 18$ for isotopes ^{106}Pd, ^{108}Pd, or ^{110}Pd.

The last column gives the totals from all Pd isotopes, weighted by their natural abundance percentages. From these values I abstract the quantities of relevance for comparison with the experiments of Iwamura et al.

1. Abundance ratio of ^{57}Fe to ^{56}Fe:

Natural abundance ratio is $^{57}Fe/^{56}Fe = 0.023$.
Theory: $^{57}Fe/^{56}Fe = 27/84 = 0.32$.
Experiment: $^{57}Fe/^{56}Fe$ = 0.036, 0.038, 0.065, 0.24, 0.66, 0.26, 0.22, 0.29, 0.45, 0.37, 0.66, 0.097, 0.03, 0.03 (range 0.03–0.66, mean 0.25; SIMS[1]),
$^{57}Fe/^{56}Fe = 0.31$ (TOF-SIMS[2]).
The theoretical value 0.32 and the experimental values 0.25 and 0.31 are in reasonable agreement.

2. Abundance ratio of mass-58 to mass-56:

Natural abundance ratio of iron isotopes is $^{58}Fe/^{56}Fe = 0.003$.
Theory: $^{58}Fe/^{56}Fe = 18/84 = 0.21$.
Experiment: mass-58/mass-56 = 0.02 (min) to 0.30 (max).
The theoretical value 0.21 and the mean experimental value 0.16 are in reasonable agreement.

3. Presence of titanium:

Theory: Ti fission fragments amount to 17% of total.
Experiment: Strong EDX signal for Ti.
Theory and experiment are compatible.

The tabulated data suggest additional measurements that can further test the theory:

a. Abundance ratio of ^{54}Cr to ^{52}Cr:

Natural abundance ratio is $^{54}Cr/^{52}Cr = 0.028$.
Theory: $^{54}Cr/^{52}Cr = 42/84 = 0.57$.

b. Abundance ratio of ^{60}Fe to ^{56}Fe:

Natural abundance ratio is $^{60}Fe/^{56}Fe = 0$.
Theory: $^{60}Fe/^{56}Fe = 51/84 = 0.61$.

c. Gamma radiation from decay of ^{60}Co:

Theory: The ^{60}Fe fission fragments decay to ^{60}Co with a half-life of 1.5 million years. Decay of the resulting ^{60}Co emits characteristic gamma radiation.

Overall the agreement between theory and experiment is consistent with the concept of palladium fission. Confirmation of the $^{57}Fe/^{56}Fe$ and $^{58}Fe/^{56}Fe$ ratios and of the presence of Ti are possible by testing palladium cathodes from earlier experiments. Measurements of $^{54}Cr/^{52}Cr$ and $^{60}Fe/^{56}Fe$ offer possibilities for extending the evidence for fission.

Detection of gamma radiation from ^{60}Co decay would provide the most compelling evidence. The ^{60}Fe fission fragments predicted by the theory have a 1.5 million year half-life, decaying to ^{60}Co. Subsequently ^{60}Co decays to ^{60}Ni with a 1900 days half-life, emitting characteristic gamma rays. Iwamura et al. found about 10^{17} atoms of Ti in the surface layers of their cathode. If Ti and Fe isotopes have proportional molar concentrations we can expect about 4×10^{16} atoms of ^{60}Fe. The rate of ^{60}Fe decay would be about 10^3 per second, and after a few years the decay rate of the Co^{60} product would rise to equal it. This level of radioactivity is measurable and a positive result would provide irrefutable proof of nuclear reaction, free of the doubts that invariably plague calorimetric measurements.

References

[1] Y. Iwamura, T. Itoh, N. Gotoh, M. Sakano, I. Toyoda, and H. Sakata, *Proceedings of the ICCF7*, Vancouver, 1998.
[2] Y. Iwamura, T. Itoh, and M. Sakano, *Proceedingd of the ICCF8*, Lerici (La Spezia), 2000.

[3] K.S. Krane, *Introductory Nuclear Physics* (Wiley, New York, 1988).
[4] J.C. Fisher, *Proceeding of the ICCF12*, Yokohama, 2005.
[5] J.K. Tuli, Nuc. Wallet Cards, *Nat. Nuc. Data Ctr.* (2005).

J. Condensed Matter Nucl. Sci. 1 (2007) 6–10

Letter to the Editor

A Particle Physicist's View on the Nuclear Cold Fusion Reaction

Tetsuo Sawada*

Institute of Quantum Science, Nihon University, Tokyo 1018308, Japan

Abstract

There are two different types of scientists who believe in the reality of the nuclear cold fusion. The researchers, who observed the excess energy by experiments, belong to the first type. On the other hand, a small number of theoreticians, who are working on the physics of the magnetic monopole, know that the nuclear reaction of the zero incident energy proceeds when the system involves a magnetic monopole. Since the former group still lacks a theory of the nuclear cold fusion based on the first principle of the natural law, I believe it is fruitful to explain to the former group how the theoretician of the particle physics comes to arrive at the conclusion that the nuclear cold fusion must occur if a magnetic monopole exists, in the framework of the quantum theory.

Keywords: Change of penetration factor, Charge quantization condition, Magnetic monopole, Nuclear cold fusion, Origin of non-reproducibility

From the charge quantization condition of Dirac [1], which says that ${}^*ee/c = \hbar/2$, where e and ${}^*e$ are the smallest electric and the magnetic charges, respectively, the magnetic counterpart of the "fine structure constant" is determined: ${}^*e^2/\hbar c = 137.036/4$. It means that the monopole is accompanied by a superstrong magnetic Coulomb field $\vec{B} = {}^*e\hat{r}/r^2$. If we remember that the nucleon has the magnetic dipole moment $\kappa_{\rm tot}(e/2m_{\rm p})\vec{\sigma}$, where $\kappa_{\rm tot}$ is 2.793 and -1.913 for the proton and for the neutron, respectively, the interaction hamiltonian between the monopole and the nucleon is $H^{\rm dip} = -(\kappa_{\rm tot}/4m_{\rm p})(\hat{r}\cdot\vec{\sigma})F(r)/r^2$, in which $F(r)$ is the form factor of the nucleon. It is remarkable that the strength of this interaction potential $H^{\rm dip}$ is two or three times larger compared to the nuclear potential $V^{\rm nucl}$ at the separation $r = 0.5$ to 3 fm.

The kinetic energy term in the external magnetic Coulomb field is $H^0 = (-i\nabla - (Ze/c)\vec{A})^2/2m$, where the vector potential $\vec{A}$ must be chosen such that rot$\vec{A}$ is the magnetic Coulomb field. Since we already know the nuclear potential $V^{\rm nucl}_{i,j}(r_{i,j})$ between the ith and the jth nucleon, the total hamiltonian of the nuclear system in the external Coulomb field becomes

$$H_{\rm tot} = \sum_{j=1}^{A} H^0_j + \sum_{j=1}^{A} H^{\rm dip}_j + \sum_{i>j} V^{\rm nucl}_{i,j}.$$

*E-mail: t-sawada@fureai.or.jp

Once the hamiltonian is given, it is the standard exercise of the quantum mechanics to calculate the physical quantities such as the energy level, radius of the orbit and the transition rate. The easiest one is the one-body problem in the external potential. The eigenfunction of the spin 0 charged particle, namely the eigenfunction of H^0, is known for long time (Tamm's solution), whose radial function is

$$R(r) = \frac{1}{\sqrt{kr}} J_\mu(kr), \quad \text{where} \quad \mu = \sqrt{(\ell + 1/2)^2 - q^2} > 0 \quad \text{and} \quad k = \sqrt{2mE},$$

in which q is the magnitude of the extra angular momentum, namely $q = Ze\,{}^*e$, and the range of the angular momentum ℓ is $\ell = |q|, |q| + 1, |q| + 2, \ldots$ Since the Bessel function is oscillatory and does not damp at large r, the system of spin 0 particle, and a monopole does not have bound state.

On the other hand, a particle of spin 1/2 forms bound states with the magnetic monopole when the anomalous magnetic moment ($\kappa_{\text{tot}} - 1$) is sufficiently large. For example, the system of the proton and the monopole has bound state, whose binding energy of the ground state is $-E = 0.188$ MeV and its radius of the orbit is $\sqrt{\langle r^2 \rangle} = 11.0$ fm [2]. We can treat the triton and the ^{3}He in the same way if the deformation of the nuclei is negligible. We found 1.52, 0.245 MeV, and 3.82, 7.37 fm, respectively, for the triton and for the ^{3}He [3]. The attractive force, which appear when the magnetic dipole moment of nuclei orients to the opposite direction of the magnetic monopole, is responsible for the formation of the bound state. We shall see the same attractive force changes the repulsive Coulomb barrier completely. Let us consider the t + p reaction. Suppose that the proton and the monopole form the bound state firstly, the potential felt by the approaching triton is the sum of the Coulomb potential and attractive potential mentioned above. The penetration potential V_1 is

$$V_1(x) = \frac{e^2}{x} - \kappa_{\text{tot}} \frac{e}{2m_{\text{p}}} \frac{{}^*e}{x^2}.$$

It is remarkable that although the peak of the Coulomb potential is around 1 MeV, the peak of $V_1(x)$ is lowered to 17 keV [3].

Furthermore, if we solve the third eigenvalue problem of the electron–monopole system, we shall find an eigenstate whose radius is one half of the electron Compton wave length namely 193.8 fm, and the monopole–proton system is shielded by the electron cloud. Therefore, the penetration potential $V_1(x)$ should be changed to the shielded Coulomb:

$$V_2(x) = \frac{e^2}{x} \exp[-2m_{\text{e}}x] - \kappa_{\text{tot}} \frac{e}{2m_{\text{p}}} \frac{{}^*e}{x^2}.$$

It is interesting to compare the penetration factor P for various potentials, in which P is

$$P = \exp[-2\tau] \quad \text{with} \quad \tau = \sqrt{2\mu_{\text{red}}} \int_a^b \sqrt{V(x) - E}\, \mathrm{d}x/\hbar,$$

where μ_{red} is the reduced mass and $[a, b]$ is the region of the penetration, and we shall put $E \to 0$ hereafter. In vacuum, $V(x)$ is the Coulomb potential, and if we choose $[a, b]$ as [1 fm, 1 Å], the penetration factor P is 5.33×10^{-106} and 6.78×10^{-92}, respectively, for d + d and for p + t. These values are forbiddingly small. On the other hand, if the magnetic monopole is involved, and so V_2 is used in place of V, P of $({}^*e - \text{d}) + \text{d}$ changes to 6.22×10^{-9}. Concerning the p + t case, there are two ways of penetration, $({}^*e - \text{p}) + \text{t}$ denotes penetration, in which the proton is trapped by the monopole at first. The penetration factors P of p + t are 5.39×10^{-4} and 2.93×10^{-7}, respectively, for $({}^*e - \text{p}) + \text{t}$ and for $({}^*e - \text{t}) + \text{p}$. Since these P have reasonable values, we can expect to find the double bound state $(\text{d} - {}^*e - \text{d})$

or (p $-$ $^*e$ $-$ t). However, since the size of the orbits are around several fm, the nuclei quickly fuse to become more stable nucleus ^{4}He. If we remember the spin 0 particle such as ^{4}He cannot form the bound state with the monopole, the ^{4}He must be emitted with the kinetic energy around 20 MeV. There remains a fresh magnetic monopole, which starts to attract surrounding nuclei again. In this way the nuclear cold fusion reaction proceeds by the help of a single magnetic monopole.

If we remember the magnetic monopole is the rare particle and if the existence of a monopole in the reaction region is responsible for the nuclear cold fusion, we expect that we have to wait for long time before the cold fusion reaction start to occur. Since in the ordinary experiment, the process that a monopole moves into and stops in the reaction region is governed by the probability, the occurrence of the nuclear cold fusion is sporadic, therefore we cannot expect the 100% reproducibility of the nuclear cold fusion. In order to recover the reproducibility of the ordinary sense, we must do the much more difficult experiment to examine the existence of the monopole along with the measurement of the excess energy.

Addition to the Abstract

Up to this point, in order to solve the problem rigorously, we considered simplified system, in which a magnetic monopole is fixed in the region where the density of the fuel nuclei is high. In the actual experiment we must stop the floating magnetic monopole. The most clean experiment will be done if we can trap the monopole electromagnetically. However, there are other methods to trap the monopole. Rare earth metal such as Eu or Gd, which has large magnetic moment (several Bohr magneton), can trap the monopole by aligning the spins of the atoms of the lattice spherically around the monopole. The estimated trapping energy is around 10 keV at the room temperature ($T = 300^{\circ}$C). Other metals, which have large magnetic permeability, such as Pd or Ni can also trap the magnetic monopole. If we consider that Pd can absorb large amount of D_2, Pd must be a good choice as the cathode.

Our primary purpose is to understand the basic mechanism of the nuclear cold fusion. In carrying out such a program, introduction of the bias, which often arises from the desire to "explain" observed phenomenon in haste, causes the fatal error. The standard mathematical manipulation of the quantum system starting from the given hamiltonian is effective in avoiding such a bias. When we simulate the quantum system there is the limitation on the number of participating particles A. So we shall restrict ourselves to the smallest system of the nuclear transmutation D + D $\rightarrow$ ^{4}He, whose nucleon number is $A = 4$. It is desirable that the phenomenon is static or close to static for the simplicity of the mathematical treatment. Therefore, the violently fluctuating system such as the plasma discharge is not suitable for our purpose.

It is interesting that two properties characteristic to the nuclear cold fusion are sufficient to narrow down the basic mechanism of the cold fusion. The properties different from the ordinary nuclear reactions in vacuum are (1) D + D reaction produces ^{4}He with the kinetic energy close to the Q-value, whose value is 23.7 MeV, (2) such a reaction starts to occur sporadic way. It is well-known that in the ordinary reaction the low-energy D + D state goes to the final state p + t or n + ^{3}He with 50% each and to $\gamma + ^4$He with very small rate, in which γ-ray carries almost all the energy Q away. If we remember from the conservations of the energy and the momentum that the reaction of (two body) $\rightarrow$ (one body) is forbidden when $Q > 0$, then the final states of the D + D reaction in vacuum mentioned above is easily understood. On the other hand, in the cold fusion, magnitude of the momentum $\vec{q}$ of ^{4}He is determined by $|\vec{q}|^2/2M_4 = Q$, where M_4 is the mass of ^{4}He. This apparent non-conservation of the momentum indicates the existence of the external potential $U(r)$ which absorbs the momentum transfer $-\vec{q}$. In our D + D $\rightarrow$ ^{4}He reaction, $cq \sim 400$ MeV, which is very large and imposes a stringent restriction on the external potential $U(r)$. Soft and spread $U(r)$ cannot do the job to receive such a large momentum transfer, and the uncertainty relation requires the size of $U(r)$ to be $\Delta r \sim 0.5$ fm. It is evident that such a highly localized potential $U(r)$ cannot be formed by the electron cloud, since its normal size is around 1 Å, moreover from the Dirac equation we know that the lower limit of the size of the electron packet is the electron

Compton wave length $\hbar/m_e c$, which is numerically 386.16 fm.

If we remember that the nucleus can respond only to three types of external fields, namely electric, magnetic or pionic fields, we can narrow down the candidate of the catalyzer which is the source particles of such external fields. When we select the candidate of the catalyzer, we must remember the required property of the catalyzer particle, namely it attracts the fuel nucleus (D), and it repels the product nucleus (^{4}He). The latter property is required to prevent for the produced particle to go back to the initial state (D + D). In summary the catalyzer particle must interact with the initial particle and the final particle oppositely. For the case of the electric field, whose source is the charged particle, for example if charge is negative it attract ^{4}He as well as D. For the pionic field, its source particle is other nucleus and the interaction arises from the ordinary nuclear potential, so it does not act oppositely to the particles of the initial, and the final states. On the other hand, for the case of the magnetic monopole, it attracts nucleus with magnetic moment such as D if its spin is oriented properly, however the spin 0 charged particle such as ^{4}He is excluded from the neighborhood of the monopole (Tamm's solution). Therefore, magnetic monopole is the only candidate as the catalyzer of the nuclear cold fusion reaction.

Finally, we must consider the non-reproducibility, which is the most important feature of the nuclear cold fusion reaction. Although most of the researchers know that the cold fusion does not start on demand, the reproducibility ratio, which must depend on the time duration of the experiments, is not well defined. It is instructive to consider an example how the non-reproducibility emerges from the fundamental law whose hamiltonian does not involve t and $\vec{r}$ explicitly, so the reproducibility in the microscopic level, and also the energy and the momentum conservation are guaranteed by the Noether's theorem. Let us consider a reaction A + B $\rightarrow$ AB in a container, and let N_A and N_B are the number of particles in the container. Suppose that, to increases the reaction speed, we add the catalyzer particle c whose number in the container is N_c. It is customary that the number of the catalyzer particle N_c is much smaller compared to N_A and N_B, however N_c as well as N_A and N_B are macroscopic numbers. We are going to examine the appearance of the fluctuation as $\langle N_c \rangle$ decreases to small number. Since the distribution of N_c has spread $\sqrt{\langle N_c \rangle}$ around $\langle N_c \rangle$, for example for $\langle N_c \rangle = 100$ the reaction speed has 10% uncertainty when we repeat the measurements. As $\langle N_c \rangle$ decreases further, the uncertainty increases, and if $\langle N_c \rangle$ becomes much <1, we must encounter an embarrassing situation. Namely the reaction does not proceed in almost all the experiment, but it occurs when a catalyzer particle comes into the container and stops in it. Occurrence of the reaction is sporadic and seldom. When we repeat experiments limited number of times we are most likely not to observe the reaction, however it does not necessarily mean that the reaction is not real. The nuclear cold fusion seems to belong to this category.

Most of the physicists welcome the magnetic monopole, since the monopole makes it possible to understand the discreteness of the electric charge in Nature and to symmetrize Maxwell equations with respect to the interchanges of the electric and the magnetic objects [1]. Despite the extensive search of the magnetic monopole, its existence is not confirmed. From the Table of the Particle Data Group [4], we can see that the search experiments have been done by using four types of devices: plastic, emulsion, counter, and induction. Among these the first three devices cannot detect the low-energy monopole. Although it is true that by induction method we can cover the low-energy monopole, there is some difficulty in detecting the very low-energy or floating monopole. In the first-half of this report, we saw that the floating magnetic monopole can make the nuclear cold fusion possible. And in the second-half of this report, we explained the logically inverse statement that the nuclear cold fusion occurs only when the magnetic monopole exists. So I am regarding the experimental apparatus of the nuclear cold fusion as the "detector" of the floating monopole. By observing that the magnetic monopole actually catalyzing nuclear cold fusion reaction, I expect to solve the two fundamental problems in physics, namely the existence of the magnetic monopole, and the basic mechanism of the nuclear cold fusion, simultaneously.

References

[1] Funfamentals of the magnetic monopole, 2006, http://www.fureai.or.jp/ t-sawada/.
[2] T. Sawada, *Found. Phys.* **23** (1993) 291.
[3] Cold Nuclear Fusion, 2002, http://www.fureai.or.jp/ t-sawada/.
[4] Review of Particle Physics, 2007, http://pdg.lbl.gov/.

J. Condensed Matter Nucl. Sci. 1 (2007) 11–15

Research Article

The Conjecture of the Neutrino Emission from the Metal Hydrides

Xing Z. Li*, Qing M. Wei, Bin Liu, Shao L. Ren

Department of Physics, Tsinghua University, Beijing 100084, China

Abstract

Selective Resonant tunneling model has been successful to explain the three major puzzles in cold fusion proposed by nuclear physicist (i.e. penetration of Coulomb barrier, no neutron emission, no gamma radiation), and successful also to explain the three major cross-section data in hot fusion(i.e. $d+t$, $d+d$, $d+He^3$). Its prediction about 3-deuteron fusion has been found in experiments as well. The reasonable inference is the neutrino emission from the metal hydrides. The feasibility of detection of this neutrino is discussed in this note.

Keywords: Condensed matter nuclear science, 3-Deuteron fusion reaction, KamLAND, Metal hydrides, Neutrino emission, Selective resonant tunneling

1. Theory—Resonance Selects Damping

Selective resonant tunneling theory predicts that there should be a state of long life-time with two deuterons inside the metal crystal lattice when deuterium gas is absorbed by a metal. This has been verified in Japan, and we further guess that this long life-time state would emit neutrino which is detectable within the sensitivity of KamLAND neutrino detector.

It is well known that hydrogen molecule will be dissociated into hydrogen atoms when hydrogen is absorbed by metal. The hydrogen atoms will be further ionized into protons and electrons in the crystal of metal. In general, those protons are trapped and separated by the lattice potential. The distance between them is similar to or even greater than the distance in a hydrogen molecule. The opportunity for them to approach each other is exponentially small due to the Coulomb barrier between two positively charged protons. The same is true for a pair of deuterons inside the metal crystal lattice. The probability for a pair of deuterons to approach each other is exponentially small as well. However, once a pair of deuterons stays together, it will form an excited state of the helium nucleus. This excited state of the helium nucleus will decay through strong nuclear interaction or electromagnetic interaction. However, according to the selective resonant tunneling theory [1,2], another kind of excited state of the helium nucleus will be generated. It is a product of the resonant tunneling through a thick and high Coulomb barrier inside the metal crystal lattice. The

*E-mail: lxz-dmp@tsinghua.edu.cn

resonant tunneling will select only the state with long life-time because the resonant tunneling would not be valid if the life-time of that state is not long enough. Hence, this state must decay through some weak interaction instead of any strong nuclear interaction or electromagnetic interaction. The most important test of this selective resonant tunneling theory is to search for this long life-time resonant state of two deuterons.

2. Experiment—Evidences for Long Life-time State

Three deuterons might interact if two deuterons stay together with a long life-time in a target while the third deuteron is impinging on this target. The longer this life-time is, the greater the opportunity to see this 3-deuteron reaction. Professor Kasagi of Tohoku University observed this 3-D fusion reaction early in 1993 in Nuclear Science Laboratory [3].

About 150 keV deuteron beam bombarded on a titanium target, which had absorbed a lot of deuterium gas in advance to form TiD_x with $x > 1.2$. Usually, we expect only the 2-body fusion reactions, because the probability of 3-body fusion reactions is almost zero. However, Kasagi observed the 3-body fusion reactions with much more probability. Every 10^5 2-body fusion reactions he observed one 3-body fusion reaction. In comparison, the theoretically expected value was only one 3-body fusion reaction in every 10^{31} 2-body fusion reactions.

In 1995–1997, Professor Takahashi of Osaka University confirmed this discovery in terms of another reaction channel [4]. Kasagi studied the reaction channel: $d + d + d \rightarrow p + n + {}^4He$ ($Q = 21.62$ MeV), and Takahashi studied the reaction channel: $d + d + d \rightarrow t + {}^3He$ ($Q = 9.5$ MeV). Kasagi found that the maximum energy of the proton and ^{4}He were 17 and 6.5 MeV, respectively. These could not be explained if only 2-body fusion reactions were involved. 3-body fusion reaction of $d + d + d \rightarrow p + n + {}^4He$ ($Q = 21.62$ MeV) explained not only the maximum energy of the proton and ^{4}He, but also the shape of the continuous energy spectrum of the protons and ^{4}He. Takahashi confirmed 3-body fusion reaction: $d + d + d \rightarrow t + {}^3He$ in terms of the energy of triton and ^{3}He (4.75 MeV), and their equal yields. Both Kasagi and Takahashi obtained the similar ratio of the 3-body reaction rate to 2-body reaction rate:$\sim 10^{-5}$. Takahashi further estimated the life-time of the state of two deuterons based on this ratio of reaction rates. The life-time of the 2-deuteron resonance state was estimated to be $10^4 - 10^5$ s, which was just in the range predicted by the selective resonant tunneling model.

3. Neutrino Emission—Feasibility of Detection

Such a long life-time state can only decay through some weak interaction, because the strong nuclear interaction or electromagnetic interaction is too strong to have such a long life-time. The weak interaction is supposed to be accompanied by neutrino emission although we do not know exactly which kind of weak interactions are involved. Is it feasible to detect such a weak neutrino emission using KamLAND neutrino detector?
The recent visit to Research Center for Neutrino Science at Tohoku University gave us the impetus to consider this feasibility with four favorable factors:

(1) *Sensitivity*. KamLAND detector requires that on its spherical surface the neutrino flux should be of the order of $10^6/s/cm^2$. The diameter of this spherical surface is of 13 m. Hence, it requires that at the center of this spherical scintillation liquid there is a neutrino source which has the intensity of 6×10^{12}/s. It corresponds to an "excess heat" power of Watts. Nevertheless, it is possible to have such amount of "excess heat" power in the metal hydride frequently [5,6] if the "excess heat" is from the recoil energy due to the neutrino emission.
(2) *Energy*. KamLAND detector has successfully detected the solar neutrino, the fission reactor neutrino, and the geo-neutrino; hence, it is easier for KamLAND detector to obtain the better ratio of signal to noise if the energy of the unknown neutrino source is greater then 5 MeV. Indeed the preliminary estimate of the energy from the metal hydride is just above 5 MeV (see Section 4).

(3) *Purification of scintillation liquid*. KamLAND detector is composed of a high-purity scintillation liquid. Its impurity is at the level of 10^{-5}. It is scheduled to further purify the scintillation liquid this year. Its impurity level would be further reduced to 10^{-7}. Hence, the ratio of signal to noise would be further enhanced accordingly.
(4) *Volume*. The volume at the center of the KamLAND detector is quite ample for the metal hydride. It is feasible to enhance the "excess heat" power level by a factor of 10–100 just based on the volumetric effect.

4. Weak Interactions

Three kinds of weak interactions are in consideration: K-electron capture, electron-catalyzed fusion reaction, and Mitsubishi–Iwamura type of nuclear transmutation.

(1) *K-electron capture*. K-shell electron of deuterium atom might be captured by the deuteron with very little probability. There are two factors which might change this situation. (i) The selective resonant tunneling is favorable to the low probability process; (ii) The K-electron would have much more chance to interact with the deuteron of which the wave function is a linear combination of two states: the helium-like excited state and the deuterium molecule-like crystal trapped state.
(2) *Electron-catalyzed fusion*. The electron might be captured by a tunneling deuteron, and form a virtual di-neutron in the nuclear well to produce a $^4H^*$ state which would be followed by a decay process to make a $^4He^*$ from this $^4H^*$ state: i.e.

$$d + d + e \rightarrow {}^4H^* + \nu_e,$$

$$^4H^* \rightarrow {}^4He^* + \tilde{\nu}_e + e.$$

The net effect is

$$d + d \rightarrow {}^4He^* + \tilde{\nu}_e + \nu_e + \text{Lattice } (Q = 23.8 \text{ MeV}).$$

It seems like an electron-catalyzed fusion reaction to emit a pair of neutrino and anti-neutrino. This anti-neutrino emission is favorable to KamLAND detector as well. The maximum energy of this anti-neutron is about 23 MeV, and the maximum recoil energy of ^4He is about 23 MeV also when lattice is involved in momentum conservation. These numbers may be compared with the experimental observation.
(3) *Mitsubishi–Iwamura nuclear transmutation*. Cesium ($^{133}_{55}Cs$) thin film on the surface of a Pd–CaO–Pd super-lattice complex might be transmuted into praseodymium ($^{141}_{59}Pr$) while a deuterium flux is permeating through this complex [7]. Four deuterons might be added into this cesium nucleus in terms of the electron-catalyzed process which might be accompanied by emission of a pair of neutrino and anti-neutrino. Although it is not quite clear about the transmutation processes, but the neutrino emission must be there if it is a weak interaction process in nature.

5. Discussion

(1) Is electron capture by deuteron in lattice a real process?
K-capture of electron in nucleus might be accompanied by a positron emission process if the mass excesses allow this positron emission. However, during K-capture of electron in deuteron, ($d+d+e \rightarrow {}^4H^*+\nu_e+0.372$ MeV,) the mass excesses do not allow the positron emission ($d + d \rightarrow {}^4H^* + \nu_e + e^+$) if $^4H^*$ is a real one (i.e. the

mass excess of $^4H^*$ takes 25.9 MeV). This consists with one aspect of the experimental fact (the products of positron annihilation, two 0.511 MeV photons, were not observed). Hence, one may expect that electron capture by deuteron in lattice might be a real process instead of a virtual process. Nevertheless, if $d + d + e \rightarrow {}^4H^* + \nu_e + 0.372$ MeV was a real process we were supposed to see the neutrino with single energy, and the neutron as the decay product of the $^4H^*$. These are not confirmed by experiments either. Indeed positron emission was not observed just due to the selectivity of resonant tunneling. Because the 3-body products in the channel of positron emission has a greater phase space available, its probability of transition is usually greater than that of the 2-body product channel (i.e. electron capture channel). As a result, the life-time for positron emission is much shorter than that of electron capture. The selectivity of resonant tunneling just picks the longer life-time for such a thick and high Coulomb barrier at low energy (see calculation in the Proceedings of ICCF-9 [8]). Thus, we assume that electron capture by deuteron in lattice is a virtual process.

(2) Is "excess heat" the recoil energy?
If the electron capture is a virtual process, and the electron just plays the role of a catalyst; then, the energy would be distributed among ^{4}He, neutrino and anti-neutrino with a little energy to lattice. The energy of ^{4}He would be in the range from 75.8 keV to 23.8 MeV. Then we are supposed to see much more ^{4}He than those observed in the "excess heat" experiments. A possible explanation is that most of the ^{4}He were trapped by lattice. ^{4}He would move out from lattice only if the temperature of palladium was higher than 1000^{o}C which is much higher than that in any electrolysis experiment or most of the gas-loading experiment.

(3) Analogy to inner conversion
When excited nucleus de-excites, the released energy may became the energy of photon, or the energy of orbital electron. At the first glance,it was easy to think of that the nuclear energy was transfer first to a real photon first; then the photo-electric effect kicked out the orbital electron. Later it was found that the nuclear energy might be transferred to orbital electron through a virtual photon without any photo-electric effect in between. Now we may imagine that the nuclear energy was transferred to neutrino and anti-neutrino through a virtue electron capture process in those weak interactions in a lattice.

6. Proposal of Experiment

All the three above-mentioned reactions emit neutrino with energy higher than 5 MeV. Hence, we may propose that putting the metal hydride in the control room of KamLAND neutrino detector near the big liquid sphere of scintillator to run the first step of experiment in order to confirm the emission of the neutrino, and measure the energy of those neutrinos.

After the confirmation of the neutrino emission, we may reconstruct the set-up of the metal hydride in order to put this metal hydride into the center of the spherical liquid scintillator, and determine the spectrum of this neutrino emission.

Early in 1989, the first generation of neutrino detector at Kamiokande was used to detect the neutron emission from the Pd–D_2O electrolytic cell. Its result of no neutron emission is still valid today, and becomes the foundation of the theory of the selective resonant tunneling in condensed matter nuclear science. We may expect that the third generation of the neutrino detector (KamLAND) might contribute to this greatest scientific exploration as well.

As long as the neutrino emission is confirmed, we may solve a long-lasting controversial puzzle in the scientific world, and a nuclear energy without strong nuclear contamination is thus feasible.

Acknowledgements

This work is supported by the Natural Science Foundation of China (No. 10475045), Ministry of Science and Technology (Division of Fundamental Research), and Tsinghua University (985-II, Basic Research Funds).

References

[1] Xing Z. Li, Jian Tian, Ming Y. Mei, Chong X. Li, Sub-barrier fusion and selective resonant tunneling, *Phys. Rev*. **C 61** (2000) 024610 .

[2] Xing Z. Li, Bin Liu, Si Chen, Qing Ming Wei, and Heinrich Hora, Fusion cross-sections for inertial fusion energy, *Laser Part. Beam* **22** (2004) 469 .

[3] J. Kasagi et al., Energetic protons and alpha particles emitted in 150-keV deuteron bombardment on deuterated Ti, *J. Phys. Soc. Japan* **64**(3) (1995) 778 .

[4] A. Takahashi et al., Anomalous enhancement of three-body deuteron fusion in titanium-deuteride with low-energy D^+ beam implantation,*Fusion Technol*. **34** (1998) 256 .

[5] G. Fralick et al., Results of an attempt to measure increased rates of the reaction $D + D \longrightarrow {}^3He + n$ in a Nonelectrochemical Cold Fusion Experiment, *NASA Tech. Memo.* (1989) 102430.

[6] Xing Z. Li et al., Correlation between abnormal deuterium flux and heat flow in a D/Pd system, *J. Phys. D: Appl. Phys.* **36** (2003) 3095–3097.

[7] Y. Iwamura et al., Elemental Analysis of Pd Complexes: Effects of D_2 gas permeation, *Jpn. J. Appl. Phys.* **41** (2002) 4642.

[8] Si Chen, X.Z. Li, Tritium production and selective resonant tunneling model, in: X.Z. Li (Ed.), *Proceedings of ICCF-9* (Tsinghua University Press, Beijing China, May 19–24, 2003) 2002, 42.

J. Condensed Matter Nucl. Sci. 1 (2007) 16–26

Research Article

Tunneling Effect Enhanced by Lattice Screening as Main Cold Fusion Mechanism: An Brief Theoretical Overview

Fulvio Frisone*

Department of Physics, University of Catania, Via Santa Sofia 64, I-95123 Catania, Italy

Abstract

In this paper are illustrated the main features of tunneling traveling between two deuterons within a lattice. Considering the screening effect due lattice electrons, we compare the d–d fusion rate evaluated from different authors assuming different screening efficiency and different d–d potentials. Then, we propose an effective potential which describe very well the attractive contribute due to plasmon exchange between two deuterons and by means of it we will compute the d–d fusion rates for different energy values. Finally the good agreement between theoretical and experimental results proves the reality of cold fusion phenomena and the reliability of our model.

Keywords: Collective plasmonic excitation, Dislocations, Fusion within a microcrack, Nuclear reaction, Tunneling effect, Vibrational frequency of the lattice

1. Introduction

The first cold fusion phenomenon has been observed in the 1926 by Paneth and Peters that passed H_2 through a high temperature Pd capillary tube and observed He spectral line [1]. Of course this episode does not sign the rise of a new branch of science since they, subsequently, declared that the helium was released from the heated glass container. Then, for about 60 years, nobody spoke about low-energy nuclear reaction, until, on March 23, 1989, Fleischmann and Pons declared the achievement of a deuterons fusion at room temperature in a Pd electrolytic cell using D_2O [2].

Since their discovery, a large amount of efforts have been spent in order to reproduce the fusion but actually the experimental knowledge and the know-how is not so far robust. However, the evidence of anomalous nuclear phenomenon had been built up in these last years [3–6].

In this paper, we want to summarize some theoretical efforts in order to understand the probably mechanism of cold fusion. In particular we focus on tunneling traveling of coulomb barrier existent between two deuterons. More exactly it will be analyzed the possible contributions of lattice in order to enhance of tunneling probability and, in this way,

*E-mail: Frisone@ct.infn.it

we will find that there is a real mechanism by means of which this probability is a lot increased: this mechanism is the screening effect due to d-shell electrons of palladium lattice.
Finally it will demonstrate that the cold fusion can be understood within a special theoretical framework which involves lattice interference on nuclear reactions but does not imply any conceptual revisions of modern physics knowledge.

2. Tunneling in Molecular D_2

After the nuclear disintegration had been discovered, it soon became clear that the laws of classical dynamics were not able to reproduce some experimental regularities as the radioactive decay law. This law involves that the time of disintegration of an atom is as independent of the previous history and of its physical condition, in other words the behavior of particles is governed by probability. Gamow [7] demonstrated that using the Copenhagen interpretation of Scrödinger equation it was possible to obtain the correct decay law expression. In this way the tunnel effect was universally accepted. Actually we are not able to understand transmutation and disintegration phenomena without the no-classical traveling of potential barrier.

In this time, the tunneling effect is a very important statement of physics 'behavior' of microscopic particles; for example a very lot of the microelectronic devices as flash memories [8] base oneself on Fowler–Nordheim tunneling.

Now, established the fusion process in terms of penetration of a particle of energy E in a region classically forbidden whose potential is V, the fusion reaction rate Λ (s^{-1}) will be determined, according to quantum mechanics, from the following expression:

$$\Lambda = A\,|\psi(r_0)|^2\,. \tag{1}$$

Here A is the nuclear reaction constant obtained from measured cross sections, the probability $|\psi(r_0)|^2$ is the square modulus of the inter-particles wave-function, and r_0 is the point of forbidden zone. Finally, it is demonstrated that for a Coulomb potential:

$$|\psi(r_0)|^2 = \left|\frac{k(r_e)}{k(r_0)}\right| \exp\left\{-\frac{2}{\hbar}\int_{r_0}^{r'} \sqrt{2\mu\,(V-E)}\;\mathrm{d}r\right\}, \tag{2}$$

where

$$k(r) = \frac{\sqrt{2\mu(V(r)-E)}}{\hbar} \tag{3}$$

and r' is the classical turning point.

Here μ is the mass of particle incoming, r_0 is a point within forbidden region, E is the energy of particle, and $k(r_e)$ is the wave number of the zero-point oscillation:

$$\frac{\hbar^2 k^2(r_e)}{2\mu} = E. \tag{4}$$

Of course the pre-factor of exponential is about 1 and the exponential term is know as Gamow-amplitude. More exactly, we define the Gamow-factor as:

$$\eta_G(r_0) = \exp\left\{-\frac{1}{\hbar}\int_{r}^{r_0} \sqrt{2\mu(V-E)}\;\mathrm{d}r\right\}. \tag{5}$$

Now compute the fusion probability between two nuclei of D_2 molecular. In this case we must consider that the average distance between two deuterons, within the D_2-molecule, is $r_0 \approx 0.74$ Å while the distance at which the nuclear force

takes place is $r \approx 20$ F. Then if we put $V = \alpha/r$, i.e. the Coulomb potential, and with μ label the reduced mass, we will compute $k \approx 1$. Finally for $E \approx 0$ we can evaluate:

$$\eta_{\mathrm{G}}(r) = \exp - \left\{ \sqrt{8\alpha\mu}(r_0^{1/2} - r^{1/2}) \right\} \approx 10^{-60}. \tag{6}$$

Using $A = 10^{22}\,\mathrm{s}^{-1}$, we obtain $\Lambda = 10^{-98}\,\mathrm{s}^{-1}$. It means that no detectable process can take place!

3. Deuterons Tunneling as Probably Cold Fusion Mechanism

The cold fusion idea came independently to Fleischmann and Pons and to Jones that if deuterium could be forced into palladium, two deuterium nuclei would come so close together as to fuse giving out more power than was being put in. On this case the d–d fusion processes involved are:

$$\begin{array}{ll} \text{(a)} & \mathrm{d} + \mathrm{d} \rightarrow {}^3\mathrm{He} + \mathrm{n}, \\ \text{(b)} & \mathrm{d} + \mathrm{d} \rightarrow \mathrm{t} + \mathrm{p}, \\ \text{(c)} & \mathrm{d} + \mathrm{d} \rightarrow {}^4\mathrm{He} + \gamma. \end{array}$$

In the previous section, we have computed that the fusion probability between two deuterons within D_2-molecular is very low. But at one time was evaluated in the 1986 that this fusion rate can be reduced [9]. In fact some mechanisms, as the replacing of the electron in a hydrogen molecular ion with a negatively charged muon, are able to increase the reduced mass and then to decrease the Gamow-factor [10]. More exactly, Siclen and Jones, starting from the possibility of creating pressures of several million atmospheres presented by diamond-anvil cell, have considered deuterons fusion rates as function of pressure and, then, of the inter-nuclear distance obtaining an theoretical average fusion rate of $10^{-74}\,\mathrm{s}^{-1}$.

They discussed in the following way. In hydrogen molecular the potential has the trend shown in Fig. 1. In this case, a Morse potential is used in the interval that included the inner turning point r_{a} and continues on toward $r = 0$, near which it is connected with the repulsive Coulomb potential $1/r$. The expression is

$$V(r) = D[\mathrm{e}^{-2\gamma(r-r_0)} - 2\mathrm{e}^{-\gamma(r-r_0)}], \tag{7}$$

here D is the depth of the potential well that is roughly equal to the dissociation energy and γ is related to the anharmonicity constant which is a measure of the curvature of the Morse potential well.

Since the vibrational levels of Morse potential can be written in this way [11]:

$$E_{\mathrm{v}} = -D\left[1 - \frac{\gamma\hbar}{\sqrt{2\mu D}}\left(v + \frac{1}{2}\right)\right]^2, \tag{8}$$

it is possible to evaluate by fitting the constant γ and D and r_0. The authors of Ref. [9] computed (in units e^2/a_0 and a_0 = Bohr radius):

$$D = 0.1743, \tag{9}$$

$$\gamma = 1.04, \tag{10}$$

$$r_0 = 1.4. \tag{11}$$

The molecular wave function has been evaluated following the method proposed by Langer [12] which now we will briefly illustrate.

The radial part of Scrödinger equation is

$$\left[\frac{\mathrm{d}^2}{\mathrm{d}r^2} + Q_0^2(r)\right]\chi(r) = 0, \tag{12}$$

where

$$Q_0^2(r) = \frac{2\mu}{\hbar^2}[E - V(r)] - \frac{J(J+1)}{r^2} \tag{13}$$

and

$$\chi(r) = r\psi(r). \tag{14}$$

The ground $v = J = 0$ molecular wave function in the interaction region is thus found to be:

$$\psi(r) = \frac{1}{4}\left(\frac{\alpha^2}{\pi^3}\right)^{1/4}\eta \tag{15}$$

with

$$\alpha = \frac{\mu\omega}{\hbar} \tag{16}$$

$$\eta = \exp\left\{-\frac{1}{2}\left[\int_r^{r_0}\left(2\,|Q(r)| - \frac{1}{r}\right)\mathrm{d}r + \ln\frac{r_\mathrm{a}}{2}\right]\right\}, \tag{17}$$

and

$$Q^2(r) = \frac{2\mu}{\hbar^2}[E - V(r)] - \frac{(J+1/2)^2}{r^2}, \tag{18}$$

where $V(r)$ is the Coulomb potential for $r < \rho$ and the Morse potential for $r > \rho$ being ρ the point at which the Morse potential is connected to the purely Coulomb potential.

Using these results Van Siclen ad Jones demonstrated the possibility of scaling down of repulsive effect between two deuterons. Moreover, they showed that the average fusion rate was much more sensitive to the choice of ρ than r (see Table 1).

4. The Screening Effect

As showed in Section 3, the increasing of deuteron fusion rate is linked to the possibility that the inter-nuclear distance between two deuterons can be minimized. In 1989 Fleischmann and Pons observed that the establishment of negative over-potential on the outgoing palladium interface shows that the chemical potential can be raised to high values and it means that within palladium it is possible to have astronomical pressure of about 10^{26} atm [13]. After the Fleischmann and Pons experiments had been published, it soon became clear the main role of palladium lattice as catalyzing.

To explain this over-potential and, consequently, the cold fusion phenomenon, many people supposed that in the lattice the coulomb potential between two deuterons is screened. To illustrate this topic we report the argument of Horowitz [14].

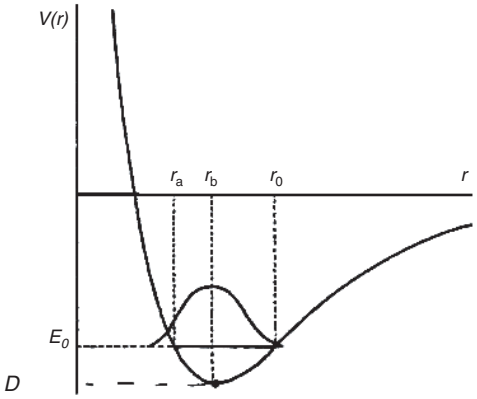

Figure 1. Molecular potential energy curve and ground-state vibrational wave function for the relative motion of two nuclei. The points r_a, r_b and r_0 are the classical turning points and the equilibrium inter-nuclear separation, respectively (from Ref. [9]).

The electrons in a metal should become a Fermi gas and the hydrogen nuclei interacting via screened coulomb potential. The effective potential between two nuclei $V(r)$ which includes the effects of electron screening is given, in a simple Thomas–Fermi model, by:

$$V(r) = \frac{e^2}{r}\exp\left[-\frac{r}{\lambda}\right] \tag{19}$$

of course λ is the screening length and depends on density. But for $r \ll \lambda$ we can write at first order:

$$V(r) = \frac{e^2}{r} - V_0. \tag{20}$$

This constant V_0 would be just the difference between electronic energy of a He isolated atom (-9.0 eV) and the binding energy of two H atoms (-51.8 eV). The fusion rate has been evaluated using:

$$A = \nu P_n, \tag{21}$$

where υ is the vibrational frequency of the crystal's zero point motion ($h\nu$ is about 1 eV) and P_n is the probability of a d–d nuclear reaction once the nuclei have made it to r_n. In other words, the fusion rate is calculated by multiplying P by the frequency of attacks on the Coulomb barrier and the probability of a nuclear reaction.

Table 1. Fusion rate evaluated in [9] as function of ρ (point where the Morse potential is linked by Coulomb, and r (force nuclear radius). The distance is reported in units of the Bohr radius

r	ρ	Λ (s^{-1})
0	0.4	3.8×10^{-70}
0	0.5	1.3×10^{-74}
10^{-3}	0.5	1.3×10^{-74}
10^{-3}	0.5	2.3×10^{-74}
10^{-3}	0.5	6.8×10^{-73}
0	0.5	5.8×10^{-79}

Put $hv = 1$ eV and $P_n = 1$ (for d–d reaction), Horowitz computes $\Lambda = 10^{-70}\,\mathrm{s}^{-1}$, for $r_0 = 0.5$ Å, but $\Lambda = 10^{-25}\,\mathrm{s}^{-1}$ for $r_0 = 0.1$ Å.

Similar argumentations were proposed by Giuliano Preparata but starting from a new formulation of condense matter theory known as Coherence Theory. In fact according to the Coherence Theory of Condensed Matter we can visualize the plasma formed by d-shell electrons as consisting of charged shells of charge $n_\mathrm{d}e$ (for palladium $n_\mathrm{d} = 10$) radius $r_\mathrm{d} = 1$ Å and thickness a fraction of 1 Å. The classical plasma frequency will be

$$\omega_\mathrm{d} = \frac{e}{\sqrt{m}}\sqrt{\frac{n_\mathrm{d}N}{V}}. \tag{22}$$

According to the coherence theory of matter we must adjust this plasma frequency of a factor 1.38. We can understand this correction observing that the formula (22) is obtained assuming a uniform d-electron charge distribution. But of course the d-electron plasma is localized in a shell of radius R (that is about 1 Å), so the geometrical contribution is

$$\sqrt{\frac{6}{\pi}} = 1.38 \tag{23}$$

and finally we can compute

$$\omega_\mathrm{d} = 41.5\,\mathrm{eV}/\hbar. \tag{24}$$

These charge oscillations produce a screening potential having an harmonic features:

$$eV(r) = -Z_\mathrm{d}\frac{ke^2}{2a_0}r^2. \tag{25}$$

In Ref. [17] putting $Z_\mathrm{d} = 10/3$ and $a_0 = 0.7$ Å, it is evaluated a screening potential of about 85 eV. It means that within a palladium lattice the Coulomb potential between two deuterons has the following expression:

$$V(r) = \frac{e^2}{r} - 85\ \mathrm{eV}. \tag{26}$$

In this case it is very easy to evaluate that the intermolecular distance between two deuterons can reach the value of 0.165 Å. Finally, by means of Eq. (1) and using $A = 10^{22}\,\mathrm{s}^{-1}$, it is computed $\Lambda = 10^{-22}\,\mathrm{s}^{-1}$.

This last value of fusion rate has been experimentally checked [15,16], and for this reason we believe that it is correct. We conclude this section affirming that within a lattice, in according to the quantum mechanics principles, the fusion probability becomes theoretically possible and experimentally observable.

5. An Effective Potential Proposed

From the results reported in previous sections, appears clear that within lattice the d–d reactions take place in a D_2-molecule whose inter-nuclear distance is reduced by screening effects. More exactly by means of works reported in references [9,14,17], we can say that within a lattice:

(1) A *compound* potential as which used by Siclen and Jones is a likely molecular potential.
(2) A screening effect that is able to reduce the inter-nuclear distance takes place

For this reason, starting to idea of Jones and Siclen, we tried to find a d–d effective potential that for distance smaller than ρ (i.e. the point where the attractive molecular potential is linked with the repulsive core) gives about the Coulomb

feature while, for the distance bigger than ρ, the Morse potential. In Ref. [18] to fit a such 'Coulomb–Morse linked' potential we have proposed the following effective potential:

$$V(r) = k\frac{e^2}{r}\left(V_{\mathrm{M}}(r) - \frac{A}{r}\right), \tag{27}$$

where

$$V_{\mathrm{M}}(r) = D'[\mathrm{e}^{-2\gamma(r-r_0')} - 2\mathrm{e}^{-\gamma(r-r_0')}]. \tag{28}$$

Here A, D', γ and r_0' are parameters to determinate by means of fitting.

Of course the problem is to know the physical values that characterize, from a point of numerical view, a potential like that used by Siclen and Jones. More exactly the principal issue, that we must solve, is to estimate:

(1) the point where the Morse potential is linked by Coulomb curve (i.e. ρ),
(2) the equilibrium distance,
(3) the well depth.

In order to evaluate the parameter relative to first bullet, we used the screening value proposed by Preparata (average: 85 eV) as starting point. In this way remembering Eq. (26), we compute $\rho = V_0/26.9$ and at last $\rho = 0.165$ Å.

Regarding the other topics (i.e. equilibrium distance r_0 and disassociation energy D) we have discussed in the following way.

In the ionized hydrogen molecular the equilibrium distance is about 1.06 Å, but in the neutral hydrogen molecular it is about 0.7 Å. We can interpret this results saying that the screening potential due to second electron whose magnitude is

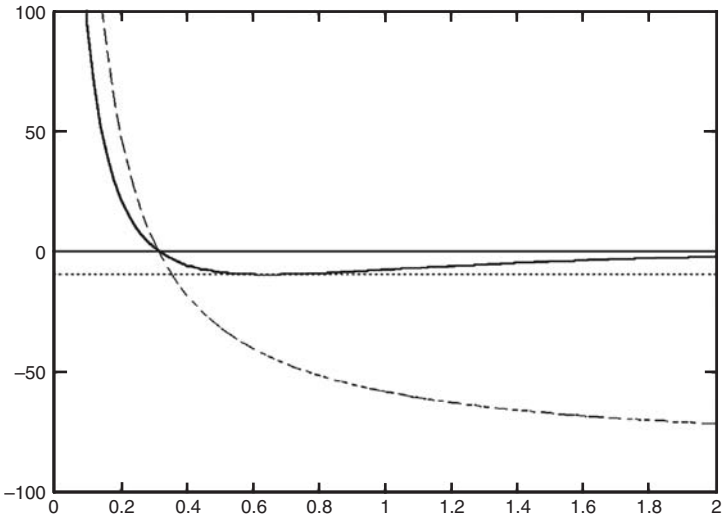

Figure 2. The solid line shows the features of potential (27) computed using the values reported in Table 2. The dashed line shows the Coulomb potential (26). Note they cross the x-axis in the same point. In the x-axis is reported the distance in Bohr radius unit and on the y-axis the energy in eV.

Table 2. In the left column are shown the physical quantities that must characterize the potential (27); in the right the model parameter values that need used in the expression (27) in order to obtain the physical values reported in the left column

$\rho = 0.165$ Å	$A = 0.0001$
$r_0 = 0.35$ Å	$r_0' = 0.99$
$D = 9.34$ eV	$D' = 0.28$
	$\gamma = 1.04$

$$2 \times \frac{26.9}{a_0} = 53.8 \text{ eV} \tag{29}$$

(here a_0 is the Bohr radius), reduces of about 34% the equilibrium distance.

Therefore, a screening magnitude of 85 eV will be able to reduce this distance of about 50%. Appling this argumentation to the neutral hydrogen molecular (and/or also to D_2-molecular, see Ref. [19]), we can suppose that inside the lattice the equilibrium distance between two nuclei of a D_2-molecular is about 0.35 Å.

A similar argumentation has been reported in order to evaluate the dissociation energy. In fact, we know that the H_2^+ dissociation energy is about 2.7 eV, whereas the H_2 dissociation energy is about 4.6 eV, i.e. a scaling of equilibrium distance of 34% is able to produce a energy growth of 70%. Then, we suppose that the scaling of 50%, in the H_2 molecular equilibrium distance, is able to increase the disassociation energy of about 103%. In this way we compute the dissociation energy of 9.34 eV.

In Table 2 are reported the ρ, r_0 and D evaluations supposed and the parameters values of potential (27) able to reproduce these quantities, while in Fig. 2 is shown the feature of potential (27) obtained using the values of Table 2. Note the good agreement with the coulomb potential for $r < \rho$.

Of course these argumentations are rough, but we believe that they are able to give a reasonable start point.

A better evaluation of point ρ, equilibrium distance and energy disassociation can be obtained from many-body theory. In fact as pointed out in Ref. [20], the deuteron interaction with the collective plasmon excitations of the palladium produces a strong attractive potential. This attractive force is due to exchange of plasmons (in Ref. [20] the authors consider only two plasmon excitations at 7.5 and 26.5 eV) between two deuteron-lines as reported in Fig. 3:

Taking into account the role of coupling between deuteron and plasmons, in Ref. [20] the authors have numerically evaluated a d–d potential having the features of potential (26). More exactly in their case ρ is about 0.2 Å, D about 50 eV and r_0 about 1 Å.

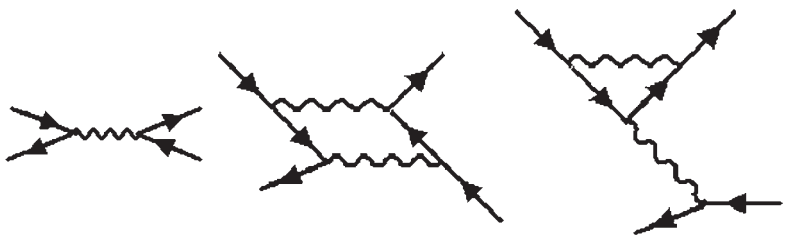

Figure 3. Plasmon exchanges. Solid lines indicate deuterons and wiggly lines plasmons.

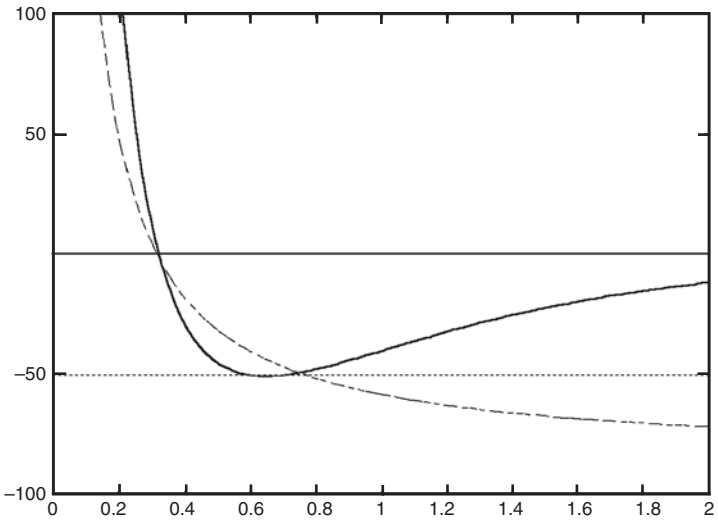

Figure 4. The solid line shows the features of potential (27) computed using the values reported in Table 3. The dashed line is the Coulomb potential (26). In the x-axes is reported the distance in Bohr radius unit and on the y-axes the energy in eV.

Of course the value of equilibrium distance very strange if compared with the energy dissociation. But as reported in Ref. [20] this result is due to assumption of un-damped plasmon and the authors declare that 'in a more realistic treatment the potential would tend more rapidly to zero'. For this reason we believe that only the D value is reasonable.

Table 3 shows the new set of parameterization values correspondently to the alternative D evaluation.

In Fig. 3 is shown the potential (27) evaluated assuming $D = 50$ eV.

We think that using this effective analytical potential, we are able to explore a very large amount of situations that can occur within lattice simply varying the parameterization constant.

Now let us discuss briefly about the role of parameters D', r'_0 and A.

Of course D' is the parameter that control the potential well, in fact for $D = 9.34$ eV we put $D' = 0.28$, for $D = 50$ eV we have $D' = 1.49$. It means that this parameter depends mainly on screening efficiency.

Regarding r'_0 it is clear that it controls the zero crossing point of potential. In fact varying only this parameter the zero crossing point moves according to the increasing or decreasing of r'_0.

It is important to observe that D' and r'_0 are correlated. In fact, it is reasonable suppose that to a bigger potential well correspond a smaller zero crossing point. Taking into account the value reported in Fig. 3 we can estimate this rough dependence:

$$r'_0 = 0.35 \times \ (50/D'). \tag{30}$$

Finally, regarding the parameters A, in the pictures shown previously it was put at 0.0001. Moreover, we can numerically prove that for small variation (of a factor less than 10) of this value, the potential does not change and its contribute appears relevant only at nuclear distance. Taking into account this observation, we can rewritte this parameter as

$$A = HR, \tag{31}$$

where R is about nuclear radius (20 F $= 3.76 \times 10^{-4}\ a_0$). It means that $H = 0.265$ eV.

This last value is about equal to the thermal energy of ions palladium that form the lattice [17]. For this reason we are conducted to put $H = KT$, where K is the Boltzmann constant and T is the lattice temperature.

Table 3. In the left column are shown the physical quantities that must characterize the potential (27) where D has been evaluated in [20]; in the right the model parameter values that need used in the expression (27) in order to obtain the physical values reported in the left column

$\rho = 0.165$ Å	$A = 0.0001$
$r_0 = 0.35$ Å	$r'_0 = 0.99$
$D = 50$ eV	$D' = 1.49$
	$\gamma = 1.04$

6. Results and Discussion

A function having a like-Morse trend seems to be the correct potential that is established between two deuterons within a lattice [9,10,20]. The expression (27) proposed in the Section 5 is an analytical function that have the proper features of a like-Morse potential linked with a Coulomb curve when the inter-nuclear distance approaches to zero.

Using the potential (27) for the two different values of model parameters reported respectively in Tables 2 and 3, we have computed the d–d fusion rate (the nuclear reaction constant was $10^{22}\,\mathrm{s}^{-1}$). From data shown in Table 4, we can see that the fusion rate appears in any case enough 'great' or, in other words, 'measurable'. Moreover, these values are in agreement with experimental data reported in [15,16,21]. More exactly in [15,16] has been reported a fusion rate of $10^{-23}\,\mathrm{s}^{-1}$ for the reaction D(d,p)T, but no significant effect were observed in the neutron and gamma-ray measurements. While in [21] has been reported a fusion rate of about $10^{-22}\,\mathrm{s}^{-1}$ regarding the reaction D(d,n)T.

Of course in order to better understand this phenomenon, it is necessary to distinguish the fusion rate expected by the theory according to the chain reaction, i.e. according to the reaction products expected. This issue has been (partially) clarified by Preparata [17].

Another main question is the following. If the occurrence of cold fusion mechanism is probably due to screening of *d-shell electron*, is it to possible enhance this effect introducing donor species? These questions will be considered in a next work.

Now let us briefly illustrate as the analytical expression of potential (27) can be extended to better handle the probably role of donor impurities on efficiency of screening.

Since the tunneling is enhanced by screening effect due to d-electron, it is clear that if we dope the lattice by means of donors atoms, the effect of electronic screening is increased. Labeled by J the impurities concentration, we have:

$$D' \to D' + GJ, \tag{32}$$

where G is a constant that depends on dopant–metal system. The other parameter r'_0 will change according to Eq. (31),

Table 4. Fusion rate evaluated using the effective potential for different values of energy and for two different sets of model parameters

$A = 0.0001$, $r'_0 = 0.99$, $D' = 0.28$, $\gamma = 1.04$, T(K) = Const., E(eV)		$A = 0.0001$, $r'_0 = 0.99$, $D' = 1.49$, $\gamma = 1.04$, T(K) = Const., E(eV)	
$E \approx 50$	$R \approx 6.32 \times 10^{-18}$	$E \approx 50$	$R \approx 3.02 \times 10^{-16}$
$E \approx 75$	$R \approx 9.71 \times 10^{-18}$	$E \approx 75$	$R \approx 9.12 \times 10^{-17}$
$E \approx 100$	$R \approx 9.95 \times 10^{-19}$	$E \approx 100$	$R \approx 8.2 \times 10^{-17}$
$E \approx 125$	$R \approx 1.05 \times 10^{-20}$	$E \approx 125$	$R \approx 1.1 \times 10^{-18}$
$E \approx 150$	$R \approx 5.6 \times 10^{-21}$	$E \approx 150$	$R \approx 9.15 \times 10^{-19}$

while regarding A we suppose that in the presence of impurities we can write:

$$A = J\xi KT, \tag{33}$$

where ξ is a constant that depends on dopant–metal system.

From a point of engineering view we can compute the new values of formulas (32) and (33) measuring the bulk plasmon excitations in function of impurities density, and then following a set of theoretical calculations as which reported in [20]. Finally, using the potential (27), we will able to evaluate the new fusion rate.
The last point that will be evaluated in another work is the role of microcrack. In fact, if within a lattice a microcrack happens a local electrical field takes place that is able to increase the deuteron energy and then according to the values of Table 4 is able to enhance the fusion probability.

To conclude, we can say that a cold fusion phenomenon is real. By means of standard theory of many body (see Ref. [20]) is theoretically possible aspect fusion rate of about $10^{-22}\,\mathrm{s}^{-1}$, i.e. measurable values. The very strange values of fusion rate as those reported in [2,22] can be considered as errors, but if we take into account other mechanisms as microcrack formation and/or the role of impurities, may be we will able to understand these spikes and, may be, reproduce them.

References

[1] F. Paneth, K. Peters, *Die Naturwissenschaften* **43** (1926) 956. English summary in *Nature* **118** (1926) 526.
[2] M. Fleischmann, S. Pons, *J. Electroanal. Chem*. **261** (1989) 301.
[3] Iwamura et al., *Japanese J. Appl. Phys. A* **41**, 4642.
[4] O. Reifenschweiler, *Phys. Lett. A* **184** (1994) 149.
[5] O. Reifenschweiler, *Fusion Technol.* **30** (1996) 261.
[6] M. H. Miles et al., *Fusion Technol.* **25** (1994) 478.
[7] Gamow, *Zeitschrift für Physik* **51** (1928) 204.
[8] S.M. Sze, C.Y. Chang, *ULSI Technology* (McGraw-Hill, New York, 1996).
[9] C. DeW Van Siclen, S.E. Jones, *J. Phys. G. Nucl. Phys*. **12** (1986) 213.
[10] J.D. Jackson, *Phys. Rev.* **106** (1957) 330.
[11] Landau, Lifshitz, *Quantum Mechanics* (Pergamon, Oxford, 1965).
[12] R.E. Langer, *Phys. Rev*. **51** (1937) 669.
[13] M. Fleischmann, S. Pons, *J. Electroanal. Chem*. **261** (1989) 301.
[14] C.J. Horowitz, *Phys. Rev. C* **40** (1989)1555.
[15] S. Aiello et al., *Fusion Technol.* **18** (1990) 115.
[16] K.E. Rehm et al., *Phys. Rev. C* **41** (1989) 45.
[17] G. Preparata, *QED Coherence in Matter* (World Scientific, Singapore, 1995).
[18] F. Frisone, *Fusion Technol.* **39** (2001)260.
[19] O.B. Christensen, *Phys. Rev. B* **40** (1989) 1993.
[20] M.Baldo, R. Pucci, *Fusion Technol.* **18** (1990) 47.
[21] Š. Miljianiè et al., *Fusion Technol.* **18** (1990) 340.
[22] S.E. Jones et al., *Nature* **338** (1989)737.

J. Condensed Matter Nucl. Sci. 1 (2007) 27–40

Research Article

Nuclear Reactions in Condensed Matter: A Theoretical Study of D–D Reaction within Palladium Lattice by Means of the Coherence Theory of Matter

Fulvio Frisone*

Department of Physics, University of Catania, Via Santa Sofia 64, I-95025 Catania, Italy

Abstract

In the last decades, an indisputable experimental evidence was built up for Low-Energy Nuclear Reaction (LERN) phenomena in specialized heavy hydrogen systems. Actually, the real problem is that, the theoretical statements of LERN are not known; in fact, no new branch of science has begun, yet. In this work, we seek to analyse the deuteron–deuteron reactions within palladium lattice by means of Preparata model of palladium lattice and we will show the occurrence probability of fusion phenomena according to more accurate, but not claimed, experiments, in order to demonstrate theoretically the possibility of cold fusion. Further, we focus on tunnelling the Coulomb barrier existent between two deuterons. Analysing the possible contributions of lattice on improving the tunnelling probability, we will find that there is a real mechanism through which this probability could be increased: this mechanism is the screening effect due to d-shell electrons of palladium lattice. Finally the good agreement between theoretical and experimental results proves the reality of cold fusion phenomena and the reliability of our model.

Keywords: Collective plasmonic excitation, Dislocations, Fusion within a microcrack, Nuclear reaction, Tunneling effect, Vibrational frequency of the lattice

1. Introduction

We have studied that within the Coherence Theory of Condensed Matter it was verified the cold fusion [1–4] phenomena. In this theory [5] it is assumed that the electromagnetic (e.m.) field, due to elementary constituents of matter (i.e. ions and electrons), plays a very important role on dynamic system. In fact considering the coupling between e.m. equations, because of charged matter, and the Schrödinger equation of field matter operator, it is possible to demonstrate that in proximity of e.m. frequency ω_0, the matter system shows a dynamic coherence. That is why it is possible to speak about the coherence domains whose length is about $\lambda_{CD} = 2\pi/\omega_0$.

Obviously, the simplest model of matter with coherence domain is the plasma system. In the usual plasma theory, we have to consider the plasma frequency ω_p and the Debey length that measures the Coulomb force extension, i.e. the

*E-mail: Frisone@ct.infn.it

coherence domain length. In order to address the crucial issue of the nuclear fusion reaction involving the deuterons that pack the Pd-lattice we must have a rather detailed understanding of the environment in which such nuclear process will eventually take place.

For a system with N, charge Q and mass m within a volume (V) the plasma frequency can be written as

$$\omega_{\vec{k}} = \omega_{\mathrm{p}} = \frac{Qe}{\sqrt{m}}\sqrt{\frac{N}{V}}. \tag{1}$$

Introducing the dimensional variable $\tau = \omega_{\mathrm{p}} t$ we can rewrite the above equations

$$\dot{\phi}_{\vec{n}}(\tau) = \frac{1}{2}\sum_{|\vec{k}|=\omega_{\mathrm{p}}}\sum_{\vec{n}'r}\langle\vec{n}|\alpha_{kr}\vec{\varepsilon}_{kr}\vec{a}^{+} - \alpha^{*}_{kr}\vec{\varepsilon}_{kr}\vec{a}|\vec{n'}\rangle\phi_{\vec{n}'}(\tau), \tag{2}$$

$$\frac{1}{2}\ddot{\alpha}_{kr} - i\dot{\alpha}_{kr} + m\lambda\alpha_{kr} = \frac{i}{2}\vec{\varepsilon}^{*}_{kr}\sum_{\vec{n}\vec{n'}}\langle\vec{n}|\vec{a}|\vec{n'}\rangle\phi^{*}_{\vec{n}}(t)\phi_{\vec{n}'}(\tau), \tag{3}$$

which, defining the state:

$$|\phi\rangle = \sum_{\vec{n}'}\phi_{\vec{n}}(\tau)\,|\vec{n}\rangle \tag{4}$$

and the e.m. field amplitude:

$$\vec{A} = \sqrt{\frac{3}{8\pi}}\sum_{r}\int \mathrm{d}\Omega_k\,\alpha_{kr}\vec{\varepsilon}_{kr}, \tag{5}$$

we can rewrite

$$\frac{\partial}{\partial t}|\phi\rangle = \sqrt{\frac{2\pi}{3}}\left(\vec{A}\vec{a}^{+} - \vec{A}^{+}\vec{a}\right)|\phi\rangle\,, \tag{6}$$

$$\dot{\vec{A}} + \frac{i}{2}\ddot{\vec{A}} + im\lambda\vec{A} = -\sqrt{\frac{2\pi}{3}}\,\langle\phi|\,\vec{a}\,|\phi\rangle\,. \tag{7}$$

If we only concentrate on one short time dynamics we can write:

$$|\phi(0)\rangle = |0\rangle\,, \tag{8}$$

then, creating a difference in Eq. (6) and using Eq. (7) with $|\phi\rangle = |0\rangle$, we can easily obtain:

$$\ddot{A}_j + \frac{i}{2}\dddot{A}_j = -\left(\frac{2\pi}{3}\right)\langle 0|\left[a_j, a_l^{+}\right]|0\rangle\,, \tag{9}$$

$$A_l = -\left(\frac{2\pi}{3}\right)A_j. \tag{10}$$

They have the same form of the equations of the coherence domains in the case in which:

$$\mu = 0,$$

$$\lambda = 0,$$

$$g^2 = \left(\frac{2\pi}{3}\right),$$

$$g_c{}^2 = \frac{16}{27} < \frac{2\pi}{3}.$$

Then, a solution for the ideal plasma exists. At any rate defining:

$$\alpha_k = \langle\phi|\, a_k \,|\phi\rangle\,, \tag{11}$$

$$g_0 = \left(\frac{2\pi}{3}\right)^{1/2}.$$

In this case the coupling critical constant of the system is

$$\dot{\alpha}_k = g_0 A_k, \tag{12}$$

$$\dot{A}_k + \frac{i}{2}\ddot{A}_k = -g_0\alpha_k, \tag{13}$$

so to admit the following holding quantity:

$$Q = \sum\left\{A_k^* A_k + \frac{i}{2}\left(A_k^*\dot{A}_k - \dot{A}_k^* A_k\right) + \alpha_k^*\alpha_k\right\}, \tag{14}$$

while for the Hamiltonian's it is easy to compute:

$$\frac{E}{N\omega_p} = H = Q + \sum\left[\frac{1}{2}\dot{A}_k^*\dot{A}_k - ig\left(A_k^*\alpha_k - A_k\alpha_k^*\right)\right]. \tag{15}$$

With the objective of seeing if there are any externals solutions, we write

$$\alpha_k = \alpha u_k e^{i\psi}, \tag{16}$$

$$A_k = A u_k e^{i\phi}, \tag{17}$$

where α and A are positive constants and u_k is a complex vector.

Changing these ones in Eqs. (12) and (13) we have:

$$\phi - \psi = \frac{\pi}{2}, \tag{18}$$

$$\alpha = g_0\frac{A}{\dot{\phi}}, \tag{19}$$

$$\frac{1}{2}\dot{\phi}^3 - \dot{\phi}^2 + g_0^2 = 0, \tag{20}$$

and by the condition $Q = 0$ (we cannot have a net charge flow in a plasma), we have:

$$1 - \dot{\phi} + \frac{g_0^2}{\dot{\phi}^2} = 0. \tag{21}$$

In this case it is easy to observe that for $g_0 = (2\pi/3)^{1/2}$ is unlikely to satisfy both Eqs. (18) and (19).

This result means that the energy of an ideal quantum plasma does not have a minimum; in other words the ideal quantum plasma does not exist.

That is not surprising because the Hamiltonian's describes, of this plasma, a system whose amplitude oscillations are arbitrary, while the limit over a certain amplitude does not exist in a real plasma.

But by:

$$\vec{\xi} = \frac{1}{\sqrt{2m\omega_{\mathrm{p}}}}(\vec{a} + \vec{a}^{+}),$$

it is easy to obtain:

$$\left\langle \vec{\xi}^{2} \right\rangle = \frac{1}{m\omega_{\mathrm{p}}}\alpha^{2}. \tag{22}$$

But in the plasma approximation as an homogeneous fluid, we suppose that our Hamiltonian's stops have to be valid for the oscillations bigger than the following:

$$\left\langle \vec{\xi}^{2} \right\rangle_{\max}^{1/2} \approx a = \left(\frac{V}{N}\right)^{1/2} \tag{23}$$

that is when the plasma's oscillations are of the same order of the inter-particle distance a. In order to create some more realistic models of plasma, we want to compute the breaking amplitude $\alpha_{\max}$ obtained by the combination of Eqs. (22) and (23) for a gas of electrons.

Using the definition of ω_{p}, we have:

$$\alpha_{\max} = \sqrt{m\omega_{\mathrm{p}}}\left(\frac{1}{3}\right)^{1/3} = (ma)^{1/4}\, e^{1/2} \tag{24}$$

taking

$$a \approx 2.5\ \text{Å}$$

it is calculated

$$\alpha_{\max} \cong 2.7\ \text{Å}.$$

This simple calculation shows how it is possible to change our quantum ideal plasma in a real plasma. For a plasma of electrons the oscillations remain very little and so a two levels model can be a good approximation (the dynamics only includes the first excited state). A consequence of this approximation, consisting in the reduction of the plasma in a homogeneous fluid, is the changing of the plasma frequency ω_{rmp}

$$\omega_{\mathrm{p}} = \frac{Q}{\sqrt{m}}\sqrt{\frac{N}{V}}. \tag{25}$$

Moreover, we study the "nuclear environment", that it is supposed existent within the palladium lattice D_2-loaded and at room temperature as predicted by Coherence Theory. In fact when the palladium lattice is loaded with deuterium gas, some physicists declared that it is possible to observe traces of nuclear reactions [1–3]. For this reason many of these physicists speak about Low- Energy Nuclear Reaction (LERN).

One of the biggest experiments tell us that in the D_2-loaded palladium case the most frequent nuclear reactions are [3,4]:

$$\text{(a)} \qquad \mathrm{D} + \mathrm{D} \rightarrow {}^{3}\mathrm{H} + \mathrm{p} + 4.03\,\mathrm{MeV},$$

$$\text{(b)} \qquad \mathrm{D} + \mathrm{D} \rightarrow {}^4\mathrm{He} + \gamma \ (23.85 \text{ MeV}).$$

In our work, we aim to propose a "coherence" model by means of which we can explain the occurrence of reactions (a) and (b) and their probability according to the most reliable experiments [6]. First of all, we will start by analysing the environment, i.e. of plasmas present within palladium (d-electron, s-electron, Pd-ions and D-ions) using the coherence theory of matter; lastly we will use the effective potential reported in [7,8] adding the role of lattice perturbations by means of which we compute the D–D tunnelling probability.

2. The Plasmas Present within No Loaded Palladium

According to the Coherence Theory of Condensed Matter, in a Pd crystal at room temperature the electron shells are in a coherent regime within coherent domain. In fact they oscillate in tune with a coherent e.m. field trapped in the coherent domains.

So we must take into account the plasma of s-electron and d-electron, in order to describe the lattice environment.

2.1. The Plasma of the d-Electrons

Similar argumentations were proposed by Preparata's but started from a new formulation of condense matter theory known as Coherence Theory.

In this theory, we can visualize the plasma formed by d-shell electrons as consisting of charged shells of charge $n_\mathrm{d}e$ (for palladium $n_\mathrm{d} = 10$) radius $r_\mathrm{d} = 1$ Å and thickness a fraction of 1 Å. The classical plasma

$$\omega_\mathrm{d} = \frac{e}{\sqrt{m}}\sqrt{\frac{n_\mathrm{d}N}{V}}, \tag{26}$$

as d-electrons plasma frequency. But according to the coherence theory of matter we must adjust this plasma frequency of a factor 1.38.

We can understand this correction by observing that the formula (26) is obtained assuming a uniform d-electron charge distribution. But of course the d-electron plasma is localized in a shell of radius R (that is about 1 Å), so the geometrical contribution is

$$\sqrt{\frac{6}{\pi}} = 1.38. \tag{27}$$

If we rewrite it with ω_d the renormalized d-electron plasma frequency, we have

$$\omega_\mathrm{d} = 41.5 \text{ eV}/\hbar \tag{28}$$

and the maximum oscillation amplitude ξ_d is about 0.5 Å.

2.2. The Plasma of Delocalized s-Electrons

The s-electrons are those which in the lattice neutralize the adsorbed deuterons ions. They are delocalised and their plasma frequency depends on loading ratio (D/Pd percentage). The formula (28) can also be written as

$$\omega_\mathrm{se} = \frac{e}{\sqrt{m}}\sqrt{\frac{N}{V}}\sqrt{\frac{x}{\lambda_\mathrm{a}}}, \tag{29}$$

where

$$\lambda_a = \left[1 - \frac{N}{V} V_{Pd}\right], \tag{30}$$

and V_{Pd} is the volume effectively occupied by the Pd-atom. As reported in [5], we obtain

$$\omega_{se} \approx x^{1/2} 15.2 \text{ eV}/\hbar. \tag{31}$$

For example for $x = 0.5$, we have $\omega_{se} \sim 10.7$ eV/$\hbar$.

2.3. The Plasma of Pd-ions

Further, we can consider the plasma due to the palladium ions forming the lattice structure; in this case it is possible to demonstrate that the frequency is Eq. (28):

$$\omega_{pd} = 0.1 \text{ eV}. \tag{32}$$

3. The Plasmas Present within D_2-Loaded Palladium

In this section, we seek to show what happens when the absorbed deuterium is placed near to the palladium surface. This loading can be enhanced using electrolytic cells or vacuum chambers working at opportune pressure [9–11]. By means of Preparata's theory of Condensed Matter it is assumed that, according to the ratio x = D/Pd, there are three phases concerning the D_2–Pd system:

(1) Phase α for $x < 0.1$,
(2) Phase β for $0.1 < x < 0.7$,
(3) Phase γ for $x > 0.7$.

In phase α, the D_2 is in a disordered and not coherent state (D_2 is not charged).

According to the other phases, we start remembering that on the surface, because of the lattice e.m., takes place the following reaction:

$$D_{lattice} \rightarrow \quad D^+ + e^-. \tag{33}$$

Then, according to the loading quantity x = D/Pd, the ions of deuterium can occur on the octahedral sites (Fig. 1) or on the tetrahedral (Fig. 2) in the (1,0,0)-plane. In the coherent theory of the so called β-plasma of Preparata's the deuterons plasma are in the octahedral site and the γ-plasma are in the tetrahedral.

Regarding to the β-plasma it is possible to affirm that the plasma frequency is given by Eq. (28):

$$\omega_\beta = \omega_{\beta_0} (x + 0.05)^{1/2}, \tag{34}$$

where

$$\omega_{\beta 0} = \frac{e}{\sqrt{m_D}} \left(\frac{N}{V}\right)^{1/2} \frac{1}{\lambda_a^{1/2}} = \frac{0.15}{\lambda_a^{1/2}} \text{eV}/\hbar. \tag{35}$$

For example if we use $\lambda_a = 0.4$ and $x = 0.5$ we obtain $\omega_\beta = 0.168\,\text{eV}/\hbar$.

In the tetrahedral sites the D^+ can occupy the thin disk that encompass two sites (Fig. 3), representing a barrier to the D^+ ions. We must underline that the electrons of the d-shell start oscillating near to the equilibrium distance y_0 (about 1.4 Å) so that the static ions have a cloud of negative charge (see [5]).

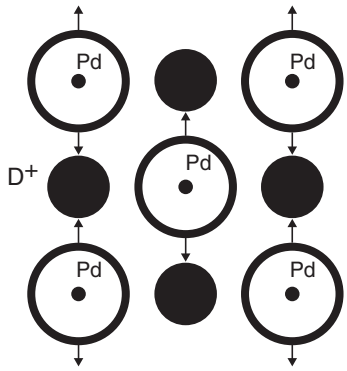

Figure 1. The octahedral sites of the Pd lattice where the deuterons take place.

Then follows:

$$\omega_\gamma = \sqrt{\frac{4Z_{\text{eff}}\alpha}{m_{\text{D}}y_0^2}} \approx 0.65 \text{ eV}/\hbar. \tag{36}$$

Of course this frequency also depends by the chemical condition of the palladium (impurities, temperature, etc…)

Due to a large plasma oscillation of d-electrons, in the disk-like tetrahedral region (where the γ-phase D^+'s are located) condenses a high density negative charge giving rise to a screening potential $W(t)$ whose profile is reported in Fig. 4.

Having mapped that Phase-γ depends on x value other can experimentally observe the new phase in [11,12], very important in the (LERN) investigation. This is demonstrated by the fact that many of the "cold fusion physicist" declare that the main point of cold fusion protocol is the loading D/Pd ratio higher than 0.7, i.e. the deuterium takes place in the tetrahedral sites.

4. The D–D Potential

In [7], it was shown that the phenomenon of fusion between nuclei of deuterium in the lattice of a metal is conditioned by the structural characteristics, by the dynamic conditions of the system and also by the concentration of impurities present in the metal under examination.

In fact, studying the curves of the potential of interaction between deuterons (including the deuteron–plasmon contribution) in the case of three typical metals (Pd, Pt and Ti), as shown in a three-dimensional model, the height of the Coulomb barrier decreases on the varying of the total energy and of the concentration of impurities present in the metal itself.

The initial potential that connects the like-Morse attraction and the like-Coulomb repulsion can be written as seen in [7,8]:

$$V(r) = k_0 \frac{q^2}{r}\left(V(r)_{\text{M}} - \frac{\Sigma}{r}\right), \tag{37}$$

where $V(r)_{\text{M}}$ is the Morse potential, $k_0 = 1/4\pi\varepsilon_0$, q is the charge of the deuteron, M_{d} the reduced mass of the deuterium nuclei, T the absolute temperature at which the metal is experimentally placed, J the concentration of impurities in the crystalline lattice and R is the nuclear radius.

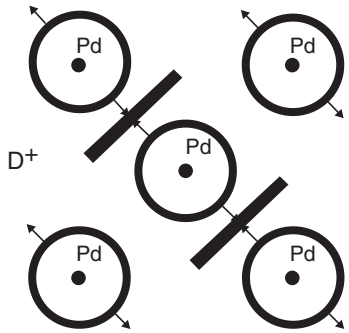

Figure 2. The thin disks of the tetrahedral sites of the Pd lattice where the deuterons take place.

In Eq. (37), $V(r)_{\mathrm{M}}$ is a like-Morse potential, and is given by

$$V(r)_{\mathrm{M}} = B\left\{\exp\left(-2\varphi(-r_0)\right) - 2\exp\left(-\varphi(r-r_0)\right)\right\}. \tag{38}$$

Here the parameters B, φ and r_0 depend by the lattice.

In fact, the potential (37) is an effective one whose reliability is demonstrated by its ability to fit the Coulomb potential for $r \to 0$ and the Morse potential in the attractive zone. So, Siclen and Jones [12] defined ρ the point where the Coulomb potential is associated to the Morse trend, r_0' the equilibrium distance and D' the well.

Of course in the free space for a D_2 molecule, ρ is about 0.3 Å, r_0' is about 0.7 Å and D' is -4.6 eV.

But within the lattice there are the screening effect and the deuteron–deuteron interaction, by means of phonon exchange, modify these parameter values.

Since the screening effect can be modulated by the giver atoms, we have considered in [7,8] the role of impurities and it has been shown that we can write $J = J_0 \exp[\beta/bkT]$.

Further, could occur some particular reactions, incorporating the impurities in the nucleus of the dislocations, as a result of the different arrangement of the atoms with respect to that of the unperturbed lattice.

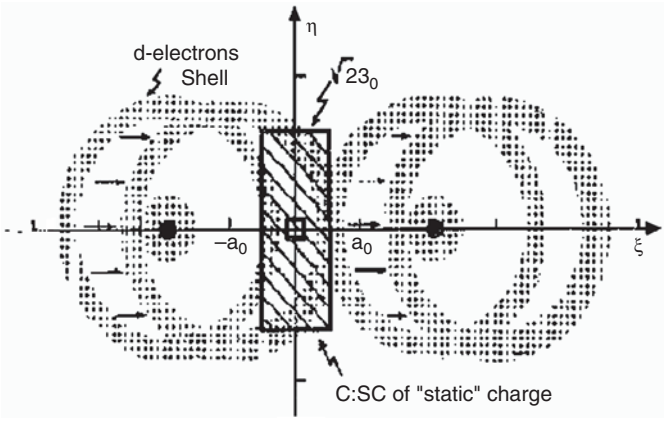

Figure 3. Possible d-electron plasma oscillation in a Pd lattice.

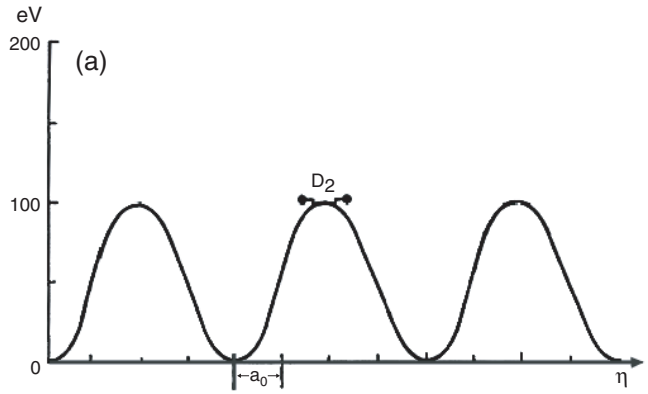

Figure 4. The profile of the electrostatic potential in a arbitrarily direction η.

This type of process has been extensively studied in the literature for metals and for the case of crystalline semiconductors at high temperature.

In the latter, for example, it is found that the concentration of interstitial impurities around a linear dislocation, with a point component, depends on the temperature according to the law written above where J_0 is the concentration of impurities in the zone with zero internal pressure, ($b^3 \simeq v_\mathrm{i}$) the volume of the ions constituting the lattice, while β is proportional to the difference ($v_d - v_i$) between the volume of the impurity atoms and that of the lattice ions.

Our conjecture is that in a metal, such as Pd, a similar phenomenon could occur between the atoms of deuterium penetrating the lattice as a result of deuterium loading and the microcracks produced by variations in temperature. In this case, the parameter β of the previous expression would be negative, determining an increase in the concentration of deuterons in the vicinity of the microcrack, which would then catalyse the phenomenon of fusion as:

$$\Sigma = JKTR \tag{39}$$

and

$$B = J/\varsigma.$$

So we can write the effective d–d potential

$$V(r) = k_0 \frac{q^2}{r}\left(V(r)_\mathrm{M} - \frac{JKTR}{r}\right), \tag{40}$$

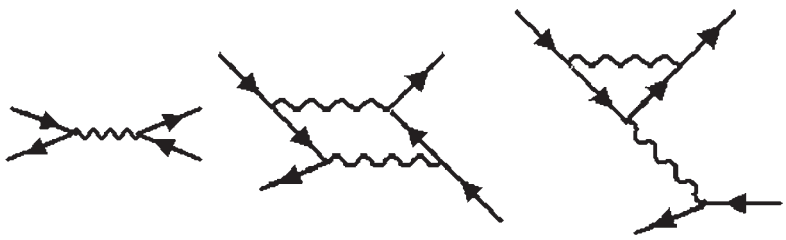

Figure 5. Plasmon exchanges. Solid lines indicate deuterons and wiggly lines plasmons.

where $V(r)_{\mathrm{M}}$ is the Morse potential, $k_0 = 1/4\pi\varepsilon_0$, q is the charge of the deuteron, M_{d} the reduced mass of the deuterium nuclei, T the absolute temperature at which the metal is experimentally placed, J the concentration of impurities in the crystalline lattice and R is the nuclear radius.

Considering the attractive force, due to the exchange of plasmons, the main contribution are those (Fig. 5):

Taking into account the role of coupling between deuteron and plasmons, in [13] it was numerically evaluated a D–D potential having the features of the potential (14) with $D' = -50$ eV and $r_0' = 0.5$ Å and $\rho = 0.2$ Å (remember that in [13] are considered only two plasmon excitations at 7.5 and 26.5 eV).

The feature of the potential (37) is shown in Fig. 6:

According to the coherence theory of condensed matter, we study the role of potential (40) in the three different phases : α, β and γ.

This section, however, needs of some important explanation, such as:

(1) what KT is,;
(2) what is the role of electrons, ions plasma?

Concerning with the first point, according to the different deuteron-lattice configurations, KT can be:

(1) the loaded lattice temperature if we consider the deuterons in the α-phase;
(2) ω_β if we consider the deuterons in β-phase;
(3) ω_γ if we consider the deuterons in the γ-phase;

The question is much more complicate for the second point. In fact the lattice environment is a combination of coherent plasmas (ion Pd, electron and deuterons plasma) at different temperature, due to different masses, that let be very difficult the description of the emerging potential.

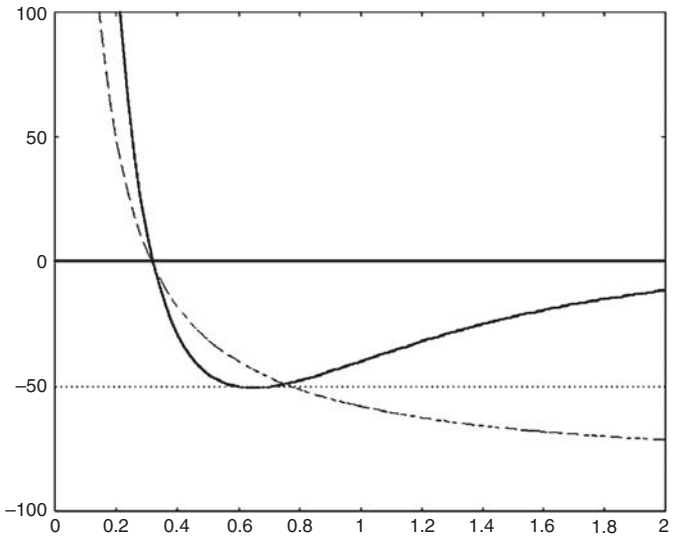

Figure 6. The solid line shows the features of potential (37) computed in order to obtain $D' = -50$ eV and $\rho = 0.165$ Å. The Coulomb potential in dashed line is computed using a screening constant of 85 eV. In the x-axis is reported the distance in Bohr radius unit and on the y-axis the energy in eV.

The method that in this work we propose is the following: to consider the total screening contribution of lattice environment at D–D interaction (i.e. V_{tot}) as random potential $Q(t)$. So in this model we have

$$V_{\text{tot}}(t) = V(r) + Q(t). \tag{41}$$

Of course we assume that

$$\langle Q(t)\rangle_t \neq 0 \tag{42}$$

that is to say that $Q(t)$ (a second order potential contribution) is a periodic potential (the frequency will be called by ω_Q) that oscillates between the maximum value $Q_{\max}$ and 0.

More exactly the oscillation charges of *d-shell* produce a screening potential having a harmonic feature:

$$eV(r) = -Z_{\text{d}}\frac{ke^2}{2a_0}r^2. \tag{43}$$

In [5] putting $Z_{\text{d}} = 10/3$ and $a_0 = 0.7$ Å, it is evaluated a screening potential V_0 of about 85 eV. In this way we can compute $\rho = V_0/26.9$ and at last $\rho = 0.165$ Å. To summarize, we can have the following cases in a palladium lattice according to the loading ratio:

4.1. α-Phase

In the phase α the deuterons are in a molecular state and the thermal motion is about:

$$0.02 \text{ eV} < \hbar\omega_\alpha < 0.1 \text{ eV}.$$

This phase takes places when x is fewer than 0.1, and since $W(t)$ is zero, the D–D potential is

$$V(r) = k\frac{q^2}{r}\left(V_{\text{M}}(r) - \frac{J\hbar\omega_\alpha R}{r}\right). \tag{44}$$

The expression (44) was partially evaluated in the previous paper [7]; in fact, we were only interested in the dependence of the tunnelling probability on impurities present within lattice. Through this work, we seek to examine the correlation between potential features and loading ratio and in the paragraph 5 we showed some numerical results.

4.2. β-Phase

When x is bigger than 0.1 but fewer than 0.7, the phase-β happens. The interaction takes place among deuteron ions that oscillate between the following energy values:

$$0.1 \text{ eV} < h\omega_\beta < 0.2 \text{ eV}.$$

In this case $W(t)$ is zero, we give this expression to the potential

$$V(r) = k\frac{q^2}{r}\left(V_{\text{M}}(r) - \frac{J\hbar\omega_\beta R}{r}\right). \tag{45}$$

Comparing the expressions (44) and (45), it seems clear that the weight of impurities is more important in the β-phase. Of course, this conclusion deals with the previous papers [7,8] in which we studied the role of temperature on tunnelling effect.

Table 1. For Pd "Impure" ($J \approx 0.75\%$), using the α-phase potential (44), has been computed the fusion probability normalized to the number of event/s for different values of energy (-50 eV $<$ E $<$ 50 eV) (Palladium $J \approx 0.75\%$, $\rho \approx 0.34$ Å, $r_0' = 0.7$ Å, $D' = -50$ eV)

$\omega_\alpha \approx 0.0025$ eV	$\omega_\alpha \approx 0.05$ eV	$\omega_\alpha \approx 0.075$ eV	$\omega_\alpha \approx 0.1$ eV
$E \approx -50$, $P \approx 10^{-100}$	$E \approx -50$, $P \approx 10^{-103}$	$E \approx -50$, $P \approx 10^{-100}$	$E \approx -50$, $P \approx 10^{-99}$
$E \approx -40$, $P \approx 10^{-99}$	$E \approx -40$, $P \approx 10^{-101}$	$E \approx -40$, $P \approx 10^{-98}$	$E \approx -40$, $P \approx 10^{-97}$
$E \approx -30$, $P \approx 10^{-97}$	$E \approx -30$, $P \approx 10^{-100}$	$E \approx -30$, $P \approx 10^{-96}$	$E \approx -30$, $P \approx 10^{-96}$
$E \approx -20$, $P \approx 10^{-95}$	$E \approx -20$, $P \approx 10^{-99}$	$E \approx -20$, $P \approx 10^{-94}$	$E \approx -20$, $P \approx 10^{-93}$
$E \approx -10$, $P \approx 10^{-94}$	$E \approx -10$, $P \approx 10^{-97}$	$E \approx -10$, $P \approx 10^{-91}$	$E \approx -10$, $P \approx 10^{-90}$
$E \approx 0$, $P \approx 10^{-92}$	$E \approx 0$, $P \approx 10^{-96}$	$E \approx 0$, $P \approx 10^{-90}$	$E \approx 0$, $P \approx 10^{-86}$
$E \approx 10$, $P \approx 10^{-91}$	$E \approx 10$, $P \approx 10^{-94}$	$E \approx 10$, $P \approx 10^{-87}$	$E \approx 10$, $P \approx 10^{-83}$
$E \approx 20$, $P \approx 10^{-90}$	$E \approx 20$, $P \approx 10^{-92}$	$E \approx 20$, $P \approx 10^{-85}$	$E \approx 20$, $P \approx 10^{-80}$
$E \approx 30$, $P \approx 10^{-89}$	$E \approx 30$, $P \approx 10^{-90}$	$E \approx 30$, $P \approx 10^{-82}$	$E \approx 30$, $P \approx 10^{-78}$
$E \approx 40$, $P \approx 10^{-86}$	$E \approx 40$, $P \approx 10^{-89}$	$E \approx 40$, $P \approx 10^{-80}$	$E \approx 40$, $P \approx 10^{-74}$
$E \approx 50$, $P \approx 10^{-84}$	$E \approx 50$, $P \approx 10^{-87}$	$E \approx 50$, $P \approx 10^{-79}$	$E \approx 50$, $P \approx 10^{-71}$

4.3. γ-Phase

Lastly, when the loading ratio is higher than 0.7, the deuteron–palladium system is in the phase-γ.

This is the most interesting case. The deuterons cross the screening through the d-electrons shell, in this sense we did a numeric simulation where we suppose that the D–D potential must be computed assuming that the well present in potential (37), because of the Morse contribution, disappears. In fact if we use a classical plasma model where the D^+ ions are the positive charge and the d-electrons the negative one, it is very "realistic" to use the following potential:

$$V(r,t) = k\frac{q^2}{r}\left(V_{\mathrm{M}}(r) - \frac{J\hbar\omega_\gamma R}{r}\right) + Q(t), \tag{46}$$

where $Q(t)$ is a not known perturbative potential. About this we can also add that

$$\langle Q(t)\rangle_t \approx \frac{W_{\max}}{\sqrt{2}}. \tag{47}$$

As said previously, we suppose that it is the screening potential, because of the d-electrons, has the role to reduce the repulsive barrier, i.e. ρ and r_0'. In the next evaluation it is given

$$\langle Q(t)\rangle_t \approx 85 \text{ eV}. \tag{48}$$

5. Conclusion

The aim of this section is to present the D–D fusion probability normalized to number of events per second regarding the D–D interaction in all different phases. More exactly, we seek to compare, at the varying of energy between –50 and 50 eV, the fusion probability in the phases α, β and γ. We also consider the role of d-electrons screening as perturbative lattice potential.

This treatment, which only interests the case where $Q(t)$ is different from zero, involves the change of the value of the point on the x-axis where the Coulomb barrier takes place; in this case, the final result is that the screening enhances the fusion probability. In order to evaluate the fusion rate (Λ) we applied this formula:

$$\Lambda = A\Gamma, \tag{50}$$

Table 2. For Pd "Impure" ($J \approx 0.75\%$), using the β-potential (45), has been computed the fusion probability P normalized to the number of event/s for different values energy (-50 eV $< E < 50$ eV) (Palladium $J \approx 0.75\%$, $\alpha \approx 0.34$ Å, $r_0' = 0.7$ Å, $D' = -50$ eV)

$\omega_\beta \approx 0.125$ eV	$\omega_\beta \approx 0.150$ eV	$\omega_\beta \approx 0.175$ eV	$\omega_\beta \approx 0.2$ eV
$E \approx -50$, $P \approx 10^{-83}$	$E \approx -50$, $P \approx 10^{-88}$	$E \approx -50$, $P \approx 10^{-86}$	$E \approx -50$, $P \approx 10^{-81}$
$E \approx -40$, $P \approx 10^{-81}$	$E \approx -40$, $P \approx 10^{-87}$	$E \approx -40$, $P \approx 10^{-85}$	$E \approx -40$, $P \approx 10^{-75}$
$E \approx -30$, $P \approx 10^{-80}$	$E \approx -30$, $P \approx 10^{-86}$	$E \approx -30$, $P \approx 10^{-83}$	$E \approx -30$, $P \approx 10^{-73}$
$E \approx -20$, $P \approx 10^{-79}$	$E \approx -20$, $P \approx 10^{-85}$	$E \approx -20$, $P \approx 10^{-80}$	$E \approx -20$, $P \approx 10^{-70}$
$E \approx -10$, $P \approx 10^{-78}$	$E \approx -10$, $P \approx 10^{-84}$	$E \approx -10$, $P \approx 10^{-74}$	$E \approx -10$, $P \approx 10^{-68}$
$E \approx 0$, $P \approx 10^{-76}$	$E \approx 0$, $P \approx 10^{-82}$	$E \approx 0$, $P \approx 10^{-73}$	$E \approx 0$, $P \approx 10^{-62}$
$E \approx 10$, $P \approx 10^{-75}$	$E \approx 10$, $P \approx 10^{-81}$	$E \approx 10$, $P \approx 10^{-72}$	$E \approx 10$, $P \approx 10^{-60}$
$E \approx 20$, $P \approx 10^{-74}$	$E \approx 20$, $P \approx 10^{-79}$	$E \approx 20$, $P \approx 10^{-71}$	$E \approx 20$, $P \approx 10^{-54}$
$E \approx 30$, $P \approx 10^{-73}$	$E \approx 30$, $P \approx 10^{-76}$	$E \approx 30$, $P \approx 10^{-70}$	$E \approx 30$, $P \approx 10^{-50}$
$E \approx 40$, $P \approx 10^{-72}$	$E \approx 40$, $P \approx 10^{-75}$	$E \approx 40$, $P \approx 10^{-69}$	$E \approx 40$, $P \approx 10^{-45}$
$E \approx 50$, $P \approx 10^{-71}$	$E \approx 50$, $P \approx 10^{-70}$	$E \approx 50$, $P \approx 10^{-65}$	$E \approx 50$, $P \approx 10^{-42}$

where Γ the Gamow factor and A is the nuclear reaction constant obtained from measured cross sections (value used was 10^{22} s^{-1}).

From an experimental point of view, in the cold fusion phenomenology, it is possible to affirm that there are three typologies of experiments [14]:

(1) those giving negative results,
(2) those giving some results (little detection signs with respect to background, fusion probability about 10^{-23} using a very high loading ratio),
(3) those giving clear positive results such as the Fleischmann and Pons experiments.

Nevertheless, we think that from the experimental point of view, the experiments of the third point are few accurate. In this sense, we believe that a theoretical model of controversial phenomenon of cold fusion is better to explain only those experiments of the points 1 and 2. In this case, it is important to consider the role of loading ratio on the experimental results. Now, let us begin from the α-phase.

In Table 1 are shown the results about the α-phase. Here we can observe that the theoretical fusion probability is very low, fewer than 10^{-74}. Consequently, it is allowed to affirm that through the loading, in the deuterium, of a percentage of $x < 0.2$ it is not possible any fusion. The same absence of nuclear phenomenon is compatible for a loading ratio of about 0.7 (Table 2) since in this case the predicted fusion probability is fewer than 10^{-42}. These predictions, of course, agree with the experimental results (for $x > 0.7$ look at [6]). The result of our model is that in the γ-phase, where we can observe some background fluctuations in which, because of a high loading ratio, we predict a fusion probability at about 10^{-22}. This is a new result, very important for [7,8] since, in those cases, the fusion probability was independent from the loading ratio.

To conclude, our aim is also to show that the model proposed in this paper (which unify nuclear physics with condensed matter) can explain some irregular nuclear traces in the solids. Regarding the experiments at point 3, on the other hand, supposing that those could be real, we want to consider other contributions as microdeformation occurrence in order to explain the very high fusion rate. The role of microcrack and impurities linked by loading ratio will be explored in other speculative works. "The nuclear physics within condensed matter" may be a new device through which it is possible to understand other new productive scientific topic.

The studied problem is the objective of proposing a theoretical model considering the *random city* of the phenomenon and that permits to those experiments (in which there is a high production of energy) to be repetitive and reproductive.

Table 3. For Pd "Impure" ($J \approx 0.75\%$), using the γ-potential (46), has been computed the fusion probability normalized to the number of event/s for different values of energy ($-50\,\text{eV} < E < 50\,\text{eV}$) (Palladium $J \approx 0.75\%$, $\rho \approx 0.165\,\text{Å}$, $r_0' = 0.35\,\text{Å}$, $D' = -50\,\text{eV}$)

$\omega_\gamma \approx 0.6$ eV	$\omega_\gamma \approx 0.65$ eV	$\omega_\gamma \approx 0.7$ eV	$\omega_\gamma \approx 0.75$ eV
$E \approx -50$, $P \approx 10^{-71}$	$E \approx -50$, $P \approx 10^{-51}$	$E \approx -50$, $P \approx 10^{-57}$	$E \approx -50$, $P \approx 10^{-50}$
$E \approx -40$, $P \approx 10^{-68}$	$E \approx -40$, $P \approx 10^{-49}$	$E \approx -40$, $P \approx 10^{-54}$	$E \approx -40$, $P \approx 10^{-47}$
$E \approx -30$, $P \approx 10^{-66}$	$E \approx -30$, $P \approx 10^{-47}$	$E \approx -30$, $P \approx 10^{-51}$	$E \approx -30$, $P \approx 10^{-44}$
$E \approx -20$, $P \approx 10^{-62}$	$E \approx -20$, $P \approx 10^{-44}$	$E \approx -20$, $P \approx 10^{-49}$	$E \approx -20$, $P \approx 10^{-41}$
$E \approx -10$, $P \approx 10^{-60}$	$E \approx -10$, $P \approx 10^{-41}$	$E \approx -10$, $P \approx 10^{-46}$	$E \approx -10$, $P \approx 10^{-39}$
$E \approx 0$, $P \approx 10^{-57}$	$E \approx 0$, $P \approx 10^{-39}$	$E \approx 0$, $P \approx 10^{-43}$	$E \approx 0$, $P \approx 10^{-36}$
$E \approx 10$, $P \approx 10^{-54}$	$E \approx 10$, $P \approx 10^{-38}$	$E \approx 10$, $P \approx 10^{-42}$	$E \approx 10$, $P \approx 10^{-33}$
$E \approx 20$, $P \approx 10^{-51}$	$E \approx 20$, $P \approx 10^{-35}$	$E \approx 20$, $P \approx 10^{-40}$	$E \approx 20$, $P \approx 10^{-32}$
$E \approx 30$, $P \approx 10^{-49}$	$E \approx 30$, $P \approx 10^{-32}$	$E \approx 30$, $P \approx 10^{-36}$	$E \approx 30$, $P \approx 10^{-29}$
$E \approx 40$, $P \approx 10^{-47}$	$E \approx 40$, $P \approx 10^{-30}$	$E \approx 40$, $P \approx 10^{-33}$	$E \approx 40$, $P \approx 10^{-25}$
$E \approx 50$, $P \approx 10^{-45}$	$E \approx 50$, $P \approx 10^{-27}$	$E \approx 50$, $P \approx 10^{-30}$	$E \approx 50$, $P \approx 10^{-21}$

Our starting point is the following: the phenomenon of the low-energy fusion critically, depends on the interaction between the d-d nuclear system and the D_2 gas system, and the lattice of the palladium.

In fact, at the variation of the loading percentage, the typical deuterium–plasma interaction of the γ phase grows up and so the electrostatic repulsion is weakened. But while the deuterium loading in the gas phase grows up, the palladium lattice is deformed.

Other theoretical and experimental studies about the electric field are in progress. In order to be more clear, we explain the main passages of the lattice reaction: firstly, we have the deformation; secondly, the dislocation; and lastly the microcrack.

If the lattice is deformed, within the microcrack one has the creation of a microscopic electric field, in which the D^+ and the plasmons come to collision, and in which the deuterium nuclei are accelerated, as it happens in a classic accelerator of nuclear physic. This acceleration can also generate the phenomenon of the low-energy fusion.

References

[1] Y. Iwamura et al., *Jpn. J. Appl. Phys. A* **41** (1994) 4642.
[2] O. Reifenschweiler, *Phys. Lett. A* **184** (1994) 149.
[3] O. Reifenschweiler, *Fusion Technol.* **30** (1996) 261.
[4] H. Melvin Miles et al., *Fusion Technol.* **25** (1994) 478.
[5] G. Preparata, *QED Coherence in Matter* (World Scientific Publishing, Singapore, 1995).
[6] S. Aiello et al., *Fusion Technol.* **18** (1990) 125.
[7] F. Frisone, *Fusion Technol.* **39** (2001) 260.
[8] F. Frisone, *Fusion Technol.* **40** (2001) 139.
[9] F. Fleishmann and Pons, *J. Electroanal. Chem.* **261** (1989) 301–308.
[10] A. De Ninno et al., *Europhys. Lett.* **9** (1989) 221–224.
[11] G. Mengoli et al., *J. Electroanal. Chem.* **350** (1989) 57.
[12] C. DeW Van Siclen, S.E. Jones, *J. Phys.G. Nucl. Phys.* **12** (1986).
[13] M. Baldo, R. Pucci, *Fusion Technol.* **18** (1990) 47.
[14] D.R.O. Morrison, Review of cold fusion, *in Eighth World Hydrogen Energy Conference*, 1990, Honolulu, Hawaii Natural Energy Institute, Honolulu, HI.

J. Condensed Matter Nucl. Sci. 1 (2007) 41–46

Research Article

Calculation of Deuteron Interactions within Microcracks of a D_2 Loaded Crystalline Lattice at Room Temperature

Frisone Fulvio*

Department of Physics, University of Catania, Via Santa Sofia 64, I-95125 Catania, Italy

Abstract

We have analysed the possibility that the coefficient of lattice deformation, linked to the formation of microcracks at room temperature and low energies, could influence the process of fusion. The calculated probability of fusion within a microcrack, in the presence of D_2 loading at room temperature and for impure metals, shows moderately elevated values compared with the probability of fusion on the surface. For all the temperatures in the 150–350 K range and for all the energies between 150 and 250 eV, the formation of microcracks increases the probability of fusion compared to non-deformed lattices, and also reduces the thickness of the Coulomb barrier. Using the trend of the curve of potential to evaluate the influence of the concentration of impurities, a very high barrier is found within the pure lattice ($J \approx 0.25\%$). However, under the same thermodynamic conditions, the probability of fusion in the impure metal ($J \approx 0.75\%$) could be higher, with a total energy less than the potential so that the tunneling effect is amplified. Finally, we analysed the influence of *forced* D_2 loading on the process.

Keywords: Collective plasmonic excitation, Dislocations, Fusion within a microcrack, Tunneling effect

1. Introduction

This study has the aim of analyzing the possible influence, which variations in temperature and energy could have on the phenomenon of deuterium fusion because of microdeformations or microcracks produced in the lattice. These could in fact be able to concentrate in their vicinity a significant fraction of the deuterons present in the metal. In particular, the author has suggested [1] that deuteron–plasmon coupling could increase the rate of fusion by acting as an effective interaction attractive to deuterium nuclei, reducing the distance at which Coulomb repulsion becomes dominant. With this in mind, a study was made of crystalline lattices with certain structural characteristics: in particular, the analysis focused on lattices with ten or more electrons in the "d" band. The present work will concentrate on palladium because, when subjected to thermodynamic stress, this metal has been seen to give results which are interesting from both the theoretical and experimental points of view.

*E-mail: Frisone@ct.infn.it

Further, it is hypothesized that the phenomenon of fusion is not only conditioned by structural characteristics and the thermodynamic conditions of the system, but also by the concentration of impurities present in the metal, correlated with the deuterium loading within the lattice itself.
The analysis will attempt to determine whether, in the case of the three-dimensional isotrope, D_2 loading can lead to the formation of microcracks in an analogous manner to that suggested for temperature variation in [1]. This would constitute an ulterior verification of the hypotheses proposed.

2. Three-dimensional Model

The aim is to determine whether, and within what limits, deuterium loading can condition the rate of fusion within a generic cubic lattice, trying to isolate the D_2 contribution from any other possible effects caused by lattice defects, or by other characteristics or thermodynamic conditions, or even by any "microdeformations" of the crystalline lattice caused by temperature variations. This type of phenomenon can be considered as a perturbation "external" to the system [2] and should be distinguished from "internal" perturbations.

In the case of external perturbations, the interaction between the impurities present and the dislocations [4] produced in the metal during microdeformation can distinctly modify the electrical properties of the material. Because of the different arrangement of the atoms with respect to the unperturbed lattice, some particular reactions can then occur so that the impurities become incorporated in the nucleus of the dislocations.

The results presented here were obtained using a numerical simulation to determine the trend of the barrier penetration factor, K, as a function of the temperature and the concentration of impurities present in the metal under examination.

In a three-dimensional model, the probability of fusion between not-free deuterium nuclei within the crystalline lattice is equal to the probability of penetrating a Coulomb potential barrier $V(r)$, given by

$$|P|^2_{\text{int}} = \exp\left(2\int_0^{\alpha} K\,(r)_{\text{int}}\,\mathrm{d}r\right), \tag{1}$$

where α is 0.11 Å and $K(r)_{\text{int}}$ is given by

$$K\,(r)_{\text{int}} = \sqrt{2\mu\,[E - V\,(r)]\,/\hbar^2} \tag{2}$$

E is the initial total energy (in eV), principally thermal in nature; μ is reduced mass of the deuteron and $\hbar$ is the Plank's constant.

The interaction potential can then be further extended to the three-dimensional isotrope case.

The potential $V(r)_{\text{int}}$ will then be expressed in the following way:

$$V\,(r)_{\text{int}} = k\frac{q^2}{r}\left[V\,(r)_{\text{M}} - J\frac{\xi k T R}{r}\right], \tag{3}$$

where $k = 1/4\pi\varepsilon_0$, q is the deuteron charge, R the nuclear radius, ξ a parameter which depends on the structural characteristics of the lattice (number of "d" band electrons and type of lattice symmetry), varying between 0.015 and 0.025, T the absolute temperature of the metal under experimental conditions and J is the percentage of impurities in the crystalline lattice.

In this case the Morse potential will be:

$$V(r)_{\text{M}} = (J/\varsigma)\ \exp\left(-2\varphi\,(r - r_0)\right) - 2\exp\left(-\varphi\,(r - r_0)\right). \tag{4}$$

In this equation, the parameters ς and φ depend on the dynamic conditions of the system, while r_0 is the classic point of inversion.

Equations (1) and (2) refer to the process of "not free" fusion, i.e. fusion within the crystalline lattice.

The "catalyzing" effect of the lattice has been studied from the theoretical point of view: in particular, it was shown [1] that, considering the interaction between deuterium nuclei and collective plasmonic excitation in the metal, fusion rate λ_f in a gas consisting of λ deuterons with densityρ is given by

$$\lambda_f = \lambda \frac{4\pi\rho\hbar}{\mu_d} \langle 1/p \rangle , \tag{5}$$

where μ_d is the mass of the deuterium nuclei, p is their impulse, and where the parentheses $\langle\rangle$ represent the thermal mean.

The aim of this work is to demonstrate the possibility of a further effect enhancing the probability of fusion, principally due to the presence of impurities in the metal.

The effect of vibrational energy, which is typically of the order of some eV for the quantum states under consideration, will be ignored here.

Electronic screening, a result of the metallic lattice, represents an important effect on the fusion reaction. Already studied by Rabinowitz et al. [3], this effect can be taken into account using a model in which the negative charge is distributed over a thin shell of radius R.

Because of the interaction potential within the metal, the "shifted" Coulomb potential can be written as:

$$V = kq^2 [(1/r) - (1/R)], \quad r_1 \leq r \leq R, \tag{6}$$

where q is the charge of the deuteron, r_1 is the nuclear radius and $k = 1/4\pi\varepsilon_0$.

This gives $V = 0$ per $r > R$.

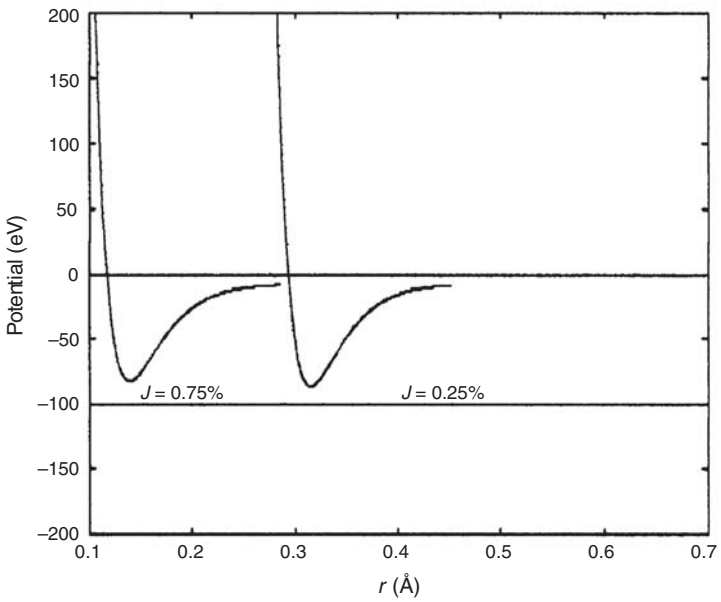

Figure 1. Semi-classic tunneling appears increased for those metals that have a concentration of impurity $J \approx 0.75\%$. The Morse potential was calculated at $T = 290$ K. The Coulomb barrier seems very high in the case of pure metals with $J \approx 0.25\%$. The "shell" potential was calculated at $T = 290$ K.

The solution for the semi-classic tunneling factor Λ is [3]:

$$\Lambda = D \exp\{-2\gamma\,(r_1)\}\,, \tag{7}$$

$$\gamma\,(r_1) = (\pi/2\hbar)\left[(2q^2/4\pi\varepsilon_0)\mu r_2\right]^{1/2}. \tag{8}$$

In Eq. (7), D is a numerical constant of the order of unity, μ the effective reduced mass of the deuteron, r_2 the classical turning point of d–d Coulomb collision process and $\hbar$ is the Plank's constant. To take into account the effect of the impurities present, the product $J\eta$ is substituted for D in Eq. (7), where J represents the concentration of impurities and η is a numerical constant.

It is now possible to consider a cubic lattice structure subjected to microdeformations and calculate the probability of fusion within a microcrack, Γ, on varying the temperature.

Indicating the volume of a single cell by $\mathrm{d}\Omega$, the deformation of the entire lattice is given by

$$D_{\mathrm{L}} = \iiint_{\omega} J\frac{\rho l^2 \nu b^2}{\alpha 2hR}\exp\left(-\frac{U_0}{kT}\right)\mathrm{d}\omega, \tag{9}$$

where ρ is the density of the mobile dislocation within the lattice at a non-constant lattice temperature, l^2 the area between the lines of separation between two adjacent dislocations, caused by a curving of the lattice [4], R is a coefficient whose value depends on the stress within the lattice, α is proportional to the thermal increment and represents the effect of the sudden variations in temperature to which the lattice is subjected and which lead to the formation of microcracks, ν^2 is the vibration frequency of the deuterons in the metal, considered constant here, b^2 the stress line which dampens the transformation of the crystalline lattice and $U_0 = 2U_j - Dbd\,(\sigma - \sigma_i)_{\varepsilon_0}$ is the activation energy.

In this last expression, $\sigma - \sigma_i$ is the stress applied to the small dislocations to a good approximation $\sigma_i \simeq \mu b/2\pi\ell$ and ℓ has the dimensions of a wavelength, while μ is an elastic constant which depends on the characteristics of the lattice. $\varepsilon_0 = \varepsilon_\beta - \beta\, t^m$ where β depends on the temperature and m is a variable which depends on the lattice (in this case it is equal to 1/3). $2U_j \simeq kT_{\mathrm{c}} \ln(X/\dot{\varepsilon})$ is obtained from the comparison of two curves with deformation velocity

Table 1. For "impure" Pd $J \approx 0.75\%$, using the Morse potential, the probability of fusion Γwithin a microcrack in the presence of D_2 loading, normalized to the number of events per minute, was calculated for different values of temperature (varying from 100 to 300 K) and energy (varying from 150 to 250 eV). It should be noted that the probability generally increases with T and E, and is systematically several orders greater than the probability of surface fusion P (Palladium $J \approx 0.75\%$, T (range) $\approx$ 100–300 K, $\alpha \approx 0.34$ Å, $\lambda = 10^{-3}$ eV/min, M_{Pd}/μg)

E (eV)	$T \approx 100$ K		$T \approx 140$ K		$T \approx 180$ K		$T \approx 220$ K		$T \approx 260$ K		$T \approx 300$ K	
	$\Gamma \approx$	$P \approx$	$\Gamma \approx$	$P \approx$	$\Gamma \approx$	$P \approx$	$\Gamma \approx$	$P \approx$	$\Gamma \approx$	$P \approx$	$\Gamma \approx$	$P \approx$
150	10^{-80}	10^{-88}	10^{-67}	10^{-69}	10^{-77}	10^{-86}	10^{-63}	10^{-65}	10^{-65}	10^{-66}	10^{-60}	10^{-68}
160	10^{-75}	10^{-86}	10^{-65}	10^{-68}	10^{-75}	10^{-85}	10^{-61}	10^{-63}	10^{-63}	10^{-65}	10^{-58}	10^{-65}
170	10^{-72}	10^{-85}	10^{-63}	10^{-65}	10^{-73}	10^{-85}	10^{-60}	10^{-62}	10^{-60}	10^{-64}	10^{-56}	10^{-62}
180	10^{-69}	10^{-83}	10^{-60}	10^{-62}	10^{-72}	10^{-84}	10^{-59}	10^{-61}	10^{-58}	10^{-63}	10^{-55}	10^{-60}
190	10^{-67}	10^{-81}	10^{-57}	10^{-60}	10^{-71}	10^{-83}	10^{-57}	10^{-60}	10^{-56}	10^{-62}	10^{-50}	10^{-58}
200	10^{-66}	10^{-79}	10^{-55}	10^{-59}	10^{-70}	10^{-82}	10^{-55}	10^{-59}	10^{-54}	10^{-61}	10^{-48}	10^{-54}
210	10^{-65}	10^{-76}	10^{-54}	10^{-58}	10^{-69}	10^{-78}	10^{-53}	10^{-57}	10^{-53}	10^{-60}	10^{-47}	10^{-52}
220	10^{-63}	10^{-75}	10^{-52}	10^{-57}	10^{-64}	10^{-77}	10^{-52}	10^{-56}	10^{-52}	10^{-59}	10^{-46}	10^{-51}
230	10^{-60}	10^{-72}	10^{-51}	10^{-56}	10^{-63}	10^{-76}	10^{-51}	10^{-55}	10^{-50}	10^{-58}	10^{-45}	10^{-50}
240	10^{-59}	10^{-67}	10^{-50}	10^{-55}	10^{-62}	10^{-74}	10^{-49}	10^{-54}	10^{-49}	10^{-57}	10^{-43}	10^{-48}
250	10^{-58}	10^{-63}	10^{-49}	10^{-53}	10^{-61}	10^{-72}	10^{-48}	10^{-52}	10^{-48}	10^{-53}	10^{-41}	10^{-46}

$\dot{\varepsilon}$, T_c is the "critical temperature" for the formation of the microcracks and $X \simeq 10^5$ in the CGS system. d indicates the distance between dislocations which have not undergone internal splitting, b can be associated with the inter-atomic distance and D depends on the time of movement of the dislocations. The aim here is to determine the probability of fusion within a deuterium loaded metal.

Further, the same problem will be treated from the aspect of the concentration of impurities contained in the metal.

If Eq. (1) is divided by Eq. (5) and multiplied by Eq. (9), it follows that

$$\Gamma \approx \frac{\exp\left(-2\int_0^{\alpha} K(r)_{\text{int}}\,\mathrm{d}r\right)}{\lambda\frac{4\pi\rho\hbar}{\mu_d}\langle 1/p\rangle} D_L. \tag{10}$$

Equation (10) represents the probability of deuteron fusion within a microcrack: it is inversely proportional to the number of nuclei absorbed by the metal.

Using Eq. (10) and adopting the Morse potential to calculate $K(r)_{\text{int}}$, the probability of fusion, normalized to the number of events per minute, was obtained by means of a numerical simulation program which utilizes the "WKB" method. The results are reported in Table 1. Within the metal, the probability of fusion given by Eq. (1) was evaluated numerically, making use of Eqs. (3) and (4) and taking the center of mass system as the reference system [1]. In the particular case of impure palladium with:

$$\alpha \simeq 0.15\,\text{Å},\ E \approx 237.2\,\text{eV},\ J = 0.75\%,\ T\ =\ 250.2\,\text{K}.$$

The result is $\Gamma_{\text{pd}} \approx 10^{-41}$, $P_{\text{int}} \approx 10^{-46}$.

For this result, and also for those obtained using the WKB method incorporated in numerical simulation programs, a range of temperatures between 100 and 300 K were considered.

The potential, Eq. (3), for Pd pure to 0.25%, was substituted by the "shell" potential, as follows:

$$V = kq^2\left((1/r) - \frac{KT}{J\varepsilon R}\right), \qquad r_1 \le r \le R, \tag{11}$$

Table 2. For "pure" Pd ($J \approx 0.25\%$), adopting the "shell" potential, the probability of fusion Γwithin a microcrack, normalized to the number of events per minute, was calculated under the same dynamic conditions as in Table 1. Also here Γis systematically several orders of magnitude greater than the probability of fusion on the surface P, but the values are systematically lower than those of the previous case (Palladium $J \approx 0.25\%$, T(range) ≈ 100–300 K, $\alpha \approx 0.34$ Å, $\lambda = 10^{-3}$ eV/min, M_{Pd}/μg)

E (eV)	$T \approx 100$ K		$T \approx 140$ K		$T \approx 180$ K		$T \approx 220$ K		$T \approx 260$ K		$T \approx 300$ K	
	$\Gamma \approx$	$P \approx$	$\Gamma \approx$	$P \approx$	$\Gamma \approx$	$P \approx$	$\Gamma \approx$	$P \approx$	$\Gamma \approx$	$P \approx$	$\Gamma \approx$	$P \approx$
150	10^{-75}	10^{-81}	10^{-76}	10^{-85}	10^{-73}	10^{-78}	10^{-69}	10^{-75}	10^{-66}	10^{-76}	10^{-65}	10^{-71}
160	10^{-74}	10^{-79}	10^{-78}	10^{-83}	10^{-70}	10^{-77}	10^{-68}	10^{-74}	10^{-65}	10^{-75}	10^{-63}	10^{-70}
170	10^{-73}	10^{-76}	10^{-76}	10^{-81}	10^{-69}	10^{-76}	10^{-67}	10^{-73}	10^{-63}	10^{-74}	10^{-60}	10^{-66}
180	10^{-71}	10^{-75}	10^{-75}	10^{-80}	10^{-68}	10^{-75}	10^{-65}	10^{-72}	10^{-62}	10^{-73}	10^{-58}	10^{-65}
190	10^{-69}	10^{-73}	10^{-73}	10^{-78}	10^{-67}	10^{-74}	10^{-64}	10^{-70}	10^{-60}	10^{-72}	10^{-57}	10^{-64}
200	10^{-67}	10^{-72}	10^{-72}	10^{-75}	10^{-65}	10^{-73}	10^{-62}	10^{-69}	10^{-58}	10^{-71}	10^{-56}	10^{-62}
210	10^{-65}	10^{-70}	10^{-67}	10^{-74}	10^{-64}	10^{-72}	10^{-60}	10^{-68}	10^{-56}	10^{-68}	10^{-55}	10^{-59}
220	10^{-64}	10^{-67}	10^{-68}	10^{-73}	10^{-63}	10^{-70}	10^{-59}	10^{-67}	10^{-54}	10^{-67}	10^{-54}	10^{-57}
230	10^{-63}	10^{-65}	10^{-66}	10^{-71}	10^{-61}	10^{-69}	10^{-57}	10^{-66}	10^{-52}	10^{-65}	10^{-50}	10^{-54}
240	10^{-61}	10^{-63}	10^{-64}	10^{-70}	10^{-60}	10^{-68}	10^{-55}	10^{-64}	10^{-51}	10^{-61}	10^{-49}	10^{-51}
250	10^{-60}	10^{-61}	10^{-63}	10^{-68}	10^{-58}	10^{-64}	10^{-54}	10^{-62}	10^{-49}	10^{-59}	10^{-45}	10^{-48}

dove KT is the mean kinetic energy of the gas, ε is the vibrational energy (typically of the order of some eV for the quantum states considered) and q is the deuteron charge. Under these particular dynamic conditions, the probability of fusion normalized to a number of events per minute was obtained for palladium. The probability of fusion within "pure" palladium, under the same dynamic conditions as the previous example, is then given by:

$$\alpha \simeq 0.15\ \text{Å},\ E \approx 237.2\ \text{eV},\ J = 0.25\%,\ T = 250.2\ \text{K}.$$

The result is $\Gamma_{\text{Pd}} \approx 10^{-45}$, $P_{\text{int}} \approx 10^{-48}$.

Other values of T, Γ, and P are reported in Tables 1 and 2.

3. Conclusions

The present work has shown that microcracks and deuterium loading in the lattice at room temperature have a significant influence on the probability of fusion.

In fact, calculating the probability of interaction within a microcrack, an increase of at least 2–3 orders of magnitude are found compared to the probability of fusion on the surface. Further, with the theoretical analysis developed it is possible to obtain relatively high values for the probability of fusion for D_2 loaded impure metals at room temperature.

On the other hand, results very close to the experimental data have already been obtained without imposing the D_2 loading (e.g. for $J \approx 0.75\%$, $E \approx 250$ eV, $T = 300$ K, $\Gamma = 10^{-21}$, and $P \approx 10^{-25}$) [5]. Judging by the comparison between the two theoretical calculations, it would seem that the experimental procedure *reduces* the rate of fusion rather than enhances it. To verify the influence of the concentration of impurities on the process from another point of view, the trend of the potential within the pure lattice ($J \approx 0.25$) was evaluated and a very high curve obtained. Therefore, crossing the barrier would require a total energy greater than the potential, as shown in Fig. 1 for palladium. If the potential barrier is evaluated for the same metal with a higher level of impurity ($J \approx 0.75\%$), under the same thermodynamic conditions of the system, it is seen that the probability of fusion may be greater than that observed for pure metals, with a total energy lower than the potential so that the tunneling effect is amplified.

References

[1] F. Frisone, Can variations in temperature influence deuteron interaction within crystalline lattices? *Il Nuovo Cimento D* **20** (10) (1998) 1567–1580.
[2] G. Chambers, Evidence for MeV particle emission from Ti charged with low-energy deuterium ions, NRL Memorandum Report 6927, 18 Dec. 1991, Naval Research Laboratory, Washington, D.C. 20375–5321.
[3] C.J. Horowitz, Cold fusion in metallic hydrogen and normal metals, *Phys. Rev. C* **40** (4) (1989) 1555–1558.
[4] J. Price Hirt and J. Lothe, Theory of dislocation, *Z. Phys.* (1960) 116–129.
[5] F. Frisone, Deuteron interaction within a microcrack in a lattice at room temperature, *Fusion Technol.* **39** (2001) 260–265.

J. Condensed Matter Nucl. Sci. 1 (2007) 47–61

Research Article

Very Sizeable Increase of Gravitation at Picometer Distance: A Novel Working Hypothesis to Explain Anomalous Heat Effects and Apparent Transmutations in Certain Metal/Hydrogen Systems*

J. Dufour†

CNAM—Laboratoire des Sciences Nucléaires, 2 rue Conté, 75003 Paris, France

Abstract

Since more than 15 years, unexplained heat effects have been reported in systems involving hydrogen isotopes (hydrogen and deuterium) and certain metals like palladium. The most studied system (palladium/deuterium) has given birth to the "Cold Fusion" concept: a special kind of DD fusion reaction, only occurring in a metallic lattice, which yields heat and helium-4 as the main reaction product. Other systems have also been studied (nickel hydrogen and caesium/deuterium for instance), showing shifts in isotopic ratio of the products of reaction and leading to the more generalized concept of Low Energy Nuclear Reaction (LENR). A novel conjecture (the pico-gravity conjecture) is presented here, that may explain all the anomalies observed in this so-called "Cold Fusion" field. According to this conjecture, the main part of the energy produced in Low Energy Nuclear Reaction could be the result of a very special kind of chemical reactions (pico-chemical reactions), induced by a considerable increase of gravity at pico-meter distances (pico-gravity). True nuclear signatures (α-particles emission for instance) could also occur according to the pico-gravity conjecture. But they should be many orders of magnitude lower than would be expected from the energy produced (which is observed experimentally). This conjecture will be tested by analysing the products of the reaction of hydrogen isotopes with selected metals.

Keywords: Cold fusion, Gravity, Isotopic shift, LENR, Low Energy Nuclear Reactions

1. Introduction

For more than 15 years since 1989, claims have been made of nuclear reactions occurring in metals (palladium for instance) at room temperature in the presence of hydrogen isotopes. During the course of electrolysis of D_2O with a palladium cathode, Fleischmann and Pons [1] observed an exothermal reaction, which they interpreted as being a special kind of deuterium nuclear fusion reaction. Claims have also been made of transmutations of chemical species, inducing

*This paper was presented in ASTI, at the 7th International Workshop on anomalies in Hydrogen/deuterium loaded metals. Following a review process, a new improved version is presented here (March 2007).

†E-mail: dufourj@cnam.fr; Tel.: +33-1-40272915

isotopic composition variations. Recently, very surprising results (transmutation of cesium into praseodymium and strontium into molybdenum) have been obtained by passing a flux of deuterium through a multi-layer composite of palladium and calcium oxide [2].

Various working hypothesis have been presented to explain the occurrence of nuclear reactions in solids at energies in the order of eV [3,4]. These hypotheses address the two main problems in the field and explain by novel quantum mechanical effects in condensed matter, the overcoming of the Coulomb barrier at room temperature and the absence of the expected characteristic radiations accompanying nuclear reactions. These hypothesis are generally rejected by mainstream scientists. In that perspective, the DOE report of 1 December 2004 [4], proposes that dedicated experiments should be founded to check two types of observations: one is the anomalous character of the heat production with deuterium, the other is the particles reportedly emitted from deuterated foils, using state of the art apparatus and methods. This is an indication that the DOE report acknowledges that something unusual might occur in certain metal/hydrogen systems.

In this DOE report, observation of apparent transmutations without radiation emission [2,5] was not taken into account. Although this might be seen as a strong proof of the occurrence of nuclear reactions in condensed matter, it will be seen that these results can indeed be rationalized by the novel working hypothesis presented below.

2. The Novel Working Hypothesis

It is commonly accepted that the electromagnetic, the weak nuclear and the strong nuclear forces, have the same intensity at the quark scale (Grand unification). It is suspected that the intensity of gravity should increase when the distance decreases and that the four interactions should have the same intensity at a sufficiently small distance (Superunification). Since 1926 and the publication of the article of Kaluza [6], who proposed a model for gravitation variations with distance, the increase of gravitation has been confined to the Plank distance, but with no experimental proof. With this very restrictive concept, gravitation should increase by a factor of some 10^{40} within a distance of 10^{-33} cm (the Plank distance), which is very questionable. The attitude towards gravitation intensity variations with distance has changed during the last 20 years [7] and a great number of theoretical models embedded in string theory and with very surprising and intellectually challenging concepts await experimental results to choose those that are backed by reality. A sizeable experimental effort is carried out at tens of μm distances [8] and so far no variations have been observed down to 50 μm. This is the upper limit for experimentally allowed gravitation variations, from the known macroscopic value (6.673×10^{-11} m^3/kg s^2), towards the ultimate one expected at Plank distance (some 7×10^{29} m^3/kg s^2). Direct measurement of the Newton constant at much smaller distances seems impossible.

It is then hypothesized that the intensity of gravitation very strongly increases at distances of the order of the inner atomic distances (0 to some 100 pm). This increase is supposed to attain such a level, that the gravitational intensity attraction between a proton (or a deuteron) and a nucleus A becomes of the same order of magnitude as their Coulomb repulsion. A simplified model of the interaction between the nucleus A and the proton (deuteron) embedded in the electronic layers of A is presented. This model is purely phenomenological, no attempt being made to modelize additional dimensions of space/time. A strong increase of the gravitational constant G is indeed considered, in the ordinary four-dimensional space/time.

It will be shown that this model predicts the possibility of bound states between the proton (deuteron) and A, with binding energies of a few hundred eV. This can explain the bulk of the anomalous enthalpy of reaction observed in certain metal/hydrogen systems. This model can also explain some very faint nuclear reactions, producing only very weak typical nuclear signatures and contributing only marginally to the enthalpy of reaction.

3. The Model

The model presented below, uses the same line of reasoning as the elementary calculation of the Bohr radius and the ionisation energy of the hydrogen atom, which is described now.

3.1. Simplified Model of the Hydrogen Atom

To calculate the radius and ionisation energy of a hydrogen atom, the following simple calculation is often used: with

$$Q^2 = \frac{e^2}{4\pi\varepsilon_0},$$

m_e, v_e the electron mass and velocity and r the distance proton/electron, the potential energy of the electron is

$$E_P = -\frac{Q^2}{r}$$

and its kinetic energy is $E_C = (1/2)\, m_e v_e^2$. A bound state of the electron has a radius r that minimizes its total energy $E = E_P + E_C$. Taking into account Heisenberg uncertainty on momentum: $m_e v_e r = n\hbar$ with $n \geq 1$ (n being an integer), the total energy of the electron is

$$E = -Q^2\frac{1}{r} + \frac{n^2\hbar^2}{2m_e}\frac{1}{r^2}. \tag{1}$$

Thus,

$$\frac{\partial E}{\partial r} = \frac{1}{r^2}\left[Q^2 - \frac{n^2\hbar^2}{m_e}\frac{1}{r}\right],$$

yielding the electron bound states:

$$r_n = n^2\frac{\hbar^2}{Q^2 m_e} = n^2 a,$$

with

$$a = 52.92\,\text{pm (Bohr radius)}$$

and

$$E_n = -\frac{1}{n^2}\frac{Q^4 m_e}{\hbar^2} = -\frac{1}{n^2}E_I,$$

with $E_I = 13.6\,\text{eV}$ (hydrogen ionisation energy).

Simplified model of bound states of a hydrogen nucleus surrounding an atom A, embedded in its electronic system and submitted to an hypothetical strong gravitational potential:

The above approach is used in Fig. 1.

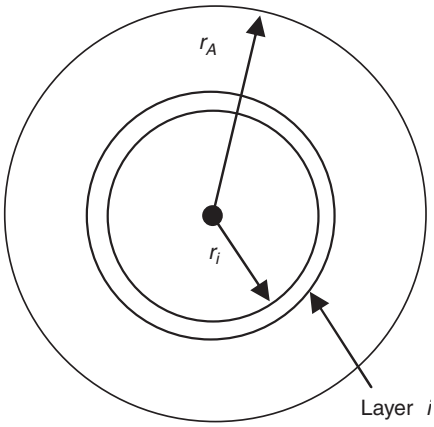

Figure 1. Simplified model of bound states of a hydrogen nucleus surrounding an atom A.

The electronic system of an atom A, having a mass number A, an atomic number Z and a radius r_{A}, is represented by a series of equidistant two-dimensional layers of electric charges, each layer having a charge equal to e, the electric charge of an electron. There are thus Z layers surrounding the nucleus of A, the innermost radius of layer i being:

$$r_i = \frac{r_{\mathrm{A}}}{Z} i \quad \text{with} \quad 0 < i \leq Z - 1.$$

A hydrogen nucleus approaching atom A from outside will be submitted to two potentials:

(1) The repulsive Coulomb potential of the nucleus of A, which will be less an less screened by the electron layers as it moves towards the nucleus of A: $E_{\mathrm{P}}^{\mathrm{E}} = (Z - i)\, Q^2 \frac{1}{r_i}$.

(2) The attractive gravitational potential of A: $E_{\mathrm{P}}^{\mathrm{G}} = -G' A m_{\mathrm{p}} m_{\mathrm{H}} 1/r_i$, G' being the increased Newtonian gravitation constant, m_{p} the mass of the proton (the mass difference between the proton and the neutron and the mass corresponding to the binding energy of the nucleus being neglected) and m_{H} the mass of the hydrogen isotope under study. The total energy of the hydrogen nucleus is thus

$$E = \left[(Z - i)\, Q^2 - G' A m_{\mathrm{p}} m_{\mathrm{H}}\right] \frac{1}{r} + \frac{n^2 \hbar^2}{2 m_{\mathrm{H}}} \frac{1}{r^2} = -k\,(Z - i)\, Q^2 \frac{1}{r} + \frac{n^2 \hbar^2}{2 m_{\mathrm{H}}} \frac{1}{r^2} \tag{2}$$

with

$$k = \frac{G' A m_{\mathrm{p}} m_{\mathrm{H}}}{(Z - i)\, Q^2} - 1 \tag{3}$$

using for (2) the same method as for (1), yields the hypothetical bounds states of the hydrogen nucleus, embedded in the electronic system of A, submitted to a combined Coulomb and gravitational potential of intensity G' and round its nucleus:

$$r_n = \frac{n^2 \hbar^2}{k\,(Z - i)\, Q^2 m_{\mathrm{H}}} = n^2 a \frac{1}{k\,(Z - i)} \frac{m_{\mathrm{e}}}{m_{\mathrm{H}}}, \tag{4}$$

$$E_n = -\frac{1}{2}\frac{k^2\,(Z-i)^2\,Q^4 m_{\mathrm{H}}}{n^2\hbar^2} = -\frac{1}{n^2}E_{\mathrm{I}}k^2\,(Z-i)^2\,\frac{m_{\mathrm{H}}}{m_{\mathrm{e}}}. \tag{5}$$

Remark: Through all this article and to distinguish the hydrogen isotopes under study, the following notations will be used for their nuclei.

Generic denomination: H for both isotopes

(1) Hydrogen (one proton) p.
(2) Deuterium (one proton, one neutron) d.

4. Discussion

For solutions to exist, k (3), must be positive. The minimum required value of the increased Newtonian gravitation constant is thus

$$G' = \frac{(Z-i)Q^2}{Am_{\mathrm{p}}m_{\mathrm{H}}},$$

obviously corresponding to a very sizeable increase of the intensity of gravitation. It can also be seen that the exact required minimum value of G' depends upon the system under study. It will be much higher for the hydrogen/hydrogen system ($A = 1, m_{\mathrm{H}} = m_{\mathrm{p}}$), than for the $^{206}_{82}$Pb/deuterium system for instance ($A = 206, m_{\mathrm{H}} = 2m_{\mathrm{p}}$).

The simpler system (in term of number of protons and neutrons involved) that has been observed experimentally to yield reactions will thus fix the value of G'. This value can then be used to study more complicated reactions. The deuterium/deuterium case seems to be a good candidate to determine G' For the sake of simplicity, we shall call "pico-gravity" the strongly enhanced gravity at picometer distances with an apparent newtonnian constant G'.

4.1. Interaction of Two Deuterium Nuclei

Although, the simple model presented is even more oversimplified in that case (the centre of mass of the system is in between the two deuterium nuclei), it is used to give an order of magnitude of G'

Equation (4) gives

$$r_1 = a\frac{1}{k_{\mathrm{d,d}}}\frac{m_{\mathrm{e}}}{m_{\mathrm{H}}} \approx a\frac{1}{k_{\mathrm{d,d}}}\frac{m_{\mathrm{e}}}{2m_{\mathrm{p}}} = 2.7\times 10^{-4}\frac{a}{k_{\mathrm{d,d}}}.$$

Thus,

$$k_{\mathrm{d,d}} = 2.7\times 10^{-4}\frac{a}{r_1}.$$

It is known that in a deuterium molecule, the distance between the two deuterium nuclei is some 74 pm. With this distance, nuclear fusion reactions between the two nuclei are extremely rare. On the contrary, in a mesic deuterium molecular ion, this distance is some 200 times smaller (0.4 pm), yielding a reaction time of a few μs. It has been observed that deuterium trapped in a palladium lattice yields very small amounts of tritium, neutron and helium 4. The amounts of helium 4 observed are much larger than would be expected from a classical "hot fusion reaction" and the helium 4 looks like the major product of the "cold fusion reaction" observed. Another plausible explanation for the apparition of sizeable amounts of helium 4 and heat in a lattice where a "cold fusion reaction" occurs will be discussed

later. For the time being, it is hypothesized that a classical "hot fusion reaction" can be catalysed by pico-gravity, through the formation of a compound with a size smaller than 74 pm, but much bigger than 0.4 pm, yielding a very small but measurable rate of "hot fusion" reactions with associated heat and classical products pattern. The determination of the exact value would require more experiments to determine the exact rate of the reaction and thus the exact value of r_1. In first approximation, r_1 is set at 20 pm, finally yielding

$$k_{\mathrm{d,d}} = 7.15 \times 10^{-4}$$

and

$$G' = \left(1 + k_{\mathrm{d,d}}\right) \frac{Q^2}{4m_{\mathrm{p}}^2} \approx 2.06 \times 10^{25}\,\mathrm{m^3\ kg^{-1}\ s^{-2}}, \tag{6}$$

which is a 3×10^{35}-fold increase compared to the measured macroscopic value ($6.67 \times 10^{-11}\mathrm{m^3\ kg^{-1}\ s^{-2}}$). It will be shown below that this increase can well have been hidden in all presently known systems, because of its very weak effects in such systems.

Using this value of G' for the pico-gravity constant, the interactions of hydrogen isotopes with atoms with mass number higher than two are now examined.

5. Interaction of Hydrogen Isotopes with Atoms with Atomic Number $Z \geq 2$ and Mass Number A

To explicit Eqs. (4) and (5), the value for G' is taken equal to the value calculated from the interaction d,d and given by (6):

$$G' = \left(1 + k_{\mathrm{d,d}}\right) \frac{Q^2}{4m_{\mathrm{p}}^2}.$$

Thus,

$$k_{\mathrm{A,H}} = \frac{G' A m_{\mathrm{P}} m_{\mathrm{H}}}{(Z-i)\,Q^2} - 1 = \frac{m_{\mathrm{H}}}{4m_{\mathrm{p}}} \frac{A}{(Z-i)} \left(1 + k_{\mathrm{d,d}}\right) - 1.$$

Thus,

$$r_n = n^2 a \frac{1}{k_{\mathrm{A,H}}\,(Z-i)} \frac{m_{\mathrm{e}}}{m_{\mathrm{H}}} = n^2 a \frac{m_{\mathrm{e}}}{m_{\mathrm{H}}} \left[\frac{1}{\frac{m_{\mathrm{H}}}{4m_{\mathrm{p}}} A \left(1 + k_{\mathrm{d,d}}\right) - (Z-i)} \right] = n^2 a \frac{m_{\mathrm{e}}}{m_{\mathrm{H}}} K\,(i)\,, \tag{7a}$$

with

$$K\,(i) = \frac{1}{\frac{m_{\mathrm{H}}}{4m_{\mathrm{p}}} A \left(1 + k_{\mathrm{d,d}}\right) - (Z-i)} \tag{7b}$$

and

$$E_n = -\frac{1}{n^2} E_{\mathrm{I}} k_{\mathrm{A,H}}^2\,(Z-i)^2 \frac{m_{\mathrm{H}}}{m_{\mathrm{e}}} = -\frac{1}{n^2} E_{\mathrm{I}} \frac{m_{\mathrm{H}}}{m_{\mathrm{e}}} L\,(i)\,, \tag{8a}$$

with

$$L\,(i) = \frac{m_{\mathrm{H}}^2}{16 m_{\mathrm{p}}^2} A^2 \left(1 + k_{\mathrm{d,d}}\right)^2 - \frac{m_{\mathrm{H}}}{2 m_{\mathrm{p}}} A \left(1 + k_{\mathrm{d,d}}\right)(Z - i) + (Z - i)^2. \tag{8b}$$

Equations (7a) and (8a), describe the possible bound states of H in the combined Coulomb + gravitational field of A. H entering the electronic layers of A from the outside, n should decrease as H approaches the nucleus of A. For the model to be coherent, n is determined as a function of i by writing:

$$r_i = \frac{r_{\mathrm{A}}}{Z} i = r_n = n^2 a \frac{m_{\mathrm{e}}}{m_{\mathrm{H}}} K\,(i)\,.$$

Thus,

$$n = \sqrt{\frac{r_{\mathrm{A}}}{a} \frac{m_{\mathrm{H}}}{m_{\mathrm{e}}} \frac{i}{Z K\,(i)}}. \tag{9}$$

In the regions of interest, n is high; r_n and E_n are thus calculated by taking the integer value of n given by (9). The discrepancy between r_i and r_n is small.

Equations (7a), (7b), (8a), (8b) and (9) shall be used to study the interaction of a proton (p) and a deuteron (d) with various atoms A and their isotopes (r_{A} is taken equal to the covalent radius of A). The values of $K(i)$ and $L(i)$ given by (7b) and (8b) are calculated for both hydrogen isotopes as will be seen below.

6. Interaction of a Proton (p) with an Atom A

In this case,

$$K\,(i) = \frac{1}{\frac{1}{4} A \left(1 + k_{\mathrm{d,d}}\right) - (Z - i)}. \tag{10a}$$

The progression of p towards the nucleus of A is limited to the layers with

$$i > Z - \frac{A}{4}\left(1 + k_{\mathrm{d,d}}\right) \approx Z - \frac{A}{4}\ (k_{\mathrm{d,d}} \text{ is small compared to } 1)$$

and the minimum value for i is

$$i_{\min} = Z - \frac{A}{4} + 1,$$

for which $K\,(i_{\min}) = 1$. In other word, when the screening by electrons becomes insufficient ($i < Z - A/4$), the Coulomb repulsion gets higher than the pico-gravity attraction and the proton is repelled. An equilibrium can nevertheless be attained, the proton oscillating between the layers $i_{\min}$ and $i_{\min} + 1$.

Hence,

$$r_{\min} = \frac{r_{\mathrm{A}}}{a} \frac{m_{\mathrm{H}}}{m_{\mathrm{e}}} a \frac{m_{\mathrm{e}}}{m_{\mathrm{H}}} \frac{i_{\min}}{Z K\,(i_{\min})} = r_{\mathrm{A}} \frac{Z - \frac{A}{4} + 1}{Z}. \tag{10b}$$

The proton p can thus never come to the close vicinity of the nucleus of A. Compounds formed will contain proton(s) embedded in the outer electronic layers of A.

$$L(i) = \frac{m_{\mathrm{H}}^2}{16m_{\mathrm{p}}^2}A^2\left(1+k_{\mathrm{d,d}}\right)^2 - \frac{m_{\mathrm{H}}}{2m_{\mathrm{p}}}A\left(1+k_{\mathrm{d,d}}\right)(Z-i) + (Z-i)^2$$
$$= \frac{A^2}{16}\left(1+k_{\mathrm{d,d}}\right)^2 - \frac{A}{2}\left(1+k_{\mathrm{d,d}}\right)(Z-i) + (Z-i)^2 \approx \left[\frac{A}{4} - (Z-i)\right]^2. \tag{11}$$

Thus, the energy of the proton is always negative, and at the layer $i = i_{\min} \approx Z - \frac{A}{4} + 1$, $L(i_{\min}) = 1$. The value of the energy at $i_{\min}$ is then

$$E_{i_{\min}} = -\frac{a}{r_{\mathrm{A}}}E_{\mathrm{I}}\frac{2K(i_{\min})L(i_{\min})}{i_{\min}} = -\frac{a}{r_{\mathrm{A}}}E_{\mathrm{I}}\frac{2}{Z-\frac{A}{4}+1}.$$

Examples of the variation of the proton energy with its distance to the nucleus of various atoms A are given below. Calculations are made using Eqs. (7a), (8a), (9), (10a) and (11).

7. Interaction of a Deuteron (d) with an Atom A

In this case,

$$K(i) = \frac{1}{\frac{1}{2}A\left(1+k_{\mathrm{d,d}}\right) - (Z-i)} \tag{12}$$

is always positive (in stable isotopes $A \geq 2Z$). The deuteron could come to contact with the nucleus of A (for $n = 1$, values of r_n are of the size of a nucleus). This might happen in rare cases, and could result in a nuclear reaction (fission, α emission, …). But in most cases it is likely that its progression is limited by Pauli exclusion principle, the electrons between the deuteron(s) and the nucleus of A having less and less energetic levels available as the deuteron d progresses towards A, in a way comparable of what is considered in the calculation of Chandrasekhar's limit for white dwarf stars. This is confirmed by the very low intensity of typical nuclear radiations experimentally observed. It is assumed that Pauli exclusion principle sets the minimum distance between the deuteron(s) and the nucleus of A. To visualize, on the graphs presented below, the possible effect of the Pauli exclusion principle, a repulsive Lennard–Jones type of potential (A/r^{12}) has been added to the combined Coulomb/gravitational potential. This potential has been set empirically, hypothesizing that the 2 s electrons are involved, which gives an order of magnitude of the distance at which the minimum total energy of the system occurs. The complex atom formed could have atomic characteristics close to but different from the product of a nuclear reaction between A and d [8]. This point will be discussed in details below.

$$L(i) = \frac{A^2}{4}\left(1+k_{\mathrm{d,d}}\right)^2 - A\left(1+k_{\mathrm{d,d}}\right)(Z-i) + (Z-i)^2 \approx \left[\frac{A}{2} - (Z-i)\right]^2 \tag{13}$$

is always positive. The total energy of the deuteron is thus always negative.

Examples of the variation of the deuteron energy with its distance to the nucleus of various atoms A are given below. Calculations are made using Eqs. (7a), (8a), (9), (12) and (13).

8. General Comments on the Proposed Model

Due to the simplified character of the model presented, only a rough order of magnitude can be expected when using it to describe this novel type of chemical reactions between a hydrogen isotope and an atom A. Anyhow, it will be seen that there is a general concordance between its predictions and what has been observed in the so-called LENR field (Low Energy Nuclear Reaction).

A second point must be stressed. An infinite range of the strong gravity has been considered, resulting in a sizeable attractive potential at the limit of the atom A (orders of hundred eV). Such a potential should already have been seen. In fact the range of strong gravity should be limited, probably at values lower than 100 pm, that is lower than typical atom size. This point will be discussed below in details. In the graphs that are presented in the following paragraph, this limitation has not been taken into account. Some of the reactions described in these graphs could not occur, if the range of pico-gravity is too small.

A third point is worth being noted: the proton and the deuteron behave differently. The mass of the latter is sufficient to insure an attractive combined Coulomb gravitational potential, even at very short distance from the nucleus of A. An equilibrium position can be found between this attractive combined potential and the repulsive potential created by the Pauli exclusion principle.

On the contrary, the progression of the proton towards the nucleus of A is limited to a minimum distance [Eq. (10b)]. Anyhow, an equilibrium could be reached, the proton oscillating round its minimum distance from the nucleus of A given by Eq. (10b), but it is likely that reactions with hydrogen should be less frequent and with a lower rate than those observed with deuterium. In other words, the pico-gravity conjecture explains heat production with deuterium. In certain favourable cases (nickel and compact atoms for instance) hydrogen could also react. This will be exemplified below.

9. Examples of Bound States of Hydrogen Isotopes with Selected Atoms A

The case of four atoms A will be examined: nickel, palladium, caesium and strontium.

9.1. Case of Nickel

The calculation has been made for the most abundant nickel isotope ($^{58}_{28}$Ni, 68%). Results are displayed in Fig. 2, giving the total energy of the hydrogen isotope as a function of the distance to the nucleus of Ni.

For deuterium, a bound state could occur with binding energy of some 200 eV. For hydrogen, as explicited above, the proton could oscillate at a distance $r_{\min}$ of some 55 pm from the nickel nucleus with a binding energy round 350 eV.

The type of radiation expected is a copious emission of very low energy X-rays, more likely to be detected as heat in the calorimeter. Heat generation has indeed been observed in the system Nickel/Hydrogen [10].

The rate of reaction should vary with the various isotopes of nickel (influence of A), giving rise to an apparent isotopic change in the remaining unreacted nickel.

As regards the products formed, they could mimic (depending upon the analytical method used) atoms A′ resulting from the addition of proton(s) or deuteron(s) to the nucleus of A. This point will be discussed in detail below in the case of caesium and strontium.

9.2. Case of Palladium

The calculation has been made for the most abundant palladium isotope ($^{106}_{46}$Pd, 28%). Results are displayed in Fig. 3, giving the total energy of the hydrogen isotope as a function of the distance to the nucleus of Pd.

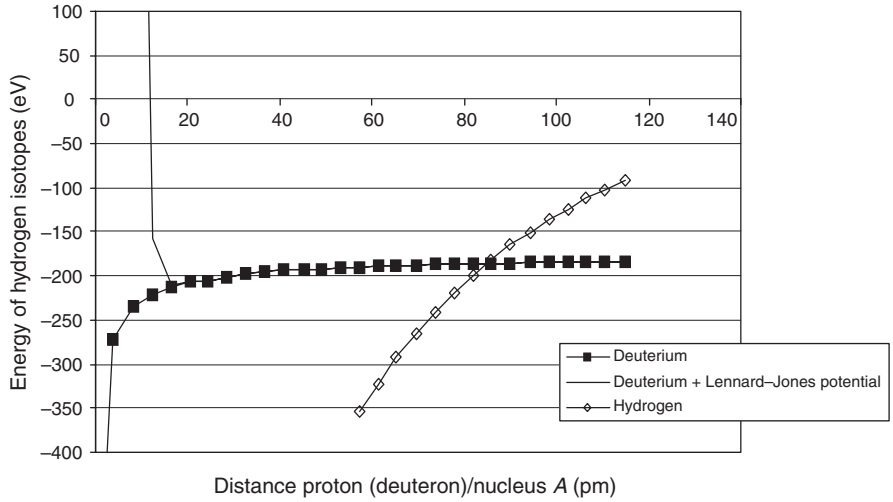

Figure 2. Bound states of hydrogen isotopes with Nickel (58).

For deuterium, a bound state could occur with binding energy of some 800 eV. For hydrogen, the binding energy should be less, round 650 eV corresponding (as for nickel) to the layer $i_{\min}$. Same considerations as for nickel, apply for the other characteristics of this reaction.

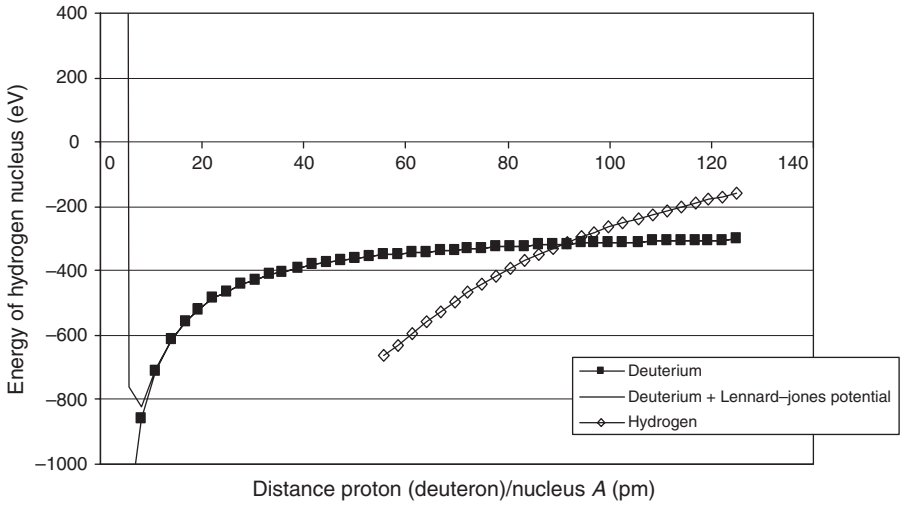

Figure 3. Bound states of hydrogen isotopes with palladium (106).

9.3. Case of Caesium

The calculation has been made for the sole stable caesium isotope ($^{133}_{55}$Cs, 100%). Results are displayed in Fig. 4, giving the total energy of the hydrogen isotope as a function of the distance to the nucleus of Cs.

For deuterium, a bound state could occur with binding energy of some 1200 eV. For hydrogen, the binding energy should be very low: 50–100 eV and decreases when the distance proton nucleus decreases.

In that case, the energy for $i_{\min}$ is very low and it is very unlikely that the proton could oscillate round $r_{\min}$ as for Nickel and hydrogen. Caesium could even not react with hydrogen, the distance at which the combined Coulomb gravitational potential becomes repulsive being some 70 pm, which might be to close to the maximum range of pico-gravity.

The case of caesium has been the object of extensive experimental studies [2,5]. By permeating deuterium through a complex layered structure of palladium and calcium oxide, containing minute amounts of caesium, the apparent following nuclear reaction has been observed (with various experimental techniques):

$$^{133}_{55}\mathrm{Cs} + 4^{2}_{1}\mathrm{H} \rightarrow {}^{141}_{59}\mathrm{Pr}, \quad Q = 50.5\,\mathrm{MeV}. \tag{14}$$

The Q-value was calculated from the mass defect of Eq. (14).

Should reaction (14) occur, copious fast neutrons would be generated (they where not observed). It is unlikely that the majority of the energy could be passed to fission fragments (because of the Coulomb barrier) or to gamma rays (because of the slow electro-magnetic transition).

Following analytical techniques were used to characterize the apparently formed praseodymium:

(1) In situ X-ray Photoelectron Spectroscopy (XPS) for most of the experiments.
(2) X-ray Absorption Near Edge Structure (XANES) for some experiments.
(3) TOF SIMS for a few experiments.

Results of in situ *XPS*: they show the clear disappearance of the caesium LM lines and the concomitant appearance of the praseodymium LM lines.

Results of XANES: they confirm the results of in situ XPS.

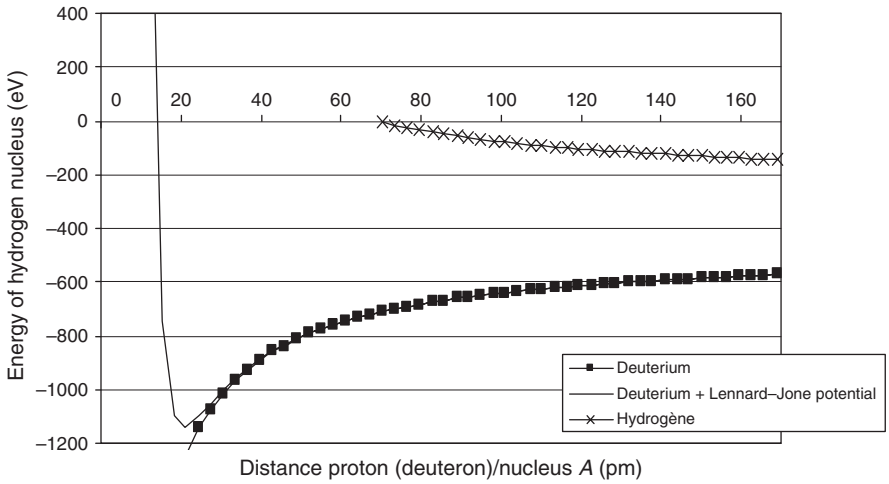

Figure 4. Bound states of hydrogen isotopes with caesium (133).

Results of TOF SIMS: they clearly show the appearance of an atom with mass 140.90 very close to the mass of praseodymium (140.908). No standard deviation of this result is given: TOF SIMS has a very high resolution, but it cannot be excluded that the absolute value found is not exactly 140.90: it could be closed to, but different from this value. This point will be discussed below.

9.4. Case of Strontium

The calculation has been made for the most abundant strontium isotope ($^{88}_{38}$Sr, 82.6%). Results are displayed in Fig. 5, giving the total energy of the hydrogen isotope as a function of the distance to the nucleus of Sr.

For deuterium, a bound state could occur with binding energy of some 800 eV. For hydrogen, the binding energy should be in the order of 50–100 eV. As for caesium, the existence of a minimum of the total energy for the proton, will depend upon the exact range of the increased gravity, which, as stated before, has not been taken into account in Fig. 5. As for caesium, strontium could even not react with hydrogen.

As for caesium, the case of strontium has been the object of extensive experimental studies [2,5]. By permeating deuterium through a complex layered structure of palladium and calcium oxide, containing minute amounts of strontium, the apparent following nuclear reaction has been observed (with various experimental techniques):

$$^{88}_{38}\mathrm{Sr} + 4^{2}_{1}\mathrm{H} \rightarrow {}^{96}_{42}\mathrm{Mo}, \quad Q = 53.5\,\mathrm{MeV}. \tag{15}$$

The Q-value was calculated from the mass defect of Eq. (15).

Following analytical techniques were used to characterize the apparently formed molybdenum:

(1) In situ XPS for most of the experiments.
(2) Secondary Ion Mass Spectroscopy (SIMS) for many experiments.

Results of in situ XPS: they show the clear disappearance of the strontium lines and the concomitant appearance of the molybdenum lines.

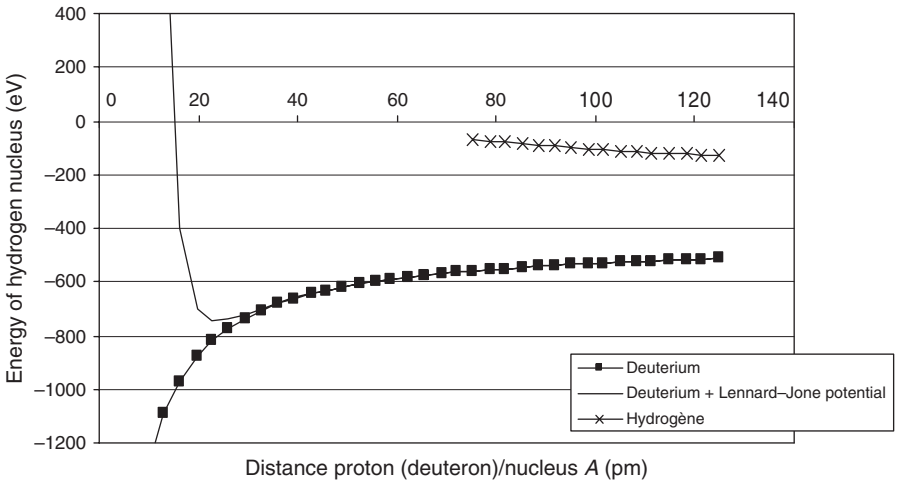

Figure 5. Bound states of hydrogen isotopes with strontium (88).

Results of SIMS: the product of strontium transformation has an isotopic composition very different from that of natural molybdenum. The major "molybdenum" peak is $^{96}_{42}$Mo. The major isotope of strontium is $^{88}_{38}$Sr. It is thus tempting to attribute the formation of Mo to reaction (15) and the similar ones for the other strontium isotopes

9.5. General Comments for the Case of Caesium and Strontium

All experimental observations described above, together with the absence of reaction with hydrogen, have been presented as strong evidence for nuclear reactions (14) and (15) to occur in solids.

The model presented here gives a simple and semi-quantitative description of another possible mechanism:

Four deuterons bind to the nucleus as described above (the proposed model is too simple to confirm or refute the assumption made that four deuterons could bind) and form a complex compound that can be written: $\left[^{88}_{38}\mathrm{Sr},4^{2}_{1}\mathrm{H}\right]or\left[^{133}_{55}\mathrm{Cs},4^{2}_{1}\mathrm{H}\right]$.

As these deuterons are close to the nucleus of strontium or caesium, the external electronic layers of the compound formed, see in fact a molybdenum or praseodymium nucleus and this is what XPS or XANES describe. The isotopic variation observed for the case of strontium is also a straightforward consequence of the model.

Remains the case of the mass of the "praseodymium" formed: the mass of $^{141}_{59}$ Pr is 140.9076.

The mass of $\left[^{133}_{55}\mathrm{Cs},4^{2}_{1}\mathrm{H}\right]$would be very close to 140.9614, a 380 ppm difference with the mass of Pr, that can be distinguished by TOF SIMS. What is questionable is the absolute calibration of the apparatus and this point would be worth being studied in details. A measure of the standard deviation is a must, together with an absolute calibration of the system.

10. Pico-gravity Conjecture and Other Observations in the Field of So-called Cold Fusion

10.1. Helium-4 Production

It has been observed experimentally (as mentioned in Section 4.1) that excess heat frequently occurs with the production of helium 4 in quantities many orders of magnitude higher than would be expected from a "hot fusion" reaction. This helium production has been ascribed to a special kind of dd fusion reaction where helium 4 is the main product. Another plausible scenario to explain this (apparent) helium 4 production is the following:

(1) Case of deuterium and palladium: the expected energy per pico-chemistry reaction in that case, is some 800 eV. It is likely that any helium 4 in the surroundings of the reacting palladium atom would get sufficient energy to be expelled from the lattice and measured as "reaction product". In these circumstances, any correlation between the energy produced and the helium measured would only reflect the initial helium 4 content of the lattice. It is interesting to note that there is a great dispersion in the measured values of the energy per atom helium 4 produced in the case of palladium (the most studied system).
(2) Case of hydrogen: as mentioned above, the reaction with hydrogen according to the pico-gravity conjecture is less probable, with a lower rate than with deuterium and likely to be limited to compact atoms like nickel. Data are lacking on a possible (apparent) production of helium 4 in that case.

10.2. "True" nuclear reactions

Nuclear signatures at very low level, as alphas or fast charged particles, have been observed in certain experiments. These can be accounted for by the pico-gravity conjecture. Consider the case of deuterium and palladium. As mentioned above, in very rare occasions the deuteron could reach the nucleus of the atom A and react with it. As an example, the following reaction could be observed:

$$^{105}_{46}\mathrm{Pd} + {}^{2}_{1}\mathrm{H} = {}^{103}_{45}\mathrm{Rh} + + {}^{4}_{2}\mathrm{He}, \quad Q = 10.8\ \mathrm{MeV}$$

yielding fast alphas and lower mass isotopes (transmutation in lighter isotopes).

11. Range of the Increased Pico-gravity and Possible Effects on Known Systems

In the modern concept of gravitation increase, additional space dimensions open at a given range.

Modelling such concept is far beyond the scope of this note. One requirement is that this opening does not conflict with known physic and chemistry. So the range of these new dimensions should be well within atom size. A range between some 50 and 100 pm seems realistic. Known chemistry would not have seen them. Inside the atom and due to the very small mass of an electron, the electronic layers would not be altered in a measurable way. There remains the case of the Lamb shift which is related to the mass of the electron. The overall mathematical treatment of the effect of the pico-gravity conjecture combined with quantum electrodynamics is probably extremely complex. Should this problem find a solution, an explanation could be found for the discrepancies observed between the predicted value and the most recent experimental measurements of this Lamb shift [11].

The finite range of these new dimensions also requires gravity to be carried along these dimensions through a massive graviton. An estimation of the mass of this graviton, is given by the Yukawa relation between its range r_G and its mass m_G:

$$r_G = \frac{\hbar}{m_G c} \quad (\text{with } c = \text{speed of light}) . \tag{16}$$

For $r_G = 50$ pm, Eq. (16) yields $m_G \approx 5$ keV. The minimum detectable mass of a particle being some 250 keV, this graviton would presently be undetectable. But this mass could explain why cross sections in reactions involving its action should be energy dependant. This might be an explanation of the discrepancies observed in the cross section of a deuteron beam and a deuterated target at very low energy of the deuteron, when compared to the cross section predicted by high-energy experiments [9].

One of the main practical problem, which could be due to the limited range of this hypothetical strong gravity, would be the need for a sizeable activation energy (tens of eV), to obtain a pico-chemistry reaction. Indeed, before reaching that range, the proton (deuteron) would be submitted to the full Coulomb repulsion of the nucleus of A. Some of the reactions presented in the above graphs, may be very difficult (if not impossible) to obtain.

Finally at femtometer scale, this increased gravitation would anyhow be some 10^{-4} weaker than the strong nuclear force and acting on quarks with mass close to 1/3 the mass of protons would have an ever weaker effect: strong gravity as required by the present model would also have been unnoticed. As regards the weak nuclear force at attometer scale, things are less clear, but two of the particles involved (electron and neutrino) have a small mass, probably closed to zero for the latter.

It is obvious that a great number of questions are still to be answered. Detailed study of the formation and characteristics of compounds such as, for example $\left[{}^{133}_{55}\mathrm{Cs}, 4{}^{2}_{1}\mathrm{H}\right]$, should shed more light on all those questions.

12. Conclusions

The novel working hypothesis proposed could open a new field of chemistry. It is proposed to call this new field "pico-chemistry". In pico-chemistry enthalpies of reaction are some 100 times higher than ordinary chemical reactions (oil combustion for instance).

Moreover, a better knowledge of the variations of the gravitational constant with distance could help reconcile quantum mechanics and relativity. A massive graviton, with mass round 5 keV is predicted.

References

[1] M. Fleischmann, S. Pons, Electrochemically induced nuclear fusion of deuterium, *J. Electroanal. Chem.* **261** (1989) 301.
[2] Y. Iwamura et al., Low energy nuclear transmutation in condensed matter induced by D_2 gas permeation through Pd complexes: correlation between deuterium flux and nuclear products, *Proceedings of the ICCF10* Cambridge, MA, 2003. Available at http://www.lenr-canr.org/.
[3] A. Takahashi, Mechanism of deuteron cluster fusion by EQPET model, *Proceedings of the ICCF 10*, Cambridge, MA, 2003. Available at http://www.lenr-canr.org/.
[4] DOE, Report of the review of low energy nuclear reactions December 1, 2004. Available at http://www.science.doe.gov/Sub/News_Releases.
[5] Y. Iwamura et al., Observation of surface distribution of products by X-ray fluorescence spectrometry, during D_2 gas permeation through Pd complexes, *Proceedings of the 12th International Conference on Condensed Matter Nuclear Science*, Yokohama, Japan, 2005.
[6] T. Kaluza, *Preuss. Acad. Wiss.* **K1** (1921) 966.
[7] L. Randall, Extra dimensions and warped geometries, *Science* **296** (2002) 1422.
[8] E.G. Adelberger, Available at http://xxx.lanl.gov/abs/hep-ex0202008.
[9] A. Kitamura et al., Experiments on condensed matter nuclear events in Kobe University *ICCF11 Proceedings* **218** (2004).
[10] F. Piantelli, Hydrogen loading of Ni and related phenomena, *Proceedings of SIENA 2005 Workshop*, see internet site http://www.iscmns.org/siena05/Montalbano.ppt.
[11] M. Weitz et al., Precision measurement of the hydrogen and deuterium 1s ground state Lamb shift, *Phys. Rev. Lett.* **72** (1994) 328–331.

J. Condensed Matter Nucl. Sci. 1 (2007) 62–85

Research Article

Deuteron Cluster Fusion and ASH

Akito Takahashi*

Osaka University, Yamadaoka 2-1, Suita, Osaka 565-0871, Japan

Abstract

This is a review of our studies on theoretical model of deuteron cluster fusion in condensed matter. Considering a transient condensation process of deuteron-cluster in focal points of metal–deuteride lattice, electron screening effect was theorized by the Electronic Quasi-Particle Screening Theory (EQPET) model for a transient deuteron cluster associating attracted electrons. Multi-body resonance fusion of deuterons was proposed by modeling charged-pion exchange for strong interaction in very condensed deuteron cluster to lead to select the tetrahedral resonance fusion (TRF) of 4D and octahedral resonance fusion (ORF) of 8D as possible major reaction channels in extreme case. ^{4}He is the final product of TRF and ORF. Tritium and ^{3}He was suggested as minor products from 3D multi-body fusion. Visible but very small level production of neutron by D + D (2D) fusion was also concluded. Further extension of EQPET model is given to propose a dynamic Bose-type condensation process by orthogonally coupled two D_2 molecules, which play a role of super screening of Coulomb barrier with quadruplet electronic quasi-particle to generate clean fusion product of ^{4}He.

Keywords: Ash, Bosonization, Deuteron cluster fusion, Electronic quasi-particle screening, 4D Fusion, 8D Fusion, Helium-4, Secondary reaction

1. Introduction

The possible occurrence of low energy deuteron fusion in condensed matter at room temperature, so called cold fusion, and other nuclear reactions in solid has been studied in the last 15 years since 1989 by number of people in the world, in spite of totally negative responses [1] by established scientific societies in 1989–1990. Many international conferences [2–10] have been held and numerous papers have been published in journals. Many claims of anomalous observation of excess heat, neutrons, helium, X-rays, charged particles, etc., which are asserted to evidences of "new" nuclear reactions in condensed matter, have been made. However, people have got failed to replicate the claimed results in most cases. Nevertheless, several groups have obtained physically same results for the following key observations.

(A) Generation of large amount of helium-4 (^{4}He), comparable to observed level of excess heat (1–100 W level) in PdDx systems of electrolysis-type experiments, has been confirmed by several groups [11–15,53,54]. In these

*E-mail:akito@sutv.zaq.ne.jp

experiments, neutrons and gamma-rays have not been observed with clearly countable level [16,17]. However, emission of continuous X-rays in the region less than 100 keV has sometimes been observed [18,19]. These results suggest us that some "unknown" nuclear reactions took place emitting energetic α-particles, which produced secondary continuous X-rays in slowing down with condensed matter (PdDx) and make energy deposit, comparable to excess heat, as lattice vibration. The known free particle d–d reaction, which is known to emit 2.45 MeV neutron plus 0.8 MeV ^{3}He and 3 MeV proton plus 1 MeV triton, cannot be candidate for explaining observed results.

In the text, d denotes deuteron-particle and D does deuteron with electron.

(B) Observations of anomalous amount of "foreign" elements on metal surface (cathode or permeation sample) region have been claimed by several groups [19–23]. Some new class of low-energy "nuclear transmutation" like "clean fission" without hard γ-ray radiation has been proposed by the researchers. Especially, the latest claim by Mitsubishi H. I. Group [24–27] is extraordinary; They have shown clear-cut results of generation of mass(A)-8-and-charge(Z, atomic number)-4 increased elements (^{96}Mo and ^{141}Pr form ^{88}Sr and ^{133}Cs, respectively), with large amount (10^{14} atoms per week or so), closely related to comparable reduction of test elements (Sr and Cs), by the deuterium gas permeation through multi-layered Pd/CaO/Pd film on which test elements were mounted. How is the selective occurrence of A-8-and-Z-4 increased transmutation made possible ? This is a big challenge to theoretical modeling.

Many theoreticians, and even experimentalists, have made great efforts to propose new theoretical models for "nuclear reaction in condensed matter" and attempted to consistently explain those anomalous observations. A comprehensive review paper [28] exists for the research period of 1989–1994; No theory work was enough consistent to match both of explaining anomalous results and not-violating established physics, although we may have some hopes to several models. Progress in theoretical study was rather slow in 1995–2001. However, well-cited models by researchers have been gradually converged to "coherent fusion" models. Dynamic behavior of deuterons in condensed matter, namely dynamics of solid-state-physics, may induce special conditions to make deuterons "coherent fusion," in either nm-size domain of metal–deuteride (MDx) lattice [28, 29] or more microscopic focal points in MDx lattice [30–34].

The author first proposed multi-body (three-body D + D + D) fusion model [35] as a cascade D-catalyzed reaction: D + D to ^{4}He*, ^{4}He*+ D to d + α + 23.8 MeV in very short time interval, to explain the original claim [36] on large excess heat with anomalous small level of tritium and neutron. Since that time, the author and his collaborators have elaborated [30–32] the multi-body deuteron fusion model in MDx dynamics, to meet the consistency requirements in views of established physics and to attempt to make quantitative studies on reaction rates of "cluster deuteron fusion process," which is another name of multi-body deuteron fusion in condensed matter. Especially in the latest paper [51], for ICCF9 Proceedings, the author has proposed the model of tetrahedral (TRF) and octahedral resonance fusion (ORF) in dynamic condition of PdDx ($x > 1$) lattice, considering the generation of transient "bosonization" of electrons at focal points to make super-screening of Coulomb repulsive force of d–d interaction to enhance resonantly strong interactions for 4D and 8D cluster fusion. Quantitative estimations of cluster fusion have ever been done [31,37,38,60,62]. Further elaboration done is reviewed in this work; the electronic quasi-particle expansion theory (EQPET) model was proposed by the author [48] and some numerical estimations were done by using calculations of screened potentials for dde* (e*; quasi-particle of electrons like Cooper pair and quadruplet-coupling) and dde*e* transient molecular states, to obtain very positive results to support the occurrence of deuteron cluster fusion as 4D or 3D multi-body fusion in PdDx lattice with so large reaction rate level as comparable to experimentally claimed level of excess heat and ^{4}He production. Nuclear transmutation by high-energy ^{8}Be emission of 8D cluster fusion was also proposed [51] to explain the extraordinary Mitsubishi results [24–26]. The model was further extended [60,62] to model super-screening mechanism by quasi-particle of quadruplet electrons with orthogonally coupled two D_2 molecules.

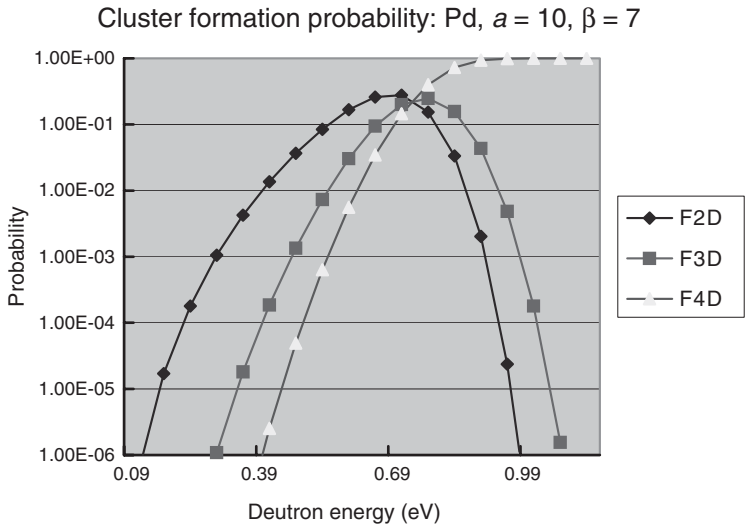

Figure 1. Cluster formation probabilities of 2D, 3D, and 4D condensation [31].

This paper first reviews the EQPET theory of deuteron cluster fusion in condensed matter, to draw a comprehensive story of the model, formulation of equations, quantitative results and discussions. Then extended theory is shown.

2. Transient Condensation of Deuteron Cluster

Since the meaningful enhancement of d–d fusion rate in steady state condition of deuterons trapped in metal lattice like PdDx is not possible [30], we have looked for dynamic conditions.

Using the implantation technique of low energy ion beam (deuteron, proton, and Si) from accelerators into titanium-deuteride (TiDx) plate-samples in vacuum, we have intensively searched if there exists any trace of deuteron cluster fusion [15,37–40,52], especially 3D (D + D + D) fusion which in conventional random motion or stochastic process of nuclear reaction should have very small reaction rate-ratio to d–d (D + D) fusion, [3D]/[2D] less than 10^{-30}. Namely, we should not observe any significant counts of produced particles (4.75 MeV t and 4.75 MeV ^{3}He, typically), according to the conventional theory of random nuclear reactions. On the contrary, our results [15,37–40] of beam implantation experiments provided very large data of [3D]/[2D] = about 10^{-4}, with increasing trend in low energy region less than 100 keV of D^+ beam energy. Namely, anomalous enhancement factor of about 10^{26}–10^{27} was obtained. To explain this with the beam-target reaction as conventional nuclear stochastic process, we need to assume the existence of close d–d pairs within 1 pm (10^{-12} m) inter-nuclear distance with 10^{-10} times population of deuterons in TiDx lattice. And experiments with proton beam [39,40] have suggested us that about half of three-body reactions (H + D + D or D + D + D) was due to the direct beam and close d–d pair reactions, and a remained half was attributed to the indirect (lattice-induced) three-body reactions that could be true deuteron cluster fusion. Therefore, to explain the enhancement factor of 10^{26}, we have sincerely to consider the mechanism of coherently induced cluster fusion in dynamic motion of TiDx and PdDx lattice.

Our preliminary model analyses were given in Refs. [30,31]; We adopted the excitation screening model. We have considered transient motion of deuterons at O-sites of PdDx lattice moving (diffusing) toward a T-site which is a candidate of focal points, for local full loading condition of PdDx, $x = 1.0$. This transient motion was conceived to be stimulated by exciting D-harmonic oscillators at O-sites near to the periodic trapping potential height of 0.22 eV.

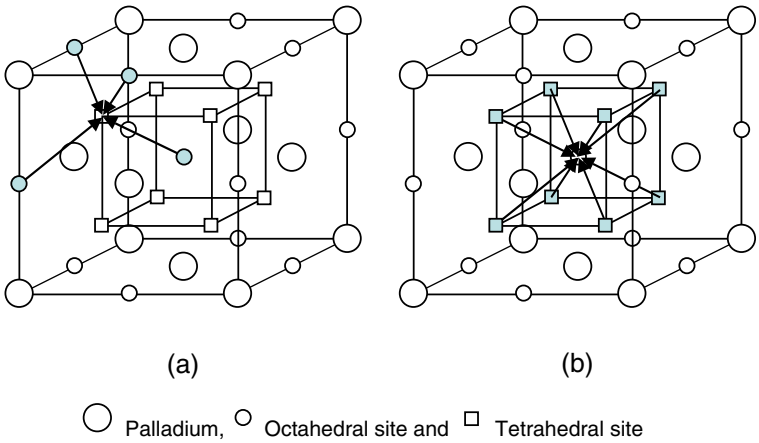

Figure 2. Tetrahedral condensation (a) and octahedral condensation (b); deuterons sit at octahedral sites for PdD and tetrahedral sites for PdD2 as local full or overloading condition.

Then cluster formation probabilities for 2D, 3D, and 4D "atomic" clusters were roughly evaluated, as shown in Fig. 1. This process of tetrahedral condensation is shown in Fig. 2a. This transient process of deuteron condensation at T-sites was considered [30,31] to be realized by squeezing many 4d-shell electrons of Pd atoms, which were quasi-free in the conduction band of Pd lattice. A two-dimensional view of this squeezing motion of deuterons and electrons into T-sites is shown in Fig. 3. Since many number of Pd atoms (more than eight), deuterons (four), and electrons (more than eight) are involved in this condensation process, an orthodox way of quantum mechanical treatment is to solve many coupled time-dependent Schroedinger equations with the potentials of three components, i.e., periodic atomic potential, Coulomb repulsive potential and nuclear strong interaction potential, in order to obtain deuteron cluster fusion rates. Of course this is a difficult task of computation.

For the treatment of zeroth order approximation, we adopted the model of strong coupling of phonons (D-harmonic oscillators) and 4d-shell electrons by D-plasma oscillation in PdDx lattice, and drew time-dependent behavior of periodic potentials which would have a transient deep potential hole (see Fig. 3 of Ref. [31]). We referred –80 eV for the depth of hole from Preparata's work [41]. In the next section, we will show the depth of hole is much deeper as –260 to –20 keV depending on the generation of transient Cooper-like pairs and/or quadruplet-coupling and octal coupling of electrons with anti-parallel spins. When a transient deep potential hole is born, e.g., four deuterons with four electrons are strongly attracted to the hole, namely at focal point (T-site in TRF case), and will accelerate to make a condensed cluster of deuterons within less than 1 pm-radius spherical domain. If we can calculate cluster fusion rates in a steady deep hole, we may convert it to time-averaged one, approximately by multiplying relative ratio of time-window for existence time of deep hole compared to plasma oscillation period, which is in the order of 10 fs. This is the way that we will extend the theory in the next section to make quantitative analysis. The EQPET model treat this by starting with assumption that total electronic wave function in transient deuteron cluster with electrons can be expanded by the linear combination of wave functions for transient molecular states like dde (namely D_2^+), ddee (D_2 molecule), dde* and dde*e* with transiently Bosonized electronic quasi-particle e* [48,49].

The INFN Frascati group of Celani et al. reported [42] very interesting and important results showing local superconductivity trend for over-D-loaded (D/Pd > 1) thin Pd wire in electrolysis. They reported resistance of wire became almost zero for 10–20 min interval and then quenched to normal resistance value of PdDx ($x = 0.7$). They also reported frequent observation of reduced resistance ratios R/R_0, probably showing tiny local superconductivity.

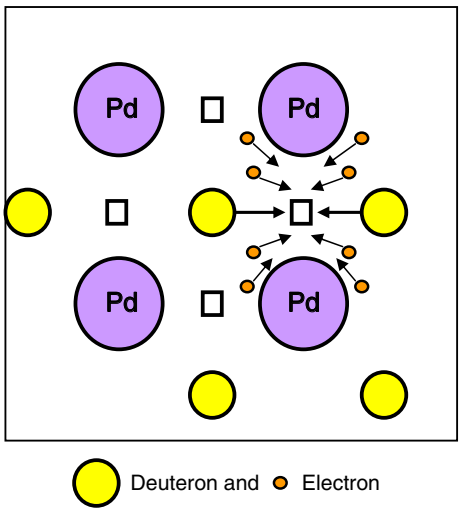

Figure 3. Squeezing of 4d-shell electrons (small circles) to focal point (T-site) of PdDx lattice.

Now we have to notify that PdDx is superconductivity material at low temperature less than 80 K, and over-D-loading ($x > 1$) will be the indication of the trend.

Recently Lanzara et al. published a paper in Nature [43] about observation of quasi-particle generation in high-T_c superconductor hole-doped copper-oxide, by means of angle resolved photo-electron emission spectroscopy. From two-peaked spectral data, they estimated about 1 ps lifetime for the electron quasi-particles (like Cooper pair). It is going to be clear that high-T_c superconductivity is induced by the generation of transient quasi-particle of electrons.

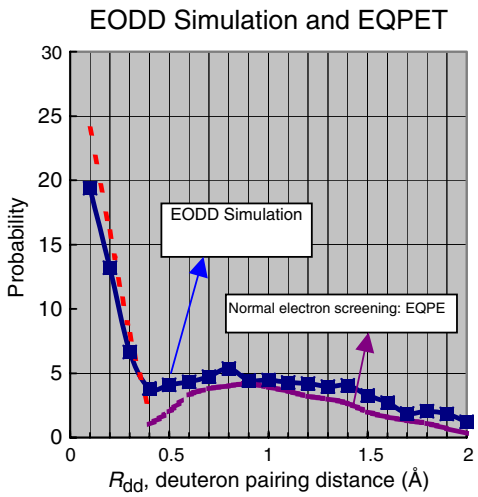

Figure 4. Transient electronic screening effects by EODD simulation [33] and EQPET [48], the lower R_{dd} component (broken line) is described by transient quasi-particle expansion.

This is anyway "transient bosonization" of electrons (fermions). We know that usually, the Pauli exclusion principle rules fermions (electrons) to block enhancement of screening of d–d Coulomb repulsive force. However, miracle of superconductivity may happen and the similar situation for generation of transient electronic quasi-particles will be true for deuteron fusion in condensed matter, by much localized transient bosonization, as we show in the next section.

The famous Japanese book of Solid State Physics [44] teaches us on superconductivity that: "behavior of charged particle in metal is well described by treating the interactions between plasma oscillation, phonons, free electrons, and shielded mutual interaction. Coupling between electron-system and phonon-system is the reason to generate superconductivity. Electron–electron interaction via phonon induces attractive force in the vicinity of Fermi surface, which compensates the shielded Coulomb repulsive force. The electron pair ($\mathbf{k}\uparrow, -\mathbf{k}\downarrow$), Cooper pair is selectively generated and annihilated in the strongly coupled state." The coherent range of Cooper pairs are regarded very long as greater than 100 nm for macroscopic superconductivity. We are going on the similar track for assuming electronic quasi-particles, but we are conceiving transient molecular states with single-particle-like e^*. Two 1S- electrons in D_2 molecule have opposite spins in each other and mutual distance of electrons is about 0.1 nm. When one of electrons gets opposite momentum from outside interaction (for instance, by phonon–electron coupling and scattering in condensed matter), Two 1-S electrons may make a transiently Bosonized state (quasi-particle) with far less mutual distance than 0.1 nm and hence e^* can be approximately treated as a single particle. So that, we do not necessarily require superconductivity condition in rather macroscopic domain, but do require localized microscopic order to generate transient electronic quasi-particle states with deuteron cluster.

Kirkinskii and Novikov [33] proposed the Electron Orbital Deformation Dynamics (EODD) model to treat the lattice dynamics in similar system as shown in Fig. 3. The EODD method is a kind of Monte–Carlo Molecular Dynamics calculation taking into account deformation of 5s + 4d shell electron-orbits by approach of two counter deuterons. They estimated the probability distribution of minimal pairing distances R_{dd} of deuterons, which showed a broadly peaked distribution in 0.5–2 Å region, probably reflecting minimum potential positions 1.1 and 0.7 Å, respectively, for dde and ddee (D_2) molecular states, and very interestingly steeply increasing component in lower R_{dd} region less than 0.2 Å as shown in Fig. 4. EODD simulation has given about 19% probability to have closely packed transient d–d pairs with less than 0.1 Å (even in 0.01 Å region) inter-nuclear distance which gives very enhanced fusion rate as 10^{-10} f/s/pair level [33]. It is regarded that this component realizes visible "cold fusion events." From our EQPET calculations [48] as reviewed in the next section, this component can be described as linear combination of Transient Electronic Quasi-Particle (TEQP) components, namely dde*(2,2), dde*(2,2), e*(2,2), dde*(4,4), and dde*(8,8), etc., as transient molecular states of EQPET theory [48]. This means that, when we will get three-dimensional EODD simulations for TRF and ORF systems, we will be able to fit the result with the combination of normal electron (dde + ddee) and transient quasi-particle screening (dde* + dde*e*) components. This should give the basis of EQPET.

3. EQPET Model

3.1. Basic Formulation

Some of MDx materials have been studied for high-temperature superconductivity trend, as typical significant effect was reported by Celani et al. [42] for full and over-loaded PdDx ($x = 1$ or > 1). The physics of low-temperature superconductivity is believed to be established by the BCS theory [50] and the physics of high-T_c (critical temperature) superconductivity has been studied, albeit not established yet, by extension of the BCS theory and Bogoliubov theory for electronic quasi-particle generation.

Deuteron at O-site (or T-site) in PdDx lattice behaves as an harmonic oscillator with phonon frequency ω_q. And motion of electrons is treated with plasma oscillation with frequency $\omega$of the lattice system with many electrons, deuterons and metal-atoms (e.g., Pd). By electron–phonon scattering, momentum $\mathbf{q} = \mathbf{k}–\mathbf{k}'$ is carried by phonon and two electrons having opposite momentum and spin may be born to generate a Cooper pair ($\mathbf{k}\downarrow$, $–\mathbf{k}\uparrow$) as an electronic

quasi-particle, due to attractive force to compensate repulsive force of Coulomb interaction, in the phonon–electron coupled motion. Shielded Coulomb interaction potential is given [50] as:

$$V(q,\omega) = 4\pi e^2/(q^2 + {k_s}^2) + (4\pi e^2/(q^2 + {k_s}^2))({\omega_q}^2/(\omega^2 - {\omega_q}^2)) \tag{3.1}$$

$$= (4\pi e^2/(q^2 + {k_s}^2))(\omega^2/(\omega^2 - {\omega_q}^2)), \tag{3.2}$$

where $1/k_s$ is the screening distance for Fermi gas. The first term of Eq. (3.1) shows normal Coulomb repulsive potential between electrons, and the second term shows phonon-mediated interaction. As clearly seen by Eq. (3.2), the potential becomes negative (attractive) if $\omega < \omega_q$. This is a driving force to produce Cooper pairs. When two deuterons with electrons are squeezing from opposite directions to T-site (or O-site) under the TRF (or ORF) transient condensation [51], the condition of opposite momentum and spin for two electrons can be naturally fulfilled (see Fig. 3). However, directions of deuterons in TRF and ORF condensation are not ideally 180° opposite, so that momentum transfer by phonon-electron coupling makes conditioning for transient Cooper-like pairs. Actually, quasi-particle state may be generated by formation of orthogonally coupled two D_2 molecules to associate electronic quadruplet, as we show in Section 4.

Effective mass m^* and effective charge e^* of Cooper-like pair can be approximately given [50] as $m^* = 2m_e$ and $e^* = 2e$. Microscopic Cooper-like pair with short life around lattice focal point can be regarded as single particle, as discussed, with mass $2m_e$ and charge $2e$. Hence we label Cooper-like pair as $e^*(m^*/m_e, e^*/e) = e^*(2,2)$. Cooper-like pair is the s-wave pairing of two electrons with opposite momentum and spin. To explain high-Tc superconductivity, generation of unconventional pairing (e.g., d-wave pairing) and very heavy fermions (several hundred times mass of electron) have been proposed (see Chapter 9 of Ref. [50]), albeit reaching no consensus yet. By considering higher order pairing (s-wave) of binary e*(2,2) quasi-particles to generate a quadruplet-coupling e*(4,4) and moreover octal coupling e*(8,8) by binary e*(4,4) quasi-particles, we may treat the state of high-T_c superconductivity, instead of assuming heavy fermions (electrons), as we see later. "Bosonized" electron wave function Ψ_N for N-electrons system in MDx lattice will be approximated, as discussed in the previous section, by a linear combination of normal electron wave function $\Psi_{(1,1)G}$ and quasi-particle wave functions $\Psi_{(2,2)G}$, $\Psi_{(4,4)G}$, and $\Psi_{(8,8)G}$ as;

$$|\Psi_N\rangle = a_1|\Psi_{(1,1)G}\rangle + a_2|\Psi_{(2,2)G}\rangle + a_4|\Psi_{(4,4)G}\rangle + a_8|\Psi_{(8,8)G}\rangle. \tag{3.3}$$

Here we consider each wave function is further a linear combination of wave functions for single and double electrons or e^*. This may be called the quasi-particle expansion of total electronic wave function. Here suffix G denotes ground state. For MDx system, the normal electron wave function $|\Psi_{(1,1)G}\rangle$ coupled with phonon may be given by a Bloch function with lattice period x_l, combined with harmonic oscillator motion for D, in one-dimensional case; Using Hermite polynomial H_n,

$$|\Psi_{(1,1)G}\rangle = \sum C_l \exp(\mathrm{i}l(x - x_l)) \sum \exp(-\alpha_n(x - x_l)^2) {H_n}^2({\alpha_n}^{1/2}(x - x_l)). \tag{3.4}$$

The ground state BCS wave function is defined as,

$$a_1|\Psi_{(1,1)G}\rangle + a_2|\Psi_{(2,2)G}\rangle = \prod(u_k + \nu_k C^*_{k\uparrow} C_{-k\downarrow}|\Psi_0\rangle, \tag{3.5}$$

where $|\Psi_0\rangle$ denotes vacuum, u_k is the un-occupied wave function of Cooper-like pair and ν_k is the occupied wave function of Cooper-like pair; hence ${u_k}^2 + {\nu_k}^2 = 1$ is the normalization condition. ${C^*}_{k\uparrow}$ and $C_{-k\downarrow}$ are generation and destruction operators, respectively.

We may define production operator C^*_{2k} and destruction operator C_{2k} for bosonized (spin zero) e*(2,2) to generate quadruplet-coupling e*(4,4) as,

$$a_1|\Psi_{(1,1)G}\rangle + a_2|\Psi_{(2,2)G}\rangle + a_4|\Psi_{(4,4)G}\rangle = \prod(u_{2k} + \nu_{2k}C^*_{2k}C_{2k})|\Psi_0\rangle \tag{3.6}$$

with ${u_{2k}}^2 + {\nu_{2k}}^2 = 1$ for normalization. Wave function for e*(8,8) is similarly defined.

To evaluate coefficients a_1, a_2, a_4, and a_8, we may apply the variational method with evaluating the BCS Hamiltonian (see Chapter 3 of Ref. [50]);

$$H = \Sigma\Sigma\varepsilon_k n_{k\sigma} + \Sigma\Sigma V_{kl}{C^*}_{k\uparrow}C^*_{-k\downarrow}C_{-l\downarrow}C_{l\uparrow} \tag{3.7}$$

and

$$\delta\langle{\Psi_N}^*|H|\Psi_N\rangle = 0. \tag{3.8}$$

The above equations are just for formality, and we need further extension to substantiate the problem. However, essential components of the problem can be analyzed as follows.

3.2. Screening Effect and Fusion Rates

For the time-window of potential deep hole [31,51], effective (time-averaged) screening potential, for a d–d pair in a transient D-cluster of 4–8 deuterons for TRF and ORF condition [51], can be defined by a screened potential of quasi-particle complex;

$$V_s(R) = b_1V_{s(1,1)}(R) + b_2V_{s(2,2)}(R) + b_4V_{s(4,4)}(R) + b_8V_{s(8,8)}(R). \tag{3.9}$$

Here R is the inter-nuclear distance of a d–d pair and $V_s(m^*/m_e, e^*/e)(R)$ is the screened potential for a dde(m^*/m_e, e^*/e) molecule, for (m^*/m_e, e^*/e) = (1,1), (2,2), (4,4), and (8,8). Time-averaging treatment for transient D-cluster condensation with electrons including transient quasi-particles is transferred here to coefficients b_1–b_8. By definition, we need to satisfy the following normalization condition.

$${b_1}^2 + {b_2}^2 + {b_4}^2 + {b_8}^2 = 1. \tag{3.10}$$

For a dde or dde* molecule (one quasi-particle approximation) within the short time-interval of D-clustering, wave function of a d–d pair (2D) is given by the solution of the following Schroedinger equation:

$$(-h^2/8\pi\mu)\nabla^2X(R) + (V_n(R) + V_s(R))X(R) = EX(R) \tag{3.11}$$

with nuclear potential $V_n(R)$ for strong interaction and reduced deuteron mass μ.

By Born–Oppenheimer approximation, we assume as,

$$X(R) = X_n(R)X_s(R). \tag{3.12}$$

Overlapping rate of $X(R)$ at $R = r_0$ gives estimation of d–d fusion rate λ_{2d} as:

$$\begin{aligned}\lambda_{2d} &= G|X(R)|^2{}_{R=r_0} \\ &= G|X_n(R)|^2{}_{R=r_0}|X_s(R)|^2{}_{R=r_0},\end{aligned} \tag{3.13}$$

where G is the scaling constant and r_0 is given to be 5 fm considering deuteron radius plus charged-pion exchange range (about 2 fm) at contact surface configuration of the moment of strong interaction for d–d fusion reaction.

Using WKB approximation for the barrier ($V_s(R)$) penetration probability,

$$|X_s(R)|^2{}_{R=r_0} = \exp(-2\Gamma_n(E_d)); \qquad \text{Barrier Factor (BF)}, \tag{3.14}$$

where E_d is the relative deuteron energy and Γ_n is Gamow integral for a d–d pair in D-cluster (n-deuterons with electrons) that is defined as:

$$\Gamma_n(E_d) = (2\mu)^{1/2}/(h/\pi)\int_{r_0}^{b}(V_s(R) - E_d)^{1/2}dR. \tag{3.15}$$

Using astrophysical S-factor for strong interaction,

$$G|X_n(R)|^2{}_{R=r_0} = vS_{2d}(E_d)/E_d. \tag{3.16}$$

Consequently we can approximately define tow-body fusion rate as:

$$\lambda_{2d} = (vS_{2d}(E_d)/E_d)\exp(-2\Gamma_n(E_d)). \tag{3.17}$$

We can estimate Gamow integral for dde* molecule, by solving Schroedinger equation to obtain screened potential $V_s(m^*/m_e, e^*/e)$ and evaluate the corresponding Gamow integral $\Gamma_n(m^*/m_e, e^*/e)$ by, for each electron and quasi-particle molecular state,

$$\Gamma_{n(m^*/m_e,e^*/e)}(E_d) = (2\mu)^{1/2}/(h/\pi)\int_{r_0}^{b}(V_{s(m^*/m_e,e^*/e)}(R) - E_d)^{1/2}d(R). \tag{3.18}$$

Using Eqs. (3.15) and (3.9) with condition of $V_s(R) \gg E_d$; $R < b$, and considering that b-parameter becomes independent own value for each quasi-particle, we can approximately obtain:

$$\Gamma_n(E_d) = b_1\Gamma_{n(1,1)}(E_d) + b_2\Gamma_{n(2,2)}(E_d) + b_4\Gamma_{n(4,4)}(E_d) + b_8\Gamma_{n(8,8)}(E_d). \tag{3.19}$$

To estimate coefficients $b_1 - b_8$, we have to solve coupled channel Schroedinger equations of normal electrons, Cooper pairs, quadru-couplings, e*(8,8) by Eqs. (3.3)–(3.8), to evaluate first relative state densities of a_1–a_8. This is a hard task to do in future. For some simplified cases as in Section 4, we have estimation.

Screened potentials $V_s n(m^*/m_e, e^*/e)(R)$ were calculated for dde* molecular states using extended solutions for dde state given in a text of quantum mechanics by the well-known technique of variational method [45] as:

$$V_{s(m^*/m_e,e^*/e)}(R) = V_h + e^2/R + (J + K)/(1 + \Delta), \tag{3.20}$$

where the Coulomb integral J, the exchange integral K, and the non-orthogonal integral Δ are given as [45]:

$$J = Z(e^2/a)[-1/y + (1 + 1/y)\exp(-2y)], \tag{3.21}$$

$$K = -Z(e^2/a)(1 + y)\exp(-y), \tag{3.22}$$

$$\Delta = (1 + y + y^2/3)\exp(-y). \tag{3.23}$$

With

$$Y = R/a, \tag{3.24}$$

$$a = a_0/Z/(m^*/m_e) \tag{3.25}$$

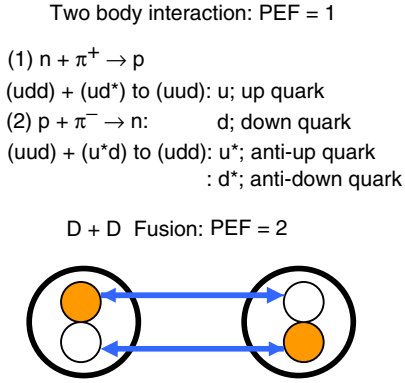

Figure 5. PEF factor to scale strong interaction for nuclear fusion.

with a_0= 0.053 nm (Bohr radius) and $Z = e^*/e$.

We also solved an atomic de* system to obtain ground state energy $V_h$as:

$$V_h = -13.6Z^2/(m_e/m^*). \tag{3.26}$$

For dde*e* molecule state with double electrons or e* s, we also extend the solution for ddee given in the text [45] and we have obtained screened potential function $V_{se^*e^*}$ as:

$$V_{se^*e^*}(R) = 2V_h + e^2/R + (2J + J' + 2\Delta K + K')/(1 + \Delta^2). \tag{3.27}$$

Here the cross-Coulomb integral J' and cross exchange integral K' are given as:

$$J' = (Z^2e^2/a)(1/y - \exp(-2y))(1/y + 11/8 + 3y/4 + y^2/6), \tag{3.28}$$

$$\begin{aligned} K' = {} & (Z^2e^2/5/a)[-\exp(-2y)(-25/8 + 23y/4 + 3y^2 + y^3/3) \\ & +(y/6)((0.5772 + \log y)\Delta^2 \\ & +(\Delta')^2E_i(-4y) - 2\Delta\Delta' E_i(-2y))] \end{aligned} \tag{3.29}$$

with

$$\Delta' = \exp(-y)(1 - y + y^2/3), \tag{3.30}$$

$$E_i(y) = -\int_0^{\exp(-y)} (1/\log x)\,dx. \tag{3.31}$$

We should note here that in these equations corrections were made for mistakes in the text book [45].
For fusion rates of multi-body (nD) reactions in a D-cluster was defined [51] as:

$$\lambda_{nd} = [vS_{nd}(E_d)/E_d]\exp(-n\Gamma_n(E_d)). \tag{3.32}$$

Here we have assumed that a simultaneous multi-body fusion process can be approximately treated by the very fast sequential process, e.g. (D + (D + (D + D))) of cascade two-body reactions for intermediate states [51]. And we have made estimate for $S_{nd}(0)$ values by using empirical scaling of known $S(0)$-values of H + D, D + D, and D + T fusion

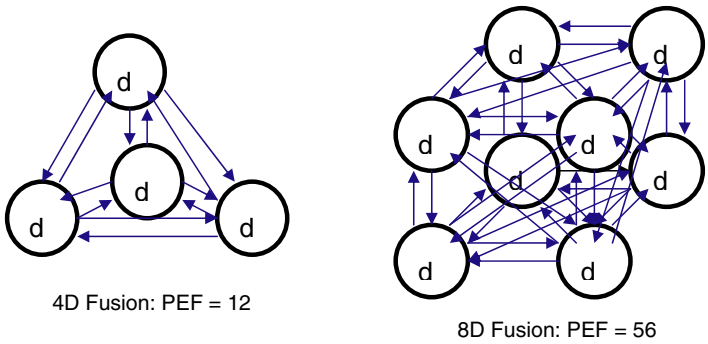

Figure 6. Charged pion exchange for 4D TRF and 8D ORF condensations.

reactions extrapolating up to unknown multi-body $S_{nd}(0)$ values as a function of pion exchange force (PEF) numbers for equilaterally symmetric configuration of strong interaction (Π^+ and Π^- exchange) in TRF and ORF condensation [51]. The second term of Eq. (32) gives multi-body barrier factor.

3.3. TRF-and ORF-Resonance of Strong Interaction

To make an empirical scaling law of effective S-values (astrophysical *S*-values) for two-body and multi-body deuteron-related fusion cross-sections, PEF parameter which is a relative measure of contact surface area of pion exchange has been defined [17,30,31,32]. The larger is the contact surface area, the larger is fusion cross section. The basic idea is illustrated in Fig. 5. Since the neutral pion exchange corresponds to scattering process between nucleons, exchange of charged pions (positive and negative) is regarded to be attributed to nuclear fusion. Single charged pion exchange between neutron and proton is defined as PEF = 1 as scaling factor of fusion-strong-interaction. By using quarks instead of pions, we obtain same results. So, we can evaluate degree of strong interaction for fusion by using charged pion exchange (Yukawa model). Using this relative PEF unit, pion exchange for D + D fusion is counted as PEF = 2. We extend the idea to others and obtain PEF = 3 for D + T, PEF = 6 for D + D + D (3D), PEF = 12 for 4D, and PEF = 56 for 8D, as illustrated interactions for 4D equilateral tetrahedron and 8D equilateral octahedron (deuteron site at face-center)

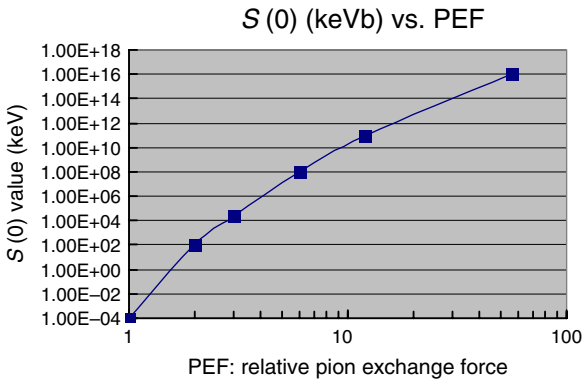

Figure 7. Speculative extrapolation of effective S-values for multi-body fusion.

in Fig. 6. TRF condensation can realize equilaterally tetrahedral configuration in charged pion exchange with same inter-deuteron distance for each deuteron: namely best condition to enhance effective contact surface of pion cloud to form virtual compound ^{8}Be* as intermediate fusion product which breaks up shortly to two α-particles. Equilateral triangle configuration for 3D fusion is next good.

For deuteron clusters of 5D, 6D, and 7D, symmetric pion-exchange condition is geometrically so violated that local 4D cluster-component may have geometrically symmetric tetrahedral configuration and resultantly 4D fusion becomes selective. For 8D cluster, symmetric condition recovers: however, interaction distances are identical and shorter to three neighboring deuterons, but identical and longer to remained four deuterons. Therefore, PEF = 56 for 8D fusion is considerably overestimation: this may mean that degree of strong interaction for fusion should be saturated for high number of nucleons. This looks true when we see changing trend of S-values of reactions between deuteron and higher mass-nuclei (^{6}Li,^{10}Be,^{12}C, and so on). However intrinsic difference, for example, between d + ^{6}Li fusion and TRF 4D fusion (both produces intermediate virtual compound ^{8}Be*) is that about half (3) of nucleons (neutron and proton) of ^{6}Li nucleus sphere are shielded with other half (3) of nucleons to make direct charged pion exchange in contact surface, while TRF 4D fusion realizes completely symmetric exchange without shielding affect. Because of above-discussed reason, we can expect resonantly strong enhancement of fusion cross sections (effectively S-values) for 3D, 4D, and 8D fusion. In addition, because of high PEF values, 4D TRF and 8D ORF may have strongest "resonance" condition. We may say that 3, 4, and 8 are "magic numbers" for deuteron cluster fusion.

Using thus counted PEF values for scaling parameter, we have obtained extrapolated S-value plot for 4D TRF and 8D ORF reactions based on known S-values of H + D, D + D, and D + T reactions, as shown in Fig. 7. We have obtained rough values of 10^{12} keV barn for 4D TRF and 10^{16} keV barn for 8D ORF, which are extremely large values compared to those of conventional two-body fusion.

Using Eq. (3.32) with estimated S-values and BF values, we have got fusion rates per cluster for 2D, 3D, 4D, and 8D fusion. Results (Table 1) will be shown in the next section.

3.4. Numerical Results and Discussions

We have done calculations of screening potentials of dde* and dde*e* molecules with heavy electrons (fermions) for $m^{*} = 1m_{e}$ to $208m_{e}$ (muon), to make comparison with screening effects by quasi-particles of e*(2,2), e*(4,4), and e*(8,8).

Figure 8 shows the effect of first-step bosonization, namely generation of Cooper-like pair, compared with screened potential of D_2 molecule (ddee system) which has minimum transient potential hole (–10.6 eV) at $R_{e} = 0.07$ nm. Value

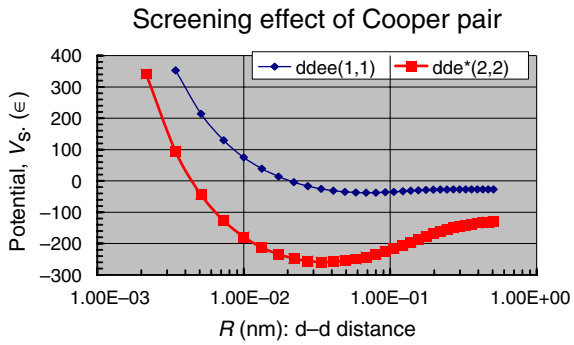

Figure 8. Screening effect of Cooper-like pair for dde* molecule, compared with D_2 molecule.

Table 1. Barrier-Factors (BF) and Fusion-Rates (FR in f/s/cl), by transient quasi-particle screening

$(m^*/m_e, e^*/e)$	2D BF (FR)	3D BF (FR)	4D BF (FR)	8D BF (FR)
(1,1)	10^{-125} (10^{-137})	10^{-187} (10^{-193})	10^{-250} (10^{-252})	10^{-500} (10^{-499})
(2,1)	10^{-53} (10^{-65})	10^{-80} (10^{-86})	10^{-106} (10^{-108})	10^{-212} (10^{-211})
(2,2)	10^{-7} (10^{-20})	10^{-11} (10^{-17})	10^{-15} (10^{-17})	10^{-30} (10^{-29})
(4,4)	3×10^{-4} (3×10^{-16})	10^{-5} (10^{-11})	10^{-7} (10^{-9})	10^{-14} (10^{-13})
(4,4)b	4×10^{-1} (4×10^{-13})	2×10^{-1} (2×10^{-7})	10^{-1} (10^{-3})	2×10^{-2} (2×10^{-1})

of b-parameter for Gamow integral is approximately given by the zero-potential crossing distance; which is essential to barrier penetration calculation. Value of b-parameter moves from 20 pm for D_2 molecule to 4 pm for dde*(2,2) Cooper-like pair. This is drastic effect: as given in Table 1, barrier factor increases from 10^{-50} with $\lambda_{2d} = 10^{-63}$, for D_2, to 10^{-7} with $\lambda_{2d} = 10^{-20}$, for Cooper-like pair dde*. Assuming macroscopic production density of 10^{20} (1% of D-density in PdDx, $x > 1$) Cooper-like-pairs/cm^3, we obtain D + D (2D) fusion yield of 1 f/s/cm^3, that is, so called Jones level and lowest countable level by usual neutron detectors. We can say that Cooper-like pair can make great effect to drastically enhance d–d fusion rate in MDx systems. This may be the first clear theoretical evidence that "cold fusion" exists. Cooper-like pair generates transient deep hole (–256 eV) to attract deuterons and initiate D-cluster condensation [51].

In Fig. 9**,** dde* potentials are compared between Cooper-like pair e*(2,2) and a heavy fermion e*(10,1). Screening effects are comparable. In Fig. 10, comparison is also made for quasi-particle of quadruplet-coupling e*(4,4) and very heavy fermion e*(100,1), to show comparable effects between the two.

Where $E_d = 0.22$ eV is assumed, which is the $n = 3$ phonon excited state of D in PdDx lattice with $h\omega_0 = 64$ meV and $E_d = (n+1/2)h\omega_0$. And (0,0): bare dd reaction, (1,1): dde- molecule, (2,1): dde* with heavy electron, (2,2): dde* with Cooper pairing, (4,4): dde* with quadru-coupled electrons, (4,4)*b*: dde* with binary quadru-coupled electrons, namely (8,8)

Muon has $m^* = 208m_e$, so that binary Cooper-like coupling, namely quadruplet-coupling e*(4,4) works as strongly as muon for D + D fusion induction. We can say that the very heavy fermion model for high-T_c superconductivity can be replaced with the binary bosonization of two Cooper pairs to make e*(4,4) quadruplet-coupling. Depth of the transient deep hole [45,51] by e*(4,4) generation is so large as –2460 eV, that can strongly attract surrounding deuterons

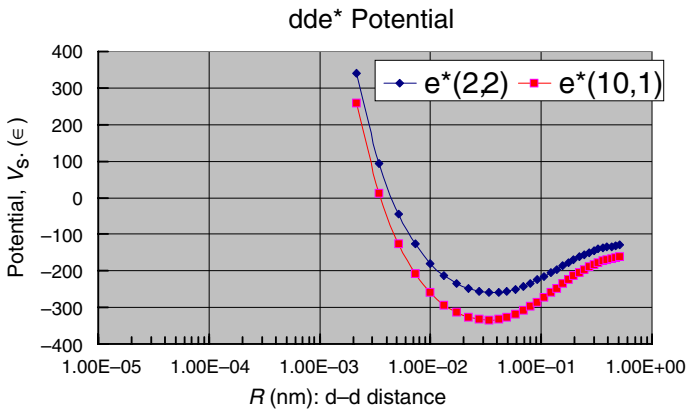

Figure 9. Comparison of screened potentials between Cooper-like pair and mass-10 heavy fermion..

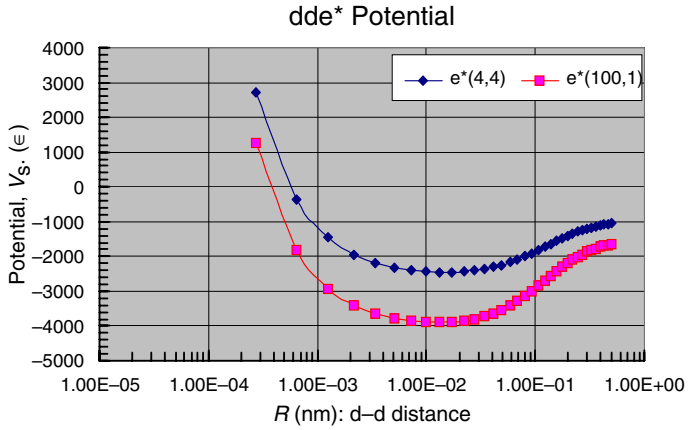

Figure 10. Comparison of screened potentials between e*(4,4) quasi-particle and mass-100 heavy fermion.

with electrons to make TRF and ORF condensations at focal points. Value of *b*-parameter for dde*(4,4) is about 0.5 pm (500 fm), to enhance D + D barrier factor to 3×10^{-4}, and 10^{-5} for 3D and 10^{-7} for 4D multi-body fusion, of which fusion rates (microscopic) are 10^{-16}, 10^{-11}, and 10^{-9}, respectively, for 2D, 3D, and 4D fusion. If we assume D-cluster density of 10^{20} cl/cm^3, we obtain fusion yield (f/s/cm^3) of 10^4, 10^9, and 10^{11}, respectively, for 2D, 3D, and 4D fusion, which are already "miracle" values to meet with major claims of "cold fusion" experiments. 8D fusion yield becomes significant level as 10^7 f/s/cm^3.

Figure 11 shows the bosonization effect of binary e*(4,4) quasi-particles, namely octal-coupling e*(8,8). When this extreme condition is realized as ORF (see Section 4), we have *b*-parameter of 70 fm within which domain deuterons can approach as classical particles to make very condensed D-cluster for very enhanced strong interaction between 3, 4, and 8 resonant deuterons [49,51] simultaneously (within Heisenberg uncertainty) as previously discussed. This screening effect of binary e*(4,4)b, namely e*(8,8) is comparable to that of heavy fermion e*(300,1). Depth of transient deep hole by e*(8,8) is very large as –20.6 keV. When we recall that the first-step goal of DT plasma temperature in TOKAMAK device is around 10 keV, e*(8,8) can provide comparable "acceleration condition," however microscopically "coherent" way. Thus, 8D fusion can be winner of D-cluster fusion as discussed previously [48,51]. 8D fusion emits two high-energy (47.6 MeV) ^{8}Be-particles, which can induce secondary capture reactions to make transmutation with mass-8 and charge-4 increment, as recently claimed by MHI experiment [27].

3.5. Discussions for Nuclear Products

In the TRF or ORF condensation process, we conceive that there happens a competing process of d + d and multi-body deuteron fusion reactions as follows.

(1) 2D → n + ^{3}He + 3.25 MeV, p + T + 4.02 MeV,
(2) 3D → Li^{6*} → t + He^3 + 9.5 MeV,
(3) 4D → Be^{8*} → 2 × He^4 + 47.6 MeV,
(4) 5D → B^{10*} (53.7 MeV),
(5) 6D → C^{12*} (75.73 MeV),
(6) 7D → N^{14*} (89.08 MeV),
(7) 8D → O^{16*} (109.84 MeV) → 2 × Be^8 + 95.2 MeV.

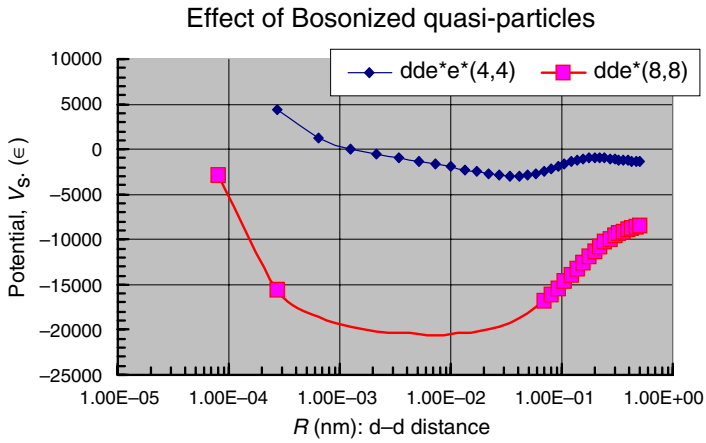

Figure 11. Bosonization effect of e*(4,4) binary quasi-particles, on screened potential.

Nuclear products of 4D fusion was discussed in detail in Ref. [31]. Here we simply assume that two ^{4}He (α-particles) with 23.8 MeV kinetic energy emit into 180° opposite directions each other, and slow down in PdDx lattice by ionization and knock-on process. 23.8 MeV α-particle has very small cross section to ionize K-shell electrons of Pd (therefore there are no emission of K-X-rays of about 22 keV), but has considerable cross sections for L-and M-shell electrons (therefore we see small component of L-and M-X-rays in several keV region). Largest component of X-rays in continuous region less than 3.5 keV is attributed to slowing down of convey electrons by α-particles.

Possible nuclear product of 8D fusion via intermediate virtual excited state of ^{16}O* is shown in Table 2. There are so many exit channels. However, we conceive only two channels are predominant. ^{16}O is a typical α-clustered nucleus. Ground state of ^{16}O is composed of four equilaterally tetrahedral α-particles in combination, and at highly excited state in collective oscillation the nucleus is deformed into two cases; (1) deformation with two ^{8}Be particles, or (2) deformation with

α-Particle and ^{12}C nucleus. Emitted ^{8}Be particles by 8D fusion have very high-kinetic energy of 47.6 MeV which is well over Coulomb barrier height of interaction with neighboring heavier nuclei to make secondary nuclear reaction as capture and fission. ^{8}Be has very short life time as 6.7×10^{-17} s and decays shortly to two ^{4}He, but has enough time to make several interactions with neighboring nuclei in the range.

Nuclear products from 3D fusion were already discussed in other reports [30,31]. 2D and 3D fusion may become minor branches in TRF and ORF deuteron-cluster condensations. This situation is quite in contrast to conventional stochastic two-body fusion reactions. Electron quasi-particles and multi-body resonance fusion play miracle role in condensed matter, which contain fully deuterons and resultantly may induce local superconductivity.

3.6. Explanation to Key Experimental Claims

Explanation to ^{4}He major products in correlation with excess heat has been already mentioned in the above discussions. The reason why we see very scarce neutrons in “cold fusion” experiments is also clear by the competition story of 2D, 3D, 4D and 8D fusion rates since 4D and 8D fusion can be winner of the competition under the strong screening and attraction by transient electronic quasi-particle generation.

The extraordinary result [24–26] of Iwamura et al. reporting mass-8-and-charge-4 increased transmutation is now on discussion. On surface of thin Pd layer they made deposit of thin test element (Sr or Cs). Back side of supporting thick

Table 2. Decay channels of 8D fusion

$8D \rightarrow {}^{16}O^*$
$\rightarrow n + {}^{15}O + 94.16$ MeV
$\rightarrow p + {}^{15}N + 97.70$ MeV
$\rightarrow d + {}^{14}N + 89.09$ MeV
$\rightarrow t + {}^{13}N + 84.79$ MeV
$\rightarrow {}^{3}He + {}^{13}C + 87.03$ MeV
$\rightarrow {}^{4}He + {}^{12}C + 102.66$ MeV
$\rightarrow {}^{6}Li + {}^{10}B + 78.95$ MeV
$\rightarrow {}^{7}Li + {}^{9}B^* + 77.76$ MeV
$\rightarrow {}^{7}Be^* + {}^{9}Be + 77.97$ MeV
$\rightarrow {}^{8}Be^* + {}^{8}Be^* + 95.2$ MeV

(0.1 mm) Pd zone was evacuated, and front side of film was filled with D_2 gas. They realized constant D-permeation (1 cm^3/min) through the multi-layered film, which would keep over-loading condition PdDx ($x > 1$) within the first thin zone of Pd, which is thought to be reaction-active zone. They observed the transmutation only in the case of existing CaO layer with D-flow; In cases of H-flow with CaO and D-flow without CaO, they observed no transmutation.

CaO zone enlarges gap of electron Fermi levels in the interface region of Pd and CaO, and same thing may happen in the interface of Pd and Sr or Cs test zone. Enlarged Fermi level gaps may help increase movement of free electrons which will enhance generation of Cooper-like pair or quadruplet-coupling of electrons, i.e., transient bosonization of electrons which would play drastic role of inducing deep potential holes to attract deuteron-clusters with electrons at focal points of T- and O-sites of regular PdDx lattice and some defect points in the interface. Local D-over-loading would have been generated. 4D TRF and 8D ORF, especially the latter was induced there to produce high energy ^{8}Be particles which would be captured by neighboring heavier nuclei as Sr or Cs to make the following transmutation reaction;

$$M(A, Z) + {}^{8}\mathrm{Be}\,(47.6\ \mathrm{MeV}) \rightarrow M(A + 8, Z + 4)^*(Ex) + KE. \tag{3.33}$$

A cartoon illustration of reactions is shown in Fig. 12. Since ^{8}Be particle with short life (unstable) is thought to be highly deformed as illustrated, we expect enhanced capture cross section by large contact surface exchanging charged pions with target heavy nucleus.

Coulomb barrier heights for reaction (3.33) are 22.5 MeV for M = Sr, and 30.1 MeV for M = Cs, which were calculated using effective contact distance for fusion as $R_f = R_1 + R_2 + \lambda$ with pion wave length λ, $R_1 = 1.2A_1^{1/3}$, $R_2 = 1.2A_2{}^{1/3}$. Possible products of reaction (3.33) for Sr and Cs are shown in Table 3. Excited energy E_x of

Table 3. Products of Be^8 absorption reaction

(1) ^{88}Sr + ^{8}Be (47.6 MeV) $\rightarrow$ ^{96}Mo*(53.43 MeV)	$\rightarrow$ ^{96}Mo($Ex.$)* + KE (deposit to lattice) or FP1 + FP2 + Energy :fission (many channels)
(2) ^{133}Cs + ^{8}Be (47.6 MeV) $\rightarrow$ ^{141}Pr*(50.47 MeV)	$\rightarrow$ ^{141}Pr(Ex)* + KE (deposit to lattice) or FP1 + FP2 + Energy :fission (many channels)

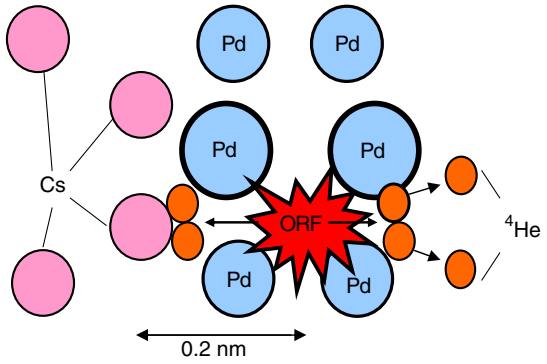

Figure 12. An imagination of 8D fusion and Be^8 capture.

intermediate compound nucleus Mo*(or Pr*) may distribute from 53.43 MeV (50.47 MeV for Pr) to 4.8 MeV (2.9 MeV for Pr) depending on the transferred energy to kinetic energy KE. Imagining liquid-drop like collision character of the reactions (3.33), most energy will be transferred to KE (Mo or Pr kinetic energy), which will make deposit to lattice vibration by heavy particle slowing down in condensed matter without emitting hard and soft X-rays. Thus, major part of experimental results can be explained by the present model. However, when E_x can be large enough to be over fission barrier (about 20 MeV for Mo, and 15 MeV for Pr), distributed mass- and Z-products may be produced. As a function of E_x, fission products distribution can be estimated by the selective channel scission theory [46,47]. Therefore, we need to know data of energy sharing between E_x and KE for reaction (3.33). This is unresolved problem and further study is expected.

4. Further Extension of EQPET Model

4.1. Deuteron Cluster Fusion

Model example of deuteron cluster fusion was proposed as the Tetrahedral Symmetric Condensation (TSC) and the Octahedral Symmetric Condensation (OSC) in PdDx lattice dynamics. As illustrated in Fig. 2, TSC may take place at locally full loaded PdD regions ($x = 1.0$), while OSC may happen much more difficultly at locally overloaded PdD_2 regions ($x = 2.0$). As discussed later on power level, we only need to require local density of 10^{-6} times (ppm order) of Pd density for the OSC condition, while much higher local density, e.g., 10% of Pd atomic density is required for the TSC condition. To generate electronic quasi-particle states, basic mechanism is thought to be the dynamic formation of quadruplet deuteron molecule, which is an *orthogonal coupling of two* D_2 *molecules*, as illustrated in Fig.13.

Three-dimensional motion of TSC can be converted to two-dimensional motion using momentum vector conversion [62]. A two-dimensional view of TSC is shown in Fig. 14. To minimize total energy of the system, charge neutral condensation in average of 4D cluster (four deuterons with alternately coupled four electrons with anti-parallel spins for counter-part electrons with reversed momentums) may cause the central point (T-site in this case) condensation from 4 O-sites of deuterons and 4-sites of electrons. Hence, transient condensate of electrons, namely quadruplet e*(4,4) may be formed at around the central T-site.

We assume a similar condition for the OSC motion, as illustrated in Fig. 15. When four electrons down-spins are happening to be arranged on upper half together with four electrons up-spins on lower half, averaged charge neutral condensation from 8 T-sites to the central O-site may become possible, to form 8D cluster with an octal-coupling state e*(8,8) of electrons at around the central O-site. This condition may realize super-screening for

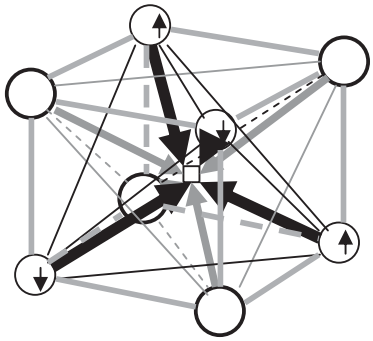

Figure 13. TSC, bigger circles for deuterons and smaller circles with arrow (spin) for electrons.

virtual d-d pairs in the 8D cluster, and 8D fusion rate can be calculated by the rapid cascade reaction model, i.e., D+(D+(D+(D+(D+(D+(D + D)))))) [60,62].

4.2. Advanced EQPET Model

A 4D cluster under TSC condition will cause 2D, 3D, and 4D nuclear fusion in competition, because the TSC state reflects the atomic level motion of deuterons in condensed matter and does not necessarily relate to 4D nuclear fusion reaction as strong interaction. In the same way, an 8D cluster causes the competition process of nuclear fusion reactions between 2D, 3D, 4D and 8D nuclear fusion reactions. We need therefore to define and estimate modal fusion rates to TSC and OSC processes [60]. Modal fusion rates are defined as:

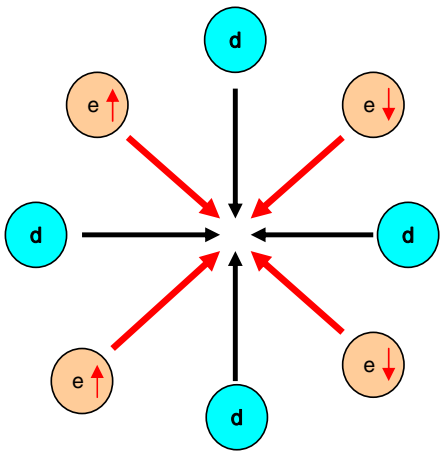

Figure 14. Two-dimensional view of TSC, plus charge for d, minus charge for e.

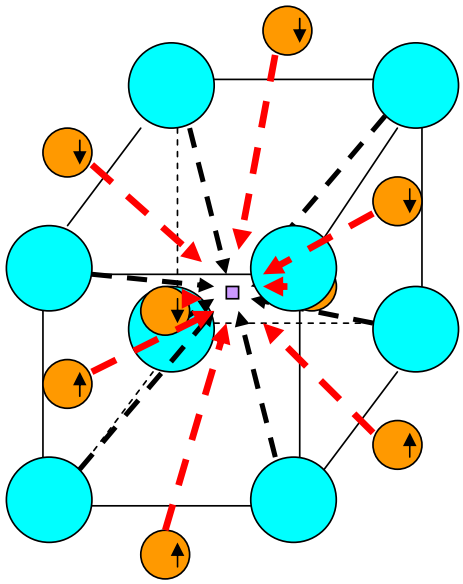

Figure 15. OSC (octahedral symmetric condensation), larger circles for deuterons, smaller circles with arrow (spin) for electrons.

$$\lambda_{2d} = {a_1}^2\lambda_{2d(1,1)} + {a_2}^2\lambda_{2d(2,2)}, \tag{4.1}$$

$$\lambda_{4d} = {a_1}^2\lambda_{4d(1,1)} + a_2^2\lambda_{4d(2,2)} + a_4^2\lambda_{4d(4,4)}, \tag{4.2}$$

$$\lambda_{8d} = {a_1}^2\lambda_{8d(1,1)} + {a_2}^2\lambda_{8d(2,2)} + {a_4}^2\lambda_{8d(4,4)} + {a_8}^2\lambda_{8d(8,8)}. \tag{4.3}$$

Here values for $\lambda_{nd(m,m)}$ intrinsic microscopic fusion rates are defined and calculated for dde*(m,m) transient molecular sates [59], and extended to multi-body fusion rates assuming rapid cascade barrier penetration and multi-body strong interactions [58–60,62]. These values are given in Table 1 of Ref. [60].

Screened Coulomb potentials for dde* EQPET molecules were calculated by the variational method of quantum mechanics [59], to be given as the following equation:

$$V_s(R) = e^2/R + V_h + (J + K)/(1 + \Delta). \tag{4.4}$$

On the right hand side of Eq. (4.4), the first term is the bare Coulomb potential and the second and third terms reflect in the screening effect by e*, which are the measure of "simply defined screening energy", as many experimentalists often use. In Table 4, effective screening energies for dde* EQPET molecules are listed up. We see that screening effects by e*(4,4) and e*(8,8) are very strong, in comparison with that a muon (mass is 208 times of electron mass) works between effects of e*(4,4) and e*(8,8). Thus, EQPET molecules may realize super screening of Coulomb potential.

In Eqs. (3.1)–(3.3), coefficients a_1–a_8 are estimated by evaluating total wave function Ψ for deuteron cluster with electrons which is expanded by wave functions $\Psi(m, m)$ of quasi-molecular states to dde*(m, m) as,

$$\Psi = a_1\Psi_{(1,1)} + a_2\Psi_{(2,2)} + a_4\Psi_{(4,4)} + a_8\Psi_{(8,8)}. \tag{4.5}$$

Table 4. Effective screening energy of dde* molecule

e*	dde*	dde*e*
(1,1)	−14.87 eV	−30.98 eV
(2,2)	−260 eV	−446 eV
(4,4)	−2460 eV	−2950 eV
(8,8)	−21 keV	−10.2 keV

In Ref. [8], approximate values of a_1–a_8 were given by taking simple quantum mechanical statistics for electron spin arrangement in TSC and OSC conditions. Calculated modal fusion rates are shown again in Table 5.

4.3. Products and Power Level of Cluster Fusion

Using modal fusion rates in Table 5, we estimated power levels of multi-body fusion rates for assumed deuteron cluster densities, as shown in Table 6. Height of periodical harmonic potential for deuteron in PdDx lattice is known to be 0.22 eV, so that 0.22 eV of deuteron (plasmon phonon) energy corresponds to excited states of trapped deuterons for dynamic motion in PdDx lattice potentials. Under this excitation condition, all deuterons trapped at O-sites move to the central T-site, and we estimate roughly the average TSC cluster density to be on the order of 10^{22} clusters per cm^3. In this condition, we get power level by 4D fusion rate to be 3 W/cm^3 (3×10^{11} f/s/cm^3) and 10 n/s/cm^3 neutron production rate by 2D fusion. Therefore neutron production rate is very small as on the 10^{-10} order of ^{4}He production rate by 4D fusion.

The OSC condition requires local PdD_2 lattice of overloaded condition, so that we assume here the OSC cluster density is very low as 10^{16} clusters/cm^3 (namely 1 ppm level of Pd atom density). Under this condition, we have still surprisingly high power level as 78 W/cm^3 (8×10^{12} f/s/cm^3) by 8D fusion rates, which produce two high-energy ^{8}Be particles per fusion.

We have speculated that 4D TSC fusion generates two 23.8 MeV ^{4}He-particles in 180° opposite directions as:

$$4D \rightarrow {}^8Be^*(47.6\ \text{MeV}) \rightarrow {}^4He + {}^4He + 47.7\ \text{MeV}. \tag{4.6}$$

However, we have at least once to consider the following possible branches of outgoing channels of threshold reactions for ^{8}Be (ground state) break-ups.

Table 5. Modal fusion rates for TSC and OSC

TSC (tetrahedral) (f/s/cl)	OSC (octahedral) (f/s/cl)
$\lambda_{2d} = 1.8 \times 10^{-21}$	$\lambda_{2d} = 7.9 \times 10^{-22}$
$\lambda_{3d} = 1.5 \times 10^{-13}$	$\lambda_{3d} = 3.5 \times 10^{-13}$
$\lambda_{8d} = 3.1 \times 10^{-11}$	$\lambda_{4d} = 7.0 \times 10^{-11}$
	$\lambda_{8d} = 7.8 \times 10^{-4}$

$$^{8}\mathrm{Be(g.s.)} \rightarrow {}^{4}\mathrm{He} + {}^{4}\mathrm{He} + 91.86\ \mathrm{keV}, \tag{4.7}$$

$$\rightarrow {}^{3}\mathrm{He} + {}^{5}\mathrm{He}\,(\mathrm{n} + {}^{4}\mathrm{He}) - 11.13\ \mathrm{MeV}, \tag{4.8}$$

$$\rightarrow \mathrm{t} + {}^{5}\mathrm{Li}\,(\mathrm{p} + {}^{4}\mathrm{He}) - 21.68\ \mathrm{MeV}, \tag{4.9}$$

$$\rightarrow \mathrm{d} + {}^{6}\mathrm{Li} - 22.28\ \mathrm{MeV}, \tag{4.10}$$

$$\rightarrow \mathrm{p} + {}^{7}\mathrm{Li} - 17.26\ \mathrm{MeV}, \tag{4.11}$$

$$\rightarrow \mathrm{n} + {}^{7}\mathrm{Be} - 18.90\ \mathrm{MeV}. \tag{4.12}$$

Other channels than (4.7) are threshold reactions with high threshold energies. Therefore, we have regarded these threshold reactions as minor channels with very small branching ratios, even with high-excited energy state of (4.6). Another possibility of minor channels in relation of (4.6) is break ups from excited states of ^{4}He which may break up to n + ^{3}He or t + p channels as those for 2D fusion. We regard branching ratios to these minor channels are also small, due to very steady core of alpha-clusters of ^{8}Be nucleus [63].

For 8D fusion, we can make a similar discussion that alpha-clustered channels dominate.

$$8\mathrm{D} \rightarrow {}^{16}\mathrm{O}^{*}(109.84\ \mathrm{MeV}) \rightarrow {}^{8}\mathrm{Be} + {}^{8}\mathrm{Be} + 95.2\ \mathrm{MeV}, \tag{4.13}$$

$$\rightarrow {}^{12}\mathrm{C} + {}^{4}\mathrm{He} + 50.12\ \mathrm{MeV}. \tag{4.14}$$

The life time of ^{8}Be(g.s.) is very short as 6.7×10^{-17} s to break up to two alpha-particles. Consequently, major products of 4D and 8D fusion are primarily high energy (23.8 MeV in kinetic energy) alpha-particles. The slowing down and ionization process by 23.8 MeV alpha-particles in PdDx condensed matter has very small cross section to emit K-alpha X-rays (22 keV) from Pd K-shell electron ionization. Major source of X-ray emission is speculated to the bremsstrahlung continuous X-rays in the region less than 3.5 keV by convey electrons, which are hard to observe, due to attenuation in experimental cells. Thus, energy deposit by 23.8 MeV alpha-particles becomes apparently radiation-less, namely “clean”.

4.4. Secondary Reactions

High energy (23.8 MeV) alpha-particles by 4D fusion can induce secondary nuclear reactions with host metal nuclei as the following capture reactions:

Table 6. Power level of 4D and 8D fusion rates

Item	TSC (tetrahedral)	OSC (octahedral)
Density	10^{22} cl/cm^3	10^{16} cl/cm^3
Power	3 W/cm^3	78 W/cm^3
Neutron	10 n/s/cm^3	< 1 n/s/cm^3

$$^{105}\mathrm{Pd} + {}^{4}\mathrm{He} \rightarrow {}^{109}\mathrm{Cd}^{*}(1.27\,\mathrm{years}), \tag{4.15}$$

$$^{106}\mathrm{Pd} + {}^{4}\mathrm{He} \rightarrow {}^{110}\mathrm{Cd}, \tag{4.16}$$

$$^{108}\mathrm{Pd} + {}^{4}\mathrm{He} \rightarrow {}^{112}\mathrm{Cd}, \tag{4.17}$$

$$^{110}\mathrm{Pd} + {}^{4}\mathrm{He} \rightarrow {}^{114}\mathrm{Cd}, \tag{4.18}$$

$$^{107}\mathrm{Pd}\,(6.5 \times 10^{6}\,\mathrm{years}) + {}^{4}\mathrm{He} \rightarrow {}^{111}\mathrm{Cd}. \tag{4.19}$$

Impurity Cd production rates in Pd cathode in the deuterium gas glow-discharge experiments by Karabut [61] may be explained by the above secondary reactions. Fission-like products also reported by Karabut [61] and Mizuno [57] can be explained by alpha-particle-induced fission process as reported by Ohta [64] in this meeting.

Even within short life of high energy ^{8}Be-particles by 8D fusion, more than ten metal nuclei exist within the range and we expect capture reactions as

$$M(A, Z) + {}^{8}\mathrm{Be} \rightarrow M(A + 8, Z + 4) + Q. \tag{4.20}$$

The kinetic energy 47.6 MeV of ^{8}Be by 8D fusion is well over the Coulomb barrier height 30.1 MeV for ^{133}Cs + ^{8}Be to ^{141}Pr reaction. Due to the liquid-drop collision-like capture process of this reaction, kinetic energy of ^{8}Be will be transferred to kinetic energy of compound nucleus $M(A + 8, Z + 4)$.

Selective nuclear transmutations reported by Iwamura [55,56] can be explained by this process, although we have few problems of possible radiation (γ-rays) emission in the process, which we will discuss elsewhere.

5. Conclusions

The EQPET model was proposed to explain super-screening for d–d pairs in condensed matter. Deuteron cluster fusion dominated will however take place by TSC and OSC conditions to make resonance multi-body fusion reactions for 3D, 4D, and 8D strong interactions. Helium-4 is the major product, and neutron production rate is very small on the order of less than 10^{-10} of helium production rate. High-energy alpha particles by 4D and 8D fusion reactions will induce secondary transmutation reactions with host or mounted heavy nuclei. Slowing down of high-energy alpha particles as products of 4D and 8D fusion reactions may emit low-energy continuous X-rays which are difficult to observe from outside of experimental cells. We can say that deuteron cluster fusion in condensed matter is clean or almost radiation-less.

References

[1] J. Huizenga, *Cold Fusion, The Scientific Fiasco of the Century* (University of Rochester Press, Rochester, 1992).
[2] *Proceedings of the First Annual Cold Fusion Conference* (University of Utah, Utah, 1990).
[3] *Proceedings of the Second Annual Cold Fusion Conference* (Italian Physical Society, Como, Italy, 1991), pp. 453–464.
[4] *Proceedings of the Third International Conference Cold Fusion* (Universal Academy Press, Nagoya, 1992), pp. 5–20.
[5] *Proceedings of the Fourth International Conference Cold Fusion*, Vol. 26, No. 4T (Fusion Technology, Maui, 1994).
[6] *Proceedings of the Fifth International Conference Cold Fusion* (Imura-E, Monte Carlo, 1995).
[7] *Proceedings of the Sixth International Conference Cold Fusion* (NEDO-Japan, Toya, 1996), pp. 425–432.
[8] *Proceedings of the Seventh International Conference Cold Fusion* (ENECO-USA, Vancouver, 1998).

[9] *Proceedings of the Eighth International Conference Cold Fusion*, Vol. 70 (Italian Physical Society, Lerici, 2001).
[10] *Proceedings of the Ninth International Conference Cold Fusion* (Springer, Beijing, 2002) (to be published).
[11] M.H. Miles, B.F. Bush, Frontier of cold fusion, *Proceedings of the ICCF2* (Universal Acadamic Press, Nagoya, 1992), pp. 189–200.
[12] Y. Arata, Y. Zhang, *J. High Temp. Soc. Jpn* **23** (1997), Special Issue.
[13] Y. Arata, Y. Zhang, *Jpn. J. Appl. Phys*. **37** (1998) L1274–L1276.
[14] M. McKubre, S. Crouch-Baker, A. Riley, S. Smedley, F. Tanzella, *Proceedings of the Third International Conference Cold Fusion* (Universal Academy Press, Nagoya, 1992), pp. 5–20.
[15] Y. Isobe, S. Uneme, K. Yabuta, Y. Katayama, H. Mori, T. Omote, S. Ueda, K. Ochiai, H. Miyamaru, A. Takahashi, Search for multi-body nuclear reactions in metal deuteride induced with ion beam and electrolysis method, *Jpn. J. Appl. Phys.* **41** (2002) 1546–1556.
[16] A. Takahashi, A. Mega, T. Takeuchi, H. Miyamaru, T. Iida, *Proceedings of the Third International Conference Cold Fusion* (Universal Academy Press, Nagoya, 1992), pp. 79–92.
[17] A. Takahashi, T. Iida, T. Takeuchi, A. Mega, *J. Appl. Electromag. Mat.* **3** (1992) 221–230.
[18] H. Fukuoka, T. Ikegawa, K. Kobayashi, A. Takahashi, *Proceedings of the Sixth International Conference Cold Fusion* (NEDO-Japan, Toya, 1996), pp. 425–432.
[19] Y. Iwamura, T. Itoh, N. Gotoh, I. Toyoda, *Fusion Technol.* **33** (1998) 476.
[20] T. Mizuno, T. Ohmori, K. Kurokawa, T. Akimoto, M. Kitaichi, K. Inoda, K. Azumi, S. Shimokawa, M. Enyo, *Denki Kagaku* **64** (1996) 1160 (in Japanese).
[21] G. Miley, J. Patterson, *J. New Energy* **1** (1996) 5.
[22] T. Ohmori, T. Mizuno, Y. Nodasaka, M. Enyo, *Fusion Technol*. **33** (1998) 476.
[23] A.B. Karabut, *Proceedings of the Eighth International Conference Cold Fusion*, Vol. 70 (Italian Physical Society, Lerici, 2001), pp. 329–340.
[24] Y. Iwamura, T. Itoh, M. Sakno, S. Sakai, Observation of low energy nuclear reaction induced by D2 gas permeation through multi-layer Pd film, *Proceedings of the Ninth International Conference Cold Fusion* (Springer, Beijing, 2002) (to be published).
[25] T. Itoh, M. Sakano, S. Sakai, Y. Iwamura, ibid.
[26] M. Sakano, T. Itoh, S. Sakai, Y. Iwamura, ibid.
[27] Y. Iwamura, T. Itoh, M. sakano, S. Sakai, *Jpn. J. Appl. Phys*. **41** (2002) 4642–4650.
[28] V.A. Chechin, V.A. Tsarev, M. Rabinowitz, Y.E. Kim, *Int. J. Theor. Phys*. **33** (1994) 617–670.
[29] S. Chubb, T. Chubb, *Fusion Technol.* **17** (1990) 710.
[30] A. Takahashi, T. Iida, F. Maekawa, H. Sugimoto, S. Yoshida, *Fusion Technol*. **19** (1991) 380.
[31] A. Takahashi, T. Iida, H. Miyamaru, M. Fukuhara, *Fusion Technol*. **27** (1995) 71.
[32] A. Takahashi, Drastic enhancement of tetrahedral and octahedral resonance fusion under transient condensation of deuterons at lattice focal points, *Proceedings of the Ninth International Conference Cold Fusion* (Springer, Beijing, 2002) (to be published).
[33] V. Kirkinskii, Y. Novikov, *Theoretical Modeling of Cold Fusion* (Novosibirsk University Publications, Novosibirsk, 2002).
[34] V. Violante, C. Sibilia, D. Di Giacchino, M. Mckubre, F. Tanzara, P. Tripodi, *Proceedings of the Eighth International Conference Cold Fusion*, Vol. 70 (Italian Physical Society, Lerici, 2001), pp. 409–418.
[35] A. Takahashi, *J. Nucl. Sci. Technol*. **26** (1989) 558.
[36] M. Fleischmann, S. Pons, *J. Electroanal. Chem.* **261** (1989) 301.
[37] A. Takahashi, K. Maruta, K. Ochiai, H. Miyamaru, T. Iida, *Fusion Technol.* **34** (1998) 256.
[38] A. Takahashi, K. Maruta, K. Ochiai, H. Miyamaru, *Phys. Lett. A* **255** (1999) 89–97.
[39] Y. Isobe, S. Uneme, K. Yabuta, H. Mori, T. Omote, S. Ueda, K. Ochiai, H. Miyamaru, A. Takahashi, *Proceedings of the Eighth International Conference Cold Fusion*, Vol. 70 (Italian Physical Society, Lerici, 2001), pp. 17–22.
[40] T. Dairaku, Y. Katayama, T. Hayashi, Y. Isobe, A. Takahashi, *Proceedings of the Ninth International Conference Cold Fusion* (Springer, Beijing, 2002) (to be published).
[41] G. Preparata, *Proceedings of the Second Annual Cold Fusion Conference* (Italian Physical Society, Como, 1990), pp. 453–464.
[42] F. Celani, A. Spallone, P. Tripodi, D. Di Gioacchino, P. Manini, A. Mancini, *Proceedings of the Sixth International Conference Cold Fusion* (NEDO-Japan, Toya, 1996), pp. 228–233.

[43] A. Lanzara, P. Bogdanov, X. Zhou, S. Kellar, D. Feng, E. Lu, T. Yoshida, H. Eisaki, A. Fujimori, K. Kishio, J. Shimoyama, T. Noda, S. Uchida, Z. Sussain, Z. Shen, *Nature* **412** (8) (2001) 510.
[44] T. Miyanaga, R. Kubo et al., *Solid State Physics* (Iwanami, Tokyo, 1961) (in Japanese).
[45] J. Pauling, A. Wilson, *Introduction to Quantum Mechanics with Applications to Chemistry* (McGraw-Hill, New York, 1935).
[46] A. Takahashi, M. Ohta, T. Mizuno, *Jpn. J. Appl. Phys*. **40** (2001) 7031–7046.
[47] M. Ohta, A. Takahashi, *Jpn. J. Appl. Phys*. **40** (2001) 7031–7046.
[48] A. Takahashi, Drastic enhancement of deuteron cluster fusion by transient electronic quasi-particle screening, *Proceedings of the Fourth Meeting of Japan CF-Research Society* (Morioka, Japan, October 2002), pp. 74–78.
[49] A. Takahashi, Y. Iwamura, S. Kuribayashi, Mass-8-and-charge-4 increased transmutation by octahedral resonance fusion model, ibid., pp. 79–81.
[50] M. Tinkahm, *Introduction to Superconductivity* (McGraw Hill, New York, 1996).
[51] A. Takahashi, Tetrahedral and octahedral resonance fusion under transient condensation of deuterons at lattice focal points, *Proceedings of the Ninth International Conference Cold Fusion* (Springer, Beijing, 2002), pp. 343–348.
[52] K. Ochiai, K. Maruta, H. Miyamaru, A. Takahashi, *Fusion Technol*. **36** (1999) 315–323.
[53] M. McKubre, Power point slide for ICCF10 Short Course, see http://www.lenr-canr.org.
[54] Y. Arata et al., *Proceedings of the ICCF10*, see http://www.lenr-canr.org.
[55] Y. Iwamura et al., *Jpn. J. Appl. Phys.* **41** (2002) 4642–4648.
[56] Y. Iwamura et al., *Proceedings of the ICCF10*, see http://www.lenr-canr.org.
[57] T. Mizuno et al., *Denkikagaku* **64** (1996) 1160.
[58] A. Takahashi et al., *Proceedings of the ICCF9*, China, 19–24 May 2002, pp. 343–348.
[59] A. Takahashi et al., *Proceedings of the JCF4*, 17–18 October 2002 (Iwate University, Japan, 2002), pp. 74–78.
[60] A. Takahashi, Mechanism of deuteron cluster fusion by EQPET model, *Proceedings of the ICCF10*, see http://www.lenr-canr.org.
[61] A. Karabut et al., *Proceedings of the ICCF10*, see http://www.lenr-canr.org.
[62] A. Takahashi, Theoretical background for transmutation reactions, Power-point slide for ICCF10 Short Course, see http://www.lenr-canr.org.
[63] A. Takahashi et al., *Fusion Technol*. **27** (1995) 71–85.
[64] M. Ohta et al., *Proceedings of the ICCF10*, see http://www.lenr-canr.org.

J. Condensed Matter Nucl. Sci. 1 (2007) 86–96

Research Article

TSC-Induced Nuclear Reactions and Cold Transmutations*

Akito Takahashi†

Osaka University, Suita, Osaka 5650871, Japan

Abstract

Tetrahedral Symmetric Condensate (TSC) of orthogonal coupling of four deuterons and four electrons behaves as charge-neutral pseudo-particle and induces nuclear interaction with host metal nuclei. Theoretical predictions are shown for processes, reaction-types and nuclear products. Some details are written for 4p/TSC + Ni and 4d/TSC + Cs reactions making transmutations and fission products.

Keywords: Tetrahedral symmetric condensate, 4p/TSC+Ni, 4d/TSC+Cs, Transmutation, Fission

1. Introduction

We reported possibility of direct nuclear interaction between proton (or deuteron) and host-metal-nucleus in condensed matter systems of metal–hydrogen/deuterium complexes [1,2]. Clean fusion reaction (4D fusion) with ^{4}He products as main ash was predicted [1,2] by Electronic Quasi-Particle Expansion Theory [3] (EQPET)/Tetrahedral Symmetric Condensate [1,2] (TSC) models. TSC is composed of four deuterons (or protons) and four electrons with anti-parallel spin arrangement in orthogonal coupling state. TSC is proposed to form in near surface area of metal–deuterium/hydrogen system. Size of TSC will become much smaller than the sizes of inner most K-shell orbits of host-metal atoms, will penetrate like neutron, due to its charge neutrality, through electron clouds of host-metal atoms, and at around its minimum-size (about 5 fm radius) state; we can expect strong nuclear interaction between TSC and host-metal nucleus. Phenomenon taken place with about 60 fs life time of TSC is modelled and numerically estimated as time-averaged treatments.

2. TSC and Self-Fusion

Dynamic squeezing motion of TSC can be treated by semi-classical model, due to its three dimensionally constrained and central squeezing motion, as the feature is illustrated in Fig. 1. It is suggested [1–3] that TSC forms dynamically

*This work is supported by Mitsubishi Heavy Industries Co., Japan.
†Work was done for submission to Siena05 Workshop on anomaly of metal–D/H systems, Siena, Italy, May 2005. E-mail: akito@sutv.zaq.ne.jp

at focal points (sites) of PdDx lattice near surface or on fractal sites at surface, although substantiation of modeling in real condensed matter conditions is yet to be studied.

Once TSC is formed in 100 pm size (1 Å) domain of condensed matter system, TSC starts central squeezing motion under three-dimensionally *frozen* condition except for directions toward the central focal point. This squeezing motion can be treated by the classical Newtonian motion due to the three-dimensional constraint of particle freedom, until when deuterons get into the range (about 5 fm) of nuclear strong interaction or electrons reach at the limit of Pauli's exclusion—classical electron diameter (5.6 fm).

For the case of 4d/TSC, formation of 4d to ^{8}Be* takes place at the minimum-size TSC state, since the charged-pion range (2.2 fm) of strong interaction is comparable to the classical electron radius (2.8 fm). Fractional fusions of 2d and 3d may happen with very small probability to be negligible [4], because of this specific condition for 4d/TSC. The nature of ^{8}Be* is thought to be collectively excited state of cluster with two alpha particles, which goes out with almost 100% weight to the break-up channel of

$$\mathrm{D} + \mathrm{D} + \mathrm{D} + \mathrm{D} \rightarrow {}^{8}\mathrm{Be}^{*} \rightarrow {}^{4}\mathrm{He} + {}^{4}\mathrm{He} + 47.6\ \mathrm{MeV}. \tag{1}$$

In very short time (of the order of fs). It is proposed [1–4] that claimed excess heat with ^{4}He production in CMNS experiments with Pd–D systems is consistently explained by clean 4D fusion of Eq. (1).

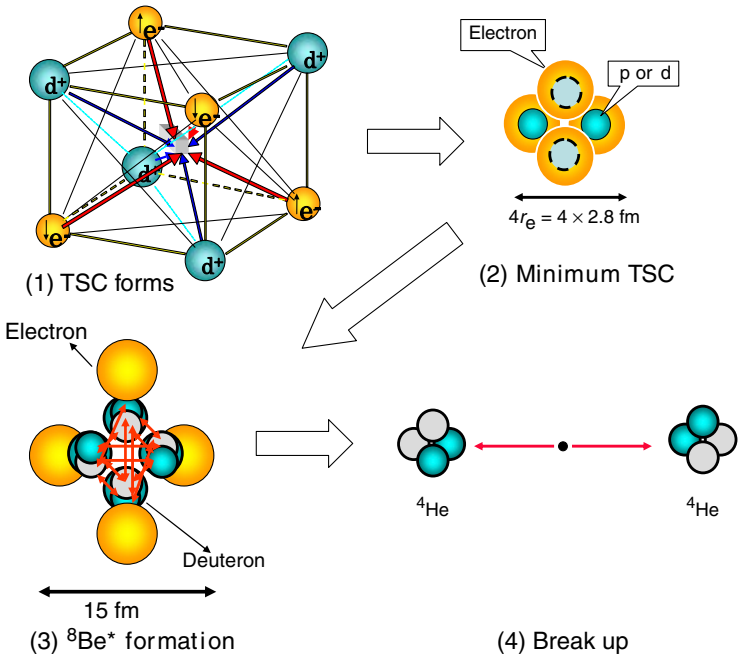

Figure 1. Squeezing and fusion process of 4d/TSC (time scale: 0–60 fs), $\langle e \rangle = (e\uparrow + e\downarrow)/2$ in QM view for four electron centers.

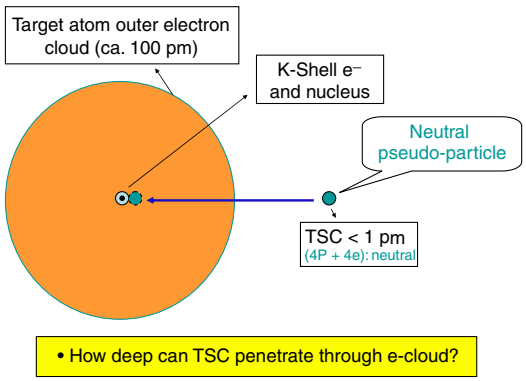

Figure 2. Illustration for TSC and host-metal atom interaction.

3. TSC–Metal Interaction

3.1. Barrier Penetration

As shown in Fig.1, TSC squeezes from about 100 pm size to its minimum-size with about 10 fm diameter and behaves as charge-neutral pseudo-particle. Life time of TSC is estimated as time difference from 100 pm size state to minimum size with velocity of the order of 10^5 cm/s; we obtain about 60 fs. During its life, TSC as charge-neutral pseudo-particle may approach to host-metal nuclei with some probability, as illustrated in Fig. 2.

Time-averaged density of TSC in metal deuteride (MDx) or hydride (MHx) is given in our previous papers [1,2] Macroscopic reaction rate Y (f/s/cm^3) for M + TSC reaction is given by

$$Y = N_{\mathrm{M+TSC}}\lambda. \tag{2}$$

Here we have to estimate the density $N_{\mathrm{M+TSC}}$ of "united molecule" M + TSC in atomic level.

$$N_{\mathrm{M+TSC}} = \sigma_{\mathrm{A}} N_{\mathrm{M}} N_{\mathrm{TSC}} v \tau_{\mathrm{TSC}}. \tag{3}$$

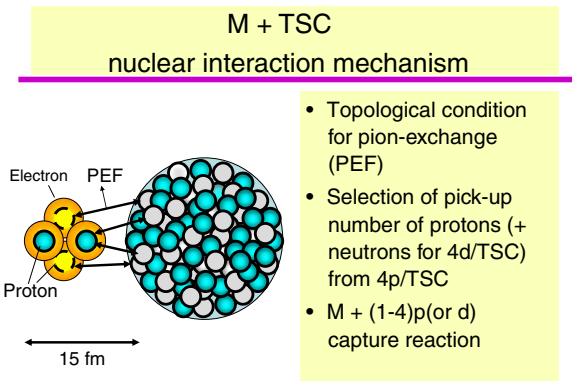

Figure 3. Feature of strong nuclear interaction, for closely approached TSC + M-nucleus united molecule.

N_M is the host-metal atom density, N_{TSC} the time-averaged TSC density, σ_A the atomic level cross section (about 10^{-16} cm^2) for M + TSC combination, and τ_{TSC} the mean life of TSC (about 60 fs), respectively. If we can assume $N_M = 10^{23}$ per cm^3 and $N_{TSC} = 10^{20}$ per cm^3, we obtain roughly $N_{M+TSC} = 10^{19}$ per cm^3.

3.2. Sudden Tall Thin Barrier Approximation

As shown in Fig. 1, TSC around with its minimum-size may approach closely to the interaction range of strong force between protons (deuterons) of TSC and host-metal nucleus. The situation is shown in Fig. 3.

When protons (or deuterons) start to make strong interaction by exchanging charged pions with nucleons of host-metal nucleus, charge neutrality of TSC starts to break and electrons should go outside, since electron does not make strong interaction but weak interaction. Field coupling constant for weak interaction is very small as on the order of 10^{-14} of coupling constant (1.0) of strong interaction. According to Fermi's golden rule, reaction cross section is proportional to square of transition matrix element which is proportional to field coupling constant. Therefore, weak interaction between electrons and host-metal nucleons is neglected. Pion Exchange Force (PEF) unit is relative measure of effective surface for very short range (about 2–5 fm) force of strong interaction.

Since electrons should go out of the interaction domain of strong force, protons (or deuterons) in TSC should *suddenly feel* Coulomb repulsion with host-metal nucleus, and also among protons (and deuterons) in TSC itself. The feature of stage is illustrated in Fig. 4.

We derived the Sudden Tall Thin Barrier Approximation (STTBA) [1,2] for calculating reaction rate in this stage.

4. Ni + 4p/TSC Reactions

Miley–Patterson [5] reported production of anomalously large foreign elements in their electrolysis experiments with Ni–H systems. Campari et al. [6] also reported large excess heat, anomalous foreign elements and about 660 keV gamma-ray peak. There are many other reports which claimed anomalous heat events and foreign elements production. Most authors claimed *cold transmutations* in condensed matter.

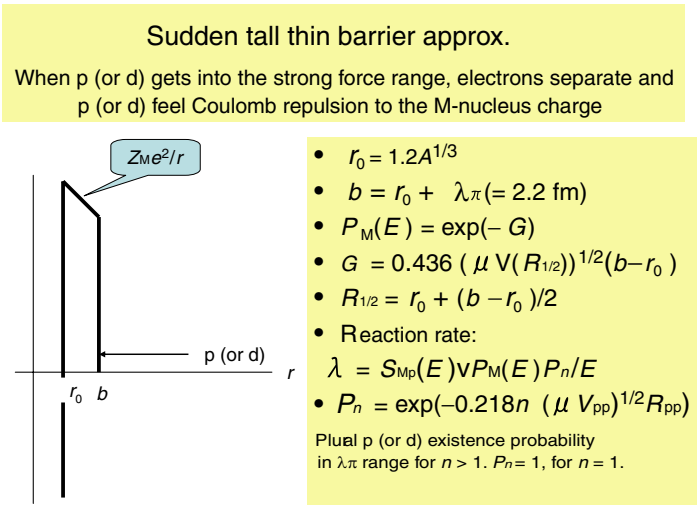

Figure 4. Sudden Tall Thin Barrier Approximation (STTBA) for TSC + M system.

Table 1. Calculated reaction rates for Ni + 4p/TSC and Ni + 4d/TSC nuclear reactions (results by STTBA calculation; M = Ni)

$P_{Mp}(E) = 9.2 \times 10^{-2}$	$V_{pp} = 1.44/6 = 0.24$ MeV
$P_{Md}(E) = 3.5 \times 10^{-2}$	$P_{2p} = 0.527$
Reaction rates	$P_{2d} = 0.404$
$\lambda_{Mp} = 3.7 \times 10^{-8}$ (f/s/pair)	
$\lambda_{Md} = 2.1 \times 10^{-7}$ (f/s/pair)	$S_{Mp}(0) = 10^8$ keV barn
$\lambda_{M4p} = 1.0 \times 10^{-8}$ (f/s/pair)	$S_{Md}(0) = 10^9$ keV barn
$\lambda_{M4d} = 3.4 \times 10^{-9}$ (f/s/pair)	
⟨Macroscopic reaction rate⟩ $= \lambda \times N_{M+TSC}$	$\lambda_{4d} = 4.9 \times 10^{-5}$
With $N_{M+TSC} = 10^{16}$ in 10 nm area, rate= 10^8 f/s/cm^2 and $Y = 10^{14}$ in 10^6 s	

The author applied STTBA for estimating reaction rates of Ni + 4p/TSC nuclear reactions, which are competing process of Ni + p, Ni + 2p, Ni + 3p and Ni + 4p reactions.

Calculated reaction rates are shown in Table 1.

We obtained considerably large values for microscopic reaction rates, and macroscopic yield 10^8 f/s/cm^2 with assuming N_{TSC+M} density = 10^{+16} (1/cm^2) in 10 nm area of Ni sample surface. Especially, Ni + 4p capture reaction rate 10^{-8} (f/s/pair) is large enough to explain claimed foreign elements as fission products of Ni + 4p to Ge* process. Before showing fission products, we show Ni + p reactions in Table 2. The excited compound state Ge* has enough excited energy (19–29 MeV for ^{60}Ni + 4p to ^{64} Ni + 4p) to induce fission. Fission products are calculated by the Selective

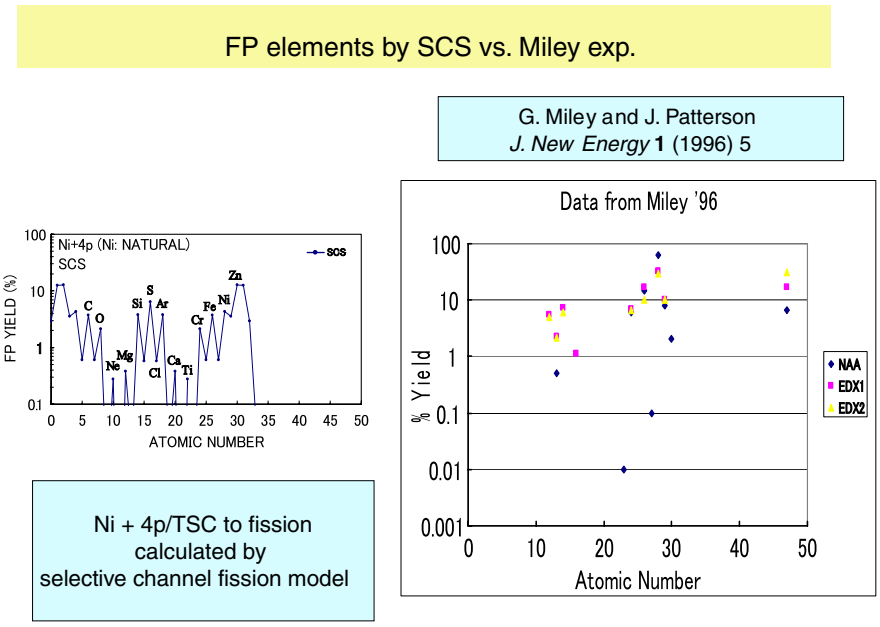

Figure 5. Comparison of calculated FP distribution (left figure) and Miley–Patterson experiment (right figure), for Ni + 4p to fission process.

Table 2. Products of Ni + p reactions

^{58}Ni + p $\rightarrow$ ^{59}Cu* (1.36 months, EC) ^{59} Ni* (7×10^4 years)	Ni–H gas system exp. By Piantelli (ASTI5);660 keV peak by NaI detector
^{60}Ni + p $\rightarrow$ ^{61}Cu* (3.3 h, EC) ^{61}Ni	
^{61}Ni + p $\rightarrow$ ^{62}Cu* (9.7 months, EC) ^{62}Ni	
^{62}Ni + p $\rightarrow$ ^{63}Cu (6.12 MeV); $E_g = 669$ keV	660 MJ excess energy
^{64}Ni + p $\rightarrow$ ^{65}Cu (7.45 MeV)	
Prompt gamma-rays emit	

Channel Scission (SCS) model [7]. Calculations were done for all nickel isotopes. FP distribution for averaged natural abundance is shown in Fig. 5.

We see good agreement, although low-Z elements (C, N, and O) were not given in the experiment, probably due to contaminants in low mass region.

Typical fission products (FP) are shown in Tables 3 and 4. Major contribution of FP is from Ni + 4p fission for higher mass isotopes of nickel. Most interesting point is that most FPs are stable isotopes and radioactive products are very weak. Therefore, this fission process is much cleaner than known fission of uranium. However, the opening of neutron emission channel is possible, although weight is small. Some FPs are decaying by electron capture (EC) process, in few cases of which there are small portion of gamma-ray emission.

5. M + 4d/TSC Reactions

In the minimum-size stage of 4d/TSC, four deuterons fuse, by exchanging charged pions, to ^{8}Be* compound state with about 2 fm radius. And electrons are kicked outside of the range of strong interaction (see Fig. 1). Therefore, M + 4D interaction becomes M + ^{8}Be* capture reaction, as illustrated in Fig. 6.

Iwamura et al. reported [8,9] selective transmutations

$$M(A, Z) + 4\mathrm{D}(\text{or } ^8\mathrm{Be}) \rightarrow M(A + 8, Z + 4). \tag{4}$$

They added ^{133}Cs or Sr atoms on surface of Pd-complex and permeated D_2 gas through the sample complex. They observed repeatedly transmutations; ^{133}Cs to ^{141}Pr or ^{88}Sr to ^{96}Mo with total transmuted amount of the order of 10^{14} to 10^{15} atoms per week.

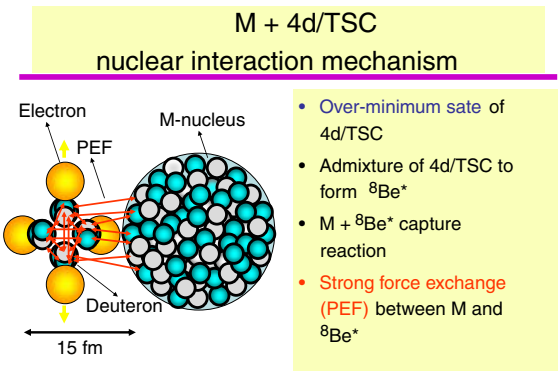

Figure 6. Strong interaction for M + 4d/TSC.

Table 3. Fission products from Ni + 4p reactions

(1) ^{58}Ni(68%) + 4p → ^{62}Ge(E_x = 11.2 MeV)
→ 8.8 MeV + ^{4}**He** + ^{58}Zn(EC)^{58}Cu(EC)^{58}**Ni**
→ 8.8 MeV + ^{28}**Si** + ^{34}Ar(EC)^{34}Cl(EC)^{34}**S**

(2) ^{60}Ni(26.2%) + 4p → ^{64}Ge(E_x = 19.1 MeV)
→ 16.4 MeV + ^{4}**He** + ^{60}Zn(EC)^{60}Cu(EC)^{60}**Ni**
→ 13.6 MeV + ^{8}Be + ^{56}Ni(EC)^{56}Co(EC)^{56}Fe
→ 13.0 MeV + ^{12}**C** + ^{52}Fe (EC)^{52}Mn(EC)^{52}**Cr**
→ 12.2 MeV + ^{16}O + ^{48} Cr(EC)^{48}V(EC)^{48}Ti
→ 13.5 MeV + ^{24}Mg + ^{40}Ca
→ 16.4 MeV + ^{28}**Si** + ^{36}**Ar**
→ 16.7 MeV + ^{32}S + ^{32}S
→ 6.5 MeV + ^{38}**Ar** + ^{26}Si(EC)Al(10^5 years)

(3) ^{61}Ni(1.1%) + 4p → ^{65}Ge(E_x = 21.3 MeV)
→ 18.9 MeV + ^{4}**He** + ^{61}Zn(EC)^{61}Cu(EC)^{61}**Ni**
→ 15.9 MeV + ^{12}C + ^{53}Fe(EC)^{53}Mn(3.7×10^6 years)
→ 11.0 MeV + ^{20}Ne + ^{45}Ti(EC)^{45}Sc
→ 17.4 MeV + ^{28}Si + ^{37}Ar(EC)^{37}Cl
→ 12.0 MeV + ^{27}Si(EC)^{27}Al + ^{38}**Ar**
→ 17.5 MeV + ^{32}S + ^{33}S

Bold font shows stable isotope.
Average kinetic energy of fission product is 9.7 MeV for Ni-natural.

The author applied STTBA analysis for modeled Pd(Cs)/D system to estimate transmutation rate. Results are shown in Table 5.

Calculated rate 4.6×10^{14} atoms per week for Cs-to-Pr transmutation showed considerable agreement with those by Iwamura's experiments.

6. 6d/OSC + M Interaction

Iwamura et al. [10] reported transmutation from ^{137}Ba to ^{149}Sm, namely mass-12 and charge-6 increased transmutation. This may be M + 6D capture process.

We considered 8D fusion process emits ^{12}C nuclei with high kinetic energy and M + ^{12}C capture process can be considered as secondary reaction. The second and more plausible process is direct 6D capture by octahedral symmetric condensate (OSC) for 6D cluster occupying six peaks (vertexes) of regular octahedron orthogonally coupled with six electrons which also occupy vertexes of regular octahedron as shown in Figs. 7 and 8. The squeezing motion of 6d/OSC can be modeled in analogous way to Fig. 1, although we need to treat three-dimensionally more complex system (cuboctahedron, dodecahedron, or regular hexagonal prism).

Self-fusion of 6d/OSC may be 6D fusion as shown in Fig. 9.

$$6\mathrm{D} \rightarrow {}^{12}\mathrm{C}^{*} \rightarrow {}^{4}\mathrm{He} + {}^{8}\mathrm{Be} + 71.3\ \mathrm{MeV} \rightarrow {}^{4}\mathrm{He} + {}^{4}\mathrm{He} + {}^{4}\mathrm{He} + 71.4\ \mathrm{MeV}. \tag{5}$$

And transmutation by M + 6d/OSC is

$$M(A, Z) + 6\mathrm{d/OSC} \rightarrow M(A + 12, Z + 6). \tag{6}$$

For example,

$$^{137}\mathrm{Ba} + 6\mathrm{D}(\text{or } ^{12}\mathrm{C}^{*}) \rightarrow {}^{149}\mathrm{Sm} + \gamma(68.23\ \mathrm{MeV}) \text{ or fission.} \tag{7}$$

Detail analysis for this process is expected. Approximate estimation of reaction rates are as follows. Microscopic 6D fusion rate for minimum state 6d/OSC is given by STTBA as

$$\lambda_{6\mathrm{d}} = (S_{6\mathrm{d}}(E)v/E)\exp(-6\Gamma_{\mathrm{STTBA}}) = 4.8 \times 10^{-2}(\mathrm{f/s/cl}). \tag{8}$$

Using PEF = 30 for 6d fusion,

$$S_{6\mathrm{d}}(E) = 10^{14}\mathrm{keV\ barn}, \tag{9}$$

$$\Gamma_{\mathrm{STTBA}} = 0.523(b^{1/2} - {r_0}^{1/2}) = 0.31. \tag{10}$$

Table 4. Fission products from Ni + 4p reactions, continued

^{62}Ni(3.6%) + 4p → ^{66}Ge(E_x = 24.0 MeV)
→ 11.0 MeV + n + ^{65}Ge(EC)^{65}Ga(EC)^{65}Zn
→ 21.4 MeV + ^{4}**He** + ^{62}Zn(EC)^{62}Cu(EC)^{62}**Ni**
→ 11.5 MeV + ^{8}Be + ^{58}Ni
→ 18.9 MeV + ^{12}**C** + ^{54}**Fe**
→ 10.5 MeV + ^{14}N + ^{52}Mn(EC)^{52}Cr
→ 8.2 MeV + ^{16}O + ^{50}Cr
→ 13.9 MeV + ^{20}**Ne** + ^{46}**Ti**
→ 15.2 MeV + ^{24}Mg + ^{42}Ca
→ 13.7 MeV + ^{27}**Al** + ^{39}**K**
→ 18.9 MeV + ^{28}**Si** + ^{38}**Ar**
→ 18.6 MeV + ^{32}S + ^{34}S
^{64}Ni(0.93%) + 4P → ^{68}Ge(E_x = 29 MeV)
→ 16.7 MeV + n + ^{67}Ge(EC)^{67}Ga(EC)^{67}**Zn**
→ 25.6 MeV + ^{4}He + ^{64}Zn
→ 10.0 MeV + ^{6}Li + ^{61}Cu(EC)^{61}**Ni**
→ 13.2 MeV + ^{8}Be + ^{57}Ni(EC)^{57}Co(EC)^{57}**Fe**
→ 10.9 MeV + ^{9}**Be** + ^{59}Ni(EC)^{59}**Co**
→ 9.9 MeV + ^{10}B + ^{58}Co(EC)^{58}Fe
→ 22.7 MeV + ^{12}C + ^{56}Fe
→ 14.8 MeV + ^{14}**N** + ^{54}Mn(EC)^{54}**Cr**
→ 12.7 MeV + ^{16}O + ^{52}Cr
→ 17.6 MeV + ^{20}**Ne** + ^{48}**Ti**
→ 12.7 MeV + ^{23}Na + ^{45}Sc
→ 17.5 MeV + ^{24}Mg + ^{44}Ca
→ 14.8 MeV + ^{27}**Al** + ^{41}**K**
→ 18.7 MeV + ^{28}**Si** + ^{40}**Ar**
→ 18.7 MeV + ^{32}S + ^{36}S

Neutron emission channel may open!
S-values for higher mass Ni may be larger than Ni-58 and Ni-60, due to more p–n PEF interaction.
Bold font shows stable isotope.

Table 5. Cs-to-Pr transmutation rate estimated by STTBA model for M + 4d/TSC reaction

STTBA prediction for Cs-to-Pr	
$S_{Mp} = 10^8$ keV barn	Suppose $N_{M+TSC} = 10^{17}$ in 10 nm layer of surface
$S_{Md} = 10^9$ keV barn	
$\lambda_{Mp} = 8.4 \times 10^{-10}$ f/s/tsc	
$\lambda_{M4p} = 2.3 \times 10^{-10}$ f/s/tsc	Macroyield $= \lambda \times N_{tsc} = 7.6 \times 10^{-9} \times 10^{17} = 7.6 \times 10^8$(f/s/cm^2)
$\lambda_{Md} = 2.8 \times 10^{-8}$ f/s/tsc	
$\lambda_{M4d} = 7.6 \times 10^{-9}$ f/s/tsc	Cs-to-Pr rate $= 4.6 \times 10^{14}$ (atoms per week per cm^2)
Where combination probability of anti-parallel spin was used for 4p/TSC	

Here we used $b = r_{ddmin} = 8$ fm and $r_0 = 5$ fm.

And M + 6d/OSC capture rate is similar order as that of M + 4d/TSC, since S-value will be a little larger and barrier factor is a little smaller.

$$\lambda_{M+6d/OSC} \approx 10^{-8}[\text{f/s/(M + OSC)}].$$

If we have $N_{M+OSC} = 10^{17}\text{cm}^{-2}$ in reaction-range (about 10 nm), we have macroscopic reaction rate of 10^9 f/s/cm^2.

Application of EQPET analysis to 6d/OSC is expected. The electronic quasi-particle e*(6,6) is composed of three Cooper pairs coupling orthogonally in three-dimensional rectangular axes, and its screening energy for d–d pair is 9600 eV, which is just near to that of muon.

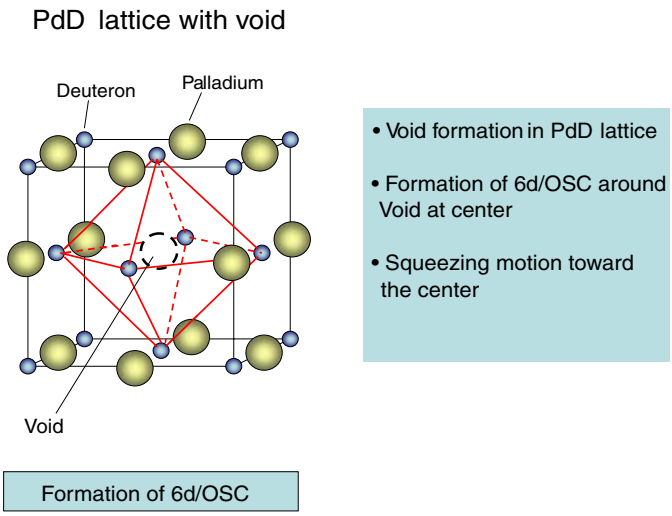

Figure 7. Formation of 6d/OSC seed by a central void in PdD lattice.

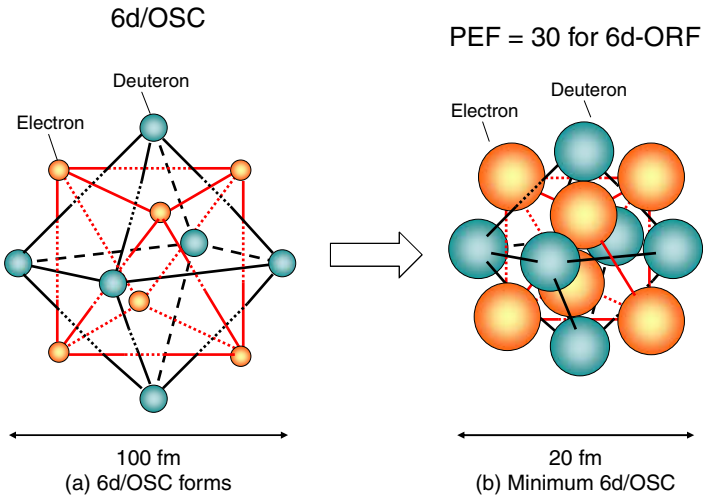

Figure 8. Formation of 6d/OSC.

7. Conclusions

The TSC of 4D (or 4H) cluster can squeeze very small as 10 fm in diameter at its minimum-size state, and will behave as charge-neutral pseudo-particle for Coulomb barrier penetration through electron clouds of host-metal atom to induced very enhanced nuclear reactions between host-metal M-nucleus and 4p (or 4d)/TSC pseudo-particle. Using STTBA model, reaction rates were estimated for Ni + 4p/TSC and M + 4d/TSC systems. Calculated results have shown good agreements with some of well-known experimental claims of transmutation and fission-products.

However, the present modeling of TSC mechanisms is still primitive and we need further elaboration. Especially, formation mechanisms near surface of host-metal complex is interested for further studies.

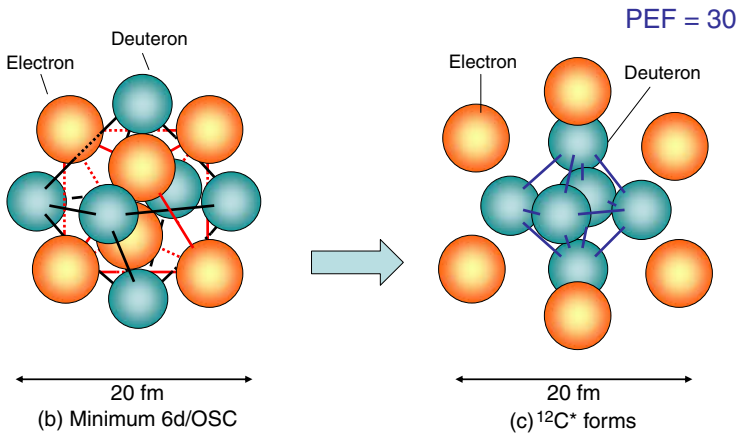

Figure 9. Formation of $^{12}C^*$ by 6d/OSC fusion.

Formation of 6d/OSC and 6D fusion in defect (void) of PdD lattice was proposed, although we need more detailed modeling of mechanism inducing central squeezing motion of 6 deuterons around central defect.

Cold transmutation scenarios as claimed by many experimentalists, also as studied in this work, are hopeful to apply for transmutation of long-lived radioactive wastes from nuclear plants.

Acknowledgments

The author is grateful to Dr. Y. Iwamura, Mitsubishi Heavy Industries Co. and Dr. F. Celani, INFN Frascati, for their kind discussions. The author thanks Dr. M. Ohta, PNC Japan, for providing fission product calculations for Ni + 4p system.

References

[1] A. Takahashi, ^{3}He/^{4}He production ratios by tetrahedral symmetric condensation, *Proceedings of the ICCF11* (Marseilles, November 2004) see http://www.iscmns.org/.
[2] A. Takahashi, *Deuteron cluster fusion and related nuclear reactions in metal deuterium/hydrogen systems, Recent Developments in Physics* (Transworld Research Network, India, issued in June 2005).
[3] A. Takahashi, Deuteron cluster fusion and ash *Proceedings of the ASTI5 Meeting* (Italy, March 2004) see http://www.iscmns.org/.
[4] A. Takahashi, A theoretical summary of condensed matter nuclear effects, *Proceedings of the Siena Workshop on Anomalies in Metal-Deuterium/Hydrogen Systems* (Siena Italy, May 2005), to be appeared in http://www.iscmns.org/.
[5] G. Miley, J. Patterson, *J. New Energy* 1 (1996) 5.
[6] E. Campari et al., Surface analysis of hydrogen loaded nickel alloys, *Proceedings of the ASTI5 Meeting* (Italy, March 2004), see http://www.iscmns.org/.
[7] A. Takahashi et al., *Jpn. J. Appl. Phys.* 41 (2001) 7031.
[8] Y. Iwamura et al., *Jpn. J. Appl. Phys.* 41 (2002) 4642.
[9] Y. Iwamura et al., *Proceedings of the ICCF10* (Boston, August 2003), see http://www.lenr-canr.org/.
[10] Y. Iwamura et al., *Proceedings of the ICCF11*, see http://www.iscmns.org/.

J. Condensed Matter Nucl. Sci. 1 (2007) 97–105

Research Article

On Condensation Force of TSC

Akito Takahashi* and Norio Yabuuchi

High Scientific Research Laboratory, Marunouchi 24-16, Tsu, Mie 514-0033, Japan

Abstract

Primitive analysis and discussion are given for possible condensing force of tetrahedral symmetric condensate (TSC) of four deuterons (or protons) plus four spin-regulated (bosonized) electrons. Once TSC is formed by the ordering-constraint-organization process in condensed matter of metal-D(H) system, there may happen strong central squeezing force (and negative Coulomb energy of total TSC system) until when four deuterons (protons) get into the range of strong interaction (or Pauli repulsion at classical electron radius). After elementary quantum-mechanical results for D(H)-atom and, $D_2(H_2)$-molecule, primitive estimations are done for TSC.

Keywords: Deuteron cluster fusion, Central squeezing force, Four deuterons, Tetrahedral symmetric condensate

1. Introduction

As a theoretical model for Condensed Matter Nuclear Effects (CMNE), Electronic Quasi-Particle Expansion Theory with Tetrahedral Symmetric Condensate (EQPET/TSC) has been proposed [1] and elaborated [2–7]. Qualitative and quantitative results of EQPET/TSC have provided reasonable agreements with major results of CMNE experiments [5], although some of key conditions for TSC formation and squeezing motions are of open questions; for example, where TSC can be generated and how is the mechanism in condensed matter, how TSC can condense transiently into a very small charge-neutral pseudo-particle and what is the driving force of squeezing condensation motion into central focal point, and so on. We need further elaboration to make the model more substantial.

This paper gives a primitive analysis on possible condensing force of TSC by Coulombic interaction under Platonic symmetry [8] and discusses the relation to biding forces of D(H)-atom and $D_2(H_2)$-molecule.

*E-mail: akito@sutv.zaq.ne.jp

2. Coulomb Energy of D(H)-Atom

The ground state electron wave function of H(D)-atom is the 1S-wave function as given (see standard text books of quantum mechanics) as

$$\Psi_{100}(r) = \frac{1}{\sqrt{\pi a^3}} \mathrm{e}^{-r/a}. \tag{1}$$

Here a becomes Bohr radius ($a_\mathrm{B} = 52.9$ pm) for H(D)-atom, and is modified for EQPET atom de* [4,7]. The system Coulomb energy is given by

$$\langle \Psi_{100} | E_{\mathrm{C-D}} | \Psi_{100} \rangle = \int_0^\infty (-\mathrm{e}^2/r)\Psi_{100}^2 4\pi r^2 \mathrm{d}r = -1.44/r \quad \text{with} \quad r = a_\mathrm{B}. \tag{2}$$

Here Coulomb energy is given in unit of keV with r in pm unit. Using Bohr radius 52.9 pm, we get

$$\langle E_{\mathrm{C-D}} \rangle = -27.2\,\mathrm{eV}. \tag{3}$$

The total system energy is given as kinetic energy plus potential energy, by evaluating Hamiltonian integral

$$\langle H \rangle = \langle \Psi_{100} | H | \Psi_{100} \rangle = \left\langle \Psi_{100} \left| -\frac{\hbar^2}{2m}\nabla^2 - \frac{e^2}{r} \right| \Psi_{100} \right\rangle = E_0 = -13.6\ \mathrm{eV}. \tag{4}$$

Using

$$\langle H \rangle = \langle E_\mathrm{k} \rangle + \langle E_{\mathrm{C-D}} \rangle, \tag{5}$$

we get mean kinetic energy of electron as $\langle E_\mathrm{k} \rangle = 13.6$ eV. Please note that in classical QM, we equate centrifugal force and Coulomb attractive force for orbital electron, $\frac{mv^2}{r} = \frac{e^2}{r^2}$ to get the same result.

$$\langle E_\mathrm{k} \rangle = \frac{1}{2}mv^2(r = a_\mathrm{B}) = \frac{e^2}{2r} = 13.6\,\mathrm{eV}. \tag{6}$$

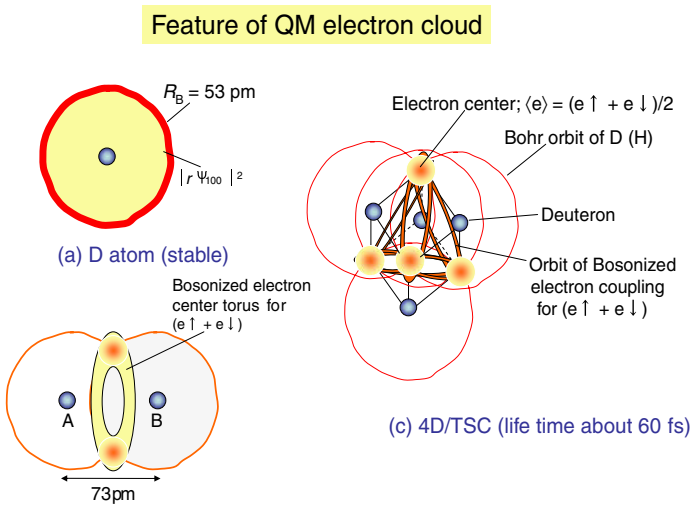

Figure 1. Weight-distributions of electron wave functions for D(H)-atom, $D_2(H_2)$-molecule, and 4D(H)/TSC transient pseudo molecule.

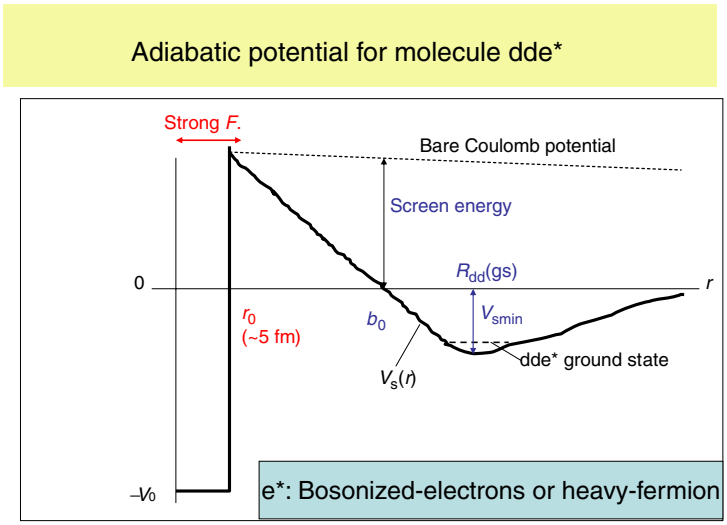

Figure 2. Conceptual view of dde* molecular potential; scales in X–Y are deformed (not linear), enlarged very much strong interaction range and depressed barrier height.

Also note that we use the normalization condition as

$$\int_0^\infty (\Psi_{100}(r))^2 4\pi r^2 \mathrm{d}r = \int_0^\infty 4\pi (r\Psi_{100}(r))^2 \mathrm{d}r = 1. \tag{7}$$

Therefore, the function $|r\Psi_{100}(r)|^2$ having peak at Bohr radius draws the radial distribution of electron weight for H(D)-atom, as shown in Fig. 1. This feature corresponds to the view of classical Newtonian motion of orbital electron at Bohr radius rotating around central plus charge of deuteron (or proton) with kinetic energy of 13.6 eV. However, in QM view, 13.6 eV is the mean kinetic energy of electron with 1S-wave function. In Fig. 1, features of electron wave functions for D_2-molecule and 4D/TSC ($t = 0$) are also drawn [5–7].

3. Coulomb Energy of $D_2(H_2)$ Molecule

Using variational method for ddee system, Pauling–Wilson–type potential (screened Coulomb potential) is derived [4] and wave function of $D_2(H_2)$ molecule is given as

$$\Psi_{2D} = \frac{1}{\sqrt{2+2\Delta}} \left[\Psi_{100}(r_{A_1})\Psi_{100}(r_{B_2}) + \Psi_{100}(r_{A_2})\Psi_{100}(r_{B_1})\right] X_s(S_1, S_2). \tag{8}$$

Here $X_s(S_1, S_2)$ is the singlet spin wave function for anti-parallel pairing of spins (S_1 and S_2) of two 1-σ electrons. And total system energy is given [5,7] as (see also Table 1, and Fig. 2) result of variational calculation to get energy eigen value,

$$\langle \Psi_{2D} | H | \Psi_{2D} \rangle = -37.8\,\mathrm{eV}. \tag{9}$$

The ground state internuclear, p–p or d–d distance is 73 pm by calculation as well known (exact value is 74.16 pm).

Approximate estimation of system Coulomb energy can be estimated from classical balance of Coulombic forces between particles (plus and minus charged) forming regular square form by alternatively positioned dede or pepe system.

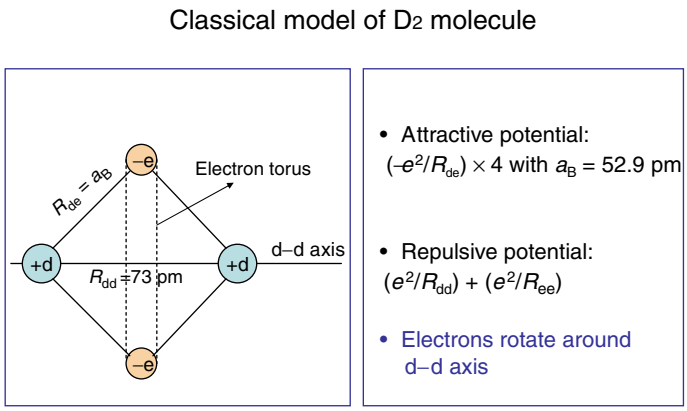

Figure 3. Classical model of D_2 molecule; electrons are rotating with mean kinetic energy of 16.25 eV around the d–d axis with radius about 37.4 pm. In QM view, mean electron orbit is the center torus of Fig. 1b.

This classical model corresponds to QM feature as follows. We know (see Figs. 1b and 3), the distance between plus-charge (deuteron or proton) and the center-circle-line of "bosonized" central electron torus is $a_B = 52.9$ pm for attraction force and d–d (or e–e) distance is $\sim \sqrt{2}a_B = 74.8$ pm (but 73 pm by QM calculation, see Table 1). We estimate system-averaged Coulomb energy as follows.

Using a classical model picture of $D_2(H_2)$ molecule as shown in Fig. 3, we obtain

$$\langle E_{C-2D} \rangle = 4\left(-\frac{e^2}{a_B}\right) + 2\left(\frac{e^2}{\sqrt{2}a_B}\right) = -70.3\ \text{eV}. \tag{10}$$

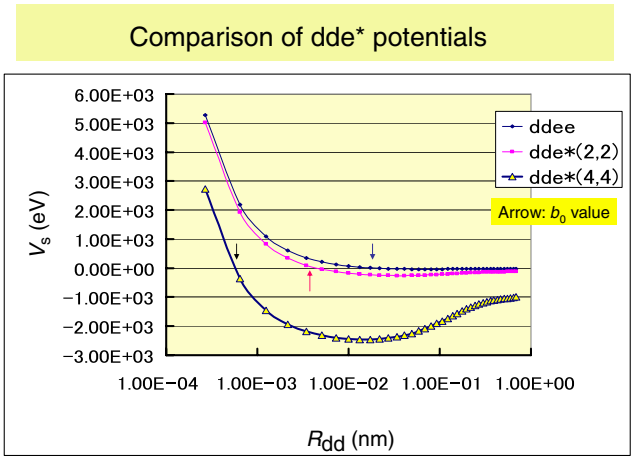

Figure 4. Shielded Coulomb potentials for ddee (namely D_2), dde*(2,2) and dde*(4,4) states with b_0-parameters (shown by arrows); Drastic decrease of b_0-parameters (see position of arrows) for the change from regular molecule D_2 to dde*(2,2) and then the change from dde*(2,2) to dde*(4,4) corresponds to the deepening of trapping potential depths (negative potential depths), which induce strong condensing force for forming 4d/TSC state [9].

Table 1. Negative Coulomb energies (trapping depths) of D_2 molecule and dde* EQPET molecule; here b_0-values are measure for barrier penetration of d–d nuclear fusion

e*(m, Z)	V_{smin}(eV)	b_0 (pm)	$R_{dd(gs)}$(pm)
Parameters of dde* potentials			
(1,1); Normal electron	−15.4	40	101
(1,1) × 2; D_2	−37.8	20	73
(2,2); Cooper pair	−259.0	4	33.8
(4,4); Quadruplet e	−2, 460	0.36	15.1
	Trapping depth		Ground state

Then averaged electron kinetic energy is given as

$$\langle E_{k-2D}\rangle = \langle H_{2D}\rangle - \langle E_{C-2D}\rangle = 70.3 - 37.8 = 32.5\,\text{eV}. \tag{11}$$

This gives average kinetic energy per 1-σ electron as 16.25 eV (cf. 13.6 eV for H(D)-atom).

By bosonization of electron pairs, dde* molecule can condense (shrink) to smaller size. As shown in Table 1, d–d distance at ground state decreases from 73 to 33.8 pm by the generation of Cooper pair e*(2,2). Orthogonal coupling of two Cooper pairs generates quadruplet e*(4,4) which makes much stronger condensation. Change of Pauling–Wilson-type potential [4,5] by bosonization of electron pairs is drawn in Fig. 4. Here b_0-parameter values correspond to the degree of barrier penetration probabilities of d–d pair through Pauling–Wilson-type shielded Coulomb potentials [5]. Diminishing shift of b_0-parameter by the bosonization corresponds to driving mechanism of transient Bose-type condensation [4,5,9].

We can consider that the bosonization (microscopic Cooper pair generation) of electron pairs may be a seed of TSC formation in metal plus deuteron systems [9].

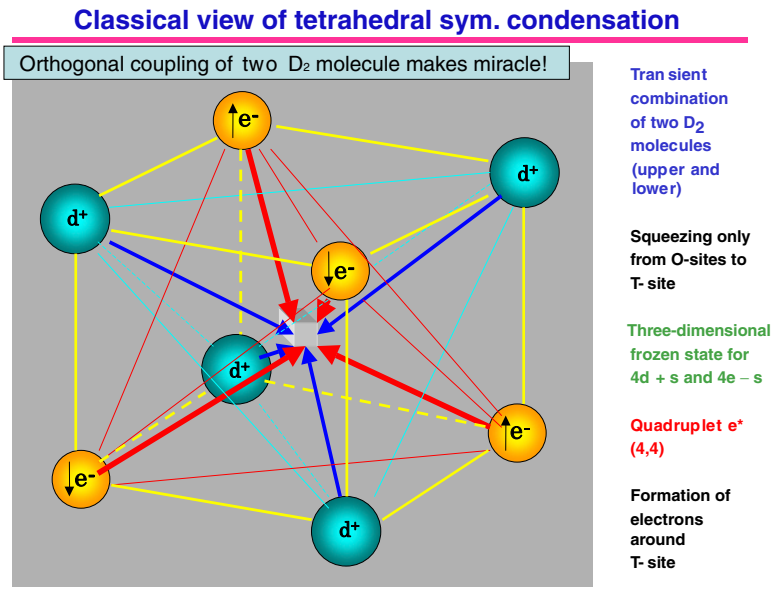

Figure 5. Classical view of TSC (tetrahedral symmetric condensate) [5].

4. Coulomb Energy and Condensing Force of TSC

Approximate wave function for TSC at $t = 0$ was given [6] as,

$$\begin{aligned}\Psi_{4D} \sim\ & a_1[\Psi_{100}(r_{A_1})\Psi_{100}(r_{B_2}) + \Psi_{100}(r_{A_2})\Psi_{100}(r_{B_1})]X_s(S_1, S_2)\\ & + a_2[\Psi_{100}(r_{A_1})\Psi_{100}(r_{D_4}) + \Psi_{100}(r_{A_4})\Psi_{100}(r_{D_1})]X_s(S_1, S_4)\\ & + a_3[\Psi_{100}(r_{A_2})\Psi_{100}(r_{C_4}) + \Psi_{100}(r_{A_4})\Psi_{100}(r_{C_2})]X_s(S_2, S_4)\\ & + a_4[\Psi_{100}(r_{B_1})\Psi_{100}(r_{D_3}) + \Psi_{100}(r_{B_3})\Psi_{100}(r_{D_1})]X_s(S_1, S_3)\\ & + a_5[\Psi_{100}(r_{B_2})\Psi_{100}(r_{C_3}) + \Psi_{100}(r_{B_3})\Psi_{100}(r_{C_2})]X_s(S_2, S_3)\\ & + a_6[\Psi_{100}(r_{C_3})\Psi_{100}(r_{D_4}) + \Psi_{100}(r_{C_4})\Psi_{100}(r_{D_3})]X_s(S_3, S_4). \end{aligned} \tag{12}$$

Here suffixes A, B, C, and D denote positions of four deuterons in TSC configuration.

Classical view of TSC configuration is shown in Fig. 5

By assuming Platonic symmetry for the wave function, namely absolute values of coefficient a_j are same and orthogonal in vector products, we can approximately estimate the system Coulomb energy. Let the distance between deuteron (or proton) and nearest electron-ball (or electron-particle in classical view) to be R_{de}. We write the d–d distance as

$$R_{dd} = \sqrt{2}R_{de}. \tag{13}$$

By assuming the balance of classical Coulomb forces between particles at vertexes of cube, we get approximate value of Coulomb energy as (see Fig. 6),

$$\langle E_{C-TSC}\rangle = 12\left(-\frac{e^2}{R_{de}}\right) + 12\left(\frac{e^2}{R_{dd}}\right) + 4\left(-\frac{e^2}{\sqrt{3}R_{de}}\right) = -\frac{8.38}{R_{de}} \tag{14}$$

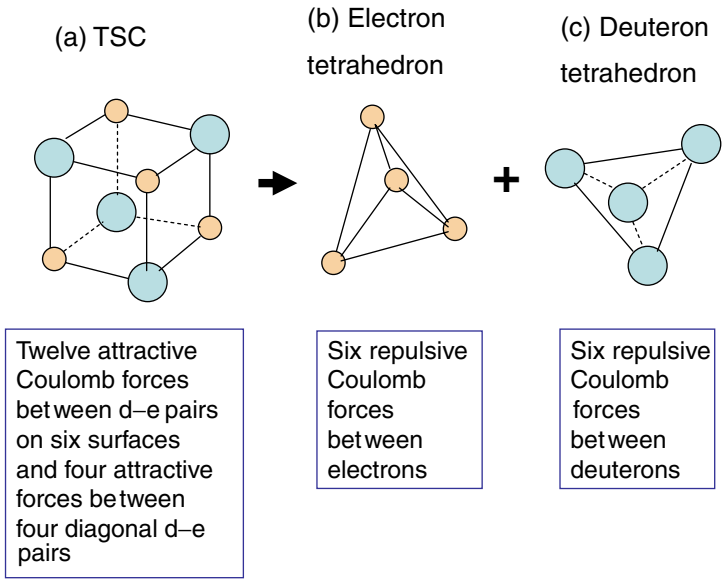

Figure 6. TSC (**a**) as combination of two regular tetrahedrons (**b**, **c**) and Coulomb forces between particles.

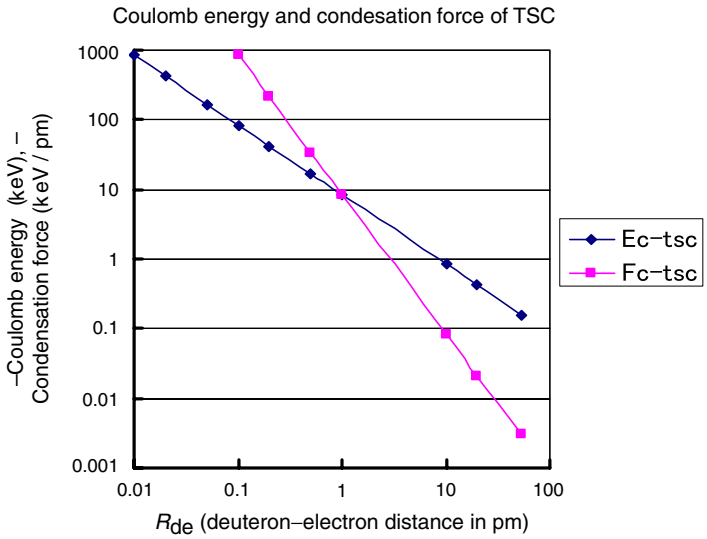

Figure 7. Coulomb energy and condensing force of TSC.

(in keV unit with pm unit for R). In three terms of Eq. (14), the first one is attractive forces on six surfaces of TSC cube, the second one is repulsive forces between d–d or e–e and the third term is the attractive forces between d–e for diagonal lines of cube.

Assuming the averaged effective kinetic energy for electron-balls are very small compared with Coulomb energy, due to coherently central squeezing motion, we can get rough estimation of condensing force of TSC by

$$F_{\mathrm{C-TSC}} = -\frac{\partial U}{\partial r} = -\frac{\partial E_{\mathrm{C-TSC}}}{\partial R_{\mathrm{de}}} = -\frac{8.38}{R_{\mathrm{de}}^2} \tag{15}$$

(in keV/pm unit with pm unit for R).

Calculated Coulomb energies and condensing forces as a function of R_{de} is shown in Fig. 7.

Here we considered that effective kinetic energy of four electron-balls on TSC represents the apparent averaged apparent kinetic energy of four "bosonized" electrons. In one of our models [5,6], we assume for TSC formation by phonon excitation in PdD lattice,

$$\left\langle E_{\mathrm{k,e-ball}} \right\rangle = 4\left(\frac{1}{2} m_{\mathrm{e}} {v_{\mathrm{d}}}^2\right) = 4\left(\frac{m_{\mathrm{e}}}{M_{\mathrm{d}}}\right) E_{\mathrm{d}} \leq 0.88\,\mathrm{eV}. \tag{16}$$

One forth of this energy was corresponded to seventh phonon-energy (one phonon 64 meV) for deuteron as harmonic oscillator in PdD lattice and nearly equal to the barrier height of Bloch potential trapping deuterons in Pd-metal O-sites (see part-II of Takahashi and Yabuuchi [7]). This very low effective kinetic energy seems to be attained by the Platonic symmetry for ordered-constrained-organized condition in forming TSC cluster in metal-D(H) systems. We should note here that local kinetic energy of electrons in a torus-orbit of a shrinking dde* molecular group in TSC would be much larger (larger than 16.2 eV for D_2 molecule), due to decreased d–d distance, if we would regard TSC as a steady state molecule. However, the process is under very rapid transient condensation motion.

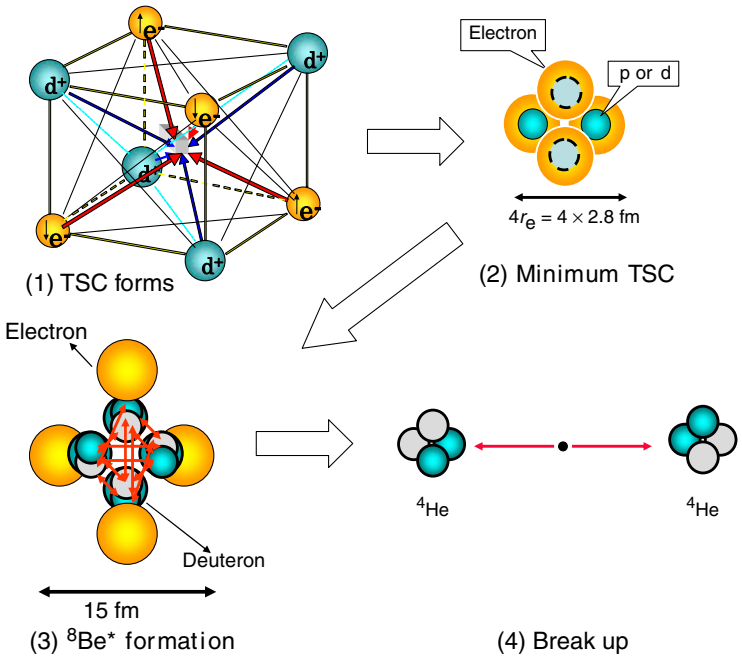

Figure 8. Feature of TSC condensation and 4D fusion reaction; (1) TSC is formed at $t = 0$, and squeezing with Newtonian motion to condense onto the central focal point, (2) end of squeezing motion at the size of TSC-minimum when getting into the range of strong force, (2) four deuterons exchange charged-pions to form shrinking ^{8}Be* intermediate compound nucleus with very short life (less than 1 fs), and charge neutrality of TSC is broken, and (3) ^{8}Be* breaks up to two alpha-particles with 23.8 MeV each [7]. It will take about 60 fs for the process.

Coulomb energy of TSC at 11 pm for R_{de}(corresponding 15 pm for R_{dd}; see Table 1) is about -0.9 keV, which can be compared to -2.46 keV of trapping depth by dde*(4,4) EQPET molecule. Bosonization of electron pair helps much condensing force increased.

As shown in Fig. 7, condensing force of TSC increases as d–e or d–d distance decreases. Consequently, once TSC is formed, it squeezes ultimately to condense into the central focal point until when some other force like strong interaction breaks the charge-neutrality of TSC. We copy [5–7] the figure of squeezing motion with 4D fusion reaction in Fig. 8.

5. Conclusion

Due to platonic symmetry in TSC formation, effective Coulomb energy and resulting condensing force of squeezing TSC-system becomes very large. The charge neutrality and balance of Coulombic forces keep this condition until TSC gets into the strong interaction range.

Bosonization of electron pairs may play a key role to trigger or generate TSC at some focal points in metal plus deuteron (proton) systems of condensed matter.

More exact quantum mechanical analysis on the mechanism of time-dependent TSC motion is to be explored in future.

References

[1] A. Takahashi, Mechanism of deuteron cluster fusion by EQPET model, *Proceedings of the ICCF10* (World Scientific, Singapore, 2006), pp. 809–818 (ISBN-891-256-564-7).

[2] A. Takahashi, ^{3}He/^{4}He production ratios by tetrahedral symmetric condensation, *Proceedings of the ICCF11* (World Scientific, Singapore, 2006), pp. 730–742 (ISBN-981-256-640-6).

[3] A. Takahashi, Deuteron cluster fusion and related nuclear reactions in metal-deuterium/hydrogen systems, *Recent Res. Dev. Phys.* **6** (2005) 1–28, ISBN: 81-7895-171-1.

[4] A. Takahashi, Deuteron cluster fusion and ash, *Proceedings of the ASTI5 Meeting* (Asti, Italy, 2004), see http://www.iscmns.org/.

[5] A. Takahashi, A theoretical summary of condensed matter nuclear effects, see also in: A. Takahashi (Ed.), *Brief Theoretical Summary of Condensed Matter Nuclear Effects, Acta Physica et Chemica, Proceedings of the Siena 2005 Workshop*, Vols. 38–39 (Debrecen, Hungary, 2005), pp. 341–356.

[6] A. Takahashi, Time-dependent EQPET analysis of TSC, *Proceedings of the ICCF12, Yokohama* (World Scientific, Singapore, 2005), to be published.

[7] A. Takahashi, N. Yabuuchi, Fusion rates for bosonized condensates, Asti2006 Workshop on Anomalies in Hydrogen/Deuterium Loaded Metals, September 2006, see http://www.iscmns.org/ ASTI.

[8] N. Yabuuchi, A. Takahashi, *Proceedings of the JCF7* (Kagoshima Japan, April 2006), to be published in http://wwwcf.elc.iwate-u.ac.jp/jcf/.

[9] A. Takahashi, N. Yabuuchi, Comments on role of CaO layer in Iwamura transmutation, ibid.

J. Condensed Matter Nucl. Sci. 1 (2007) 106–128

Research Article

Fusion Rates of Bosonized Condensates*

Akito Takahashi†

High Scientific Research Laboratory, Marunouchi 24-16, Tsu, Mie 514-0033, Japan and Osaka University, Yamadaoka 2-1, Suita, Osaka 5650871, Japan

Norio Yabuuchi

High Scientific Research Laboratory, Marunouchi 24-16, Tsu, Mie 514-0033, Japan

Abstract

In Section 1, theoretical basis for formulating fusion rates in condensed matter is summarized. Nuclear strong interaction, S-matrix, T-matrix, fusion rate for steady state dde* molecule as bosonized condensate, and fusion rate formula for collision process are briefly given. In Section 2, application for TSC-induced fusion is summarized. Fusion rate formulas for adiabatic approach in EQPET theory are summarized. Final state interaction is briefly discussed. Time-dependent approach for TSC squeezing motion is briefly introduced.

Keywords: Bosonized condensate, dde* molecule, EQPET, Fusion rate formula, Time-dependence, TSC-induced reaction

1. Basic Theory

1.1. Nuclear Potential

In general, nuclear reaction is usually theorized and analyzed in three steps; initial state interaction, intermediate compound state, and final state interaction. Transition from intermediate state to final state has various, sometimes complex, channels such as the electro-magnetic transition to ground state emitting gamma rays, the particle (neutron, proton, α-particle, etc.) emission and residual nucleus, which sometimes decay to ground state emitting gamma-rays, and the direct break-up to two or more nuclei like fission. Potential for nuclear strong force and Coulomb force in these cases can be categorized into three cases [1] of Fig. 1.

The potential state (I) shows the case that nucleons (neutrons and protons) are trapped in a very deep well of strong force. Stable isotopes of masses less than 60 have this type potential well. Fusion reactions by two light nuclei produce stable isotopes of this type.

*Submittal to the 7th International Workshop on Anomalies in Hydrogen/Deuterium Loaded Metals, September 2006.
†E-mail: akito@sutv.zaq.ne.jp

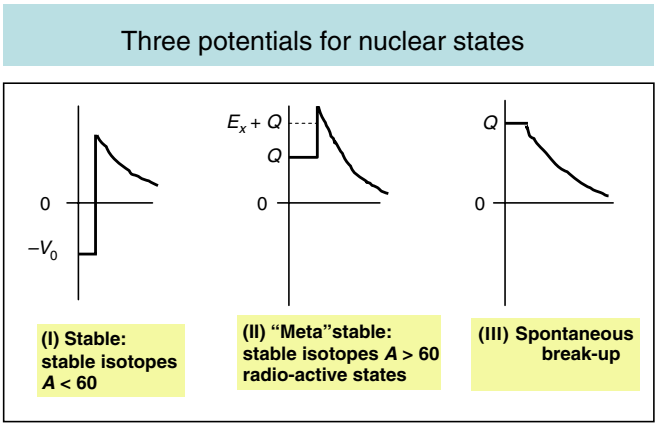

Figure 1. Three potential types for nuclear interaction.

The potential state (II) appears for intermediate compound state in general. Radioactive isotope has this kind of potential. Stable isotopes having masses greater than 60 are trapped in these type potentials, which are drawn according to the fission channels breaking-up to lighter nuclei. In this case, the depth of trapping potential is deep enough to have very long lifetime, but positive Q-value for fission channels makes height of potential tail in outer-skirt lower than the depth of trapping well. At ground state, the thickness of potential well is large enough to make the quantum-mechanical tunneling probability of fission to be "inverse-astronomically" very close to zero.

Therefore, nucleus is regarded as stable isotope. Here, Q-value is obtained by calculating mass defect between before and after reaction, using Einstein's formula $E = mc^2$. However, when the intermediate compound nucleus has high inner excited energy E_x, the thickness of outer wall of trapping potential becomes relatively thin and quantum mechanical tunneling probability for particle emission or fission can dramatically increase. Fission process for uranium and trans-uranium nuclei is induced in this way. Moreover, we may have possibility of fission for lighter nuclei with mass $A < 200$. In some of proposed theories [2–4] in the Condensed Matter Nuclear Science (CMNS), deterministic models of fission for $60 < A < 200$ nuclei have been developed.

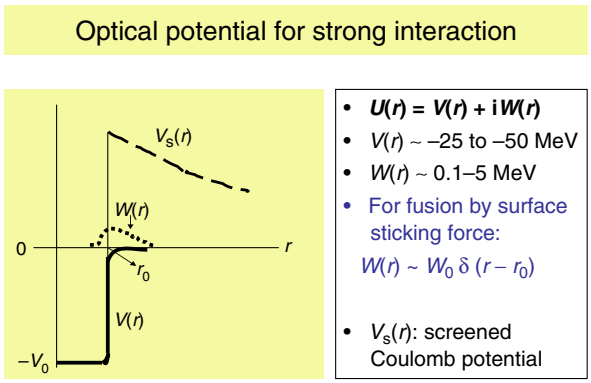

Figure 2. Optical potential for strong interaction.

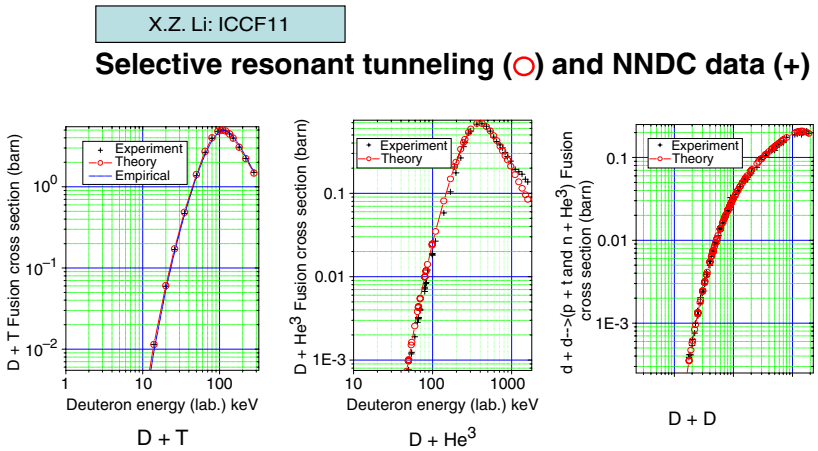

Figure 3. Fusion cross-sections for dt, d^3He and dd processes.

The potential type (III) is the case for intermediate compound nucleus having very high inner excited energy Ex, such as cases of fusion reactions of hydrogen isotopes. Compound nucleus in this case promptly breaks up to fragment-particles.

1.2. Strong Interaction

Now we explain very briefly the feature of potential by nuclear strong interaction. The reason why nucleons are trapped within very small spherical space with radius about 5 fm (1 fm $= 10^{-15}$ m) was first solved by the famous Yukawa model of pion exchange. Hideki Yukawa won Nobel Prize by this theory. Later, the theory of strong force has been deepened by the development of QCD [5] based on concept of quark and gluon. However, as the conclusion in recent views of nuclear physics, the strong interaction can be drawn accurately enough by the Yukawa model with charged pions (π^+, π^-) and neutral pion, for relative reaction energy less than about 200 MeV (less than the threshold energy of pion-generation). Especially, for fusion reaction process, charged pions play role of sticking two (or more) nuclei.

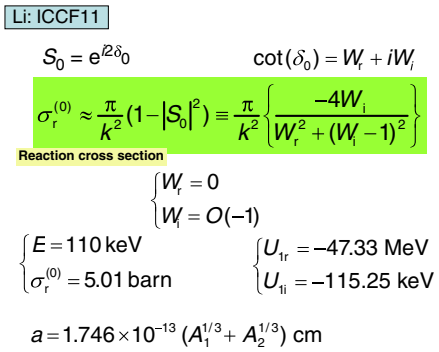

Figure 4. Fitting of dt fusion cross-sections by *S*-matrix formulas by Li et al. [9].

Nuclear fusion by strong interaction can be simulated by the catch-ball model of charged pions between nuclei for fusing. Due to the very short range of de Broglie wave length (about 2 fm) of pion, the strong interaction for fusion becomes very short range force, namely "almost on surface" sticking force. For example, when relatively large ($A > 6$) two nuclei approach closely, fusion force by exchanging charged pions (between neutron and proton for counter-part nuclei) becomes the sticking force near at surface ($R = r_0$). Exchange of neutral pion for scattering (repulsive) force between nucleons of counter-part nuclei also happens in the region relatively near at surface.

Especially, nuclear fusion reactions at very low energy as cold cluster fusion and transmutation as modeled by EQPET/TSC theory (see Section 2), largeness of surface area for exchanging charged pions governs the largeness of reaction cross-section. This is specific character of "nuclear reactions in condensed matter".

1.3. Optical Potential

Global optical potential [6], written by complex number, is used for nuclear potential of strong interaction for scattering and sticking forces. Image of global optical potential is drawn in Fig. 2. The real part, namely deep trapping potential $V(r)$ is a well with rather round shape near at surface of nucleus (Woods–Saxon type), but is approximated to be constant value V_0 within in nucleus.

$$U(r) = V(r) + iW(r). \tag{1}$$

V_0 is about -25 MeV for deuteron. V_0 value saturates to about -50 MeV for nuclei of $A > 24$.

Imaginary part $W(r)$ corresponds to the interaction of charged-pion exchange, and locates near at surface ($r = r_0$) to be approximated by delta-function $W_0\delta(r - r_0)$. When we use this delta-function approximation, fusion rate formula becomes simple.

1.4. T-matrix and Reaction Cross-section

Now we briefly summarize quantum mechanical basis of scattering and reaction process.

Asymptotic wave function [6,7] after scattering (interaction) is written by Eq. (2).

$$\Psi(r) \approx \mathrm{e}^{ikz} + f(\theta)(\mathrm{e}^{ikr}/r). \tag{2}$$

Differential cross-section of process is defined by

$$\frac{\mathrm{d}\sigma}{\mathrm{d}\Omega} = |f(\theta)|^2. \tag{3}$$

S-matrix is defined by the phase-shift analysis [6,7] as using Legendre polynomial expansion for scattering amplitude $f\ (\theta)$,

$$f(\theta) = (1/2ik)\sum_{l=0}^{\infty}(2l+1)(S_l - 1)P_l(\cos\ \theta), \tag{4}$$

$$S_l = \mathrm{e}^{2i\delta_l}. \tag{5}$$

In general reaction process, not only elastic scattering but also absorption, fusion, particle emission processes are taking place as transition. To treat the transition from (α, β) to (α', β') channel, evaluation of T-matrix elements are usually done. T-matrix is defined [7] by the following Lippmann–Schwinger equation,

$$T = U + UG_0T, \tag{6}$$

$$G_0 = (E - H_0 + i\delta)^{-1}, \tag{7}$$

$$H = U + H_0. \tag{8}$$

Here, G_0 is the Green operator for H_0 Hamiltonian with kinetic energy and spin Hamiltonian only. So, U is regarded as the effective interaction Hamiltonian.

Scattering amplitude is defined by,

$$f(\theta; \alpha\beta \to \alpha'\beta') = -(2\pi/h^2)\left\langle \Psi_{\alpha'\beta'}|T|\Psi_{\alpha\beta}\right\rangle. \tag{9}$$

If we approximate $T = T^{(0)} = U$, formula (9) becomes the Born approximation.

Lippmann–Schwinger equation can be regarded as an integral type equation of Schroedinger differential equation. The first-order approximation of T is given by inserting $T = U$ in Eq. (6), and we get $T^{(1)} = U + UG_0U$. The second-order approximation is then given as $T^{(2)} = U + UG_0T^{(1)}$, and the nth order approximation gives $T^{(n)} = U + UG_0T^{(n-1)}$. This successive treatment is known as Neumann series solution [8] of integral equation.

We can treat reaction cross-section including transition by evaluating T-matrix elements.

For the optical potential of $V + iW$ type with constant V and W values, formulas of reaction cross-section are given in standard text book of nuclear physics (Chapter 9 of Ref. [6], for example) for S-wave ($l = 0$).

$$\sigma_{r,0} = \pi\bar{\lambda}^2 \frac{-4kR\,\mathrm{Im}\,f_0}{(\mathrm{Re}\,f_0)^2 + (\mathrm{Im}\,f_0 - kR)^2}, \tag{10}$$

$$K = \frac{1}{\hbar}\sqrt{2M(E + V + iW)}, \tag{11}$$

$$f_0 = KR\ \cot\ KR. \tag{12}$$

And relations between S-matrix and T-matrix for Legendre coefficients are:

$$T_\ell = \mathrm{e}^{i\delta_\ell}\ \sin\ \delta_\ell, \tag{13}$$

$$S\ell = 1 + 2iT_\ell. \tag{14}$$

By evaluating T-matrix elements, we can treat reaction with channel transition.

As shown in Figs. 3 and 4, Li evaluated [9] fusion cross-section for dd, dt and d^{3}He reactions using S-matrix formulas. Fusion cross-sections are shown in Fig. 3. S-matrix formula and evaluated values of V and W (written as U_{1r} and U_{1i} in Fig. 4) for dt reaction are shown in Fig. 4.

Li used the reaction cross-section formula with S-matrix elements as shown in Fig. 4. He obtained averaged values of V and W of optical potential by fitting calculated curves to experimental cross-sections.

As explained in nuclear physics text books [6], S-matrix elements by the phase-shift analysis can be used for estimating not only elastic scattering cross-section but also total reaction cross-section. However, the phase-shift analysis does not give information on out-going channels and products by final state interaction.

1.5. Imaginary Part of Optical Potential

Now we move to the explanation of physical meaning for the imaginary part W of optical potential. From the conservation of quantum mechanical probabilistic density flow (a kind of continuity equation), we can take meaning of the imaginary part.

The forward Schroedinger equation is

$$i\hbar\frac{\partial\Psi}{\partial t} = \left[-\frac{\hbar^2}{2M}\nabla^2 + V + iW\right]\Psi \tag{15}$$

and the backward or adjoint equation is

$$-i\hbar\frac{\partial\Psi^*}{\partial t}=\left[-\frac{\hbar^2}{2M}\nabla^2+V-iW\right]\Psi^*. \tag{16}$$

Here we used complex conjugate potential for the adjoint (backward) equation.

We multiply Ψ^* on Eq. (15) from the left side, multiply Ψ on Eq. (16) from the left side and make mutual subtraction to get for the left hand side:

$$i\hbar\left(\Psi^*\frac{\partial\Psi}{\partial t}+\Psi\frac{\partial\Psi^*}{\partial t}\right)=i\hbar\frac{\partial\Psi\Psi^*}{\partial t}=i\hbar\frac{\partial\rho}{\partial t}. \tag{17}$$

Here,

$$\rho=\Psi\Psi^*. \tag{18}$$

And we get for the right hand side:

$$i\hbar\frac{\partial\rho}{\partial t}=-\frac{\hbar^2}{2M}\left[\Psi^*\nabla^2\Psi-\Psi\nabla^2\Psi^*\right]+i\left[2W\rho\right]=-i\hbar\,\mathrm{div}\,\vec{j}+i\left[2W\rho\right]. \tag{19}$$

Here we used formulas of quantum mechanical current flow as

$$\begin{aligned}\vec{j}&=\frac{\hbar}{2im}(\Psi^*\vec{\nabla}\Psi+\Psi\vec{\nabla}^*\Psi^*)\\&=\frac{\hbar}{2im}(\Psi^*\vec{\nabla}\Psi-\Psi\vec{\nabla}\Psi^*),\end{aligned} \tag{20}$$

$$\begin{aligned}\mathrm{div}\,\vec{j}&=\frac{\hbar}{2im}(\vec{\nabla}(\Psi^*\vec{\nabla}\Psi)-\vec{\nabla}((\Psi\vec{\nabla}\Psi^*))\\&=\frac{\hbar}{2im}(\Psi^*\nabla^2\Psi+(\vec{\nabla}\Psi^*)(\vec{\nabla}\Psi)-\Psi\nabla^2\Psi^*-(\vec{\nabla}\Psi)(\vec{\nabla}\Psi^*))\\&=\frac{\hbar}{2im}(\Psi^*\nabla^2\Psi-\Psi\nabla^2\Psi^*).\end{aligned} \tag{21}$$

Consequently, we obtain the modified continuity equation for probabilistic density flow:

$$\frac{\partial\rho}{\partial t}=-\mathrm{div}(\vec{j})+\frac{2}{\hbar}W\rho. \tag{22}$$

It is obvious that the second term of Eq. (22) corresponds to the absorption rate term of the balance. (We do not have the second term in the continuity equation of fluid.)

Mean-free-path of particle in the strong force field of optical potential is given as (velocity) × (lifetime), namely:

$$\Lambda=(\hbar/2)v/W(r). \tag{23}$$

1.6. Fusion Rate for Steady Molecule

We now move to formulate fusion rate formulas for pseudo-molecule (EQPET molecule) [10–19] of two deuterons and bosonized electrons (quasi-particle) $\mathrm{e}^*(m/m_\mathrm{e}, Z)$. Here, m_e is the electron mass and Z is number charge of quasi-particle.

For deriving the trapping Coulomb potential, we will treat it later. Here, we assume an EQPET molecule is trapped in a shielded Coulomb potential similar to the Morse potential [8]. We illustrate the image of shielded Coulomb potential $V_\mathrm{s}(r)$ with optical potential in Fig. 5. Scales are deformed for easy understanding the feature.

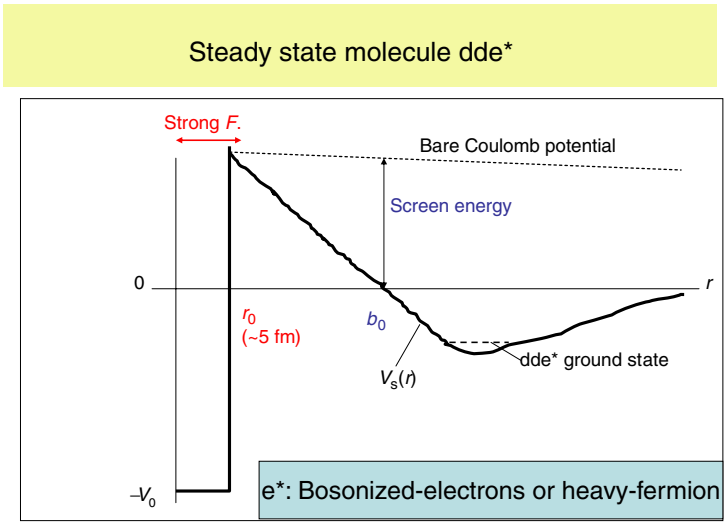

Figure 5. Trapping Coulomb+strong force potential for steady EQPET molecule of dde*.

Range of strong nuclear force is very short in several fm regions, and concentrated in near surface ($r = r_0$) of nucleus. On the other hand, Coulomb interaction as electro-magnetic force distributes from r_0 to nm long region effectively.

As a result, fusion rate for low energy under the strong interaction at around $r = r_0$ can be treated by adiabatic

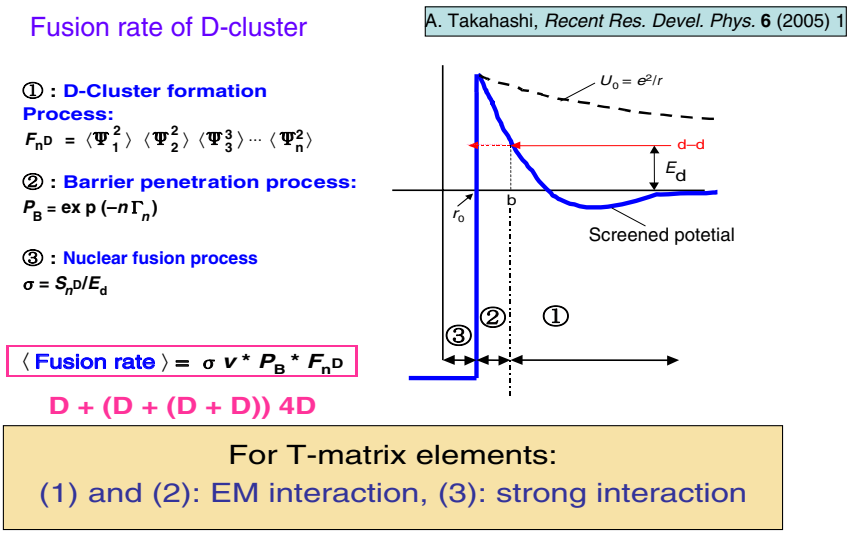

Figure 6. Three adiabatic steps for formulating fusion rate in condensed matter.

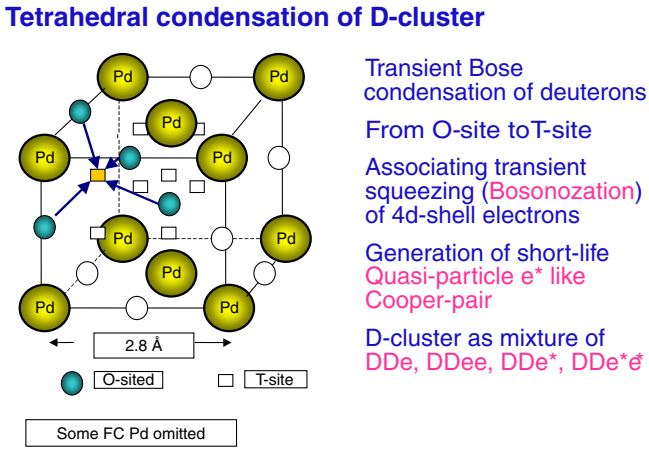

Figure 7. Model-A for TSC formation in PdD lattice under D-phonon excitation.

approximation (namely Born–Oppenheimer approximation in quantum mechanics) to take product of the absorption rate by nuclear optical potential (imaginary part) and the tunneling probability of dd pair at $r = r_0$.

Fusion rate per dd pair is therefore defined as

$$\lambda_{\mathrm{dd}} = T_{\mathrm{n}} |\Psi(r_0)|^2, \tag{24}$$

$$T_{\mathrm{n}} = (2/\hbar)\, \langle \Psi_{\mathrm{f}} | W(r) | \Psi_i \rangle\, . \tag{25}$$

Here, $|\Psi(r_0)|^2$ is equivalent to the quantum mechanical tunneling probability of dd pair through the shielded Coulomb potential $V_{\mathrm{s}}(r)$, as given by the WKB approximation [7]. Fusion rate for muonic molecule dde*(208,1) can be approximately given by Eq. (24), assuming the lifetime of muon is long enough. Actually the lifetime of muon is 2.2 μs, and trapping potential should be regarded as adiabatic.

1.7. Fusion Rate for Dynamic Process

For more transient and dynamic process than muonic dd molecule, it is better to use formulas (Fermi's second golden rule) for cross-section. Especially, for fusion rate calculations of EQPET molecules dde*(2,2), dde*(4,4), dde*(6,6), dde*(8,8), lifetimes of pseudo-molecules are much shorter (assuming on the order of femto-second) than muonic dd molecule.

Fusion rate is formulated as

$$\lambda = \sigma v = (1/\hbar) v T^2 \rho(E'), \tag{26}$$

$$T = \langle \Psi_{\mathrm{f}} | H_{\mathrm{int}} | \Psi_i \rangle\, . \tag{27}$$

Here v is the relative velocity for d–d interaction, $\rho(E')$ is the final state density, and H_{int} is the effective interaction Hamiltonian as given by the approximate solution of Lippmann–Schwinger equation.

Fusion rate per dd pair is given by $\langle \sigma v \rangle$. Cross-section σ is proportional to the square of T-matrix. To evaluate T-matrix elements, we need to treat many steps of physics as the formation process of EQPET dde* molecule by the consequence of electromagnetic interaction in ordered (or constrained) space in condensed matter—solid state

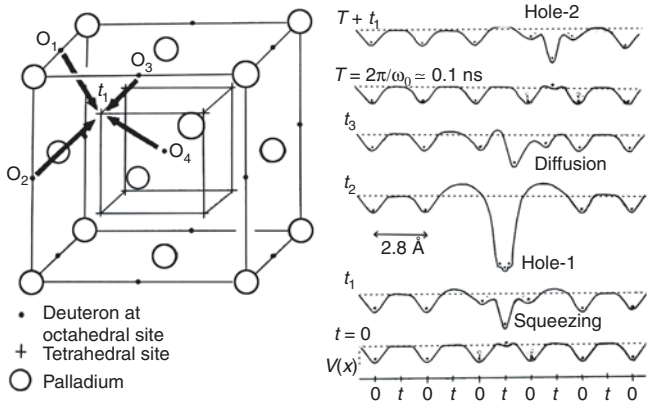

Figure 8. Image of lattice potential change by D-phonon excitation.

physics calculation of dynamic behavior of deuterons in lattice Bloch potential, atomic physics calculation to evaluate shielded Coulomb potential $V_s(r)$ and strong interactions by global optical potential. After that, we need to evaluate the intermediate compound state with excited energy and spin-party state. Finally, we have to evaluate out-going channels and branching ratios of the final state interaction. In every step, we need to evaluate T-matrix elements.

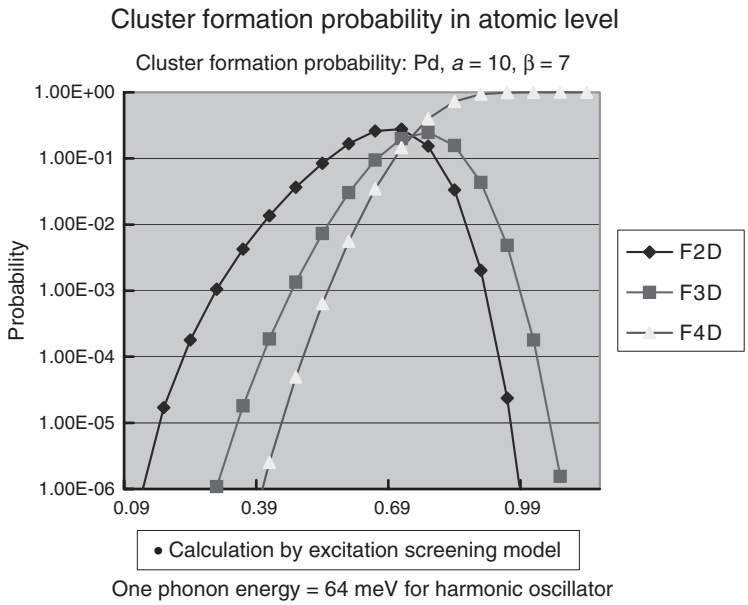

Figure 9. Example of estimation of D-cluster formation probability [20].

2. Example: EQPET/TSC Model

2.1. Tetrahedral Symmetric Condensate (TSC)

As a seed of cold fusion or more extendedly condensed matter nuclear effects, a charge-neutral entity (pseudo-particle) of Platonic regular polyhedron composed with alternative positioning of deuteron (or proton) and electron at vertex of polyhedron has been porposed [9–19]. A representative one is the tetrahedral symmetric condensate (TSC), which is composed of four deuterons forming a regular tetrahedron and four electron balls also forming a regular tetrahedron. Each particle or ball sits at vertexes of cube. An electron ball at vertex depicts effective electron center of coupled two electrons having opposite spins each other. TSC is a transient pseudo-particle with short life (on the order of 100 fs at shortest). Exact place and condition for TSC production is still open question, but two models were proposed [11–17]. One (Model A) is the transient formation of TSC at T-sites of PdD under D-phonon excitation. The other (Model B) is the resonant coupling of two D_2 molecules at some focal points (corner hole, defect, etc.) in near surface of metal-deuteride. TSC can make time-dependent squeezing motion under three-dimensional constraint to condensate at central focal point to become transiently a very small (on the order of 10 fm) charge-neutral pseudo-particle, which will make self-fusion of four deuterons within strong interaction (charged-pion exchange) range or will make deuteron-cluster-capture reaction with host metal nucleus [11–17].

Estimation of fusion rate by the TSC squeezing motion has been formulated by evaluating T-matrix elements in three adiabatic steps, as illustrated in Fig. 6.

The first adiabatic process is for estimating D-cluster formation probability in condensed matter.

$$F_{\mathrm{nd}} = \left\langle {\Psi_1}^2 \right\rangle \left\langle {\Psi_2}^2 \right\rangle \left\langle {\Psi_3}^2 \right\rangle \left\langle {\Psi_4}^2 \right\rangle \cdots \left\langle {\Psi_n}^2 \right\rangle, \tag{28}$$

where Ψ_n is the "lattice" wave function for the nth deuteron. To estimate the D-cluster formation probability F_{nd} is most important for predicting experimental conditions. However practical modeling is of open question for future research.

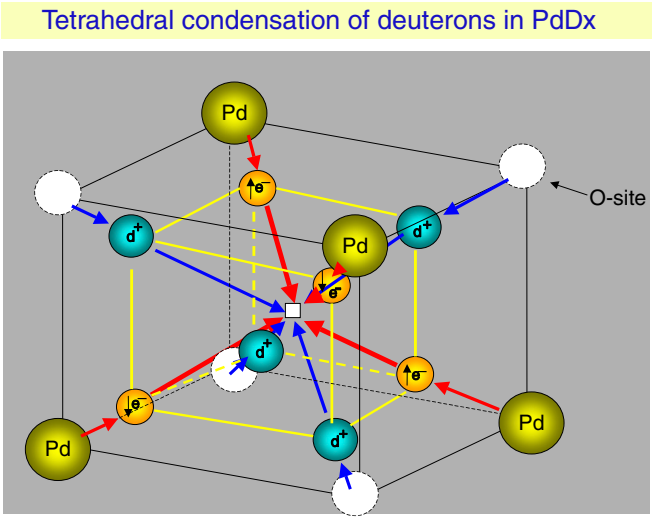

Figure 10. Image of TSC formation in PdD lattice under statistical coherence by phonon excitation.

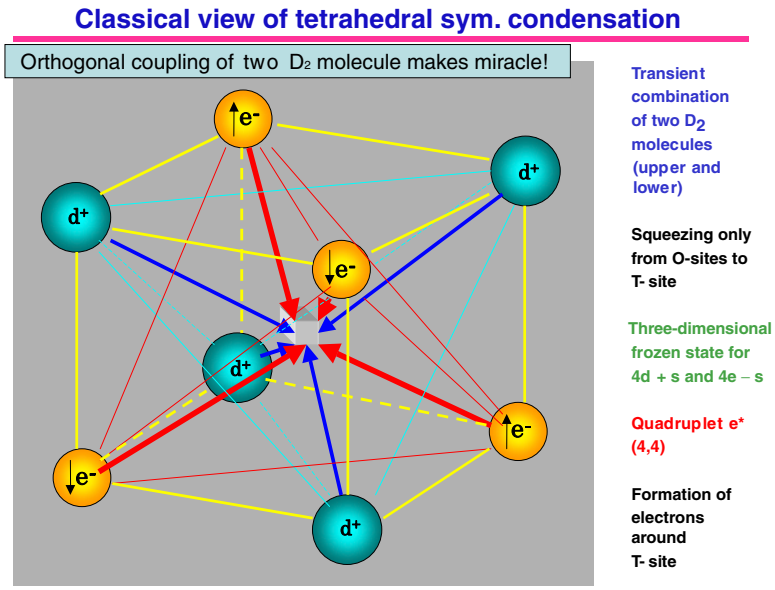

Figure 11. Semi-classical view of TSC (tetrahedral symmetric condensate) for four deuterons and four electron-balls (here electron balls are drawn as single electrons).

The second adiabatic process is for estimating quantum mechanical barrier penetration probability P_{B}. P_{B} is approximately given by the WKB method [7] as

$$P_{\mathrm{B}} = \exp(-n\Gamma_{\mathrm{n}}), \tag{29}$$

where Γ_n is Gamow integral for n-deuterons cluster and given as,

$$\Gamma_n = (\sqrt{2\mu}/h)\int_{r_0}^{b}\sqrt{V_{\mathrm{s}}(r) - E_{\mathrm{d}}}\mathrm{d}r. \tag{30}$$

Here μ is the reduced mass and r_0 and b are given in Fig. 5. For very low energy fusion reaction, b is approximately given by b_0. Once the adiabatic screened potential, as illustrated in Fig. 5, is calculated, for example as we show later by the EQPET model [11–19], the Gamow integral can be numerically obtained by Eq. (30). The barrier penetration probability for multi-body fusion process is given in Eq. (29) by assuming that multi-body interaction takes place as very rapid cascade process of two-body interactions.

The third adiabatic process is for estimating cross-section of multi-body strong interaction. Instead of evaluating T-matrix directly, it is more practical to use S-value, the astrophysical S-value, to write fusion cross-section by strong interaction only as,

$$\sigma_{\mathrm{strong}} = S_{\mathrm{nd}}/E_{\mathrm{d}}. \tag{31}$$

Pure theoretical estimation of S-values for multi-body interaction is difficult because of so many-body (exchanging more than six charged pions for 3d, 4d, 6d, and 8d fusion) problems. We introduce instead an empirical extrapolation as shown later.

Model A for TSC formation is illustrated in Fig. 7. We assume local fulfillment of $x = 1$ for PdDx lattice. We do not necessarily require the $x = 1$ condition (full D-loading) for balk Pd sample. The local $x = 1$ condition may

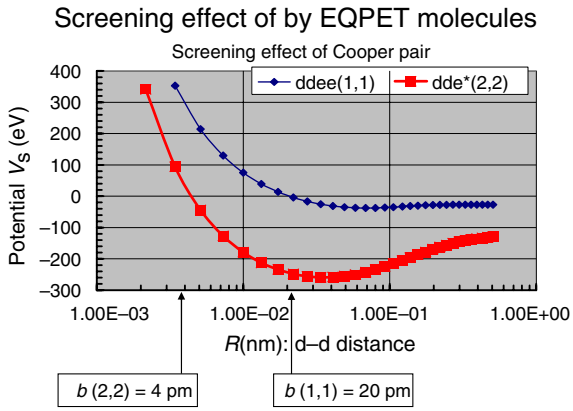

Figure 12. Screened Coulomb potential for ddee (D_2 molecule) and dde*(2,2) (EQPET molecule with Cooper pair); change of b-parameter with deepening of negative potential depths results in condensing force for dde* pseudo-molecule.

be fulfilled in near surface zone of Pd sample in experiment. Then we assume that D-in lattice is excited to higher phonon energy state by external stimulation. Laser beam irradiation on Pd sample surface may be a stimulation method for optical phonon excitation. It is known that D in PdDx lattice sits as Harmonic oscillator with $\hbar\omega = 64\,\text{meV}$ and $E_0 = 32\,\text{meV}$.

As a function of phonon energy, we can estimate D-cluster formation probabilities at central T-sites, as example of such calculation is shown in Fig. 9. However this process is essentially time-dependent (transient), and we have to treat more exactly the process as illustrated in Fig. 8. We may first estimate the D-cluster formation probability within a small time-interval of "deep trapping hole" in Fig. 8, by treating adiabatically the state (adiabatic dde* state). Then we will make time-averaging for the periodical oscillation process. The adiabatic dde* state is regarded as the most squeezed state (MSS). Numerical calculation for screened potential $V_s(r)$ will be then done (shown later) by EQPET.

The example of D-cluster formation probability for Model A, as shown in Fig. 9, is the treatment [20] with quantum mechanical statistics, which does not include anti-parallel spin configuration for pairing electrons forming electron balls, neither treating the three dimensional constraint of squeezing motion under Platonic symmetry yet.

Centralized point-symmetric coherence of momentum-vectors for four deuterons and four-electron balls is required to form TSC. This condition cannot be expected in random motion of particles in plasma. The squeezing motion under three-dimensional constraint (or ordering, or self-organization process) in lattice dynamics can realize that condition.

The semi-classical image of 4D cluster (TSC) is shown in Fig. 10. Pd atom has 10 outer most electrons in 4d-shell. Pd atom is unique atom having largest number of valence electrons among atoms in nature. Electrons in 4d-shell contribute as quasi-free conduction-band electrons in Pd metal lattice.

Transition of physical system happens to realize the system-energy minimum state. The local energy minimum condition is formulated by the variational principle of quantum mechanics [7,8]. Eigen-value problem is led to solve secular equation.

However, under the ordering process (or self-organization process) in three-dimensional constrained motion, the Platonic symmetry (regular polyhedron) for alternative positioning of deuteron (proton) and electron-ball makes obviously the averaged system electric charge zero. Namely TSC realizes minimum system Coulomb energy. Hence the TSC state can be a particular solution of variational method.

The semi-classical image of TSC is shown in Fig. 11. Pair of counter-part two electrons is the combination of anti-parallel spins, combination probability of which can be estimated simply. When momentum vectors of pairing two

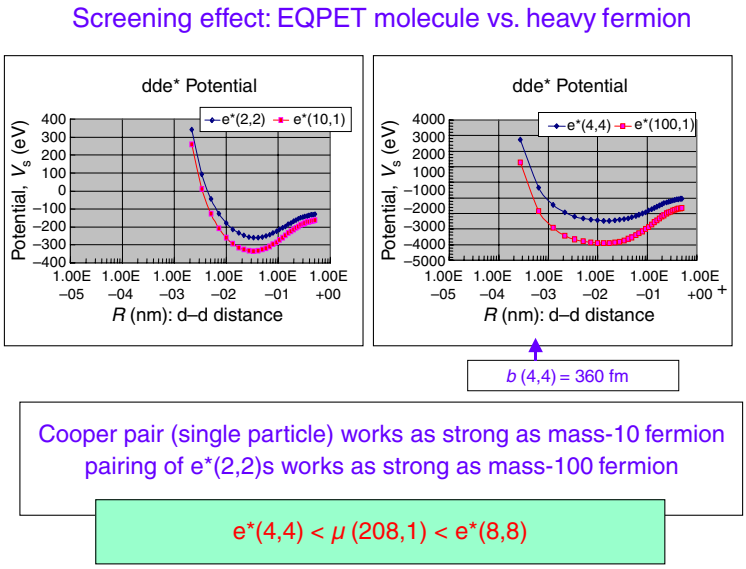

Figure 13. Comparison of screened Coulomb potentials between EQPET molecules and virtual molecules with heavy fermions; muon works as much as e*(6,6), cf. Tables 1 and 2.

electrons are 180° opposite configuration, the transient Cooper pair e*(2,2) is formed. Moreover, in TSC configuration, two Cooper pairs may couple orthogonally to form the quadruplet quasi-particle e*(4,4). As a general concept, this is the *bosonization* of electrons. Here, more exact quantum mechanical image for electron-ball is a pseudo-particle of 1/2 of coupling of two electrons with anti-parallel spin each other. More exact image is shown later in the time-dependent problem.

2.2. EQPET Model

It is difficult to evaluate directly the total TSC wave function because of so many-body problems. The EQPET (electronic quasi-particle expansion theory) model assumes that the total TSC wave function can be written by the

Table 1. Calculated screening energies by EQPET model

e*	U_s (eV)		b_0 (pm)	
	dde*	dde*e*	dde*	dde*e*
(1,1)	36	72	40	20
(2,2)	360	411	4	3.5
(4,4)	4000	1108	0.36	1.3
(8,8)	22,154	960	0.065	1.5
(208,1)	7579	7200	0.19	0.20
(6,6)	9600		0.15	

Screening energy of EQPET molecules $U_s = -e^2/b_0$ for $V_s(b_0) = 0$

linear combination of partial wave functions for EQPET molecules dde* for e*(2,2) and e*(4,4) and regular molecules dde (D_2^+ ion) and ddee (D_2 molecule).

$$|\Psi_N\rangle = a_1 \left|\Psi_{(1,1)}\right\rangle + a_2 \left|\Psi_{(2,2)}\right\rangle + a_4 \left|\Psi_{(4,4)}\right\rangle + a_6 \left|\Psi_{(6,6)}\right\rangle + a_8 \left|\Psi_{(8,8)}\right\rangle. \tag{32}$$

Here equation is written for including the case of OSC (octahedral symmetric condensate). For TSC, a_6 and a_8 are zero.

Fusion rate formula for dde* is given [11–19] by,

$$\lambda_{(i,j)} = v\,(S_{2d}/E_d)\exp\left(-2\Gamma_{(i,j)}\right), \tag{33}$$

$$\Gamma_{(i,j)} = 0.218 \int_{r_0}^{b(i,j)} \sqrt{V_{s(i,j)}\,(R_{dd}) - E_d}\ \mathrm{d}R_{dd}. \tag{34}$$

Here R_{dd} is the inter-nuclear distance between two deuterons in D-cluster.

The modal fusion rate for TSC system is given by

$$\lambda_N = {a_1}^2\lambda_{(1,1)} + {a_2}^2\lambda_{(2,2)} + {a_4}^2\lambda_{(4,4)} + {a_6}^2\lambda_{(6,6)} + {a_8}^2\lambda_{(8,8)}. \tag{35}$$

Formulas for screened Coulomb potentials V_s of EQPET molecules were given [11–19] by applying the solution for D_2^+ ion and D_2 molecule, based on the variational method [21], as for dde*,

$$V_{s(i,j)} = \frac{e^2}{R_{dd}} + V_h + \frac{J+K}{1+\Delta}, \tag{36}$$

$$V_h = -13.6(e^*/e)^2\left(m^*/m_e\right). \tag{37}$$

Here V_h is the virtual binding energy of EQPET atom de*. And,

$$i = e^*/e \tag{38}$$

is the number charge of e*, and

$$j = m^*/m_e. \tag{39}$$

The Coulomb integral J is given as

$$J = (Ze^2/a_B)\left[-\frac{1}{y} + \left(1+\frac{1}{y}\right)\exp(-2y)\right]. \tag{40}$$

The electron exchange integral K is given by

$$K = (Ze^2/a_B)(1+y)\exp(-y). \tag{41}$$

Table 2. Main parameters of screened Coulomb potentials

Parameters of dde* potentials			
Trapping depth		Ground state	
e*(m, Z)	V_{smin}(eV)	b_0 (pm)	R_{dd} (gs) (pm)
(1,1)	− 15.4	40	101
(1,1) × 2; D_2	−37.8	20	73
(2,2)	−259.0	4	33.8
(4,4)	−2460	0.36	15.1

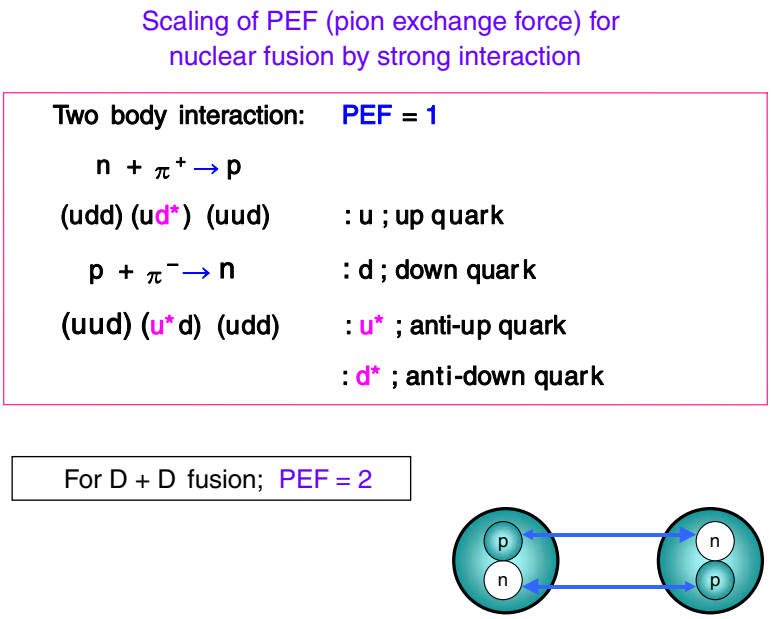

Figure 14. Definition of scaling measure PEF for fusion reaction.

The non-orthogonal integral is

$$\Delta = \left(1 + y + \frac{y^2}{3}\right) \exp(-y) \tag{42}$$

with

$$y = R_{\mathrm{dd}} / \left(a_{\mathrm{B}} / Z / \left(m^* / m_{\mathrm{e}}\right)\right). \tag{43}$$

Here $aB = a_{\mathrm{B}}/Z/(m^*/m_{\mathrm{e}})$, a_{B} is Bohr radius (52.9 pm) and $Z = \mathrm{e}^*/\mathrm{e} = i$.

Fusion rate for multi-body reaction is given approximately by

$$\lambda_{\mathrm{nd}(i,j)} = v\,(S_{\mathrm{nd}}/E_{\mathrm{d}}) \exp\left(-n\Gamma_{(i,j)}\right). \tag{44}$$

Modal fusion rate of multi-body fusion for TSC is then given by

$$\lambda_{N\mathrm{nd}} = \sum_i a i^2 \lambda_{\mathrm{nd}(i,j)}. \tag{45}$$

Calculated results of screened Coulomb potentials for EQPET molecules are shown in Figs. 12 and 13.

Compared to the bare Coulomb potential, a low energy d–d pair can come closer to the position b_0 classically and then penetrates quantum mechanically to the point $r = r_0$ of strong interaction range. It is well known that muonic molecule dde*(208,1) realize large dd fusion rate. Shielded Coulomb potential for dde*(4,4) is equivalent to the one for dde*(100,1), and dde*(6,6) has almost the same shielded Coulomb potential as muonic molecule. Here muon mass is used 207 plus 1 considering one electron added.

Screening energy by e* is estimated by calculating bare Coulomb energy at $r = b_0$. Calculated screening energies are given in Table 1.

Table 3. Calculated barrier factors and fusion rates (per cluster) for dde*

(m*,e*)	Barrier factor (BF)				Fusion rate (f/s/cl.) (FR)			
	2D	3D	4D	8D	2D	3D	4D	8D
(0,0)	10^{-1685}				10^{-1697}			
(1,1)	10^{-125}	10^{-187}	10^{-250}	10^{-500}	10^{-137}	10^{-193}	10^{-252}	10^{-499}
(2,1)	10^{-53}	10^{-80}	10^{-106}	10^{-212}	10^{-65}	10^{-86}	10^{-108}	10^{-211}
(2,2)	10^{-7}	10^{-11}	10^{-15}	10^{-30}	10^{-20}	10^{-17}	10^{-17}	10^{-29}
(4,4)	(3×10^{-4})	10^{-5}	10^{-7}	10^{-14}	(10^{-16})	10^{-11}	10^{-9}	10^{-13}
(8,8)	(4×10^{-1})	(2×10^{-1})	(1×10^{-1})	2×10^{-2}	(10^{-13})	(10^{-7})	(10^{-3})	10^{-1}

$E_d = 0.22$ eV and ( ) indicates that the value is virtual rate

2.3. Multi-Body Strong Interaction

We now move to explain the empirical formulas for extrapolating S-values of intrinsic cross-section terms of two-body and multi-body strong interaction in fusion reaction process.

Basic measure pion exchange force (PEF) is defined as the scale of effective surface area for very short range attractive force, that is the catch-ball of charged pion between neutron–nucleon and proton–nucleon between two fusing nuclei. One PEF is defined as the number of string between n and p, as illustrated in upper figure of Fig. 14.

As discussed in Section 1, sticking force of fusion happens at near surface of fusing nuclei.

The larger is the sticking surface area, the larger is the fusion cross-section. Using the PEF measure, PEF = 1 for HD fusion, PEF = 2 for DD fusion, and PEF = 3 for DT fusion, respectively, as example for DD fusion is drawn in the lower figure of Fig. 14.

Let us consider fusion reaction of deuteron with heavier nucleus, for example ^{6}Li + d fusion. As drawn by the right figure of Fig. 15, catch-ball of charged pions is interfered for about half of nucleons in ^{6}Li nucleus due to self-shielding by more front nucleons. As consequence of the self-shielding effect, PEF value would be around 3. For more heavy nuclei, PEF value should saturate to effective PEF values for interacting surface area.

On the contrary, multi-body deuteron fusion under the Platonic polyhedral configuration (e.g., regular tetrahedron for 4d fusion), there is no self-shielding effect. We can expect perfect exchange of charged pions among all deuterons of regular tetrahedral configuration as drawn in the left figure of Fig. 15. Thus, PEF = 12 is given for 4d fusion. Similarly PEF = 6 is given, for 3d fusion. We can say that effective sticking surface for multi-body fusion becomes very large as scaled by PEF number.

Table 4. All possible decay channels from ^{8}Be*

Decay-channel of ^{8}Be
4D → ^{8}Be + 47.6 MeV:
^{8}Be → ^{4}He + ^{4}He + 91.86 keV: Major Ch.
→ ^{3}He + ^{5}He(n + ^{4}He) − 11.13 MeV
→ t + ^{5}Li(p + ^{4}He) − 21.68 MeV
→ d + ^{6}Li − 22.28 MeV
→ p + ^{7}Li − 17.26 MeV
→ n + ^{7}Be − 18.90 MeV

^{8}Be excited state may open to threshold reactions

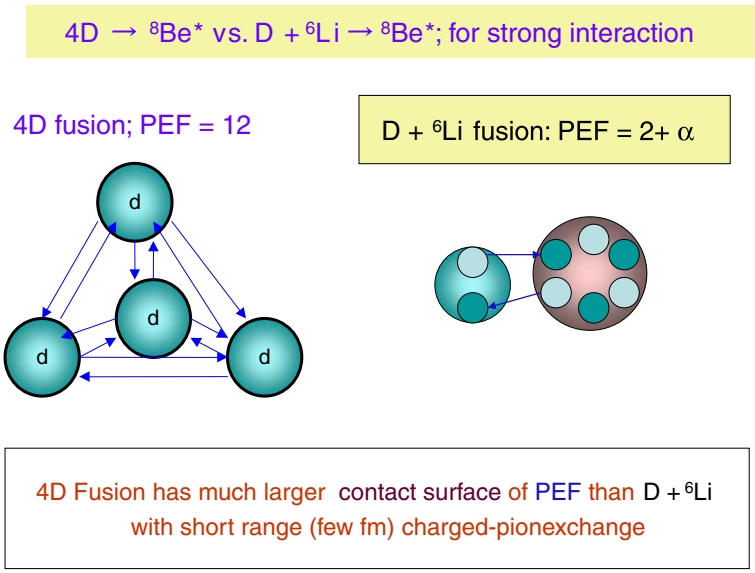

Figure 15. Estimation of effective sticking surface for fusion reactions, by the PEF measure for strength of charged pion exchange.

Here we recognize that ^{8}Be* is intermediate compound state both for the ^{6}Li + d and 4d reactions. And 4d fusion due to Platonic symmetry will have much larger cross-section than the ^{6}Li + d reaction.

Pion exchange force values, hence fusion cross-sections for 6d and 8d fusions in OSC condition may become much larger than 4d fusion.

Using known experimental $S(0)$-values for boson-related fusions, as pd, dd, and dt fusion, we draw plot of $S(0)$ values as a function of PEF value, and extrapolate to multi-body fusion using scaling formula, as shown in Fig. 16.

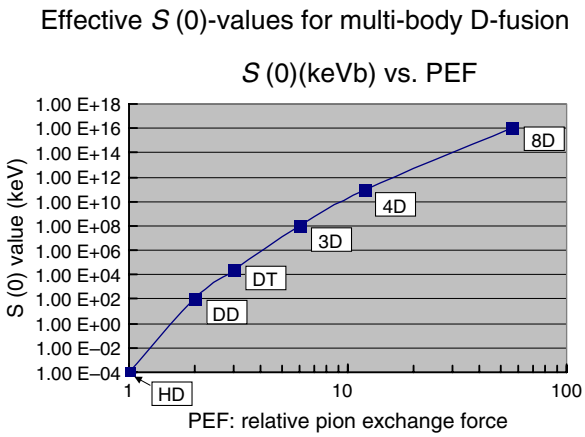

Figure 16. Empirical extrapolation of $S(0)$ values as a function of PEF (effective sticking surface of fusion reaction) number, for multi-body fusion.

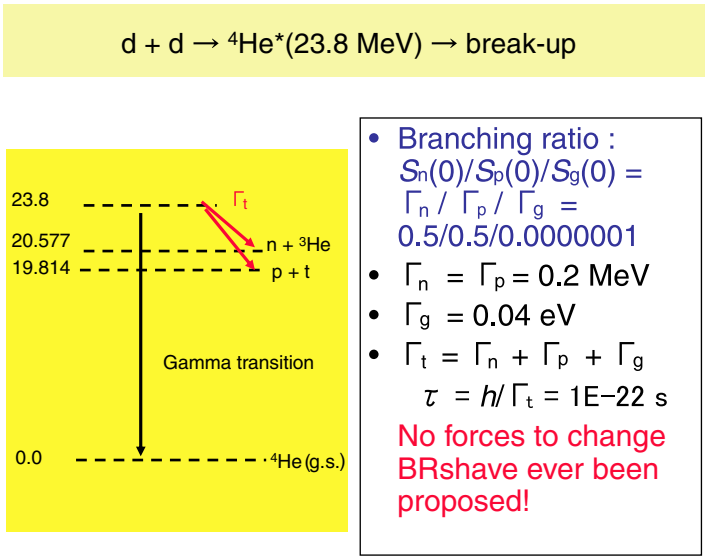

Figure 17. Final state interaction and branching ratios for dd fusion.

See also Fig. 2.

$$S_{\mathrm{n}}(0) \propto {T_{\mathrm{n}}}^2 \propto (\mathrm{PEF})^N. \tag{46}$$

Using $S_{\mathrm{dd}} = 100$ keVb and $S_{\mathrm{dt}} = 2 \times 10^4$ keVb, we estimated as scaling exponent $N = 11.4$ and we got $S_{4\mathrm{d}} = 1 \times 10^{11}$ keVb.

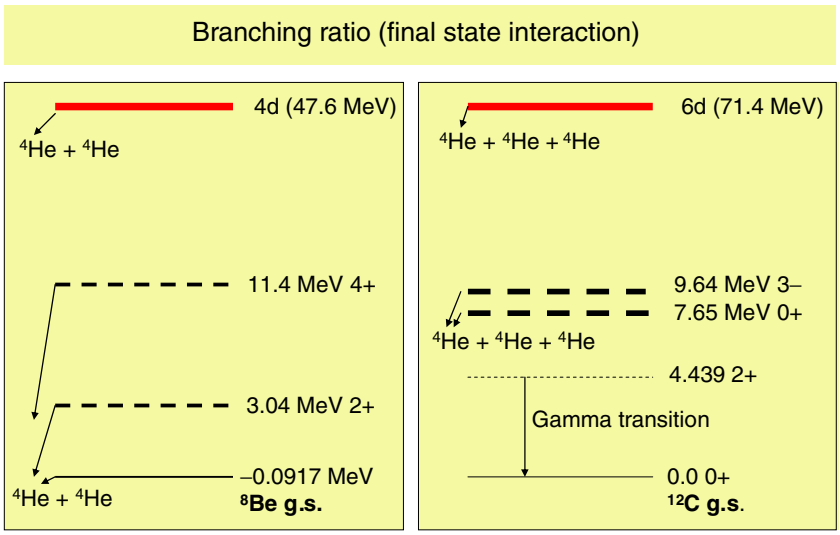

Figure 18. Final state interactions for 4d and 6d fusion reactions in condensed matter.

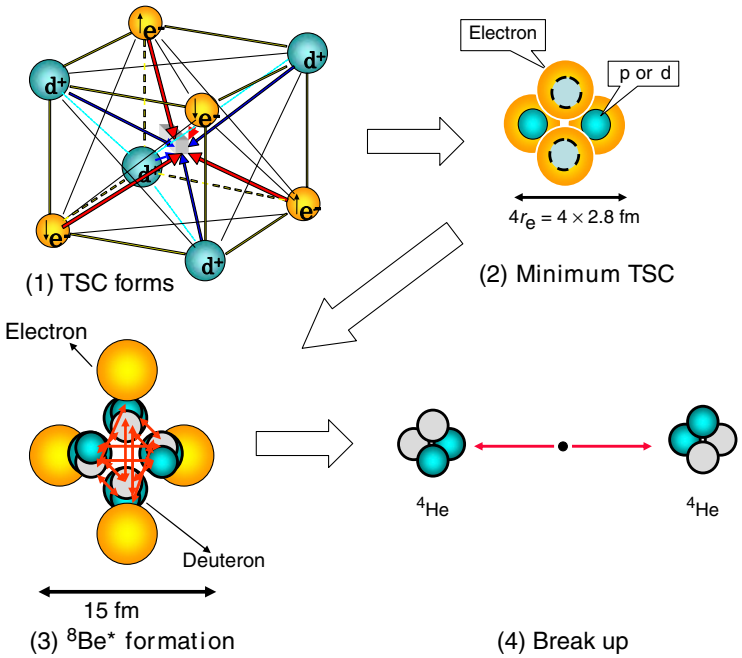

Figure 19. Semi-classical view of TSC squeezing motion and self-4d fusion reaction, here electron with spin should be electron-ball of 1/2 of two bosonized electrons in QM view.

Now we have finished preparation for fusion rate calculation. Calculated barrier penetration probabilities and fusion rates are shown in Table 3 for dde* EQPET molecules.

2.4. Final State Interaction

We now briefly summarize on the final state interactions and branching ratios to plural out-going channels.

The out-going break-up channels and branching ratios for dd fusion are very well established as shown in Fig. 17.

Unless we could change the intermediate excited state ^{4}He*($E_x = 23.8$ MeV) by some external forces putting in (see the lower figure of Fig. 14, for d–d reaction), we have no way to change the branching ratios. Namely, major channel for ^{4}He generation never happens otherwise. The electromagnetic interaction (QED, phonon coupling, etc.) is too weak to change the intermediate compound state. In the view of author, to put additional charged pion exchange into

Table 5. Time-averaged fusion rates by TDEQPET model, compared with values at $t = 0$

e*(m, Z)	$\langle\lambda_{2d}\rangle$ (f/s/cl.)	$\langle\lambda_{4d}\rangle$ (f/s/cl.)	$\lambda_{2d}(0)$ (f/s/cl.)	$\lambda_{4d}(0)$ (f/s/cl.)
TDEQPET cal. for EQPET molecules				
(1,1)	4.3×10^{-44}	7.8×10^{-63}	1.9×10^{-60}	7.3×10^{-93}
(2,2)	2.9×10^{-25}	2.5×10^{-24}	2.4×10^{-37}	1.1×10^{-50}
(4,4)	$(2.1 \times 10^{-17})^*$	5.5×10^{-8}	$(5.5 \times 10^{-22})^*$	5.9×10^{-20}

$(\,)^*$: virtual value

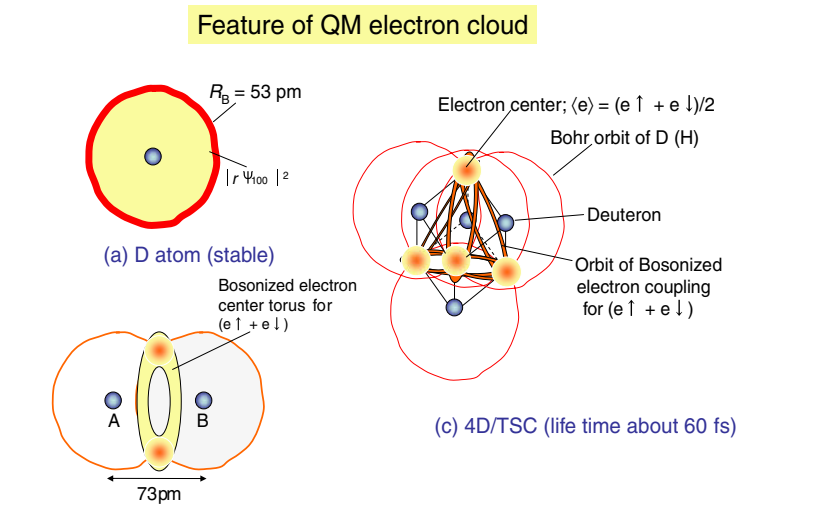

Figure 20. Initial state TSC wave function, compared with wave functions of D atom and D_2 molecule.

the d–d interaction by participating additional hadrons is actually possible way to get to the ^{4}He production: however, this idea leads ones automatically to the multi-body (or cluster) fusion process.

In Fig. 18, the final state interaction is drawn. The table of possible out-going channels is given in Table 4. The highly excited state ^{8}Be* can be regarded as a collectively deformed nucleus of two α-clusters, because of very hard formation of α-cluster in ^{8}Be nucleus. The very high (47.6 MeV) excited energy is therefore rarely redistributed to single nucleon (n or p), or d, or t-cluster for particle emission. Here one remembers that binding energy per nucleon for ^{4}He nucleus is 7 MeV and so total binding energy of ^{4}He nucleus is 28 MeV. This is the reason that α-cluster formation in light nuclei is very plausible.

We can speculate that all threshold reactions in Table 4 will not open in the final state interaction from 4d fusion, due to collective deformation of two α-clusters. Therefore, ^{8}Be* will decay with almost 100% weight to two ^{4}He with 23.8 MeV kinetic energy per ^{4}He, as illustrated in Fig. 18. The decay channel of 6d fusion by OSC is also shown in the right figure of Fig. 18. This process will give also 23.8 MeV per ^{4}He.

We know that p + ^{7}Li and n + ^{7}Be channels appear in the ^{6}Li + d beam-target reaction.

We understand that these branches are caused by stripping reactions taking n or p from deuteron approaching to ^{6}Li nucleus. The purely symmetric strong force exchange in the Platonic polyhedral condition, e.g., in the case of 4d/TSC reaction in PdD lattice, ignores the stripping process.

2.5. Time-dependent Approach

Detail of time-dependent analysis is given in Ref. [19]. Brief feature is illustrated in Fig. 19. The semi-classical squeezing motion of TSC will get to its minimum size state with about 10 fm diameter in about 74 fs. Calculated effective time-interval for 4d fusion is about 0.04 fs, namely very much short.

The TSC wave function at the starting point ($t = 0$) can be drawn by superposition of six D_2 molecule wave functions on six surfaces of cube, as shown in Fig. 20c. To calculate approximately time-dependent fusion rates, we

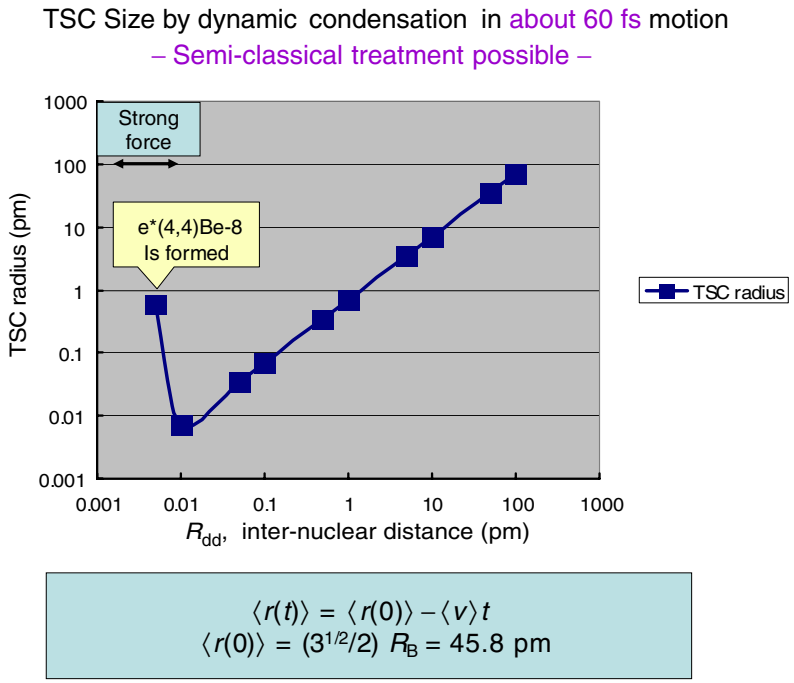

Figure 21. Linear decrease of TSC size by semi-classical Newtonian motion.

can use adiabatic dde* potentials, dividing into three time intervals for; normal electron state, Cooper pair state and quadruplet state, respectively. For more accurate analysis, we need to develop an algorithm of molecular dynamics under three-dimensional constraint motion. This is our future task.

Time-dependent squeezing motion of TSC was first treated by the time-dependent EQPET (TDEQPET) model [18].

$$a_i \Psi_{4D}(r,t) = a_1 \Psi_{(1,1)}(r,t) + a_2 \Psi_{(2,2)}(r,t) + a_4 \Psi_{(4,4)}(r,t), \tag{47}$$

$$\langle r(t)\rangle = \langle r(0)\rangle - \langle v\rangle t. \tag{48}$$

Because of the three-dimensionally and symmetrically constraint motion with averaged charge-neutrality for total TSC system, there is no force to stop squeezing motion until TSC size gets into the range of strong interaction (range of pion exchange). Therefore, the squeezing motion can be treated by the semi-classical Newtonian motion, as illustrated in Fig. 21.

To calculate time-dependent barrier penetration probability, we assumed that time-dependent change of potential can be replaced with three adiabatic potential V_s for D_2 molecule, dde*(2,2) and dde*(4,4) in three time intervals sequentially, according to the change of $\langle r\rangle$ value comparing with b_0-parameters of adiabatic potentials.

Time-dependent Gamow integral is defined as

$$\Gamma(t) = 0.218 \int_{r_0}^{b(t)} \sqrt{V_s(R_{dd}) - E_d}\ \mathrm{d}R_{dd}. \tag{49}$$

Here $b(t)$ is set to $\langle r(t)\rangle$ for $\langle r(t)\rangle > b_0$ parameter in each time interval for assumed adiabatic potential, namely e* state.

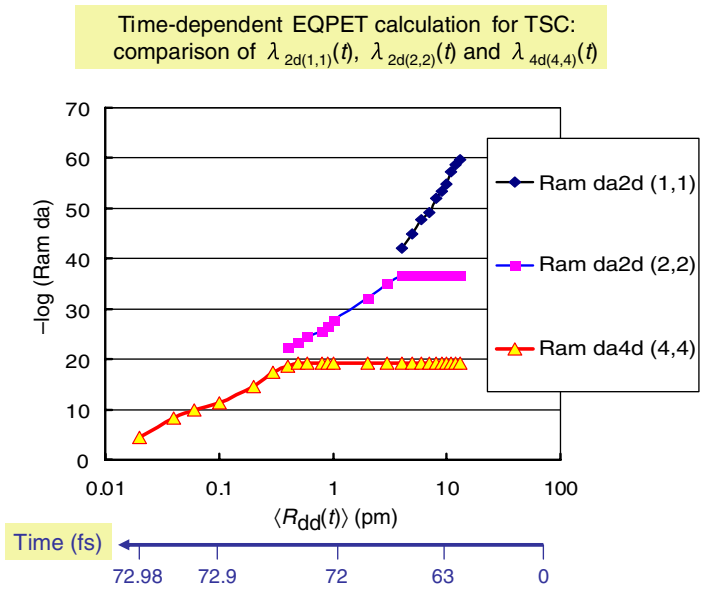

Figure 22. Calculated time-dependent fusion rates by TDEQPET model.

Time dependent fusion rates were calculated, as shown in Fig. 22. Time-averaged fusion rates were obtained as listed in Table 5.

Maximum TSC density possibly produced in PdD lattice is on the order of 1×10^{22} TSC/cm^3. Multiplying this number to cluster fusion rates in Table 5, we obtain dd fusion rate, which emit neutrons on the order of 3×10^{-3} n/s/cm^3. This level of neutron emission is difficult to detect by usual detectors. On the contrast, we obtain 4d fusion rate as $5.5 \times 10^{14}\alpha$ /s/cm^3 which corresponds to 55 kW/cm^3 power level. Thus, neutron free clean fusion reaction producing large heat density and ^{4}He ash, as reported by experiments of Arata, McKubre, de Ninno, Violante, Isobe, etc. can be now theoretically explained.

References

[1] J.M. Blatt, V.F. Weisskopf, *Theoretical Nuclear Physics*, Chapter VIII (Springer, Berlin, Heidelberg, New York, 1979).
[2] A. Takahshi et al., *JJAP* **41** (2001) 7031–7046.
[3] M. Ohta, A. Takahashi, *JJAP* **42** (2002) 645–649.
[4] A. Takahashi, Theoretical backgrounds for transmutation reactions, ppt slides for Sunday School of ICCF10, see http://www.lenr-canr.org/ Special Collection for ICCF10.
[5] B. Povh, K. Rith, C. Scholtz, F. Zetsche, *Teilchen und Kerne* (Springer, Berlin, Heidelberg, New York, 1994).
[6] K. Yagi, *Nuclear Physics* (Asakura, Tokyo, 1971) (in Japanese).
[7] L.I. Schiff, *Quantum Mechanics* (McGraw-Hill, New York, 1955).
[8] P.M. Morse, H. Feshbach, *Methods of Theoretical Physics* (McGraw-Hill, New York, 1953).
[9] X.Z. Li et al., *Phys. Rev. C* **61** (2000) 24610.
[10] A. Takahashi, Condensed matter nuclear effects, *Proceedings of the. International Meet. Frontiers of Physics*, Kuala Lumpur, 25–29 July, 2005, *Malays. J. Phys.* to be published.

[11] A. Takahashi, Deuteron cluster fusion and related nuclear reactions in metal-deuterium/hydrogen systems, *Recent Res. Dev. Phys.* **6** (2005) 1–28, ISBN: 81-7895-171-1.
[12] A. Takahashi, *Proceedings of the ICCF9*, pp. 343–348, see Ref [2].
[13] A. Takahashi, Mechanism of deuteron cluster fusion by EQPET model, *Proceedings of the ICCF10*, see Ref [3].
[14] A. Takahashi, *Proceedings of the JCF5, 6*, see http://wwwcf.elc.iwate-u.ac.jp/jcf/.
[15] A. Takahashi, *Proceedings of the ICCF11*.
[16] A. Takahashi, Deuteron cluster fusion and ash, *Proceedings of the ASTI5 Meeting*, see Ref [5].
[17] A. Takahashi, A theoretical summary of condensed matter nuclear effects, in: A. Takahashi (Ed.), *Proceedings of the Siena2005 Workshop*, see also: *Brief Theoretical Summary of Condensed Matter Nuclear Effects*, Debrecen, Hungary, 2005, *Acta Phys. et Chem.* **38–39**, 341–356.
[18] A. Takahashi, Time-dependent EQPET analysis of TSC, *Proceedings of the ICCF12*, Yokohama, 2005.
[19] C.J. Pethic, H. Smith, *Bose-Einstein Condensation in Dilute Gases* (University of Chicago Publication, Chicago, 2001).
[20] A. Takahashi, H. Numata, Y. Iwamura, H. Yamada, T. Ohmori, T. Mizuno, T. Akimoto, *Nuclear Reactions in Solids* **(**Kogakusha, Tokyo, 1999) (in Japanese).
[21] S. Shirato, *Atomic Physics-II* (Nippon Rikou Publ., Tokyo, 1984) (in Japanese).

J. Condensed Matter Nucl. Sci. 1 (2007) 129–141

Research Article

A Theoretical Summary of Condensed Matter Nuclear Effects*

Akito Takahashi†

Osaka University, Yamadaoka 2-1, Suita, Osaka 5650871, Japan

Abstract

Key experimental results are compared with the results of Electronic Quasi-Particle Expansion Theory/Tetrahedral Symmetric Condensate (EQPET/TSC) models. Screening energy for d–d pair by theory is 360 eV and is comparable with 310 eV by Kasagi experiment for PdDx. Helium-4 production with scarce neutron is modeled by strong 4D fusion of minimum state 4d/TSC reaction. Maximum level of 4d/TSC fusion is 46 MW/cm^3-Pd and 23 keV/Pd, comparable to 24.8 keV/Pd by El Boher experiment. Transmutation with mass-8 and charge-4 increase is explained by 4d/TSC + host metal reactions. Fission-like products by Ni–H systems are in agreement with fission products of 4p/TSC + nickel nuclear reactions.

Keywords: d-d Screening, EQPET/TSC model, Excess power level, Experimental results, 4D Fusion, Fission, Helium-4, Selective transmutation

1. Introduction

Most impressive experimental results in Condensed Matter Nuclear Science (CMNS) research in last several years are (1) anomalous enhancements of d–d and 3D fusion rates by low energy (1–10 keV) d-beam/metal-target reactions [1,2]. (2) Intense production of helium-4 (^{4}He) atoms by electrolysis and laser irradiation experiments [3,4], in correlation with excess heat generation. (3) Very intense excess heat production by super-wave electrolysis [5] with high gain (25 times input) was reported in ICCF11. (4) Selective [6] and fission-like [7] transmutations were reported by deuterium permeation through Pd-complexes [6] and Ni–H systems [7].

A series of elaborated theories on deuteron cluster fusion model is reviewed in two papers [8,9]. The Electronic Quasi-Particle Expansion Theory (EQPET) model was proposed and applied for numerical analyses of D- and H/D-mixed cluster fusion in PdDx systems. Formation and squeezing of Tetrahedral Symmetric Condensate (TSC) were modeled with numerical estimations by Sudden Tall Thin Barrier Approximation (STTBA) [9]. Obtained numerical results could explain major claims of CMNS experiments.

*This work is supported by Mitsubishi Heavy Industries Co., Japan.
†Work is done for submission to Siena WS on Anomalies in Metal-D/H Systems, Siena, May 2005. E-mail: akito@sutv.zaq.ne.jp

Table 1. Summary results, experiment versus theory

Item	Experiment author/method/results	EQPET/TSC models
Screening of d–d fusion	Kasagi/D-beam, PdDx/U_s = 310 ± 30 eV Takahashi/3D, TiDx/ $\langle dd \rangle = 1 \times 10^9$ in range	U_s = 360 eV, by dde*(2,2) $(1 \times 10^{13})\tau$ with τ = 0.1 ms
$^4He/^3He$ production	McKubre/electrolysis/31 ± 13 MeV/^{4}He Arata/nano-Pd, El./[^{3}He]/[^{4}He] = 0.25	23.8 MeV/^{4}He by 4D → ^{4}He + ^{4}He + 47.6 MeV, [^{3}He]/[^{4}He] = 0.25, for H/D = 0.6
Maximum heat	El Boher/super-wave El./24.8 keV/Pd gain = 25	23 keV/Pd 46 MW/cm^3-Pd by 4d/TSC
Transmutation	Iwamura/Pd-complex, gas/Cs to Pr Miley/Ni–H, electrolysis/fission-like FP	4d/TSC or ^{8}Be capture, FP by Ni + 4p/TSC

In this paper, we review short summary of theoretical models, in comparison with key experimental results, as briefly listed in Table 1. We have seen very consistent agreements between key experimental results and numerical estimations by EQPET/TSC models.

2. Screening Effects for d–d Fusion in Condensed Matter

When low-energy d-beam is implanted into condensed matter, e.g., PdDx, incident d^+ picks up and conveys an electron, which is quasi-free in conduction band of PdDx lattice to make charge neutralization. A target D-atom (d + e) is waiting for incoming (d + e) as illustrated in Fig. 1.

Incident d gives same velocity to convey electron, which has therefore enough momentum of 180° opposite direction to another electron with target deuteron. We easily expect two electrons form a Cooper pair e*(2,2) with 50% weight for anti-parallel arrangement of spins.

In our previous paper [8], numerical (graphical) result of screened Coulomb potential for d–d interaction $V_s(r)$ is given using the formula, for dde*(m,n) EQPET molecules,

$$V_s(r) = e^2/r + V_h + (J + K)/(1 + \Delta), \tag{1}$$

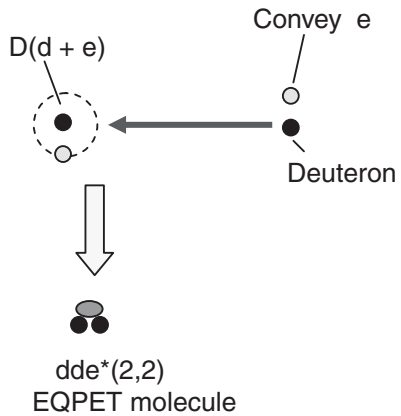

Figure 1. Formation of dde*(2,2) molecule by d-beam injection into condensed matter.

Table 2. Screened energies for various EQPET molecules

e*(m*/me, e*/e)	Screening energy U_s (eV)		b_0 (pm)	
	dde*	dde*e*	dde*	dde*e*
(1,1); Normal electron	36	72	40	20
(2,2); Cooper pair	360	411	4	2
(4,4); Quadruplet	4000	1108	0.36	1.3
(8,8); Octal coupling	22 154	960	0.065	1.5
(208,1); Muon	7579	7200	0.19	0.20

$$V_h = -13.6Z^2/(m_e/m^*) \text{ (in eV unit)}. \tag{2}$$

By defining b_0-parameter to satisfy,

$$V_s(b_0) = 0. \tag{3}$$

We obtain screening energy U_s by

$$U_s = -e^2/b_0 = -1.44/b_0 \text{ (in eV and nm unit)}. \tag{4}$$

Calculated b_0-parameters and screening energies are listed in Table 2.

Kasagi et al. [1] gave $U_s = 310 + -30$ eV for Pd target with 1–10 keV d-beam irradiation, by measuring proton yield from d + d to the p + t + 4.02 MeV reaction channel. Huke [10] gave 320 eV for similar beam target experiments. These experimental values considerably agree with theoretical value 360 eV by dde*(2,2), namely EQPET dd molecule with Cooper pair. These values for screening energy are very large, compared to 72 eV for ddee (D_2).

Takahashi et al. [2] reported anomalously enhanced yield ratios [3D]/[2D] for 3D fusion over 2D fusion, by 50–300 keV d-beam irradiating TiDx ($x > 1.6$) targets with cooling. They gave [3D]/[2D] values on the order of 1×10^{-4}, which were drastically larger than 1×10^{-30} calculated by conventional random nuclear process. They concluded that close d–d-pair ⟨dd⟩ in pico-meter inter-nuclear distance should exist with 1×10^9 pairs in the range (about 1 μm) of incident d-beam. They used 1–10 μA d-beam, so that there would be ⟨dd⟩ numbers on the order of $(1 \times 10^{13}) \times$ (lifetime of ⟨dd⟩. To meet with experimental ⟨dd⟩ numbers, life-time of ⟨dd⟩ would be on the order of 0.1 ms, which is significantly large life compared with d-plasma harmonic oscillation period (few fs) trapped in Bloch potential with 0.22 eV depth for PdDx lattice.

3. Formation of TSC

We have proposed multi-body deuteron fusion process by formation of TSC and Octahedral Symmetric Condensate (OSC) [8,9]. Some numerical results were given by EQPET analyses, which could explain 3–78 W/cm^3 power with $1 \times 10^{11} - 1 \times 10^{13}$ f/s/cm^3 of ^{4}He-atoms production by 4D and 8D fusion reactions, with less than 10 n/s/cm^3 neutron production.

There are remained open questions about where TSC is formed. We have proposed two mechanisms, as transient motion forming deuteron-clusters with short lifetime (60 fs).

(A) In the near surface region of PdDx cathode, deuterium full loading ($x = 1$; PdD) may be attained by electrolysis, gas discharge or gas-permeation, at least locally. No experimental techniques have been developed to measure local distribution of x-value, although we know that it should be key information. With very small density (namely 1 ppm was assumed in our paper [8]) PdD_2 states may exist.

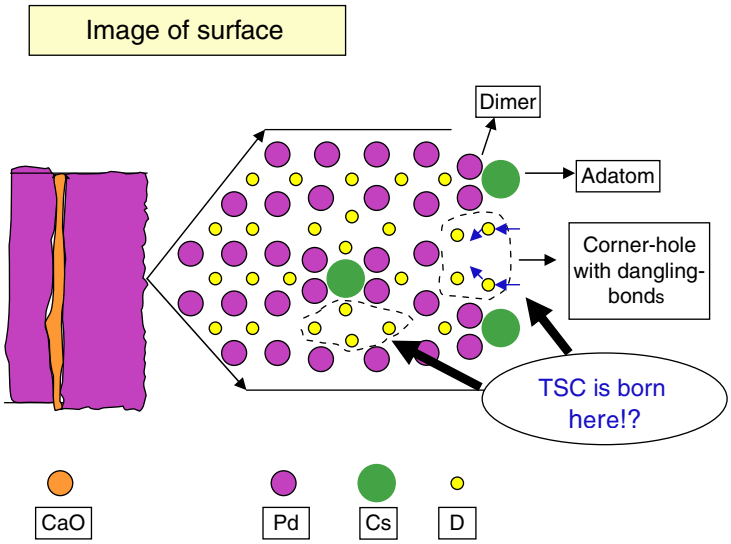

Figure 2. Image of Pd-complex surface.

Trapped D in Bloch potential has discrete energies with 32 meV ground state and 64 meV one phonon energy for excited states. Over 0.22 eV, all D-ions in lattice diffuse out of solid. By exciting with external UV or EUV laser, due to classical Drude model, transient cluster of TSC can be formed with certain probabilities [8].

(B) We know surface of metal is complex and fractal with ad-atoms, dimmers, and corner-holes, for example, as illustrated in Fig. 2. Somewhere, for instance in corner holes, incident D_2 molecules are trapped by dangling bonds. Free D_2 molecule has freedom of rotation and vibration. Trapped D_2 would lose freedom of rotation, but can vibrate for changing distance between pairing two deuterons, and waiting for incoming D_2 molecule.

When incoming D_2 molecule meets near to trapped D_2, incoming D_2 rotates with 90° maximum against waiting D_2 molecule to neutralize charge (minimize Coulomb repulsion energy) and form an orthogonally coupled two D_2 molecules when there meets coherence in vibration modes and electron-spins are anti-parallel for counter part electrons. In this way, TSC may be formed on surface. Since the scenario is still very speculative, we need further substantiating studies.

4. 4D Fusion by 4d/TSC Itself

Trial to explain excess heat with ^{4}He production based on d + d two-body fusion in condensed matter has two intrinsic difficulties to overcome;

(1) Maximum level of d–d fusion rates should saturate on the order of 10 mW/cm^3 (1×10^9 f/s/cm^3), due to the constraint of trapped deuterons in Bloch potential and not large $S(0)$ value (1.1×10^2 keVbarn) enough to increase power level [11].
(2) The dreamed scenario of d + d to ^{4}He+lattice-energy (23.8 MeV) has no reason supported by nuclear physics (see Appendix).

Macroscopic reaction rate (yield) of two-body and multi-body fusion rate with D-cluster condensates as TSC and OSC is given by

$$Y = N_{\mathrm{nd}} \lambda_{\mathrm{nd}}. \tag{5}$$

Table 3. Typical results by EQPET/TSC for fusion rates, power level and products, for TSC in PdDx, assuming $N_{4D} = 1 \times 10^{22}$ (1/cm^3)

Multi-body	Microscopic fusion rate (f/cl/s)	Macroscopic yield (f/s/cm^3), power (W/cm^3)	Ash (fusion products)
2D	1.9×10^{-21}	1.9×10(f/s/cm^3), 1.9×10^{-11}(W/cm^3)	Neutron; 10 n/s/cm^3
3D	1.6×10^{-13}	1.6×10^{9}(f/s/cm^3), 1.6×10^{-3}(W/cm^3)	Tritium; 8×10^{8} t/s/cm^3
4D	3.1×10^{-11}	3.1×10^{11}(f/s/cm^3), 3.1 (W/cm^3)	Helium-4; 3×10^{11} h/s/cm^3

Here, N_{nd} is the time-averaged nD-cluster ($n = 2, 4, 8$) density and λ_{nd} is the microscopic modal fusion rate [8,9], given by

$$\lambda_{nd} = v(S_{nd}(E)/E)\exp(-n\Gamma_{nd}). \tag{6}$$

$S_{nd}(E)$ is the astrophysical S-factor and Γ_{nd} is Gamow integral for d–d interaction in nD-cluster system. The microscopic modal fusion rate for 4D cluster is defined by EQPET as

$$\lambda_{nd} = {a_1}^2\lambda_{nd(1,1)} + {a_2}^2\lambda_{nd(2,2)} + {a_4}^2\lambda_{nd(4,4)}. \tag{7}$$

Here EQPET assumes that the total wave function ψ_{4D} of 4D-cluster is approximated with linear combination of partial wave functions for EQPET molecules, $\psi_{(1,1)}$, $\psi_{(2,2)}$, and $\psi_{(4,4)}$, for normal electron (1,1) state, Cooper pair (2,2) state, and quadruplet state (4,4), respectively.

$$\psi_{4D} = a_1\psi_{(1,1)} + a_2\psi_{(2,2)} + a_4\psi_{(4,4)}. \tag{8}$$

In our previous papers [8,9], we have given calculated microscopic fusion rates for EQPET molecules, dde(1,1), dde*(2,2), and dde*(4,4), using,

$$\lambda_{nd(m,Z)} = v(S_{nd}(E)/E)\exp(-n\Gamma_{nd(m,Z)}). \tag{9}$$

And the Gamow integral for dde*(m, Z) EQPET molecule is given by

$$\Gamma_{nd(m,Z)} = \int_{r_0}^{b} (V_s(r) - E)^{1/2}\mathrm{d}r/((h/\pi)/(2\mu)^{1/2}). \tag{10}$$

Some numerical results are re-listed in Table 3.

Here typical break-up channels of reactions are:

$$2D \rightarrow n + {}^3\mathrm{He} + 3.25\,\mathrm{MeV}(50\%),\ \mathrm{p} + \mathrm{t} + 4.02\,\mathrm{MeV}(50\%), \tag{11}$$

$$3D \rightarrow \mathrm{t} + {}^3\mathrm{He} + 9.5\,\mathrm{MeV}\ (\text{about } 50\%\ ), \tag{12}$$

$$4D \rightarrow {}^4\mathrm{He} + {}^4\mathrm{He} + 47.6\,\mathrm{MeV}\ (\text{almost } 100\%\ ). \tag{13}$$

This calculation (Table 3) shows that 4d/TSC fusion is clean with ^{4}He main ash with very low neutron production ($<1 \times 10^{-10}$ order of ^{4}He rate), although power level (about 3 W/cm^3-Pd) is rather low. Tritium production rate (1×10^{-3} order of ^{4}He rate) is however rather high.

Modal fusion rate given by Eq. (7) for 4D fusion is attributed almost 100% to the quadruplet EQPET molecule dde*(4,4) state. Therefore, the accuracy of this model is closely related to what the minimum size sate of 4d/TSC is.

Later [9], we have considered that the squeezing motion of TSC can be more simply treated by a semi-classical model, because of the three-dimensionally constrained motion of 4d and 4e particles in TSC into the central focal point. Figure 3 illustrates the feature of the semi-classical treatment. Every particle in TSC can make central squeezing motion with same velocity, to keep charge neutrality of total TSC system – in other words to satisfy minimum system energy state (as calculated by the variational principle of quantum mechanics). Therefore this squeezing motion can be treated as Newtonian mechanics until when four deuterons get into the range (about 5 fm) of strong nuclear interaction.

$$\langle r(t)\rangle = \langle r(0)\rangle - \langle v\rangle t. \tag{14}$$

$$\langle r(0)\rangle = (3^{1/2}/2)R_{\mathrm{B}} = 45.8\,\mathrm{pm}. \tag{15}$$

Here, R_{B} is Bohr radius (52.9 pm) and $t <$ TSC lifetime (about 60 fs).

In Fig. 3, TSC will form in the near surface region of condensed matter by the mechanism (A) or mechanism (B) as discussed in Session 2, with certain probability depending on methods of experiments and near-surface physics of condensed matter: Step 1 (TSC forms). Then TSC starts Newtonian squeezing motion to decrease linearly its size from about 100 pm radius size to much smaller size and reaches at the minimum size state: Step 2 (minimum TSC). Classical squeezing motion ends when four deuterons get into the strong force range (5 fm) and/or when four electrons get to the Pauli's limit (about 5.6 fm for e–e distance). Here for the Pauli's limit, we used the classical electron radius of 2.8 fm, which is determined by equating the static Coulomb energy (e^2/R_{e}) and the Einstein's mass energy ($m_{\mathrm{e}}c^2$) to obtain

$$R_{\mathrm{e}} = e^2/m_{\mathrm{e}}c^2 = 2.8\,\mathrm{fm};\ \text{classical electron radius}. \tag{16}$$

Since the range of strong interaction (about 5 fm) is comparable to the classical electron diameter (5.6 fm), as shown in Fig.3(2), the intermediate nuclear compound state ^{8}Be* will be formed just after the minimum size state ("over-

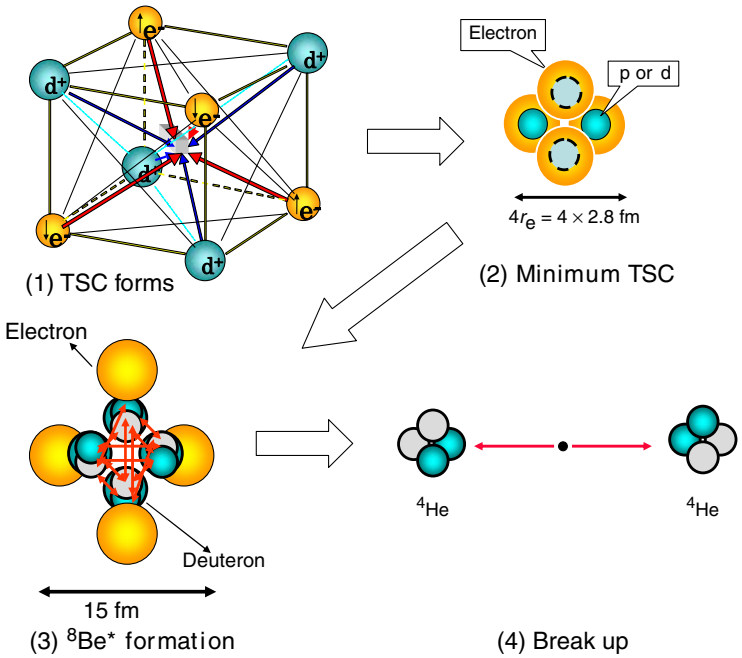

Figure 3. Semi-classical view of squeezing motion of TSC, $\langle e\rangle = (e\downarrow + e\uparrow)/2$ for QM view at four electron centers.

minimum" state); Step 3: ^{8}Be* formation. Immediately at this stage, 4d-cluster shrinks to much smaller size (about 2.4 fm radius) of ^{8}Be* nucleus, and four electrons should go outside due to the Pauli's repulsion for fermions. Shortly in about few fs or less (note; Lifetime of ^{8}Be at ground state is 0.67 fs), ^{8}Be* will break up to two ^{4}He particles, each of which carries 23.8 MeV kinetic energy; Step 4: Break up. It will take about 60 fs from about 100 pm initial size of TSC to its minimum size about 10 fm. About 60 fs is regarded as rough measure of TSC lifetime for this very transient squeezing motion.

Figure 4 shows feature of electron orbits when TSC is just formed. Using linear combination of hydrogen atom wave functions for four deuterium-states, variational method can be applied to calculate coupled electron orbits. As a result, averaged electron position (electron center of $\langle \mathrm{e} \rangle = (\mathrm{e}\uparrow + \mathrm{e}\downarrow)/2$, Bosonized electron pair for exchange force) $\langle r(0) \rangle$ locates at vertexes of regular cube with tetrahedral combining orbits and outer dilute clouds. At $\langle r(0) \rangle$, three Bohr wave functions superpose and electron density is about nine times larger than that of outer dilute cloud. Therefore, the semi-classical treatment of central squeezing motion by Newtonian is approximately fulfilled for "coherent" central averaged momentums for eight particles.

When four electrons start to separate at minimum TSC state, four deuterons suddenly start to *feel* mutual Coulomb repulsion. Nuclear interaction at this stage can be approximately treated by STTBA. Figure 5 illustrates the barrier penetration and strong interaction with negative well potential, for STTBA.

Gamow integral of STTBA [9] is given by

$$\Gamma_{\mathrm{nd}} = 0.218(\mu^{1/2}) \int_{r_0}^{b} (V_{\mathrm{B}} - E_{\mathrm{d}})^{1/2} \mathrm{d}r. \tag{17}$$

And bare Coulomb potential is

$$V_{\mathrm{B}}(r) = 1.44 Z_1 Z_2 / r, \text{ in MeV and fm units.} \tag{18}$$

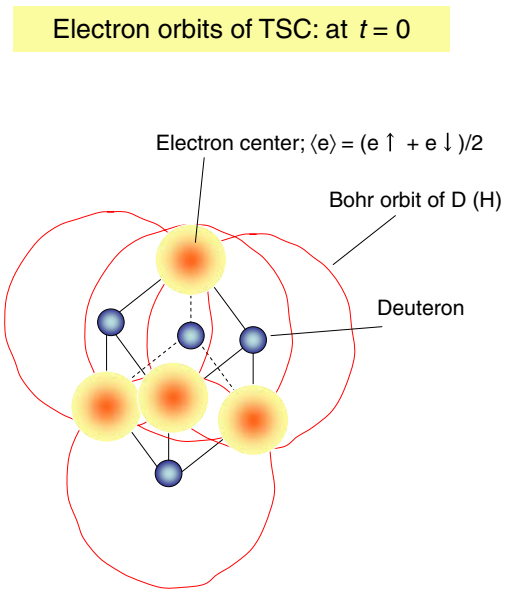

Figure 4. Electron orbits of TSC at $t = 0$, namely orthogonally coupled state of two D_2 molecules as transient motion, with lifetime about 40–80 fs.

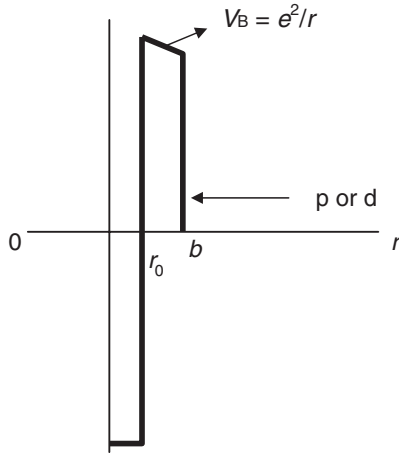

Figure 5. Potential for Coulomb barrier penetration and strong negative well, for Sudden Tall Shin Barrier Approximation (STTBA).

And barrier penetration probability is

$$P_{nd}(E_d) = \exp(-n\Gamma_{nd}). \tag{19}$$

For $V_B \gg E_d$,

$$\Gamma_{nd} \simeq 0.523(Z_1 Z_2 \mu)^{1/2}(b^{1/2} - {r_0}^{1/2}). \tag{20}$$

Using $b = 5.6$ fm and $r_0 = 5$ fm, we obtained; $P_{4d} = 0.77$ with $V_B = 0.257$ MeV and using S_{4d} value in Refs. [8,9], we obtained: $\lambda_{4d} = 2.3 \times 10^{-4}$ f/s/cl. This microscopic fusion rate is 1×10^7 times larger value than one given in Table 3. We consider therefore that EQPET model gave significant underestimation for 4D fusion rate when rigid constraint of motion in three-dimensional space is attained as shown in Fig. 3.

Macroscopic reaction rate with $N_{4D} = 1 \times 10^{22}$ (1/cm^3) is then given as $Y_{4D} = 4.6 \times 10^{18}$ f/s/cm^3-Pd, which is equivalent to 46 MW/cm^3-Pd and 23 keV/Pd-atom.

In ICCF11, El Boher et al. reported [5] very intense excess power for about 17 h, by their super-wave D_2O/Pd-thin-pate electrolysis technique, to give 24.8 keV/Pd-atom. This experimental value is close to 23 keV/Pd-atom by the over-minimum state 4D fusion by 4d/TSC. El Boher et al. did not measure helium, and gave no information about nuclear mechanism behind. If they will find corresponding level of helium atoms, we can say very good agreement between experiment and theory.

If we apply $\lambda_{4d} = 2.3 \times 10^{-4}$ f/s/cl for modal fusion rates in Table 3, neutron production level drops to the order of 1×10^{-17} of ^{4}He production rate and tritium production rate also drops to the order of 1×10^{-9} of ^{4}He production rate. These results are nearer to experimentally observed levels of neutrons and tritium-atoms in CMNS studies [12].

In our 4D cluster fusion model by TSC formation and condensation, two 23.8 MeV α-particles are produced in 180° opposite directions by the final state interaction of ^{8}Be* (excited state) break-up. With known knowledge of ionization and X-ray producing cross-sections of 23.8 MeV α-particle in, e.g., PdDx, production of about 22 keV Pd K-X-rays should be with very small rate and main radiation would be bremsstrahlung X-rays in the region less than about 4 keV by slowing down of convey-electrons of α-particle. Components by L- and M-X-rays (in less than 5 keV region) may appear with visible weights (peaks). Production of secondary neutrons by D(α,n) process by 23.8 MeV α-particle is also with very small rate, since cross-sections are small. Most kinetic energy of 23.8 MeV α-particle will be lost

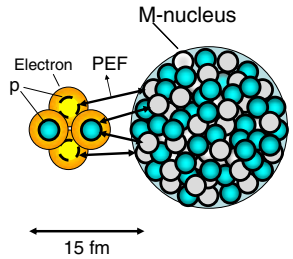

Figure 6. Strong interaction for M-nucleus + 4p/TSC.

by ionization and knock-on with atoms of PdDx (effectively with Pd atoms), associating with soft X-rays by convey electrons, to deposit finally the released nuclear energy as lattice vibration (phonon) energy of PdDx. Therefore, the detection of Soft X-rays is of key issue. However, due to strong attenuation of soft X-rays in the PdDx layer and cell materials, observation from outside will be difficult.

5. TSC+Metal Interaction

Since TSC is a charge-neutral pseudo-particle and its minimum size is about 10 fm in diameter, TSC behaves as like neutron and may penetrate through electron clouds (100 pm for outer most shell and 1 pm for inner most K-shell) surrounding host metal nucleus. Hence, we expect direct nuclear interaction between TSC and host metal nucleus, with certain rate, which we have to study deeply [9].

For 4p/TSC+M-nucleus interaction, four protons do not make fusion in the minimum size state [Fig. 3(2)] of TSC and therefore each proton exchanges charged pion with neutron-states of host metal nucleus (see PEF in Fig. 6). There is competing process between one, two, three, and four protons pick-up by M-nucleus, consequently. We applied STTBA calculation for Ni+4p/TSC reaction rates [9]. We can consider Ni+p, Ni+2p, Ni+3p, and Ni+4p capture processes [9]. Estimated level of reaction rates was considerably high as 5 mW/cm^2 for 1 μm surface Ni layer.

In the case of Ni + H interaction, we estimated fission product distribution and compared with Miley–Patterson experiment [7] for their major products [9], as referred in Fig. 8. Good agreement is seen for two peaked components in higher Z elements, although low-Z elements like C, N, and O are not measured in experiment due to high background of impurities in the low-Z area. Fission products by Ni + 4p reaction become mostly stable isotopes [9] and coming with higher weights from heavier Ni-isotopes as Ni^{62} and Ni^{64}.

For 4d/TSC + host-metal–nucleus interaction behaves different from that of 4p/TSC, because of the tight formation of ^{8}Be* compound state by strong interaction within TSC. This situation makes M + 4D (or ^{8}Be) capture process

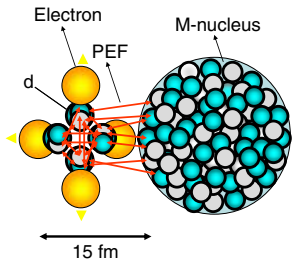

Figure 7. Strong interaction for 4d/TSC + M-nucleus.

predominantly selective (see Fig. 7). Assuming that this process happened in Iwamura experiment [6], we estimated production rate for Cs to Pr transmutation.

$$^{133}\mathrm{Cs} + 4\mathrm{d} \rightarrow {}^{141}\mathrm{Pr}(E_x = 50.49\,\mathrm{MeV}) \rightarrow {}^{141}\mathrm{Pr}(\mathrm{GS}) + \gamma\text{-ray}(50.49\,\mathrm{MeV}) \tag{21}$$

or

$$\rightarrow \text{Fission products.} \tag{22}$$

$$[\text{Transmutation rate}] = 4.6 \times 10^{14}\text{Pr-atoms per week.} \tag{23}$$

This transmutation rate is in agreement with Iwamura's experiment.

Another important possibility for formation of 6d/OSC around defect/void of PdD lattice and its induced 6D fusion and M + 6d/OSC is discussed in other paper to this workshop [14].

6. Conclusions

Some essential results of cluster fusion model for condensed matter nuclear effects were summarized in this work. Major experimental results as d–d screening effects, ^{4}He production without visible neutron emission, correlation of excess heat and ^{4}He production, very intense excess power level as 46 MW/cm^3-Pd, selective transmutations and fission-like products, were almost consistently explained by the EQPET/TSC models.

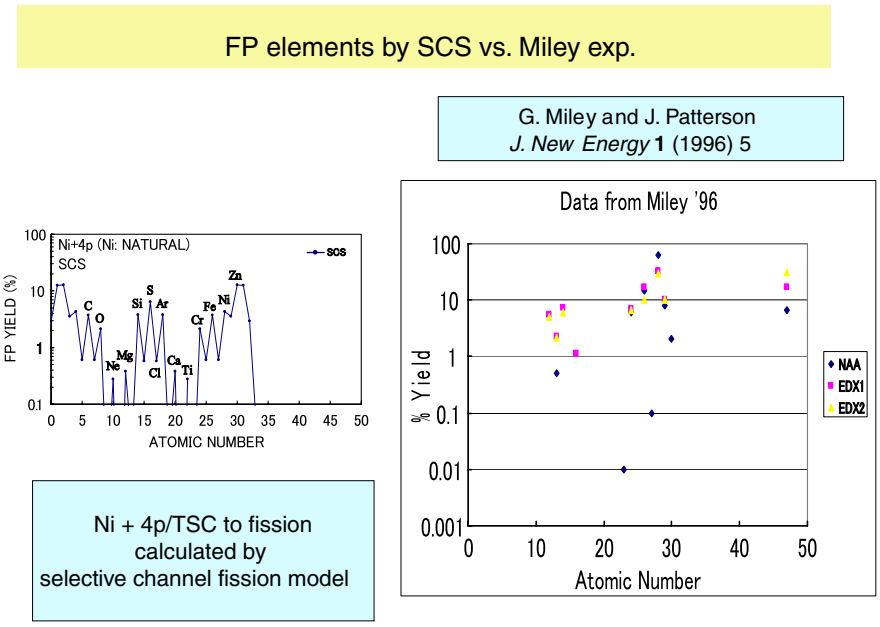

Figure 8. Fission products by Ni + 4p/TSC reaction, calculated by SCS model [13] and experimental data by Miley and Patterson [7].

However, theories are still in primitive stage and further elaborations are expected. Some key conditions like TSC formation mechanism and places are speculative, and we need substantiation of problems in views of condensed matter and surface physics.

Time-dependent EQPET analysis of TSC is underway (presented in ICCF12).

Acknowledgements

The author acknowledges Dr. Y. Iwamura, Mitsubishi Heavy Industries Co. and Dr. F. Celani, INFN Frascati, for their kind discussions to this work.

Appendix

(1) Oppenheimer-Phillips Process
(Q) OP proposed that if deuteron is polarized to n and p we may have enhanced pick up of triton channel by d–d fusion, because of p–p Coulomb repulsion in d–d reaction?
Is this process explainable to observed anomalous tritium generation in CF experiments?

(A) Deuteron never polarizes as so. If d were polarized to n and p, n will decay to p + e in about 10 min and d should disintegrate: we know this never happens and d is stable isotope. Strong interaction binding "virtual" p and n in d-nucleus, by exchanging charged pions (or equivalently glueons between quarks), is so fast that we cannot distinguish which one is neutron or proton, say changing from p to n or from n to p with very high frequency and there is no chance to be "neutron" for making β-decay of weak interaction, and therefore nucleus is stable.
Tritium preferred d–d reaction is therefore not plausible.

(2) d + d to ^{4}He process:
(Q1) Very narrow resonance of d–d interaction in condensed matter may exist and make lifetime of ^{4}He* (or close pair of d–d admixture) very long and 23.8 MeV excited energy can be transferred "gradually" to lattice phonons without emitting hard radiation?

(A1) No mechanisms, which are consistent with known nuclear physics have ever been proposed to change lifetime of ^{4}He*. If lifetime of ^{4}He* would become very long, this state is less competing to short lives (about 1×10^{-22} s) of n + ^{3}He (and p + t) out-going channel and branching ratio of ^{4}He production would become much less than 1×10^{-7} that is for $^4\mathrm{He} + \gamma$ channel. See Fig. 9.
Note that: branching ratio is given as ratio of energy width $\Delta - E/\Delta - E$-total. The total width is $\Delta - E_{(\mathrm{n})} + \Delta - E_{(\mathrm{p})} + \Delta - E_{(\gamma)}$. And we know for d–d reaction $\Delta - E_{(\mathrm{n})} = \Delta - E_{(\mathrm{p})} =$ about 0.2 MeV, and $\Delta - E_{(\gamma)} =$ about 0.04 eV (corresponding lifetime is on the order of 1×10^{-15} s, namely 1 fs). By Heisenberg uncertainty principle, lifetime is given by $h/\Delta - E$. So, if energy width of ^{4}He* would become 1 μeV (corresponding lifetime is about 10 ps) by "very narrow resonance," branching ratio to ^{4}He emission becomes 1×10^{-11}. When one said that lifetime of ^{4}He* were on the order of several seconds, branching ratio should be on the order of 1×10^{-22}.

So, no way is there to produce ^{4}He predominantly in d–d reaction, unless energy width could become far greater than 0.2 MeV. Unfortunately, upper most value of possible energy width is 23.8 MeV which could anomalously increase branching ratio to ^{4}H/n/t = 100/1/1, if at all, and still we should have lethal neutrons from d–d reaction if excess heat were due to such case.
We know the coupling constant of field (force) exchange for electro-magnetic interaction (or QED) is on the order of 1×10^{-2} (1/137 in exact) of nuclear strong interaction. Nuclear reaction cross-section is

proportional to square of transition matrix. Transition matrix is proportional to interaction Hamiltonian. Interaction Hamiltonian is proportional to field coupling constant. Ratio of cross-sections (EM/ Strong) is therefore less than the square (1×10^{-4}) of that ratio of field coupling constants. So we have to conclude that the above case of predominant ^{4}He channel is not plausible.
Even if we assume mega-seconds life for a close d–d pair, if at all, we have nothing to do with changing the lifetime (on the order of 1×10^{-22} s) of ^{4}He* in d–d reaction: this means that normal d–d reactions should take place in stochastic way within the assumed mega-seconds lifetime of the close d–d pair!
The coupling constant of nuclear weak interaction is on the order of 1×10^{-14} of nuclear strong interaction. Therefore, any significant enhancement by weak interaction (including EC — electron capture process) for changing drastically the branching ratios is not plausible, either.
Here you note; Fusion cross-section of two-body interaction is given by

$$\sigma(E) = (S(E)/E)P(E).$$

And $S(E)$ is the intrinsic strong interaction factor, so called astrophysical S-factor, E is the relative energy of two-body system ($1/E$ is the square of de Broglie wave length, i.e., corresponding to geometrical cross-section of incident wave) and $P(E)$ is the barrier penetration probability through shielded (screened) Coulomb potential.

For cold d–d fusion, $S_{dd}(0) = 1.1 \times 10^2$ keVb: this is strong interaction.

For cold p–p fusion, $S_{pp}(0) = 3.4 \times 10^{-22}$ keVb: this is weak interaction and governing reaction in the fusion reaction cycles in the sun.

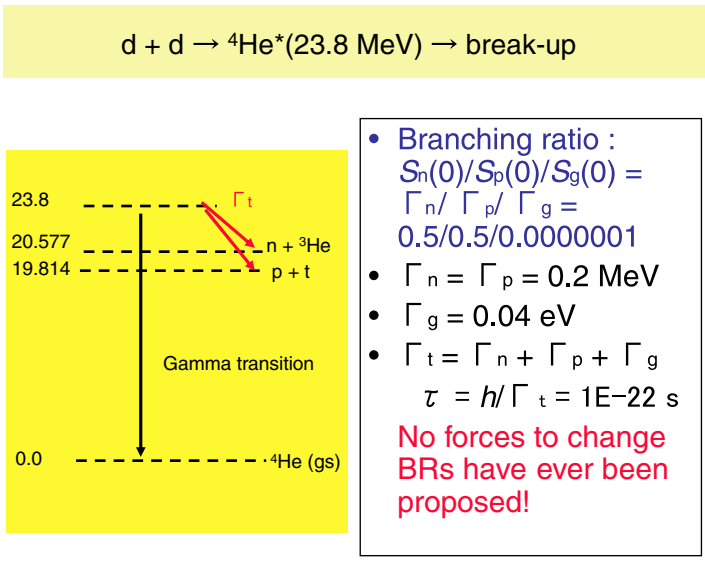

Figure 9. Break-up channels of d–d fusion reaction.

So, we roughly estimate the order of $S_{pp}/S_{dd} = 1 \times 10^{-24}$. You understand how weak the weak interaction is. The sun has huge mass and gravitational confinement fusion of p–p reaction can produce huge energy with very much slow speed (more than 1 billion years lifetime) due to very small S_{pp}-value. Hence a scenario to relate observed excess heat to weak interaction is not plausible. We have abandoned to observe p–p fusion in laboratory experiments, because the reaction level is too weak.

(Q2) There has been asserted by some theories that "two deuteron atoms join together to form one helium-4 + lattice energy." Is it theoretically proved to be correct?

(A2) The "dreamed" reaction d + d to ^{4}He (lattice energy) is simply NOT POSSIBLE from nuclear physics point of view because there is no STRONG nuclear force scenario (ever proposed by theorists with certain quantitative estimation of branching-ratio changing effect) to change known reaction out-going branches of n + ^{3}He and p + t products with 50–50% branching ratio. Please see Q1 and A1.

So their conjecture is to say Cheating Nuclear Physics (Strong Interactions), by a priori "desire." And furthermore, if one conceives the process d + d to ^{4}He (E_x = 23.8 MeV)* as intermediate compound excited state of ^{4}He with very short life as 1×10^{-22} s, the nuclear excited energy ($E_x = 23.8$ MeV) cannot go to lattice phonons (we have to require more than 1 million lattice atoms, say palladiums locating within 30 nm domain, to receive its energy with much faster photon speed -by QED; quantum electrodynamics; coupling is thought there – than light velocity: hence in contradiction to Einstein relativity!).

The Arata-Zhang 5 nm diameter Pd particles experiment with intense ^{4}He production clearly showed that their conjecture is wrong since 5 nm Pd crystal has about 1000 Pd atoms which can receive only about 30 keV (about 0.1% level of 23.8 MeV) in order not to be displaced from lattice (not destroying lattice, namely not destroying story of condensed matter-related reaction). The generation of ^{4}He should be attributed to some other process than the d + d to ^{4}He hypothetical (and wrong, the author thinks) scenario. In author's opinion, we need participation of third and fourth hadrons in d–d system to change reaction products as proposed in this paper and our previous works [8,9,11].

References

[1] J. Kasagi et al., *J. Phys. Soc. Jpn.* **71** (2002) 2881.
[2] A. Takahashi et al., *Phys. Lett. A* **255** (1999) 89.
[3] M. McKubre et al., *Proceedings of the ICCF10*, Boston, 2003, see http://www.lenr-canr.org/.
[4] Y. Arata, *Il Nuovo Aggiatore* **38** (2005) 66–71.
[5] El Boher et al., *Proceedings of the ppt Slide of ICCF11*, Marseilles, November 2004, see http://www.iscmns.org/.
[6] Y. Iwamura et al., *Jpn. J. Appl. Phys.* **41** (2002) 4642.
[7] G. Miley, J. Patterson, *J. New Energy* **1** (1996) 5.
[8] A. Takahashi, Deuteron cluster fusion and ash, *Proceedings of the ASTI5 WS*, Italy, March 2004, see http://www.iscmns.org/.
[9] A. Takahashi, Deuteron cluster fusion and related nuclear reactions in metal-deuterium/hydrogen systems, Recent Developments in Physics, Transworld Research Network, India, issued June 2005.
[10] A. Huke, Ph.D. Thesis, Technical University of Berlin, 2004.
[11] A. Takahashi et al., *Fusion Technol.* **27** (1995) 71.
[12] See many papers in http://www.lenr-canr.org/.
[13] A. Takahashi et al., *Jpn. J. Appl. Phys.* **41** (2001) 7031.
[14] A. Takahashi, TSC-induced nuclear reactions and cold transmutations, this Workshop.

J. Condensed Matter Nucl. Sci. 1 (2007) 142–147

Research Article

Theory of Fusion During Acoustic Cavitation in C_3D_6O Liquid

Fu-Sui Liu* and Yumin Hou
Physics Department, Beijing University, Beijing 100871, China

Wan-Fang Chen
CCAST(World Lab.), P. O. Box 8730, Beijing 100080, China and
Graduate School, Chinese Academy of Science, Beijing 100080, China

Abstract

This paper demonstrates that an exact calculation for transition probability of deuteron under the phonon–deuteron interaction leads to violation of Fermi golden rule. Considering the violation of Fermi golden rule, the zero-point oscillation, and the energy uncertainty relation, this paper demonstrates that the neutron emission during acoustic cavitation comes from D(entered)–D(entered) fusion in C_3D_6O liquid instead of in cavitation vapor bubbles. This paper gives some predictions. The most important prediction is that the water can be taken as energy source producing fusion instead of C_3D_6O liquid.

Keywords: Acoustic cavitation, Fermi golden rule, Fusion, Green function, Phonon–deuteron interaction, Transition probability

1. Introduction

Taleyarkhan et al. measured time spectra of neutron in acoustic cavitation experiments with chilled deuterated acetone [1–3]. Statistically significant neutron emission was measured. The neutron emission rate was up to $\sim 4 \times 10^5$ n/s, where n indicates neutron. Taleyarkhan et al. thought that the neutron emission is due to D–D fusion inside the cavitation vapor bubbles nucleated in highly tensioned deuterated acetone by means of fast neutrons. Here, D indicates deuteron. The D–D fusion mechanism imagined by Taleyarkhan et al. is as follows. The intense implosive collapse of bubbles, including acoustic cavitation bubbles, can lead to extremely high compression, temperature (about 10^9 K), and density of D. Their duration is large enough. These conditions yield the D–D fusion inside the cavitation vapor bubbles.

The difficulty of Taleyarkhan et al.'s mechanism of D–D fusion is that there is no direct experimental evidence to show the high temperature of 10^9 K in the cavitation vapor bubbles. As far as we know, there is still no exact microscopic theory for the D–D fusion during acoustic cavitation. Basing on the exact calculation of the transition

*E-mail: fsliu@pku.edu.cn

probability of deuteron under phonon–deuteron interaction, this paper proposes a microscopic theory for the D–D fusion. Our mechanism is as follows. During the acoustic cavitation a large number of D inside the bubbles enter the spherical surface layer of the chilled deuterated acetone by means of high compressions and high density of D. Note that the spherical surface layer surrounds the cavitation vapor babbles. We call the D entered the spherical surface layer the entered D, and is expressed as D_e or D(entered). The state of D_e in the spherical surface layer is of non-equilibrium and of high density. We call the spherical surface layer D_e–C_3D_6O system. There is D_e–phonon interaction in the spherical surface layer. We will demonstrate that the D_e–phonon interaction leads to the D_e–D_e fusion in the spherical surface layer. In view of the importance of exact calculation of the transition probability to this paper, we introduce two another examples in Section 2, taken from Ref. [4]. In Section 3, we demonstrate that the transition probability of D_e under D_e–phonon interaction violates Fermi golden rule, and give a microscopic theory for the D_e–D_e fusion in the spherical surface layer. In Section 4, we make some predictions.

2. Departure from Fermi Golden Rule

Liu et al. pointed out that it has to be emphasized that two assumptions were made in calculating the transition probability previous to Ref. [4]. Suppose the Hamiltonian H can be put in the form: $H = H^{(0)} + V$, where $V = A\exp(\mathrm{i}\omega t) + A^{+}\exp(-\mathrm{i}\omega t)$, $|a\rangle$ is a discrete state of $H^{(0)}$, $|b\rangle$ is the state in a continuous spectrum of $H^{(0)}$, B is the domain of $|b\rangle$, A is a time-independent operator, and that at initial time t_0, which is taken to be zero, the system is in the state $|a\rangle$. The probability $P_{a\to B}$ of transition into one of the states in the domain B at time t by absorbing an energy $\hbar\omega$ has been given in Ref. [4].

$$P_{a\to B} = \int_B P_{a\to b}\rho_b(E_b)\,\mathrm{d}E_b, \tag{1}$$

$$P_{a\to B} = \frac{1}{\hbar^2}|A_{ba}|^2 f(t, \omega_b - \omega_a - \omega), \tag{2}$$

$$f(t, \omega_b - \omega_a - \omega) = \frac{\sin^2[(\omega_b - \omega_a - \omega)t/2]}{[(\omega_b - \omega_a - \omega)/2]^2}, \tag{3}$$

$$\lim_{t\to\infty} f(t, \omega_b - \omega_a - \omega) = 2\pi t\delta(\omega_b - \omega_a - \omega), \tag{4}$$

where $\rho_b(E_b)$ is the density of states at E_b, $E_b = \hbar\omega_b$, $E_a = \hbar\omega_a$, and $A_{ba} = \langle b|A|a\rangle$. Taking $-\epsilon/2 < E_b < \epsilon/2$. The first assumption in calculating the integral in Eq. (1) is that the width ϵ is so sufficiently small that A_{ba} and ρ_b remain practically constant over the integral so that they can be taken outside the integral sign in Eq. (1). The second assumption is that t is sufficiently large for ϵ to be much greater than the period of oscillation of the f function in Eq. (3), i. e., $\epsilon \gg 2\pi\hbar/t$, so that Eq. (4) can apply. Under the two assumptions $P_{a\to B}$ is then [4]

$$P_{a\to B} = \frac{2\pi}{\hbar}|A_{ba}(E_b)|^2\rho_b(E_b)t. \tag{5}$$

The $P_{a\to B} \propto t$ may then be called the Fermi golden rule. Ref. [4] demonstrated that the exact calculations of transition probability, without using the two assumptions, lead to violation of Fermi golden rule in the cases of hydrogen ionization and KWW relaxation.

3. Departure from Fermi Golden Rule and Theory of D_e–D_e Fusion

The intense implosive collapse of cavitation vapor bubbles can lead to extremely high compressions and high density of D [3]. During this process, a large number of D inside the bubbles enter the spherical surface layer, surrounding the cavitation vapor bubble, of the chilled deuterated acetone, and form a D_e–C_3D_6O system. The C_3D_6O is a liquid. The model of translational motion in liquid, proposed by Kruus [5] and Larsson [6], is as follows. Assume a molecule to undergo vibration in its cell on the average for a time τ_0. It then is displaced into another cell through some distance l, where it again oscillates for a time τ_0, etc. We can describe such collective and translational motion by longitudinal phonon [5,6]. The density oscillations can also be described by the longitudinal phonons [5,6]. Neutron scattering data for liquid had been interpreted in terms of the presence of longitudinal phonon successfully [5,6].

For the D_e–C_3D_6O system the explicit form of the D_e-longitudinal phonon interaction Hamiltonian, $H_{\rm int}$, in the deformation potential approximation is [7, 8]

$$H_{\rm int} = \sum_{m,p} c_{\rm m}^{+} a(\mathbf{p}) c_{\rm m} C i \left[\frac{\hbar}{2NM\omega}\right]^{1/2} \mathbf{p}\cdot\mathbf{e}(\mathbf{p}) + h.c., \tag{6}$$

where N is number of C_3D_6O molecules in the D_e–C_3D_6O system, $c_{\rm m}$ the annihilation operator of D_e at site m, $a(\mathbf{p})$ the phonon annihilation operator, M the mass of C_3D_6O molecule, $\mathbf{e}(\mathbf{p})$ the longitudinal polarization unit vector, $\mathbf{p}\cdot\mathbf{e}(\mathbf{p}) = p$ for longitudinal phonon, p is the wave number of phonon, ω the phonon frequency, C the deformation potential coefficient. Let us estimate the value of C in C_3D_6O liquid. The density of C_3D_6O liquid is 0.79 g/cm^3 [9]. The average volume occupied by one C_3D_6O in C_3D_6O liquid is thus (4.93 Å)^3. The average volume occupied by one atom in a C_3D_6O molecule of C_3D_6O liquid is thus $\Omega = (2.28\ \text{Å})^3$. The average charge of every atomic nucleus in C_3D_6O molecule is -1.8 e, where e is the free electron charge. For C_3D_6O liquid, the average interaction between D_e and atomic nucleus of C_3D_6O molecule is $\epsilon = 1.8e^2/2.28$ Å. From Ref. [8], $\delta\epsilon = C\delta(N_1\Omega)/(N_1\Omega)$, where N_1 is the number of atoms in C_3D_6O liquid. Thus, we obtain $C = -6.03\times10^{-12}$ erg.

Let us assume that the D_e is at m at $t = 0$. The probability amplitude of finding the D_e still at m at $t > 0$ is the following Green function of time at a finite temperature [7]

$$G(t) = -i\langle T c_{\rm m}(t) c_{\rm m}^{+}(0)\rangle. \tag{7}$$

A waiting-time distribution $Q(t)$ is $Q(t) = |G(t)|^2$ [10]. The lifetime of D_e at m, $\langle t\rangle$, is given as [10]

$$\langle t\rangle = -\int_0^\infty t\ \mathrm{d}Q(t). \tag{8}$$

From an exact derivation, Ref. [7] gives

$$Q(t) = \mathrm{e}^{-P(t)}. \tag{9}$$

$P(t)$ is then expressed as [7]

$$P(t) = \frac{2C^2}{\hbar NM}\sum_p [2n(\mathbf{p})+1]\frac{p^2}{\omega}\frac{\sin^2(\omega t/2)}{\omega^2}, \tag{10}$$

where $n(\mathbf{p})$ is the Bose distribution of the phonon. We will now just consider the zero-point energy term in Eq. (10). Because the signs of the two terms in Eq. (10) are the same the $P(t)$ will become larger if we consider also the term with the Bose distribution of the phonon. For the zero-point energy term, Eq. (10) can be transformed into the integration

$$P(t) = \frac{2C^2}{\hbar N M} \int_0^{\omega_{up}} \mathrm{d}\omega \rho(\omega) \frac{p^2}{\omega} \frac{\sin^2(\omega t/2)}{\omega^2}, \tag{11}$$

where $\rho(\omega)$ corresponds to the density of states of longitudinal phonon, and ω_{up} is the upper limit of spectral density function. Here, we meet the same function as Eq. (1). We do not use the two assumptions mentioned in Section 2, and make an exact calculations for Eq. (11). We know from Eq. (4.6) of Ref. [11] that for a completely random lattice the p^2 in Eq. (11) represents $|\mathbf{k} - \mathbf{k}'|^2$, where $\mathbf{k}$ and $\mathbf{k}'$ are the wave vectors of a particle before and after absorption of a phonon. The $|\mathbf{k} - \mathbf{k}'|^2$ does not depend on the energy for a completely random lattice [11]. The average value of $|\mathbf{k} - \mathbf{k}'|$ in the Brillouin zone, $|\mathbf{k} - \mathbf{k}'| = \bar{p} = \pi/(2a)$, is taken for a completely random lattice [11]. For a perfect lattice $|\mathbf{k} - \mathbf{k}'| = p = \omega/v$ where v is the longitudinal sound velocity [11]. However, considering that the phonons in liquid have a much-shorter lifetime and pathlength than in crystalline solids [5] and that liquids have short-range order ($\sim$ 20 Å) [5], one often takes $p = \omega/v$ in liquid theory approximately [5]. Actually, $p = \omega/v$ is correct only for a perfect lattice. Actual solid and liquid have more or less deviations from the perfect lattice. Especially, the long-range disorder in liquid still has a little influence to the relation $p = \omega/v$. Therefore, we should imitate Refs. [4, 11] to take

$$p = \left(\frac{\omega}{v}\right)^{1-\beta'} \bar{p}^{\beta'}, \tag{12}$$

where $\bar{p} = \pi/(2 \times 4.93\ \text{Å})$, and $\beta' \approx 0$ for C_3D_6O liquid. To obtain the express of $\rho(\omega)$ in Eq. (11), we make the following analyses. We will show that the D_e–D_e fusion is induced by the D_e-longitudinal phonon interaction in C_3–D_6O liquid. To have this interaction the D_e in the C_3D_6O liquid should be in non-equilibrium state, and thus can move. In this movement, the D_e can absorb longitudinal phonon. If the D_e is trapped in some place of the C_3D_6O liquid, and thus moves together with the molecule C_3D_6O, then the movement of the D_e becomes a part of the oscillation of molecule C_3D_6O. In this case there is no D_e–phonon interaction. We assume for specification that the non-equilibrium state of D_e just occurs in the spherical surface layer whose thickness is only one C_3D_6O molecule. For this quasi-two-dimensional D_e–C_3D_6O system, the average density of states of phonon, $\rho(\omega)$, is $10^{13}S/(4\pi v^2)$ [12]. The S is the total area of the spherical surface layer of the D_e–C_3D_6O system. The v is the longitudinal sound velocity in C_3D_6O liquid. $v = 1174$ m/s at 25°C [9]. If we set $\beta = 1 - 2\beta'$, then $\beta \approx 1$. Let $A = C^2\pi^{2\beta'}S/[\pi\hbar N M v^{4-2\beta'}(2 \times 4.93\ \text{Å})^{2\beta'}]$, then Eq. (11) becomes

$$p(t) = A \int_0^{\omega_{up}t} \mathrm{d}(\omega t) \frac{\sin^2(\omega t/2)}{(\omega t)^{2-\beta}} t^{1-\beta}. \tag{13}$$

Now let us assume that at $t = 0$ we have a D_e at site m with energy E_m and a phonon with frequency ω_{up}, and at $t > 0$ we have only a D_e at the site m. For this physical system, the uncertainty relation for energy, Eq. (44.1) of Ref. [13], gives $\omega_{up}t = 1$ for any value of t. Assume $\beta = 0.8$. Numerical calculation for the integral in Eq. (13) gives 0.1335. Eq. (13) then becomes

$$P(t) = 0.1335At^{0.2}. \tag{14}$$

From Eq. (14) we see that the Fermi golden rule is violated seriously. However, we should believe this result because it comes from exact calculations for Eq. (11) without using the two assumptions in Section 2.

Set

$$\tau = (0.1335\ A)^{-1/0.2}, \tag{15}$$

then

$$P(t) = \left(\frac{t}{\tau}\right)^{0.2}. \tag{16}$$

Substituting Eq. (16) into Eqs. (9) and (8) gives that the lifetime of D_e at m under the influence of D_e-longitudinal phonon interaction is

$$\langle t\rangle = \tau\Gamma\left(1+\frac{1}{0.2}\right), \tag{17}$$

where Γ indicates Gamma function. Numerical calculations give $\langle t\rangle = 3.8\times10^{-26}$ s. Considering that the D_e with radius 10^{-13} cm has possibility to move to all directions, the probability of D_e to move to a specific D_e is $P = \pi(10^{-13})^2/4\pi a^2$, where a is the nearest distance between two moving D_es in the spherical surface layer of C_3D_6O liquid.

If we take $a = 2$ Å, then $P = 6.25\times10^{-12}$. The D_e in the D_e–C_3D_6O system makes random thermal movement. At 300 K, the velocity of D_e is thus $v_D = 1.1\times10^5$ cm/s. If we do not consider that the D_e has possibility to move to all directions, then the collision rate of a D_e with another D_e is $v_D/2$ Å. If just before the wink of collision between two D_es one D_e absorbs a phonon, then its lifetime is 3.8×10^{-26} s, and the energy given by the energy uncertainty relation is 2.76×10^{-2} erg. Noting that even at 10^9 K the energy of D_e is only 1.38×10^{-9} erg, we can say that the fusion of the two D_es can occur definitely. (If $\beta = 0.9$, then the lifetime is 2.28×10^{-36} s, and the energy given by the energy uncertainty relation is 5×10^8 erg.) In our numerical calculations the estimative value of C is rather rough because it is based on the average volume and the average charge. The larger the value of C, the shorter the lifetime. If $C = -3\times10^{-12}$ erg instead of -6×10^{-12} erg, then the lifetime is 4.0×10^{-23} s instead of 3.8×10^{-26} s. In this case the energy given by the energy uncertainty relation is 2.76×10^{-5} erg, which is still much larger than 10^9 K. The nearest distance between two D_es is 2 Å. The number of D_es in this length of 2 Å is, in principle, $2\times10^{-8}/10^{-13} = 2\times10^5$. If the D_e absorbs only one phonon in the length of 2 Å, then the probability to absorb a phonon by D_e just before collision wink is only $P' = 5\times10^{-6}$. Considering all the factors, the rate that a moving D_e comes into collision with another D_e and produces D_e–D_e fusion is $R = P'Pv_D/2$ Å $= 3.3\times10^{-4}$/s. If the number of cavitation vapor bubbles in the chilled deuterated acetone is 100 and the radius of the bubbles is 120 nm in average, then the total volume of the spherical surface layer of the 100 vapor bubbles is 9.7×10^{-15} cm^3. Noting that the nearest distance between two moving D_es is 2 Å, then the total number of moving D_e in this volume is $N_t \approx 9.7\times10^{-15}/(2\times10^{-8})^3 = 1.2\times10^9$. The total fusion rate is $RN_t = 4\times10^5$/s. This is just the observed value in Ref. [3]. The observed radius of the cavitation bubble is from tens of nanometers to several hundreds of nanometers [3]. If we take the nearest distance between two moving D_es $a = 3$ Å instead of 2 Å, then the total fusion rate is 0.8×10^5/s, which has no change of order of magnitude in comparison with 4×10^5/s. Therefore, we can say that, considering the energy uncertainty relation, the violation of Fermi golden rule, and the zero-point oscillation in the D_e–C_3D_6O system, the experimental results in Refs. [1–3] can be explained by D_e–D_e fusion on the whole.

4. Predictions

Our theory supports the D_e–D_e fusion in Refs. [1–3] and predicts that there should be excess heat. From ${}^2_1\mathrm{D} + {}^2_1\mathrm{D} \longrightarrow {}^3_2\mathrm{He} + {}^1_0\mathrm{n} + 3.3$ MeV and the observed neutron emission rate ($\approx 4 \times 10^5$ n/s), we know the excess heat rate is $\approx 1.3 \times 10^6$ MeV/s. The reason that the excess heat is difficult to be observed in Ref. [3] is that the volume of the total spherical surface layer is too small (only 9.7×10^{-15} cm^3), and thus the number of moving D_es are too small. The fusion imagined by Refs. [1–3] occurs in the cavitation bubbles. However, our theory demonstrates that the fusion occurs in liquid.

In our theory for the D_e–D_e fusion during acoustic cavitation, the sufficient conditions for occurrence of the D_e–D_e fusion are the existences of D_es in high density non-equilibrium state and the longitudinal phonons in a condensed matter system. If the compression and the density of moving H in the acoustic cavitation vapor bubbles in water are high enough, then a number of moving H can enter the spherical surface layer surrounding the cavitation bubbles and form non-equilibrium state of the entered H, at least, in a layer with thickness of one molecule of water. The H(entered)-H(entered) fusion can also occur in the spherical surface layer outside the bubbles, i. e., in water. However, there was no statistically significant neutron emission, when one used C_3H_6O liquid instead of C_3D_6O liquid [3]. We think that the H(entered)-H(entered) fusion already occurred in Ref. [3], when one used C_3H_6O liquid. The reason why is simple. The last products of H(entered)-H(entered) fusion are ${}^4_2$He and excess heat. Therefore, that there is no neutron emission does not imply that there is no H(entered)-H(entered) fusion in C_3H_6O liquid. If the H(entered)-H(entered) fusion in water can be realized in suitable acoustic cavitation conditions, then the water can provide nearly infinite energy source for mankind. The cavitation vapor bubbles in water can be nucleated by fast neutron or by laser.

Considering that the energy given by the energy uncertainty relation is very large (2.76×10^{-2} erg), the moving D_e (or H(entered)) can overcome the high potential barriers between the moving D_e (or H(entered)) and any atom in C_3D_6O (or C_3H_6O and H_2O). Therefore, we predict that there are fusions between D_e (or H(entered)) and any atom of C_3D_6O (or C_3H_6O and H_2O) as well.

After the finding of neutron emission during acoustic cavitation in Refs. [1–3], most people doubt the correctness of quantum mechanics. Our theory clearly shows that the fusion in Refs. [1–3] is true, and the quantum mechanics is correct. Although the exact calculations in this paper and in Ref. [4] show that the Fermi golden rule is broken in many cases, yet the Fermi golden rule is not the foundation of quantum mechanics. Our theory just shows that when one uses the Fermi golden rule, one should be careful enough.

References

[1] R.P. Taleyarkhan, R.I. Nigmatulin, R.T. Lahey Jr., *Science* **295** (2002) 1868.
[2] R.I. Nigmatulin, R.T. Lahey Jr., R.P. Taleyarkhan, *Science 2002* Online, WWW.Sciencemag.org/cgi/content/full/295/5561/1868/DC1.
[3] R.P. Taleyarkhan, J.S. Cho, C.D. West, R.T. Lahey Jr., R.I. Nigmatulin, R.C. Block, *Phys. Rev. E* **69** (2004) 031609.
[4] Liu Fu-sui, Peng Kuang-ding, Chen Wan-fang, *Inter. J. Theor. Phys.* **40** (2001) 2037.
[5] P. Kruus, *Liquids and Solutions* (Marcel Dekker, New York, 1977), pp. 164, 399, 467, 497, 460, 57 and 400.
[6] K.E. Larsson, *Faraday Symp. Chem. Soc.* **6** (1972) 122.
[7] G.D. Mahan, *Many-Particle Physics* (Plenum, New York, 1981), pp. 90, 269, 270 and 277.
[8] J. Callaway, *Quantum Theory of the Solid State* (Academic, New York, 1991), p. 620.
[9] R. Weast, *Handbook of Chemistry and Physics* (Chemical Rubber Co., Cleveland, OH, 1971), p. E–41.
[10] Liu Fu-sui, Wen Chao, *Phys. Rev. B* **40** (1989) 7091.
[11] G. Bergman, *Phys. Rev. B* **3** (1971) 3799.
[12] N.M. Ashcroft, N.D. Mermin, *Solid State Physics* (Holt, Rinehart and Winsron, New York, 1976), p. 464.
[13] L.D. Landau, E.M. Lifshitz, *Quantum Mechanics* (Pergamon Press, Oxford, 1962), p. 150.

J. Condensed Matter Nucl. Sci. 1 (2007) 148–154

Research Article

Search for Isotopic Anomalies in Alchemical Silver Coins from the Germanischen National Museum in Nuremberg

Hervé Bottollier-Curtet
1 Avenue Brassens, 13100 Aix en Provence, France

Oliver Köberl
467 Bd. Général Charles de Gaulle, 84120 Pertuis, France

Robert Combarieu
CEMEF, Ecole des Mines de Paris, UMR CNRS 7635, BP 207, 06904 Sophia Antipolis, Cedex, France

Jean-Paul Biberian*
CRMCN, CNRS, 163 Avenue de Luminy, 13288 Marseille Cedex 9, France

Abstract

We analyzed six silver coins of supposedly alchemical origin. They were manufactured during the 17th and 18th centuries, and kept in the Germanischen National Museum in Nuremberg in Germany. We did both nondestructive chemical and isotopic analysis. Silver has two stable isotopes, and our measurements indicate that the silver of all the coins have natural isotopic composition. We conclude that the silver contained in these coins is not of artificial origin. This does not prove that alchemists did not succeed in transmuting metals, but we have shown that the silver of these six coins is most likely of natural origin.

Keywords: Alchemy, Cold fusion, Isotopic anomalies, Museum, Silver, Transmutation

1. Introduction

According to science, it is impossible to produce nuclear reactions by chemical means. However, with the discovery of Cold Fusion [1], experimental demonstrations of low-energy nuclear reactions have resulted in transmutation of elements by electrolysis [2]. Moreover, recently Iwamura et al. [3] have shown that transmutation occurs without electrolysis. All these recent results indicate that in the past, alchemists may have found a way to do the same. Recent

*E-mail: biberian@crmcn.univ-mrs.fr

Figure 1. Photograph of both sides of the coins analyzed. Ref 8882, Krohnemann.

isotopic analysis of these transmutations obtained by electrochemical or chemical means indicates that the isotopic ratios of the newly formed elements differ from natural elements, inciting us to perform isotopic analysis of metals allegedly produced by alchemy.

In the last two millennia, numerous people from different continents, civilizations and historic eras, claimed that they were able to transmute base metals such as mercury or lead into noble metals such as gold or silver. During the 17th and 18th centuries in Europe, many adepts of alchemy organized public exhibitions of their art in the presence of their protector and counselors. Even coins and commemorative medals were minted with this allegedly transmuted, a few dozens of which are kept today in several museums throughout the world.

Some of these objects have undergone chemical analysis, confirming that they are actually mostly made of gold or silver, with some other minority or trace elements such as copper, lead, mercury, silicon, etc. But to our knowledge, none of these objects has undergone any nuclear analysis, the only class of analysis providing potential evidence of nuclear reactions such as those claimed by the alchemists.

We measured the isotopic composition of the silver contained in six "alchemical" coins from the collection of the Germanischen National Museums (GNM) in Nuremberg, Germany, with a Time Of Flight Secondary Ion Mass Spectrometer (TOF-SIMS). These isotopic compositions are all normal, i.e. identical to the isotopic composition of natural (terrestrial) silver. These results demonstrate unambiguously that the metals used to mint these six "alchemical" coins come from landmines, and are not the result of alleged alchemical transmutations.

Alchemy is the ancestor of modern chemistry and, as such, is worthy of investigation. Adepts have always stated that they have succeeded in transmuting metals, i.e. in triggering nuclear reactions. With their equipment (athanors,

Table 1. Name and year of production of the coins

GNM No.	Year	Name
Mü 8882	1679	Krohnemann
Med 5941	1679	Krohnemann
Med 6010	1705	Unbekannt
Med 5948	ca 1700	Rosenkreuser
Med 5937	Unknown	Lune
Med 6215	Unknown	Solis

Figure 2. Photograph of both sides of the coins analyzed. Ref : 5941, Krohnemann.

alambics, crucibles, etc.) they were capable of producing chemical reactions, but at the present time are not believed to trigger nuclear reactions because of the huge difference in the energy threshold level: typically 1 eV per atom for a chemical reaction and 1 MeV per atom for a nuclear reaction, i.e. six orders of magnitude higher. That is why transmutations obtained by these adepts are viewed as absolutely impossible by modern scientists.

The isotopic distribution of metals in nature coming from the fact that heavy metals were formed in a dying star. If an element is produced artificially, the isotopic composition is very likely to be different from that of the natural element. As gold has only one stable isotope, we could not lok for isotopic anomalies in transmuted gold. However, silver has two stable isotopes and therefore any deviation from the natural composition can be looked for. Standard isotopic compositions are compiled and published by the International Union of Pure and Applied Chemistry [4]. For Silver, the standard isotopic composition is, in at.%: 51.839% for ^{107}Ag and 48.161% for ^{109}Ag. This standard isotopic composition is constant wherever the landmine is located throughout the world, within a range of a few parts per thousand (‰).

2. Silver Isotopic Compositions of the Six "Alchemical" Coins of the Nuremberg Museum

2.1. Description of the Coins

This collection has been carefully studied from a historical point of view [5], and we are sure that they are supposedly been produced by alchemists. We analyzed one coin and five medals (for the sake of simplicity, we will use the generic

Table 2. Chemical analyses of coins

Coin	Ag	Cu	S	Hg	Si
Hercules	100.0	–	–	–	–
Marie Curie	100.0	–	–	–	–
Mü 8882	95.0	5.0	–	–	–
Med 5941	95.0	2.0	3.0	–	–
Med 6010	89.3	1.8	2.5	0.3	6.1
Med 5948	95.5	1.5	0.5	–	2.5
Med 5937	84.6	4.6	8.8	2.0	–
Med 6215	52.0	6.0	26.0	13.5	2.5

Figure 3. Photograph of both sides of the coins analyzed. Ref 6010 : Unbekannt.

term of "coins"). Table 1 gives the museum reference, the year of production and the name of the various coins. Figures 1–6 show photographs of both sides of the six coins that have been studied.

In addition to these six "alchemical" coins, we analyzed two French contemporary silver collection coins (99.99% of Ag) in order to get a benchmark for our measurements:

A 50 Francs coin "Hercules", minted in 1974,

A 100 Francs coin "Marie Curie", minted in 1984.

2.2. Chemical Analysis

Surface chemical analyses have been performed by X-rays fluorescence in a JEOL Scanning Electron Microscope (SEM) at the CRMCN Laboratory by Energy Dispersive Spectroscopy (EDS). Precision of measurements being 1.0%.

For each coin, measurements have been done between 2 and 5 times on heads and tails of the coins, at different locations. Here are the results in at.% (Table 2).

These six "alchemical" coins are mostly made of silver. Copper is measured, as it is the case in regular silver coins (Sterling, Thaler, etc.). Sulphur and mercury were expected since these two elements were widely used by alchemists. Silicon is likely attributable to the use of crucibles made of refractory materials.

2.3. Isotopic Composition Measurements

2.3.1. *Procedure*

Non destructive mass analysis was performed at the Ecole des Mines with a Charles Evans TOF-SIMS. A gallium ion gun sputters surface atoms that are ionized by impact of the incident beam, and then depending on their mass arrive at the detector at different times.

The spectrometer has a mass resolution of 9000 at mass 28 on silicon wafer, but only mass resolutions of 4000 can be obtained on such coins due to roughness of their surfaces. However, this is enough to easily separate metallic ions from hydrocarbons ions having same atomic masses. Sensitivity varies with elements analyzed, and this technique is not good for quantitative analysis. However, for atomic ratios this is a very convenient tool, with a unique advantage of being almost non destructive, since only a few atomic layers are sputtered away during analysis.

Figure 4. Photograph of both sides of the coins analyzed. Ref 5948, Rosenkreuser.

2.3.2. *Results*

We first checked our spectrometer by measuring isotopic compositions of natural silver contained in the two regular coins "Hercules" and "Marie Curie". Within precision of our measurements ($\sigma = 1.0\%$), these two measured isotopic compositions are the standard ones. We then measured isotopic compositions of silver contained in the six "alchemical" coins. Here also, within precision of our measurements, these six measured isotopic compositions are equal to the standard ones. For these "alchemical" coins, we also checked isotopic compositions of other elements contained in the coins, even though there was no reason why their isotopic composition would have not been standard. Copper, mercury, sulfur and silicon all had standard isotopic compositions.

3. Discussion

For these alchemical coins, the isotopic composition of silver is equal to the standard isotopic ratio. If this silver was of alchemical origin, i.e. transmuted from another metal, then the probability that its isotopic composition be equal to the standard one would have been close to zero, not to say zero.

Figure 5. Photograph of both sides of the coins analyzed. Ref : 5937, Luna.

Figure 6. Photograph of both sides of the coins analyzed. Ref 6215 : Solis.

Actually, the probability depends on precision of measurements: 1% in our case. That is why we can state unambiguously that the silver contained in these coins is natural.

However, only six silver "alchemical" coins were analyzed out of a total of 34 silver coins stored in the museums of Nuremberg, Wien, Dresden and Munich [6].

4. Conclusion

We measured the isotopic composition of the silver contained in six "alchemical" coins coming from the collection of the Germanischen National Museums (GNM) in Nuremberg, Germany, with a TOF-SIMS. These isotopic compositions are normal, i.e. identical to the isotopic composition of natural (terrestrial) silver. These results demonstrate unambiguously that metals used for minting these six "alchemical" coins come from landmines, and are not the result of some alleged alchemical transmutations.

With these results of nuclear analysis, the first to our knowledge, we propose a method capable of providing a definitive and irrefutable answer to the question of the allegedly transmutation of a base metal into silver, proclaimed by numerous adepts of alchemy for centuries.

These results are not a definitive proof that alchemy never existed because they are partial: only six silver "alchemical" coins have been analyzed out of a total of at least 34 kept in museums. But it is a serious hint.

To have a definitive answer, since the analysis is totally non-destructive, we invite the aforesaid museums to lend us their silver "alchemical" coins for analysis.

Acknowledgments

The authors wish to thank Dr. Hermann Maué, Germanischen National Museums in Nuremberg, for the loan of the coins and Dr. Vladimir Karpenko, University of Prague, for fruitful discussions.

References

[1] M. Fleischmann, S. Pons, *J. Electroanal. Chem.* **261** (1989) 301–308 .
[2] G.H. Miley, J.A. Patterson, *J. New Energy* **1**(3) (1996) 5.
[3] Y. Iwamura, M. Sakano, T. Itoh, *Jpn. J. Appl. Phys. A* **41** (2002) 4642.
[4] Ph. Taylor et al., Isotopic compositions of the elements 1997, *Pure Appl. Chem.* **70**(1) (1998) 217–235.

[5] V. Karpenko, Alchemistische Münzen und Medaillen, *Anzeiger des Germanischen Nationalmuseums Nürnberg*, 2001, pp. 49–72.
[6] V. Karpenko, Coins and medals made of alchemical metal, Ambix, **25** (Part 2) (1988) 65–76.